Interactions tectono-magmatiques au cours de l'extension des marges volcaniques : nouvelle lecture de l'évolution de la province Afar en tant qu'analogue actif

Martin Stab

- Thèse de doctorat -

Interactions tectono-magmatiques au cours de l'extension des marges volcaniques : nouvelle lecture de l'évolution de la province Afar en tant qu'analogue actif

présentée par

Martin Stab

Pour obtenir le titre de

Docteur de l'Université Pierre et Marie Curie – Paris VI

Soutenance publique à Nancy le 30 Novembre 2015
devant le jury d'examen composé de :

Pr. Othmar Müntener,	Université de Lausanne, Suisse,	Rapporteur
Pr. Laurent Geoffroy,	Université de Brest, France,	Rapporteur
Pr. Laurent Jolivet,	Université d'Orléans, France,	Examinateur
Dr. Claudio Rosenberg,	Université Paris VI, France,	Examinateur
Dr. John Armitage,	IPGP, France,	Examinateur
Dr. Marc Lescanne,	Total, France	Invité
Dr. Dereje Ayalew	Université d'Addis Abeba, Éthiopie	Invité
Dr. Nicolas Bellahsen,	Université Paris VI, France,	Directeur de thèse
Dr. Raphaël Pik,	Université de Lorraine, France,	Directeur de thèse
Dr. Sylvie Leroy,	Université Paris VI, France,	Directrice de thèse

Remerciements

J'adresse bien entendu mes premiers remerciements à Laurent Geoffroy, Othmar Müntener, Laurent Jolivet, John Armitage, Claudio Rosenberg, Marc Lescanne et Dereje Ayalew pour avoir accepté de lire et d'évaluer (et pour les deux premiers d'avoir rapporté !) ce manuscrit. Merci à Actions Marges et Total pour avoir financé cette thèse.

Je suis profondément heureux de remercier Sylvie Leroy, Raphaël Pik et Nicolas Bellahsen pour m'avoir encadré et accompagné pendant ces presque quatre années de thèse. Merci d'avoir été disponibles et passionnés, tolérants quand j'étais à l'arrache et attentifs quand je ne l'étais pas. Merci particulièrement à Sylvie, sans qui il n'y aurai pas eu de thèse du tout, de m'avoir appris à regarder des coupes sismiques, de m'avoir parlé d'autres marges que celle de l'Afar ; à Raphaël de m'avoir accueilli dans le laboratoire où j'ai passé le plus clair de mon temps, à m'avoir appris à mesurer des gaz rares, emballer des échantillons dans le désert, plus généralement de m'avoir *emmené* dans ledit désert, à m'avoir montré la géochimie ; à Nicolas pour m'avoir appris les failles, à tenir une boussole, et à dessiner des coupes, entre autres. C'était un grand plaisir d'avoir travaillé ensemble.

Merci à Philippe Werner et Patrick Unternehr pour leur aide avec les coupes sismiques. Je remercie Dereje pour sa grande aide sur le terrain et pour les discussion sur les basaltes et les rhyolites, et aussi parce qu'il sait faire la différence entre les deux même à 30 km, ce qui fait gagner du temps. Merci à Xavier Quidelleur pour sa disponibilité et pour la patience avec laquelle il m'a formé sur la technique K-Ar dans son laboratoire, sans crier. Merci à Thomas Boulesteix pour m'avoir aidé à bien préparer les échantillons pour que Xavier ne crie pas. Merci à Emmanuel Davy pour son aide dans toutes les affaires de sciage, broyage, séparation qui m'auront sérieusement occupé. Merci à Bouchaïb Tibari pour sa grande aide avec le spectromètre. Merci à Alain Rabaute pour les précieux conseils et techniques qui ont attrait au SIG.

Je remercie mes pétulants collègues du CRPG : Émilie, Maïa, Yves, Guillaume M, Flo, Magali, les Nico Puchol et Meyer, Sarah, Marie, Julien A., Jesse, Aurélien, Léo, Dimitri, Romain, Guillaume A, Rémi B., Gaelle, Evelyn, Laurent, Delphine, François, Lydéric, PH, Gaston, Mary, Julien C., Léa, Yumi, Aurélie, Cati, Isabelle et Martine, Yannick, Pierre, et j'en oublie. Ceux de l'ISTEP : Félicie, Alex, Jordane, Chloé, Arnaud, Nico et les autres.

Merci à tous les amis de Nancy pour avoir été présents : Nastasia, Marko, Marie, Anthony, Laurette, Julien, Marianne, Anne. Merci à la meute du 67 pour avoir pris au sérieux cette vaste expérience et d'avoir été doux et glorieux.

Merci à mes parents de m'avoir supporté, encouragé, et rassuré. Merci à Camille pour m'avoir épaulé pendant les longues heures de rédaction, pour son indéfectible soutien et sa grande patience.
Merci à Pete pour tous les moments.

Résumé

Les marges passives volcaniques, qui représentent plus des trois-quarts des marges passives sur Terre, sont les témoins privilégiés des processus d'extension lithosphérique menant à l'ouverture de nouveaux bassins océaniques. Elles sont caractérisées notamment par une grande quantité de magma sous-plaqué, intrudé et extrudé sous forme de grands prismes de laves – les *seaward-dipping reflectors*, ou SDR - au cours de l'extension et de l'amincissement lithosphérique qui forment la transition océan-continent (TOC). L'origine et de la formation de ces objets géologiques, directement liée aux interactions entre processus de rifting et fusion du manteau, est encore largement débattue. Cela est dû en partie au fait que l'observation de la TOC reste un défi : inaccessible, puisque située à de grandes profondeurs sous la surface des océans, et difficilement observable du fait de la présence de grands volumes de roches volcaniques qui en masquent les structures.

Cette thèse se propose d'explorer les relations structurales et temporelles qui existent entre le développement des grandes structures qui accommodent l'extension et l'amincissement, et la production magmatique qui lui est associée *pendant* le développement d'une marge volcanique naissante, accessible à l'observation directe : le point triple Afar en Éthiopie. Nous produisons une nouvelle lecture de la province Afar en tant qu'analogue en devenir des marges volcaniques. Nous présentons dans ce travail une approche triple. La première approche consiste – au moyen d'une étude de terrain et de datation du volcanisme - en la caractérisation du timing de la déformation *crustale* et du style structural du rift depuis les phases les plus précoces du rifting jusqu'à l'actuel. La seconde approche consiste en la détermination de l'évolution des régimes de fusion *mantellique* au cours de l'extension, au travers de l'examen de la géochimie des laves. La troisième est la construction d'un modèle synthétique à l'échelle des plaques Nubienne et Arabe qui traite de l'évolution des marges volcaniques associées au point triple Afar en lien avec leur segmentation.

Les principaux résultats suggèrent que l'extension est accommodée de façon distribuée en surface en Afar Central, en association avec d'importants volumes de sous-plaquages qui ré-épaississent la croûte pendant le rifting. Ceci est compatible avec l'existence de grands détachements crustaux. Nous montrons que des phases tectoniques ponctuelles alternent avec des périodes de magmatisme plus prolongées. La production de grands volumes de *flood basalts* se produit après l'amincissement crustal et lithosphérique tardif, ce qui suggère que la formation des SDR est contrôlée par des épisodes tectoniques antérieurs. Nous montrons qu'il existe une différence entre l'Afar Central, marge longue, asymétrique et fortement sous-plaqué, avec les marges volcaniques de la Mer Rouge et du Golfe d'Aden plus courtes et symétriques où l'amincissement et la mise en place des prismes de SDR sont synchrones. Nous suggérons que cette différence est due en premier lieu à l'absence ou la présence de

manteau lithosphérique sous ces deux types de marges et en second lieu à la segmentation précoce héritée de l'initiation du rifting qui renforce cet effet en distribuant inégalement le magma sous-plaqué et erupté. Enfin, nous proposons que le break-up aux marges volcaniques se traduit par l'amincissement extrême de la croûte continentale initiale, qui est progressivement remplacé par du sous-plaquage mafique et des laves subaériennes pour finir par former la première croûte océanique.

Abstract

Volcanic passive margins, that represent more than the three quarters of continental margins worldwide, are privileged witnesses of the lithospheric extension processes that form new oceanic basins. They are characterized by voluminous amounts of underplated, intruded and extruded magmas, under the form of massive lavas prisms (seaward-dipping reflectors, or SDR) during the course of thinning and stretching of the lithosphere, that eventually form the ocean-continent transition. The origin and mechanisms of formation of these objects, which are directly linked to rifting and melting interactions, are still largely debated today. This is partly due to the fact that mature margins are hardly accessible, buried beneath some kilometers of post-rift sediments underwater. Furthermore, SDR often act as an observation mask, rendering geophysics observations a challenging exercise.

This thesis proposes to explore the structural and temporal relationships that exist between the development of the major thinning and stretching structures and the magmatic production associated to them. To do so, we will focus our work of the Afar triple junction, Ethiopia, a nascent volcanic passive margin that present the advantage of being accessible and offers a unique and complete record of both the syn-rift lava pile and tectonic structures. The rationale of this work is threefold. First, we present fieldwork analysis with lavas geochronology to determine the timing and style of the rift formation, since the early syn-rift period to present days. Second, we determine how the melting regime evolved in response to the deformation of the crust, through a geochemical study of the pre- to syn-rift lavas. Third and last, we present a synthetic model a the scale of the Nubia and Arabia plates, that describes the evolution of the volcanic margins associated with the triple junction, in relationship with their segmentation.

The mains results of this thesis suggest that extension is primarily accommodated over a wide area at the surface, in association with important volumes of underplated mafic material that compensate crustal thinning. This is done by major crustal-scale detachments that help localize the thinning and underplating at depth. In line with this 'magmatic wide-rift' mode of extension, we demonstrate that episodic extension steps alternate with more protracted magmatic phases. The production of syn-rift massive flood basalts occur after thinning of both the crust and the lithosphere, which suggests that SDR formation, is controlled by previous tectonic event. There exist a difference between Central Afar that is a wide, heavily underplated, extensively thinned and asymmetric margin and volcanic margins offshore Yemen, which is shorter, with syn-tectonic classically pictured SDR wedges. We propose that this difference is provoked in a first place by the absence of presence of a competent lithospheric mantle beneath those two types of volcanic margins and their associated melting regimes; and to a further extent by the early syn-rift

segmentation that enhances the aforementioned morphological features by distributing the magma unequally. Finally, we suggest that the break-up at volcanic margins occurs after the crust is efficiently thinned and replaced by underplating and SDR to form the first oceanic crust.

Table des matières

Chapitre 1 : Introduction générale 1
1. L'extension lithosphérique 2
1.1. Le rifting 2
1.2. Les causes du rifting, les forces extensives et l'effet du magma 3
1.2.1. Rifts actifs vs. passifs 3
1.2.2. Rifting assisté par injection de magma 4
1.2.3. Le break-up 5
2. Les marges passives volcaniques (MPV) 5
2.1. Les types de marges 5
2.2. Structure des marges volcaniques 8
2.2.1. Architecture sismique 8
2.2.2. Structure d'une marge volcanique 8
2.3. Origine des marges volcaniques 14
2.3.1. Large Igneous Province 15
2.3.2. Panaches mantelliques 15
2.3.3. Un rôle actif du manteau dans l'initiation de l'extension et des *flood basalts* ? 16
2.3.4. ... où un rôle passif ? 17
2.4. Modèles génétiques des marges volcaniques 19
2.4.1. Rôle du manteau 20
2.4.2. Rôle de grands détachements crustaux 21
2.4.3. Rôle de la segmentation 25

Chapitre 2 : Problématique, objet d'étude et démarche 29
1. Questionnement scientifique et problématique 29
2. La dépression des Afars 32
2.1. Physiographie et structures 32
2.1.1. Les zones marginales de la dépression Afar 33
2.1.2. La partie centrale de la dépression Afar 34
2.2. Formations géologiques 35
2.2.1. Pré-rift 35
2.2.2. Syn-rift précoce (Miocène) 36
2.2.3. Syn-rift tardif (Plio-Pléistocène) : série Stratoïde 36
2.2.4. Volcanisme actuel : segments actifs 37
2.3. Nature de la lithosphère 38
2.3.1. L'état du manteau 38
2.3.2. Structure de la croûte 40

2.4. Style structural des segments de rift et développement de la TOC 43
2.4.1. Des styles structuraux contrastés 44
2.4.2. Le développement d'une TOC 46
3. Démarche de la thèse 48

Chapitre 3 : Évolution tectono-magmatique de l'Afar central 51
Article accepté à *Tectonics*: Modes of rifting in magma-rich settings : tectono-magmatic evolution of Central Afar.
Abstract 52
1. Introduction 53
2. Geological setting 57
2.1. Present-day extension and strain accommodation 57
2.2. Mantle beneath Ethiopia 60
2.3. Nature of the crust, magma intrusions and underplating 60
2.4. Crustal thinning 61
2.5. Stratigraphy and volcano-tectonic history 62
2.6. Synthesis and main objective 63
3. Methods 64
3.1. Geochronology 64
3.1.1. K-Ar 64
3.1.2. (U-Th-Sm)/He 66
3.2. Balancing cross-sections: polyphase faulting and tilted blocks 67
4. Results 70
4.1. Volcano-stratigraphy of Central Afar 70
4.1.1. Oligocene flood basalts 70
4.1.2. Miocene basalts and rhyolites 71
4.1.3. Pliocene flood basalts 71
4.2. Structural features of Central Afar 73
4.2.1. Arabati (flexure area) 73
4.2.2. Sullu Adu (area of highly tilted blocks) 78
4.3. Composite balanced cross-section 81
4.3.1. Amount of extension at the surface 81
4.3.2. Total thinning factor and excess lower crust 83
4.3.3. Structural style, mid-crustal shear zone, and underplating 84
5. Discussion 86
5.1. Timing of deformation 86
5.2. Extension discrepancy and extra lower crust 90
5.3. Magma-compensated crustal thinning during rifting 92
5.4. Mid-crustal shear zone model 95
5.5. A 'magmatic wide-rift' during the Mio-Pliocene 97
5.6. Segmentation and Seaward Dipping Reflector (SDR) formation 98

5.7. Comparison with Volcanic Passive Margins 99
6. Conclusions 102
Acknowledgements 103

Chapitre 4 : Évolution des régimes de fusion mantellique en réponse à l'extension 105
Article en préparation pour *Geochemistry, Geophysics and Geosystems* : Mantle melting regime and lithospheric thinning constrained by basalts geochemistry at the Central Afar nascent volcanic passive margin.
Abstract 110
1. Introduction 111
2. Context 113
2.1. Geological settings 113
2.2. Magmatic series 114
3. Rationale, dataset and methods 115
3.1. Rationale 115
3.2. Dataset and methods 116
4. Fractional crystallization 117
4.1. Major elements 117
4.2. Trace elements 119
4.3. Liquid lines of descent (LLD) calculation 121
4.4. Correction of low-pressure fractional crystallization 122
5. Fe-Na-Ti systematics of initial magmas 123
6. REE systematics of initial magmas 126
7. Thermobarometry of initial magmas 128
8. Discussion 130
8.1. Significance of the P-T results 130
8.2. P-T conditions of the mantle 132
8.3. Mantle cooling vs. lithospheric thinning 134
8.4. Evolution of the melting regime 136
9. Conclusions 141
Appendix 142
A. LLD determination for major elements 142
B. LLD determination for trace elements 145
C. Non-modal batch melting of lherzolite peridotite 147

Chapitre 5 : Influence de la segmentation syn-rift sur la distribution du magmatisme et du style structural 151
Article en préparation pour *Terra Nova* : Early syn-rift segmentation control on the Cenozoic tectono-magmatic evolution of the Afar-Red Sea-Gulf of Aden system.
Abstract 152

1. Introduction 152
2. The diachronous evolution of the Afro-Arabia rift system 155
3. Seismic cross-sections 156
3.1. Southern Red Sea (Eritrean – Yemeni conjugate margins) 156
3.2. The Gulf of Aden volcanic margin offshore Yemen and the SESFZ ...159
4. Tectono-volcanic evolutionary model of the Afro-Arabia rifts system 160
5. An asymmetric rift system 164
6. Conclusions 165
Acknowledgements 165

Chapitre 6 : Discussion générale 167
1. Synthèse des résultats principaux 167
2. Accommodation de la déformation et signification du sous-plaquage 171
3. Amincissement crustal et break-up 173
4. Construction des SDR 175

Chapitre 7 : Conclusions et perspectives 179
1. Conclusions 179
2. Perspectives 179

Bibliographie 183

Annexe 213
Article en révision à *Geostandards and Geoanalytical Research* (manuscript n° GGR-0375-R1): An alternative protocol for single zircon dissolution with application to (U-Th-Sm)/He thermochronometry.

CHAPITRE 1
-
INTRODUCTION GÉNÉRALE

Les marges continentales passives, à la transition entre masses continentales émergées et océans profonds, sont les archives – géologiquement – éphémères des mouvements tectoniques qui façonnent la surface de la Terre. La dénomination même de « marge » est bien choisie, car si elles constituent bel et bien l'espace en bordure qui sépare les domaines continentaux vieux de milliard d'années des domaines océaniques constamment recyclés dans le manteau terrestre et renouvelés au cours des cycles de Wilson, le questionnement scientifique qui entoure leur genèse s'inscrit lui aussi à la limite de champs interdisciplinaires. En effet, poser la question de comment fabriquer une marge passive, question qui revient à demander comment « ouvrir » un océan et qui constitue la base de la tectonique des plaques, requiert d'interroger les interactions fines et complexes qui existent entre la lithosphère et les forces extensives auxquelles elle est soumise, et l'activité mantellique qui lui est ou non associée.

La grande majorité des marges passives sur Terre sont dites « volcaniques », car elles présentent, à la transition entre domaines continental et océanique, de grands volumes de magmas, ou « trapps ». Bien qu'elles surpassent en nombre leurs équivalents « non-volcaniques », les marges volcaniques sont moins bien documentées et les processus qui mènent à leur formation moins bien compris, tant les difficultés techniques et conceptuelles qu'induisent la surabondance de magmatisme sont grandes, pour des raisons que nous détaillerons par la suite.

Plus particulièrement, le questionnement porte ici sur les interactions croûte-manteau et tectono-magmatiques lors de la genèse des marges volcaniques. La nature des structures qui accommodent l'extension et le magmatisme depuis l'initiation de l'ouverture continentale jusqu'à la rupture lithosphérique est fortement débattue. En d'autres termes, l'histoire des interactions tectono-magmatiques pré-océaniques des marges volcaniques, pourtant fondamentale dans la compréhension de la tectonique des plaques à l'échelle du globe, est mal connue. Cette thèse se propose d'explorer et d'expliquer ces interactions en prenant l'exemple d'un lieu où l'on assiste à la naissance d'une marge volcanique, le point triple des Afars en Afrique de l'Est.

1. L'extension lithosphérique

La lithosphère est définie comme l'enveloppe contenant la croûte terrestre et la partie la plus superficielle du manteau, le manteau lithosphérique. Elle est morcelée en douze plaques principales et un certain nombre de micro-plaques. Ces entités sont plus rigides et moins denses que le manteau asthénosphérique sur lequel elles évoluent et interagissent entre elles lors de leur mouvement, définissant ainsi des zones "frontalières" de différents types : 1) les *zones de convergence,* où la rencontre de deux plaques provoque notamment la subduction de l'une sous l'autre ; 2) les *zones transformantes* où deux plaques se déplacent latéralement l'une par rapport à l'autre et 3) *les zones de divergence*, qui sont les lieux d'extension et de création de lithosphère nouvelle. Les forces convergentes permettent la création de fosses océaniques ou d'orogènes. Les forces extensives, à l'inverse, déforment la lithosphère et l'amincissent parfois jusqu'à la rupture totale. Ce processus, appelé rifting, est responsable de la fragmentation des continents et parfois précurseur de la formation des rides océaniques.

1.1. Le rifting

Le rifting est le processus qui en un lieu donné étire et amincit la lithosphère. Ses modalités sont fonctions de paramètres cinématiques : vitesse d'extension, processus continu ou discontinu ; et mécaniques : structure rhéologique, thermique et héritage structural au moment du rifting.

Conceptuellement, il existe plusieurs types de modèles cinématiques simples mettant en lumière différents aspects du processus de rifting (Fig. 1). De nombreux travaux (*McKenzie,* 1978, *Lister,* 1989, *Buck,* 1991 et *Brun,* 1999) décrivent l'accommodation de l'extension par la création de failles dans la partie cassante de la lithosphère ou du jeu de détachements crustaux, tandis que la partie ductile de la lithosphère se déforme par fluage. Selon les propriétés rhéologiques (c'est à dire thermiques et mécaniques) de la lithosphère, l'extension est tantôt localisée sur une zone étroite (Mer Rouge, Golf de Suez, rift Est-Africain, rift Baïkal) ou bien très large (Basin and Range, USA). Certains rifts fonctionnent grâce au jeu de failles de détachements crustaux (*Lister,* 1989).

Il est important de noter qu'il existe des rifts continentaux "avortés" ou "paléo-rifts" et des rifts continentaux "actifs" (*Ruppel,* 1995). Les rifts actifs présentent des caractéristiques témoignant d'une activité tectonique ou magmatique. Il est donc intéressant de se demander pourquoi des rifts peuvent s'inactiver.

Dans tous les cas, lorsque le processus de rifting est complet et qu'on atteint la rupture continentale, on crée de part et d'autre de la zone de rupture des marges conjuguées dont la morphologie (taille, architecture) est fonction du "style" de rifting qu'elles auront subi.

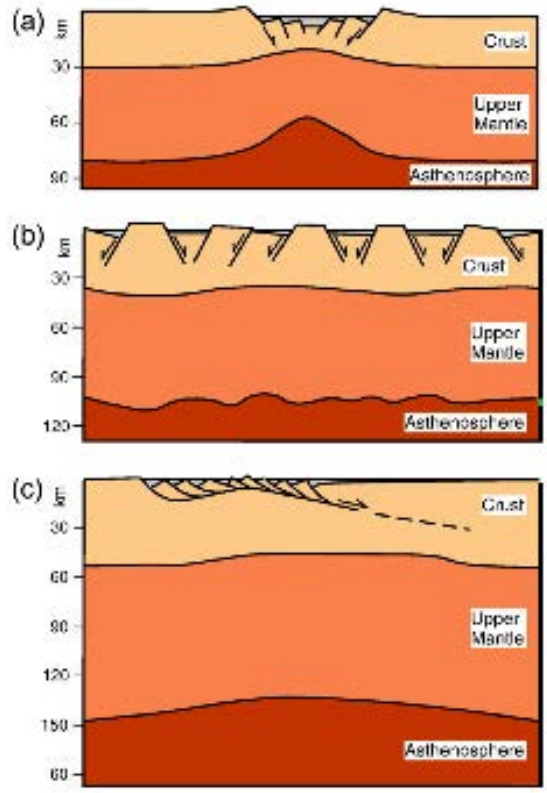

Figure 1. Trois modes conceptuels de rifting, d'après Rosenbaum, *2008. a) Narrow rift mode (*Buck, *1991 ;* Brun, *1999), le rift est symétrique et caractérisé par le jeu de failles normales cassantes dans la croûte supérieure et une remontée du manteau supérieur et de l'asthénosphère par isostasie. b) Wide rift mode (*Buck, *1991 ; 1999), développement d'une zone d'extension au-dessus d'une asthénosphère anormalement chaude, zone de rift très large. Dans ce mode, on n'atteint jamais la rupture lithosphérique. c) Core complex mode (*Lister, *1989), l'extension est accommodée par le jeu d'un détachement d'échelle crustale qui mène à l'exhumation de la croute inférieure.*

1.2. Les causes du rifting, les forces extensives et l'effet du magma

Les modèles invoqués plus haut (Fig. 1) expliquent le rifting dans le cas d'une divergence appliquée à la lithosphère où les forces horizontales suffisent à dépasser la résistance de la lithosphère. Ainsi, si le rifting s'initie facilement lorsque la lithosphère est déjà amincie ou fragile, les forces "disponibles" aux limites de plaques sont insuffisantes dans le cas où la lithosphère est anormalement épaisse (*Buck,* 2004). Ainsi, le magma pourrait faire office de "troisième force" pour compenser le déficit et permettre le rifting.

1.2.1. Rifts actifs vs. passifs

Sengör et Burke (1978) ont décrit les rifts passifs ou actifs (Fig. 2). La distinction entre les deux types de rifts porte à la fois sur les caractéristiques concernant leur initiation et leur évolution.

Les premiers sont induits puis dirigés par des contraintes tectoniques à très grande échelle générées aux limites de plaques. La lithosphère s'étire et s'amincie sous les forces exercées et l'asthénosphère remonte passivement par réponse isostatique pour combler l'espace vide laissé par le "manque" de lithosphère.

Les rifts actifs sont dominés par des mouvements dans l'asthénosphère (cellules de convection, points chauds) qui érodent thermiquement la lithosphère sus-jacente, soit par la remontée des isothermes vers la surface, soir par des mouvements de convection qui en délaminent la base. Le resserrement des isothermes vers la surface

provoque le bombement de la lithosphère, un maintien dynamique qui donne une subsidence nulle et crée des forces gravitaires.

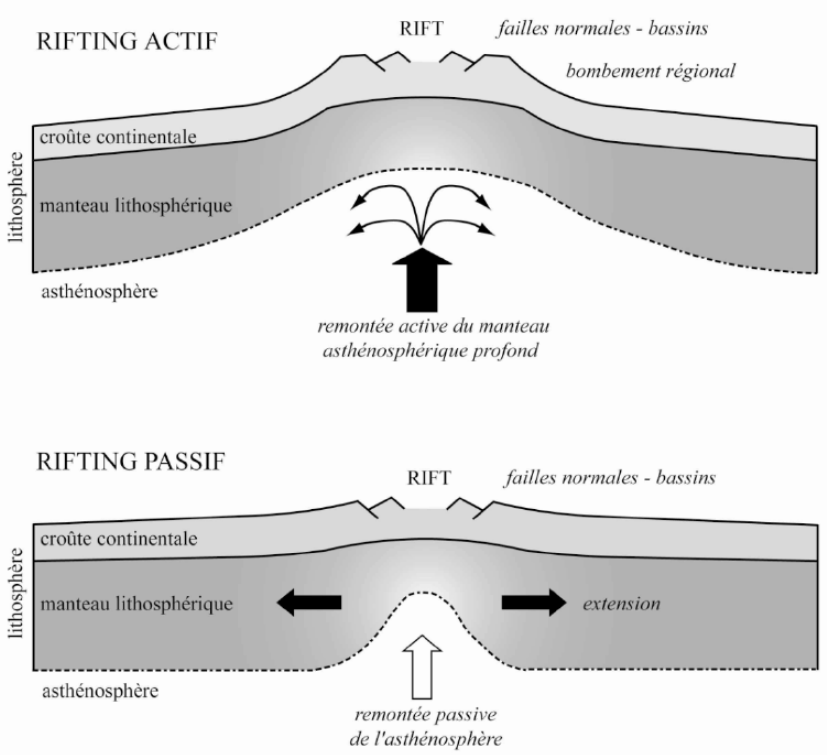

*Figure 2. Illustration des notions de rifting actif et passif (*Péron-Pinvidic*, 2006). Rift actif : anomalie de température dans le manteau asthénosphérique (induite par des mouvements convectifs ou des remontées types points chauds) qui bombe la lithosphère (doming) et provoque le rifting. Rifting passif : forces tectoniques aux limites de plaques qui provoquent le rifting aux zones faibles des plaques continentales.*

Bien que la dichotomie entre rifts passifs ou actifs soit encore débattue la notion de rifting actif introduit l'effet du magma comme moteur, ou tout du moins comme paramètre majeur influençant l'extension.

1.2.2. Rifting assisté par injection de magma

Il a été proposé qu'on pouvait initier le processus de rifting même avec de faibles forces disponibles aux limites de plaques si on est en présence de magma (Fig. 3) (*Buck,* 2004 ; 2006). La figure 3 montre que si du magma est disponible, alors l'extension peut s'effectuer sous de plus faibles contraintes par injection verticale de magma. Donc, lors du rifting dit "actif " on retrouve à la fois des failles normales et des dykes injectés qui accommodent l'extension. On note que ces deux types de déformation n'affectent pas la lithosphère de la même manière. Lors de la divergence aux limites, le jeu des failles normales crée une dépression dans la croûte supérieure et des épaules de rift de part et d'autre de la zone de déformation qui subside. Le

manteau remonte vers la surface par isostasie. Au cours d'un étirement purement magmatique, la lithosphère est étirée sans qu'aucun mouvement vertical n'ait lieu car la mise en place du dyke accommode l'essentiel de la divergence.

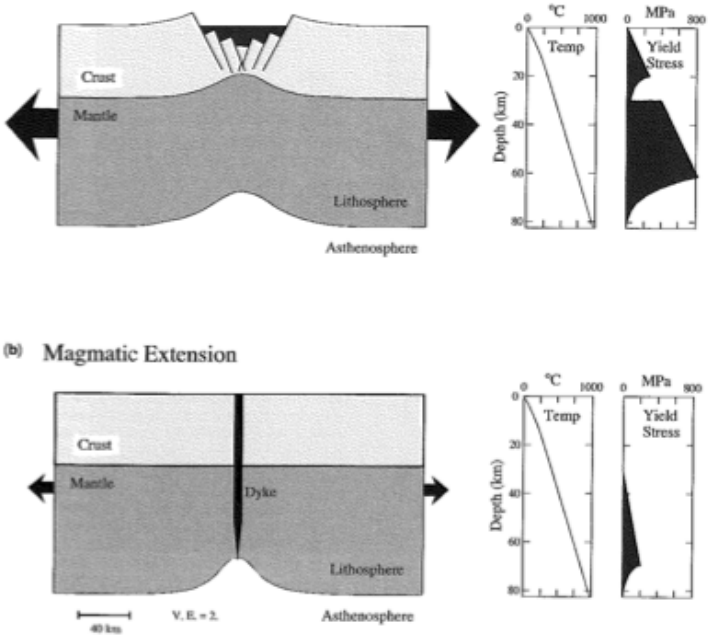

Figure 3. Deux manières d'étirer une lithosphère d'épaisseur normale. a) sans et b) avec magma. Noter la différence de résistance (surface grisée dans le diagramme P-profondeur) dans les deux cas. (Buck, *2006).*

1.2.3. Le break-up

Lorsque l'interaction des paramètres de rifting (i.e. vitesse de divergence, rhéologie de la lithosphère et de l'asthénosphère, héritage structural) est favorable, la lithosphère s'étire et s'amincie jusqu'à atteindre possiblement une épaisseur nulle : c'est le break-up. Deux plaques continentales se forment avec la formation d'une jeune dorsale qui fabriquera la lithosphère océanique en continu. On nomme *marges conjuguées* les deux extrémités de ces domaines continentaux ayant enregistré la déformation du rifting. C'est la région dans laquelle s'effectue la transition d'une croûte continentale à une croûte océanique.

2. Les marges passives volcaniques (MPV)

2.1 Les types de marges

On distingue deux types de marges : les marges passives et les marges actives, qualificatifs qui décrivent en réalité l'activité sismique qui leur est associée. En effet, une marge active est une limite de deux plaques en convergence où la croûte océanique entre en subduction sous la croûte continentale. Une marge passive représente plutôt une transition entre la croûte continentale et océanique.

Les marges passives se subdivisent à leur tour en deux types : les marges passives sédimentaires (MPS) et les marges passives volcaniques (MPV) (Fig. 4 et 5). La distinction entre marges volcaniques et non volcaniques n'est pas systématiquement évidente d'une marge à l'autre. Les architectures des marges varient entre les deux *extrêmes* et l'attribution des qualificatifs "volcanique" et "non volcanique" s'opère sur la base de la quantité de magma mise en place pendant le rifting *et/ou* le break-up, sous forme de larges prismes de laves extrudés en surface (SDR) et de sous-plaquage imagé en géophysique. Aussi, de manière générale, la quantité de magma générée augmente systématiquement lorsqu'on arrive au break-up et à l'accrétion de croûte océanique. C'est pour cela que le terme de "marge non volcanique" est d'un certain point de vue inapproprié (*Planke et al.,* 2013).

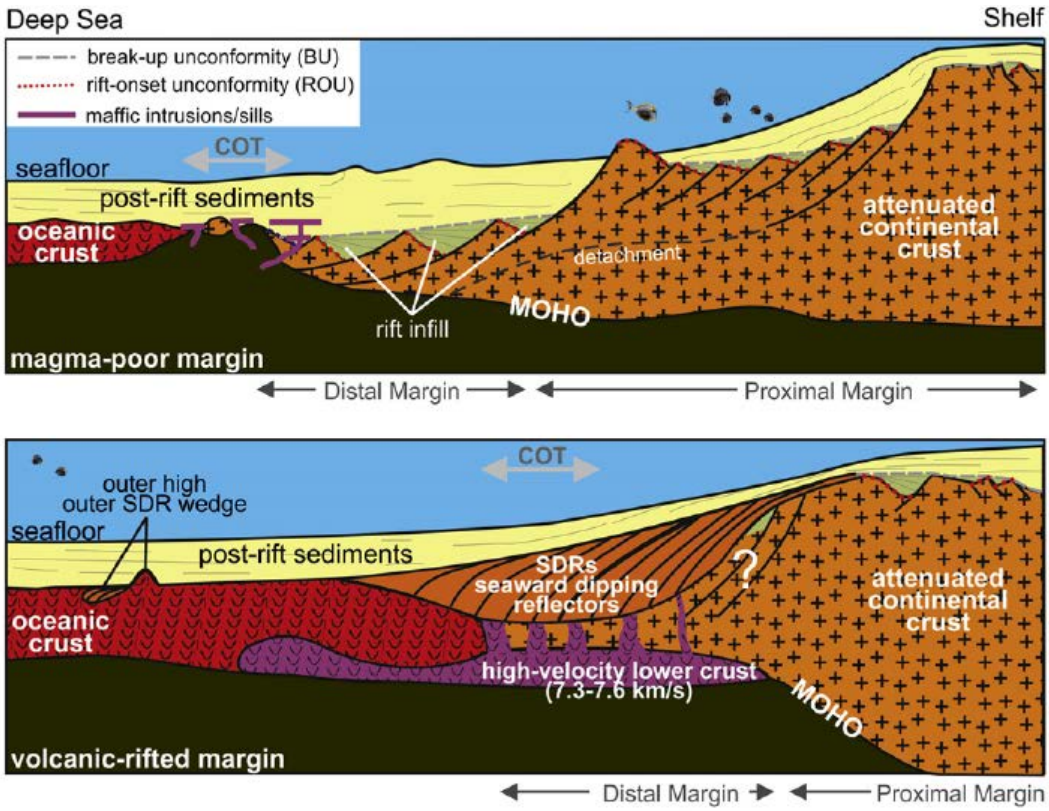

*Figure 4. Représentation stylisée d'une marge sédimentaire (panneau du haut) et d'une marge volcanique (panneau du bas) (*Franke et al., *2013). Les marges sédimentaires, ou non-volcaniques, sont caractérisées par des blocs basculés, une zone d'amincissement progressif jusqu'à l'épaisseur nulle, une zone d'exhumation du manteau et une croûte océanique d'épaisseur normale. Les marges volcaniques sont caractérisées par des produits magmatiques éruptifs (SDR, voir texte) et sous-plaqués, et une croûte océanique plus épaisse. Noter la vergence des failles normales dans les deux cas.*

Les exemples les plus connus de marges non volcaniques sont les marges Brésil-Angola (e.g. *Aslanian et al.,* 2009), la marge NW Australienne (*Karner and Driscoll,* 1998), les marges Ibérie-Terre Neuve (e.g. *Manatschal and Bernoulli,* 1999 ; *Péron-Pinvidic et Manatschal,* 2009 ; *Reston,* 2007), et les marges Aden-Est (e.g. d'Acremont et al., 2010 ; *Leroy et al.,* 2012). Les marges non-volcaniques sont caractérisées par l'absence de produits magmatiques extrusifs, par des blocs crustaux basculés par des failles normales à vergence vers l'océan et dont le jeu engendre une architecture sédimentaire syn-rift en prismes, par une croûte fortement amincie (*Péron-Pinvidic et Manatschal,* 2009), par une zone de transition qui consiste en l'exhumation de manteau serpentinisé à la surface généralement par le fonctionnement de grands détachements crustaux (*Péron-Pinvidic et Manatschal,* 2009) et enfin par une croûte océanique "normale" d'épaisseur de 6 à 8 km.

Ces marges sédimentaires, pauvres en matériel volcanique et magmatique constituent en fait plutôt l'exception que la règle, puisqu'il est maintenant établi que plus de 70% des marges passives actuelles ont un caractère volcanique (*Skogseid,* 2001 ; *Menzies et al.,* 2002 ; Fig. 5). Ce constat intervient relativement tard dans l'histoire de l'étude des marges continentales car il était plus aisé à l'heure du développement des méthodes de sismique réflexion-réfraction de produire des images à travers les sédiments et la croûte amincie qu'à travers le basalte. Ainsi, les principales VPM développées sont les marges de l'Atlantique Nord (*White et al.,* 1987 ; *Eldholm et Grue,* 1994 ; *Mjelde,* 2007, *Quirk et al.,* 2014 ; *Abdelmalak et al.,* 2015), du Groenland Ouest (*Karson et al.,* 1998 ; *Geoffroy et al.,* 1998, 2001), la marge Est Américaine (*Holbrook et Kelemen,* 1993), les marges de l'Atlantique Sud (*Hinz,* 1981, *Bauer et al.,* 2000 ; *Blaich et al.,* 2013 ; *Stica et al.,* 2014 ; *Clerc et al.,* 2015), Ouest indienne (*Sheth,* 1999 ; *Ajay et al.,* 2010), le Golfe d'Aden occidental (*Tard,* 1991 ; *Leroy,* 2012).

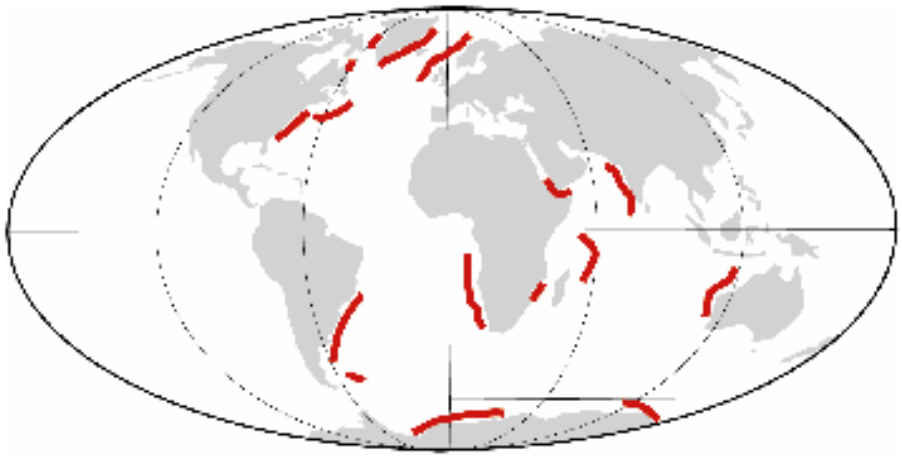

Figure 5. Carte localisant les marges volcaniques actuelles (Callot, 2002).

2.2. Structure des marges volcaniques

2.2.1. Architecture sismique

La figure 6 montre un profil de variation de vitesses sismiques des marges Nord Atlantiques. On y distingue trois couches : la première, épaisse d'environ 6 km montre un profil de vitesse qui augmente avec la profondeur. Elle correspond à des intercalations de laves, de cendres et de sédiments. C'est dans cette couche précisément que l'on trouve les larges prismes de laves caractéristiques des marges volcaniques, ou *seaward dipping reflectors* (SDR), que nous décrirons par la suite plus en détails. La vitesse des ondes sismiques dans cette croûte extrusive augmente de 3,5 à 6-6,5 km/s du sommet à la base du fait du changement de vergence dans les craquelures des joints de refroidissement des laves (en effet, plus on se dirige vers le bas de la pile de SDR, plus le pendage des laves augmente). La deuxième couche montre un gradient plus faible avec des vitesses de l'ordre de 6,5-7 km/s. La troisième couche, épaisse de 10 km, a une vitesse associée de 7 à 7,9 km/s. C'est la HVZ (High Velocity Zone, *Eldholm & Grue,* 1994 ; *White et al.,* 2008) : les vitesses y sont trop basses pour le manteau supérieur (> 8 km/s).

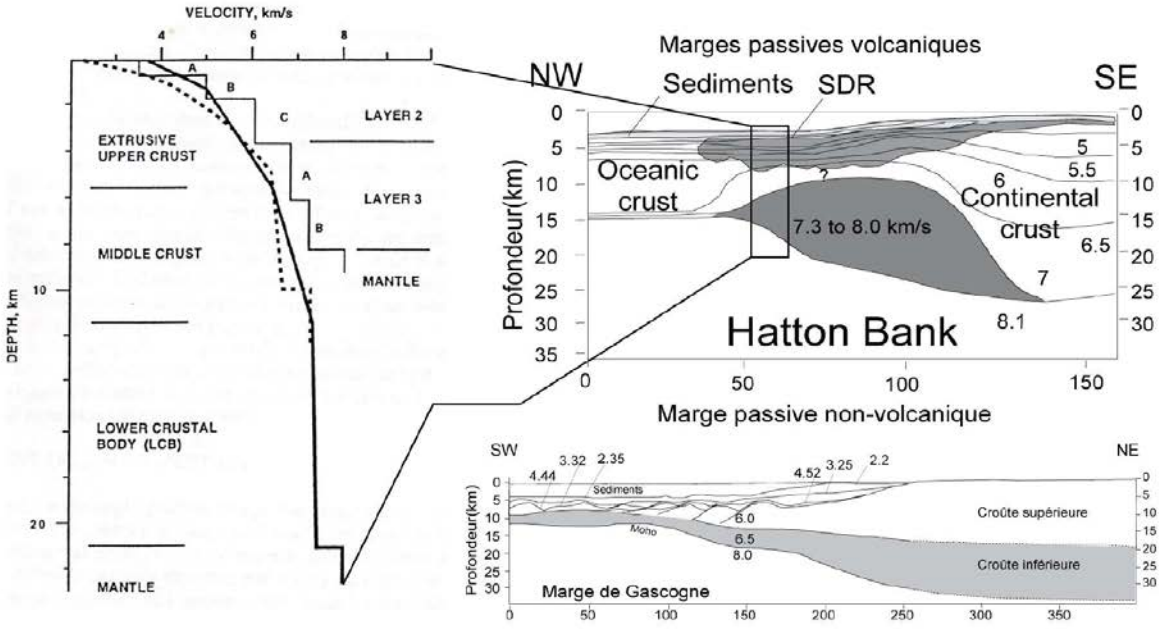

Figure 6. Comparaison d'une marge volcanique (Hatton Bank) et non-volcanique (marge de Gascogne en bas à droite. Profil de vitesses sismiques au niveau de Hatton bank à gauche (d'après Abdelmalak*, 2010).*

2.2.2. Structure d'une marge volcanique

Les marges volcaniques présentent des éléments structuraux originaux qui les différencient complètement de leurs homologues non-volcaniques. Les éléments structuraux caractéristiques de ces marges se trouvent localisés dans la mince zone de

la transition océan-continent, aussi serait-il plus juste de parler d'éléments structuraux de la transition océan-continent d'une marge volcanique. La figure 7 illustre schématiquement ces éléments.

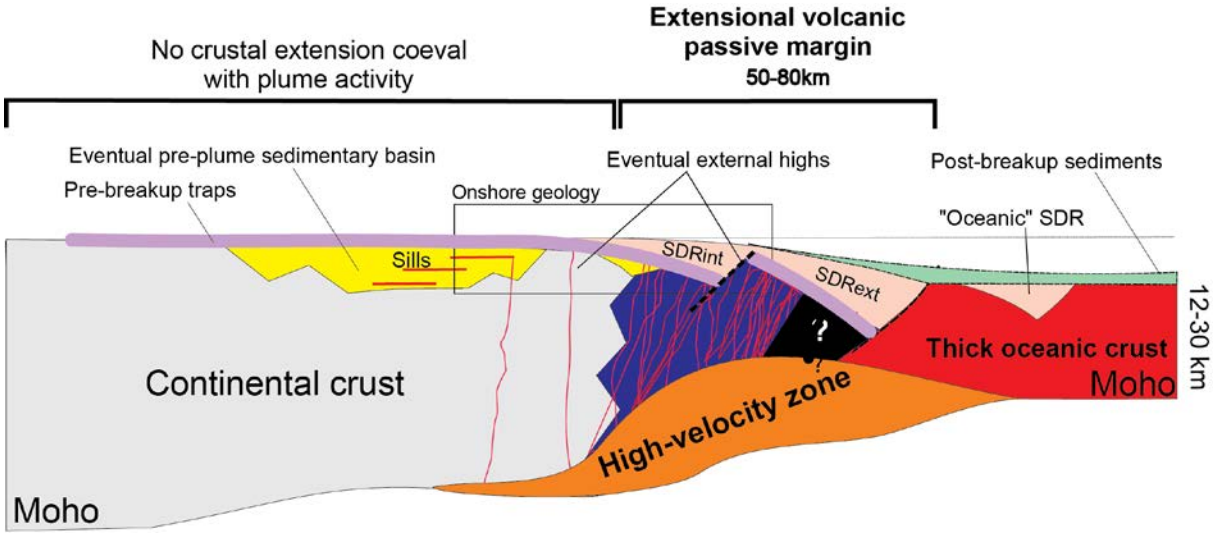

*Figure 7. Modèle conceptuel de marge volcanique (*Geoffroy, *2005). Cette coupe montre les différents éléments constitutifs d'une marge volcanique. La transition du domaine continental au domaine océanique se fait à la TOC (Transition océan-continent), et comprend trois niveaux de produits magmatiques associés : i) de larges prismes de laves (SDR) ii) des intrusions magmatiques dans la croûte continentale amincie (en violet) iii) un corps sous plaqué correspondant à une zone de vitesse élevée des ondes P.*

Les failles à vergence vers le continent et les blocs basculés

La déformation est accommodée, entre autres, par des failles normales à vergence majoritaire vers le continent, à l'opposé des marges non volcaniques. On observe des failles listriques sur les profils sismiques qui séparent les différentes rangées de prismes de SDR et qui pendent vers le domaine non étiré. A terre, notamment au Groenland, on observe des prismes de laves discordants séparés par des failles normales à vergence vers le continent également (*Geoffroy,* 2005), et des blocs basculés en domino (*Morton and Black*, 1975). Certains auteurs ont tenté de reproduire le développement de telles failles normales en laboratoire (*Lagabrielle et al.,* 2001 ; *Mulugeta et Ghebreab*, 2001 ; *Acocella,* 2010). L'expérience montre qu'on peut favoriser le développement de failles à pendage vers le continent, antithétiques de grandes failles bordières, si la lithosphère subit dès l'initiation du rifting un épisode brutal d'étirement et de subsidence. Si ces modèles permettent de reproduire à l'échelle crustale les géométries en blocs basculés observés aux marges volcaniques, notamment à terre (*Morton & Black,* 1975, *Wolfenden et al.,* 2005), ils souffrent de ne pas prendre en compte la topographie dynamique engendrée par un manteau anormalement chaud, d'ordinaire présent sous ces marges.

Les corps sous-plaqués

Les marges volcaniques possèdent typiquement une zone en profondeur où la vitesse des ondes sismiques est anormalement importante, fréquemment décrite comme étant du sous-plaquage. On l'appelle la High Velocity Zone (ou HVZ). Cette zone correspond à une section de ~15 km d'épaisseur dans la croûte (Fig. 6). La vitesse des ondes P dans la HVZ est de 7,0 – 7,7 km/s, soit le même intervalle que la croûte océanique inférieure gabbroïque (*White et al.,* 1987) sachant que la vitesse des ondes P dans croute inférieure n'excède rarement 7,0 km/s (voir à ce sujet *Hammond et al.,* 2011). Cette croûte inférieure à haute vitesse se trouve confinée dans une bande qui ne dépasse pas les 50 km de largeur (*White et al.,* 2008). Il n'y a pour le moment pas de définition précise de la HVZ : *White et McKenzie* (1989) prédisent que pour une croûte océanique d'épaisseur normale (7,1 ± 0,8 km, *White,* 1992) et de vitesse observée autour de 6,9 km/s, les vitesses caractéristiques de la HVZ de 6,9-7,2 km/s seraient le produit de fusion partielle avec le manteau. *Franke* (2013) suggère de définir la HVZ comme la croûte inférieure d'une marge volcanique dans laquelle les vitesses des ondes P se propagent entre 7,2 et 7,9 km/s. Il n'y a pas de consensus à ce jour concernant l'origine d'une telle croûte. Les hypothèses sont : des intrusions massives, du sous-plaquage mafique, du manteau partiellement serpentinisé ou des roches métamorphiques héritées de haut grade (*Gernigon et al.,* 2004 ; 2006).

La croûte de transition

La croûte continentale amincie sur laquelle se déposent les SDR et sous laquelle sont sous-plaqués les HVZ est dite "de transition" puisque ses caractéristiques sont intermédiaires entre celles d'une croûte continentale et océanique (ce qui est illustré par la synthèse de *Hammond et al.,* 2011). La vitesse des ondes sismiques y est de 6,5-7,2 km/s, soit plus élevée que dans la croûte continentale felsique (maximum 6,5 km/s, *Chapman et Furlong*, 1992). Cette croûte continentale est intrudée par des essaims de dykes centrés sur des réservoirs magmatiques dont la densité de population augmente à mesure que l'on se rapproche de la zone de break-up. Au Groenland, une telle croûte est à l'affleurement et on y documente la géométrie flexurée des intrusions : les dykes les plus anciens sont basculés au cours de l'extension et sont surimposés par des dykes de plus en plus jeunes et verticaux (*Lenoir et al.,* 2003).

Les Seaward Dipping Reflectors

Ces prismes de laves ont été décrits pour la première fois sur les lignes sismiques de l'Atlantique où l'on voit des réflecteurs à pendage vers l'océan (seaward dipping reflectors) en forme d'éventail présentant des discordances internes (*Hinz,* 1981 ; *Mutter et al.,* 1982) (Fig. 8). Leur épaisseur varie de 4 à 15 km selon les marges, et il peut y avoir un unique prisme ou une succession de deux à trois d'entre eux séparés par des hauts topographiques interprétés comme étant des morceaux de

croûte transitionnelle ou des volcans. Ils se mettent en place en général pendant ou juste après le break-up et la formation de la première croûte océanique. Les SDR se développent non seulement au niveau de la croûte transitionnelle mais aussi au dessus de la croûte continentale. *Planke et al.* (2000) distinguent ces deux types (respectivement SDR externes et SDR internes). Les SDR internes du domaine continental ont une géométrie fortement affectée par la géométrie du bassin préexistant. Leur mise en place est exclusivement subaérienne avec des intercalations sédiments-laves (*Franke et al.,* 2013). Les SDR externes se développent dans le domaine océanique en conditions subaquatiques et sont composés de pillow-lavas et de hyaloclastites.

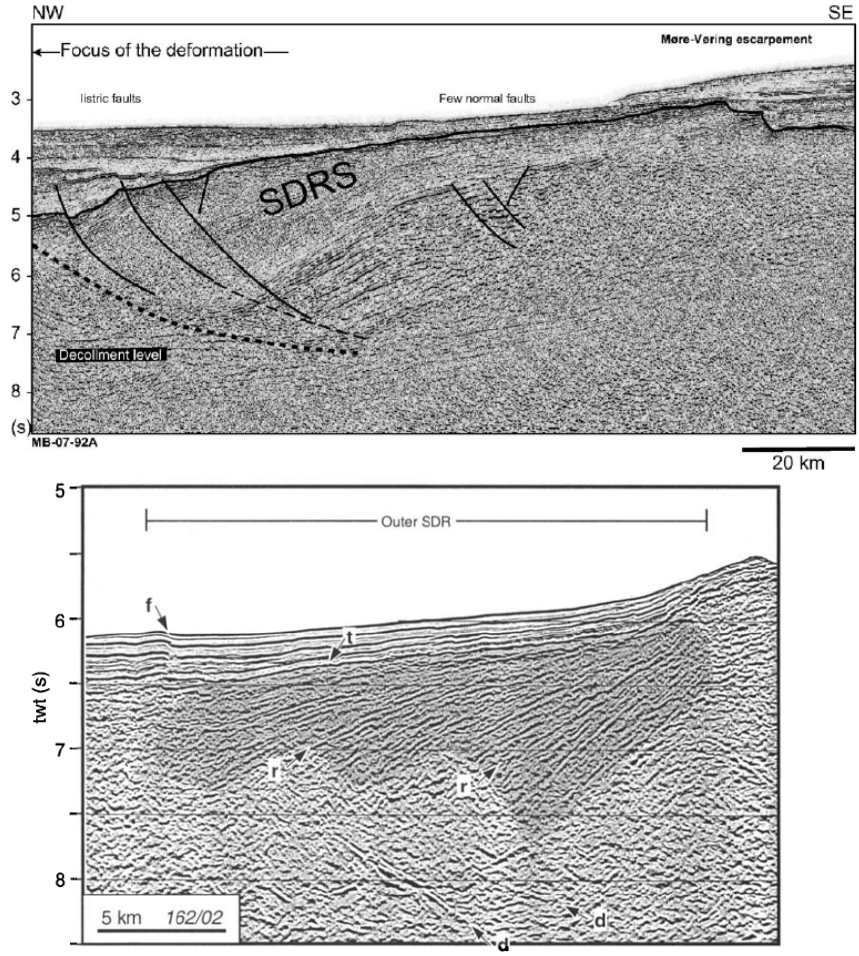

Figure 8. SDRs offshore imagés en sismique. Panneau du haut : Gernigon et al. *(2006), panneau du bas :* Planke et al. *(2000).*

Les modalités de formation de tels empilements volcano-sédimentaires sont sujettes à débat (Fig. 9). *Mutter et al.* (1982) propose un modèle d'accrétion dans lequel les laves sont d'abord éruptées en contexte subaérien par un dyke vertical. Le poids des laves induit une flexure progressive et le passage vers un environnement marin favorisent une mise en place en contexte subaquatique (Fig. 9). Ce modèle, purement gravitaire, ne tient pas compte de l'effet de l'allongement crustal. *Gibson et*

Gibbs (1987) proposent un modèle de formation par jeu de failles listriques à vergence vers le continent qui contrôlent la flexure progressive des laves vers l'océan, impliquant des détachements à l'échelle crustale (Fig. 9). Il a également été montré que les failles normales (à vergence vers le continent) de différentes dimensions sont synthétiques d'une faille bordière plus grande, qui accommode la flexure en roll-over du prisme et dont le jeu est syn-magmatique (*Geoffroy*, 2005). Ces failles basculent pendant la flexure et le remplissage magmatique, puis sont progressivement inactivées au fur et à mesure que migre le dépôt-centre des laves vers la zone de break-up.

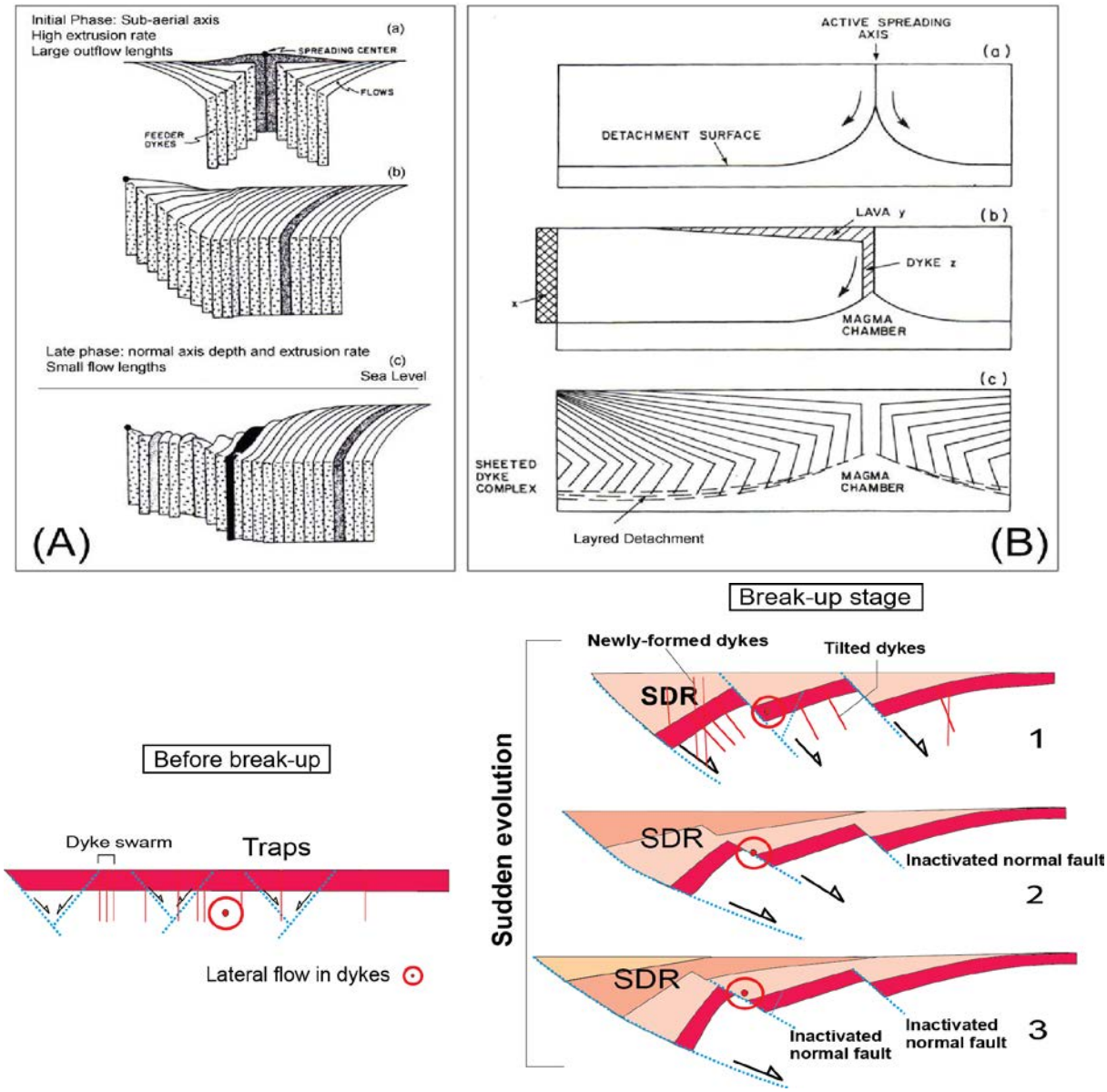

*Figure 9. Hypothèses de mécanisme de formation des SDR. A) Accrétion gravitaire (*Mutter et al., *1982). B) Détachements listriques* (Gibson & Gibbs, *1987). Panneau du bas : flexure en roll over anticlinal des prismes magmatiques, inactivation progressive des failles à mesure que la déformation migre vers l'océan* (Geoffroy, *2005).*

La flexure continentale

La flexure continentale est un élément structural caractéristique des marges volcaniques, fréquemment observé à terre. Il s'agit d'une flexure monoclinale en direction de l'océan des laves mises en place *avant* ou *pendant* la déformation (*Sheth et al.,* 1999 ; *Klausen,* 2008). C'est un terme ambigu dans le sens où cela peut désigner à la fois *le processus tectonique* de formation de la flexure (e.g. *Sheth et al.*, 1998, Fig. 10), où bien « *l'objet-flexure* », qui, aux marges volcaniques, représente un analogue à terre de SDR en cela qu'il est constitué de laves empilées en éventail et contrôlé par une faille listrique à vergence continentale (e.g. *Abdelmalak et al.,* 2015, Fig. 11). Au sens le plus large, la flexure continentale désigne toujours un objet à terre, directement observable.

Le *processus* de flexure est caractérisé par une augmentation progressive des pendages d'une couche volcanique donnée (les trapps pré-extension dans la figure 10) en direction de l'océan. Dans ce cas de figure, la flexure des trapps est post-magmatisme.

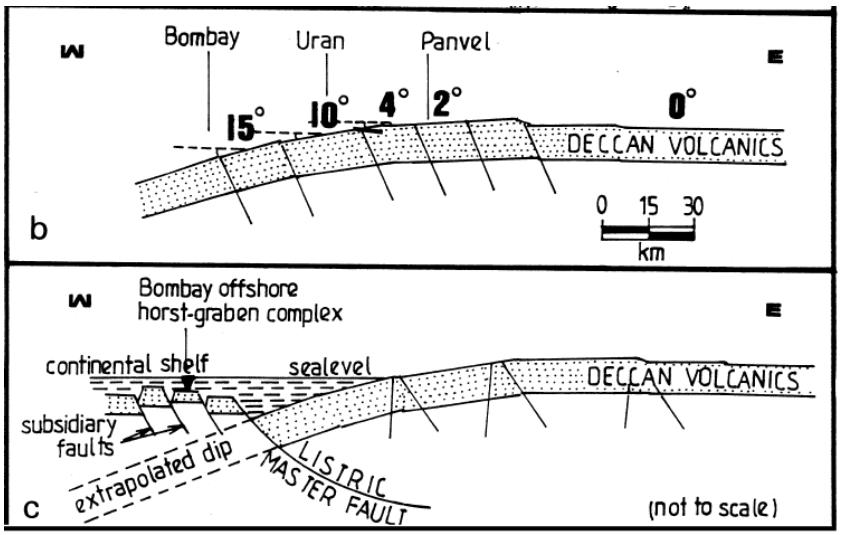

Figure 10. Flexure de panvel (Sheth, *1999). La flexure est ici post-magmatique.*

Lorsque les laves se mettent en place *pendant* la formation de la flexure continentale, il est alors possible de dater sa mise en place en datant directement les laves (e.g. *Lenoir et al.,* 2003 au Groenland). Le temps de formation est court (~2 Ma) et les épisodes éruptifs brutaux (*Klausen,* 2008). Une interprétation possible, exemplifiée par *Abdelmalak et al.* (2015), considère la flexure continentale comme l'analogue de ce qui se produit *en base* de SDR (Fig. 11). Les nombreux dykes qui coupent les sédiments/laves les plus basculés sont interprétés comme pouvant être compatibles en taille et en nombre avec ceux qui nourrissent les coulées importantes des SDR en mer.

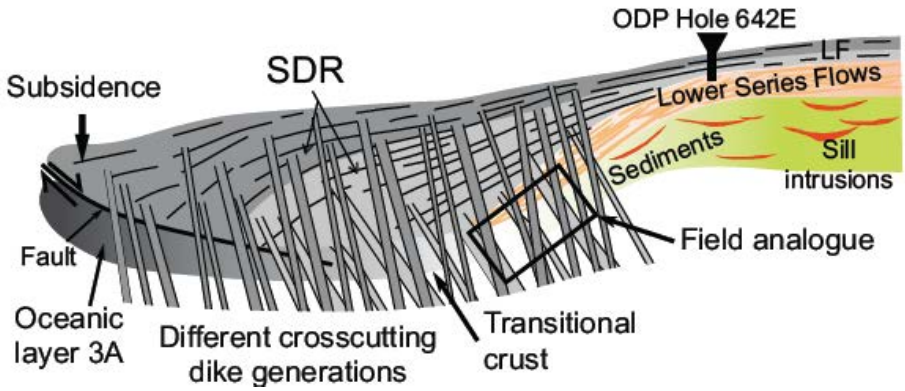

*Figure 11. Représentation schématique d'un SDR, avec plusieurs épisodes de dyking successifs (*Abdelmalak et al., *2015). Ici, les flexures continentales sont tenues pour être des fenêtres sur ce qui se passe en base de SDR.*

2.3. Origine des marges volcaniques

Il a été établi que les marges volcaniques sont en étroite relation avec les Large Igneous Provinces (ou LIP). Les LIP, ou "trapps", sont des épanchements de laves basaltiques et/ou siliceuses de plusieurs kilomètres d'épaisseur sur des superficies de plusieurs dizaines de milliers de kilomètres carrés. Ces immenses quantités de magmas associées à la nature volcanique des VPM constituent l'argument majeur en faveur de l'origine "active" (en terme de rifting actif décrit plus haut) de ces objets. La figure 12 montre la disposition des principales provinces volcaniques. La corrélation des structures des cartes des figures 5 et 12 corrobore au premier ordre cette observation. Cependant, il existe des arguments en faveur d'un développement des marges volcaniques indépendant de l'action des points chauds. L'objectif de cette partie est de présenter l'état des connaissances à ce sujet.

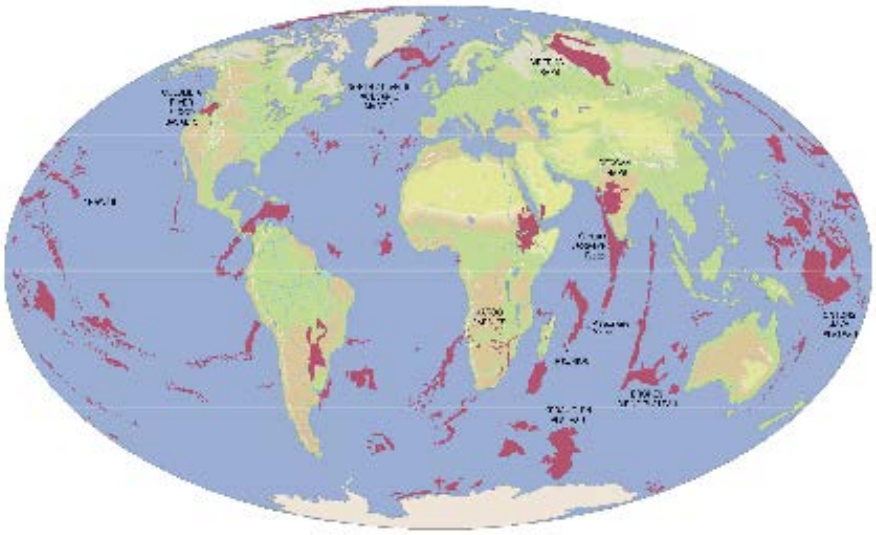

Figure 12. Localisation des LIP sur Terre, d'après Coffin & Eldholm *(1994). Il faut distinguer les provinces "onshore" et "offshore". Les provinces onshore, donc à terre,*

sont des "trapps", épanchements massifs de laves basiques à siliceuses, parfois bi-modales. Les trapps dans les provinces offshore sont souvent masquées par les sédiments ou l'érosion ancienne, ou recouvert par des produits volcaniques plus récents. Ainsi, ces LIP subaquatiques regroupent trapps et SDR sous une même dénomination.

Il ne faut pas confondre "point chaud", qui désigne un endroit géographique sur Terre qui est le lieu d'emplacement d'une "Large Igneous Province" ou "Trapps" et "Panache" qui désigne un modèle physique pour expliquer la mise en place des trapps et qui explique leur morphologie. Indépendamment des notions de point chaud et de panache intervient celle de convection mantellique qui désigne l'ensemble des théories décrivant notamment les sources dans le manteau des magmas des trapps.

2.3.1. Large Igneous Provinces

Le terme de Large Igneous Provinces a été proposé pour la première fois par *Coffin et Eldholm* (1994). Il désigne les extrusions massives de laves mafiques intraplaque, dont la mise en place est essentiellement fissurale, par des processus autres que le magmatisme lié à l'activité des rides océaniques. Les grandes provinces magmatiques sont caractérisées par des volumes de magma de l'ordre de 10^6 km^3, mises en place très rapidement (1~3 Ma, *Anderson,* 1994 ; *Sheth,* 1999). Elles se trouvent en domaine océanique et continental.

Du fait de l'activité tectonique, seules les LIP les plus récentes (mises en place depuis le Permien) sont facilement observables aujourd'hui (*Courtillot et al.,* 1999) bien qu'on puisse observer des reliques de provinces magmatiques plus anciennes (*Ernst et al,* 2008), notamment les grands essaims de dykes du craton canadien datées à 1.26 Ga.

2.3.2. Panaches mantelliques

Le modèle des panaches mantelliques est établi par *Morgan* (1972) à partir de l'observation d'alignements volcaniques intra-plaques. Le modèle suppose une remontée de matériel mantellique chaud stationnaire par rapport au mouvement des plaques lithosphériques. Selon Morgan, la tête du panache génère des trapps sur une surface qui dépend du degré d'interaction entre la tête et la lithosphère (*Hill,* 1992). Lorsque la tête se dissipe, la queue du panache produit des îles volcaniques alignées du fait du mouvement relatif de la lithosphère au-dessus de l'asthénosphère. Il existe plusieurs hypothèses concernant la forme et la profondeur d'origine de tels panaches. *Courtillot et al.* (2003) proposent une synthèse des différents types de panaches à partir des données de tomographie sismique et de géochimie provenant de 49 points chauds et provinces volcaniques sur le globe (Fig. 13). Les panaches qui prennent source à la transition D'' (la limite manteau-noyau) ont une durée de vie longue (panaches de type I). Ils sont associés à la formation des provinces de trapps. Les

panaches de type II prennent source au sommet des super-panaches et ne sont pas associés à une province volcanique. Les panaches de type III sont d'origine asthénosphérique et se développent en réponse à l'extension lithosphérique. *Montelli et al.* (2006) propose que la plupart des panaches s'enracinent dans le manteau profond mais qu'aucun d'entre eux de possèdent effectivement de tête.

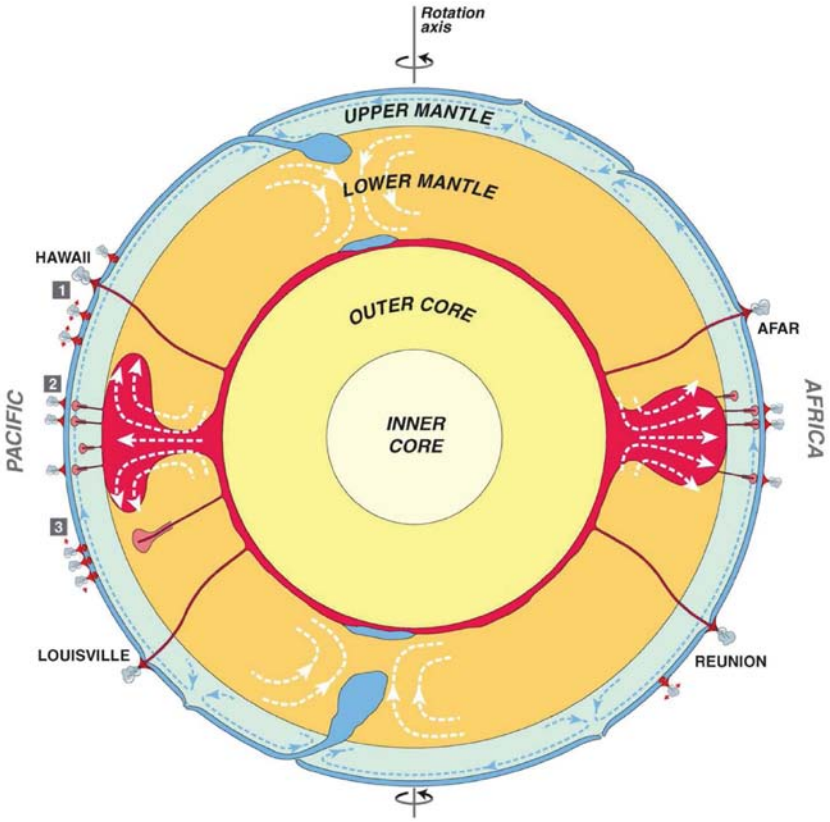

*Figure 13. Les différents types de panaches mantelliques (*Courtillot et al., *2003). Les types I (Hawaii, Louisville, Afar, Réunion) prennent leur source directement depuis la transition D''. Les types II sont associés aux super-plumes et les types III à l'extension lithosphérique.*

2.3.3. Un rôle actif du manteau dans l'initiation de l'extension et des *flood basalts* ?

Les marges volcaniques sont souvent associées aux LIP (*Coffin et Eldholm,* 1994), où le magmatisme se produit généralement dans des temps géologiques très courts de l'ordre de ~1-2 Ma (*Courtillot et al.,* 1999 ; *Ukstins et al.,* 2002 ; *Coulié et al.,* 2003). Bien que la plupart des LIPs offshore soient seulement identifiables indirectement, les SDR associées tendent en général à avoir le même ordre de grandeur en terme de volume de magma que les LIPs onshore (*Coffin and Eldholm,* 1994). Par exemple, *Gladczenko et al.* (1997) ont estimé les volumes éruptés au large de l'Argentine/Uruguay et de son conjugué en Afrique de l'Ouest à $0{,}6 \cdot 10^6$ km^3, soit l'ordre de grandeur des trapps de Paraná-Etendeka qui est de $1{,}5 \cdot 10^6$ km^3 (*Richard et al.,* 1989). La similitude des ordres de grandeurs des volumes de lave des SDR et

des LIP suggère que les conditions de formations des objets magmatiques des marges et des épanchements de trapps sont les mêmes, c'est à dire un manteau anormalement chaud (anomalie de 150-200°C) présent sous le rift. Il a été proposé que de telles anomalies, liées aux panaches mantelliques et aux points chauds, puissent causer le rifting (*Richards et al.,* 1989) ou que l'accumulation à la base de la lithosphère de ce matériel chaud provoque l'amincissement thermique et la décompression adiabatique nécessaires pour produire des quantités de magma beaucoup plus importantes qu'au dessus d'un manteau à température normale (*White et McKenzie,* 1989). Il a été proposé que le magmatisme en Atlantique Nord ait été causé par la remontée passive et la décompression du manteau asthénosphérique, bien que ce manteau puisse aussi être associé au point chaud d'Islande (*White,* 1989).

2.3.4. …Où un rôle passif ?

Théories des causes passives

Il existe plusieurs hypothèses alternatives qui s'opposent au lien génétique unissant marges volcaniques et panaches mantelliques. Celles-ci s'appuient sur deux sortes d'arguments. 1) D'un point de vue géologique l'étude des lignes sismiques montre un diachronisme entre magmatisme et initiation du rifting. 2) Des travaux montrent qu'on peut se passer d'anomalie de température initiale pour produire de larges quantités de magma. Des processus liés à l'extension et à la nature de la lithosphère pourraient suffire avec par exemple l'influence de la convection du manteau (*Van Wijk et al.,* 2001), sa richesse en éléments volatils (*Anderson,* 1992), ou encore un amincissement lithosphérique antérieur (*Armitage et al.,* 2010).

Une observation majeure : le diachronisme rifting / magmatisme

La mise en place de la séquence «trapps et SDR» des marges volcaniques se produit presque toujours après une (ou plusieurs) phase(s) d'extension amagmatique parfois longue de plusieurs dizaines de Ma (*Courtillot et al.,* 1999). Dans la région Nord Atlantique, l'extension est lente, discontinue et diachrone au Paléozoïque et au Mésozoïque. Au Paléocène, la mise en place des trapps est concomitante avec le *doming* de la lithosphère et le break-up survient à l'Eocène, synchrone de l'émission des larges prismes de laves qui forment les SDR (i.e. *Geoffroy et al.,* 2005). Cette composante volcanique, tardive dans l'histoire de ces marges, est associée à une anomalie thermique du manteau (*Bauer et al.,* 2000, *Geoffroy et al.,* 2001). En Atlantique Central, *Blaich et al.* (2011) décrivent des réflecteurs correspondant à des détachements crustaux inactivés pré-datant la mise en place d'un volume élevé de lave pendant le break-up. Aussi, l'initiation de plusieurs rifts montre un diachronisme avec l'emplacement de trapps/SDR : les deux évènements sont synchrones en Atlantique Sud, décalés de 15 Ma en Atlantique central, de 70 Ma dans l'océan

Indien et de presque 280 Ma pour les marges Norvège-Groenland (*Nikishin et al.,* 2002 ; *Ziegler et Cloething,* 2004).

Cela montre que la mise en place de *flood basalts* n'est pas nécessairement un prélude à l'extension continentale.

Des trapps sans panache mantellique ?

La mise en place de flood basalts n'est pas non plus nécessairement tributaire d'une anomalie mantellique de départ, mais peut-être largement contrôlée par des processus physiques et chimiques.

Les théories qui ont la faveur de la littérature sont celles qui invoquent une déstabilisation physique du manteau pendant l'extension, liée à des effets dynamiques. La lithosphère n'est pas une entité rhéologique totalement homogène limitée par une isotherme à 1300°C. Sa base est soumise à des mouvements de convection à petite échelle (*Jaupart et Mareschal,* 1999 ; *Morency et al.,* 2002). Cette dynamique mantellique suffit à expliquer les volumes de magma observés aux marges volcaniques (*Huismans et al.,* 2001). De plus, l'état de la lithosphère joue un rôle important. *Ballmer et al.* (2007) montrent par exemple que l'on peut produire jusqu'à 4 fois plus de magma pour une température du manteau donnée si l'on fait varier la rigidité (qui dépend de l'âge) de la lithosphère. *Anderson* (1994) montre que lors de l'extension d'une lithosphère hétérogène en épaisseur, la convection permet non seulement d'initier la mise en place des premiers magmas mais de prolonger le phénomène en réalimentant la zone de fusion partielle. Ce modèle explique en outre le fait que beaucoup de marges volcaniques se trouvent en bordure de craton. Ceci suggère que les anomalies thermiques du manteau associées aux grands volumes de magma des MPV sont *engendrées* par des processus de convection lithosphérique à petite échelle résultant d'une première phase prolongée d'extension passive. *Anderson et al.* (1994) propose qu'au cours du Crétacé, période qui a vu des épisodes majeurs de rifting continental et de réorganisation des plaques, l'extension conjuguée à un manteau refertilisé par la subduction d'ancienne lithosphère océanique aient localement permis la mise en place de grands volumes de trapps (*Anderson*, 1992).

Rifting assisté par le magma : pas besoin d'extension préexistante

Il existe toutefois des contre exemples à la précédente hypothèse. En Afar par exemple, on assiste au développement de marges volcaniques juste après la mise en place des trapps à l'Oligocène sur une lithosphère panafricaine cratonique. Comment peut-on *quand même* déformer une lithosphère épaisse très résistante et générer immédiatement une MPV alors que la cette première phase passive, *a priori* nécessaire, n'est pas enregistrée ? *Buck* (2006) démontre ainsi que l'on peut initier le rifting en mode actif en présence de magma qui serait disponible d'entrée de jeu, sans passer par une phase de déformation passive (voir Fig. 14).

Les forces tectoniques disponibles aux limites de plaques (slab pull) suffisent à initier le rifting passif avec une potentielle phase active tardive (i.e. Atlantique Nord/Sud, Australie), ou une déformation passive intégrale (i.e. Ibérie-Newfoundland) lorsque le manteau lithosphérique est déjà chaud (par exemple dans la province des *Basins and Ranges*) ou lorsque la croûte est surépaissie (dans le cas des orogènes). Par contre, le rifting ne peut s'initier qu'en présence de magma et donc en mode actif dès lors que la lithosphère a une épaisseur "normale" comme dans le cas du système Afro-Arabe.

Il existe de fait beaucoup d'arguments dans la littérature en faveur d'un découplage temporel entre la mise en place de hotspots et l'initiation de l'extension. De ce point de vue, le terme de « rifting actif » de Sengör et Burke qui semble aujourd'hui obsolète ne doit pas être confondu avec ce que nous appellerons par la suite un « rôle actif » ou « rôle passif » du manteau *au cours* de l'extension. Cela signifie que nous ne ferons pas de distinction *a priori* sur le manteau en tant que *cause* de l'extension, mais nous discuterons le rôle du manteau en tant qu'*agent* de l'extension, au sens où il exercera ou non un effet sur la morphologie des marges.

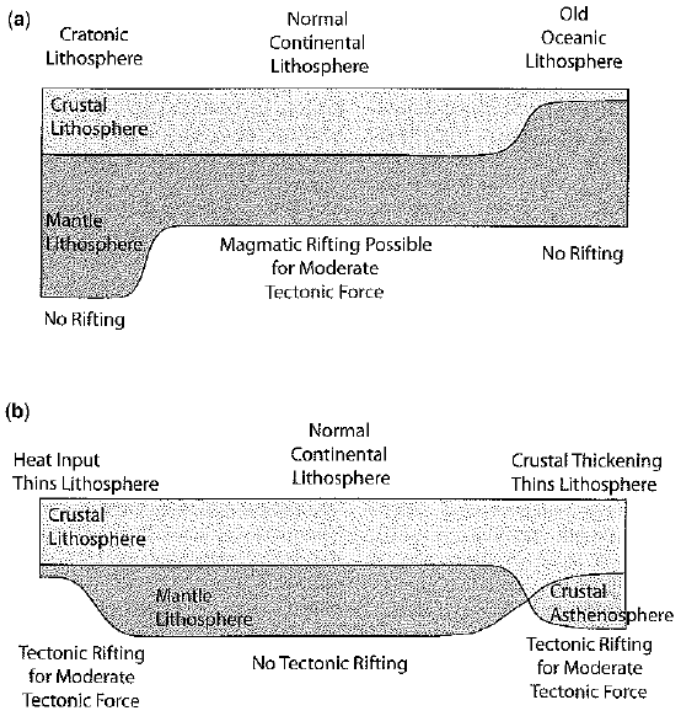

Figure 14. Schéma illustrant les conditions de rifting selon l'épaisseur de la lithosphère, Buck, 2006.

2.4. Modèles génétiques des marges volcaniques

Ce n'est qu'avec le développement de techniques très haute résolution que la sismique réflexion est à même de fournir des images de l'architecture des marges volcaniques à l'échelle crustale (i.e. *Clerc et al.,* 2015). Jusqu'à présent, il était impossible d'observer directement les structures qui amincissement la croûte (e.g.

Franke et al., 2000, Fig. 8). Ce type d'imagerie de grande qualité est toutefois loin d'être disponible pour l'ensemble des marges volcaniques ; il présente cependant l'intérêt de confronter par l'exemple les différents modèles de formation d'une marge volcanique, ce que nous faisons dans cette partie.

Le débat est actuellement centré autour (i) du rôle du manteau, (ii) du rôle des détachements et du couplage croûte cassante / croûte ductile, (iii) de la segmentation des marges.

2.4.1. Rôle du manteau

Théorie des soft-points

La théorie des soft-points (Fig. 15) (*Geoffroy,* 2005 ; *Gac et Geoffroy,* 2009) se propose d'expliquer le synchronisme magmatisme / extension et l'architecture 3D des flexures magmatiques, qui au vu de la répartition des dykes montrent que les zones de fusion partielle associées aux failles à vergence continentale sont très localisées dans la croûte (*Geoffroy et al.,* 2005). Ces zones très localisées sont appelées '*soft-points'* du fait de la faiblesse rhéologique du réseau de dykes / sills encore chaud dans une croûte encaissante froide et dure. *Callot et al.* (2001 ; 2002) ont modélisé l'effet de telles faiblesses rhéologiques localisées dans la croûte inférieure. Ils ont produit des marges conjuguées courtes où la zone de necking est très étroite, en accord avec les caractéristiques des marges volcaniques atlantiques (i.e. *White et McKenzie,* 1989 ; *Menzies et al.,* 2002 ; *Stica et al.,* 2014). De plus, ce modèle permet de reproduire la segmentation très prononcée, en « zig-zag », des marges volcaniques de l'Atlantique Nord (*Callot et al.,* 2002 ; *Gac et Geoffroy,* 2009 ; *Koopmann et al.,* 2014). Selon ce modèle, la segmentation des marges est héritée directement d'upwellings locaux de l'asthénosphère (*Gac et Geoffroy,* 2009).

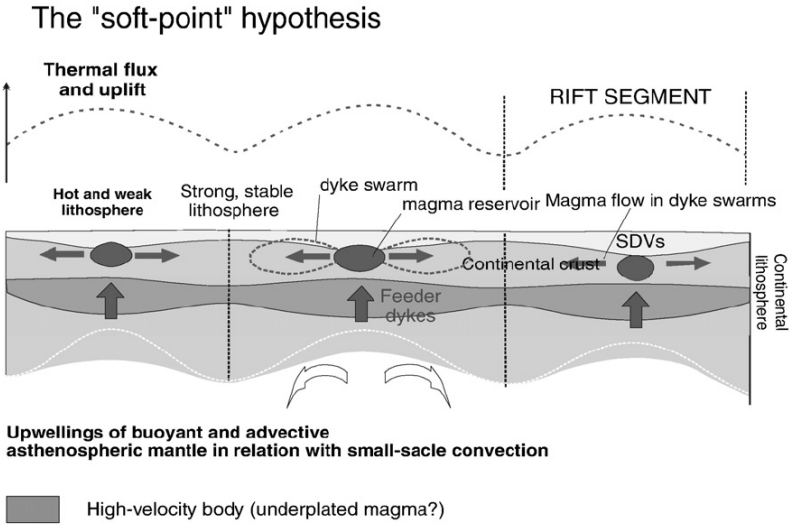

*Figure 15. Schéma conceptuel de l'extension au dessus de soft points (*Gac et Geoffroy, *2009). Un « soft point » est donc un point mou rhéologique dans le*

manteau lithosphérique, correspondant à une zone localisée de fusion partielle. Ils sont dus à des petits upwelling asthénosphériques causés par la convection du manteau, à l'aplomb desquels se concentre l'activité magmatique : abondance de sous-plaquage et éruption de SDR (ici nommés SDV pour seaward dipping volcanics*).*

De grand détachements contrôlés par le fluage du manteau

Pour expliquer la vergence vers le continent des failles normales qui accommodent la flexure et les SDR, *Geoffroy et al.* (2005) propose un rôle mécanique actif pour le manteau : l'upwelling de l'asthénosphère « tire » le manteau lithosphérique ductile en direction de la future zone de break-up, induisant un mouvement relatif opposé dans la croûte inférieure ductile (Fig. 16). Ceci implique l'existence de grands détachements qui accommodent l'amincissement de la marge (Fig. 16).

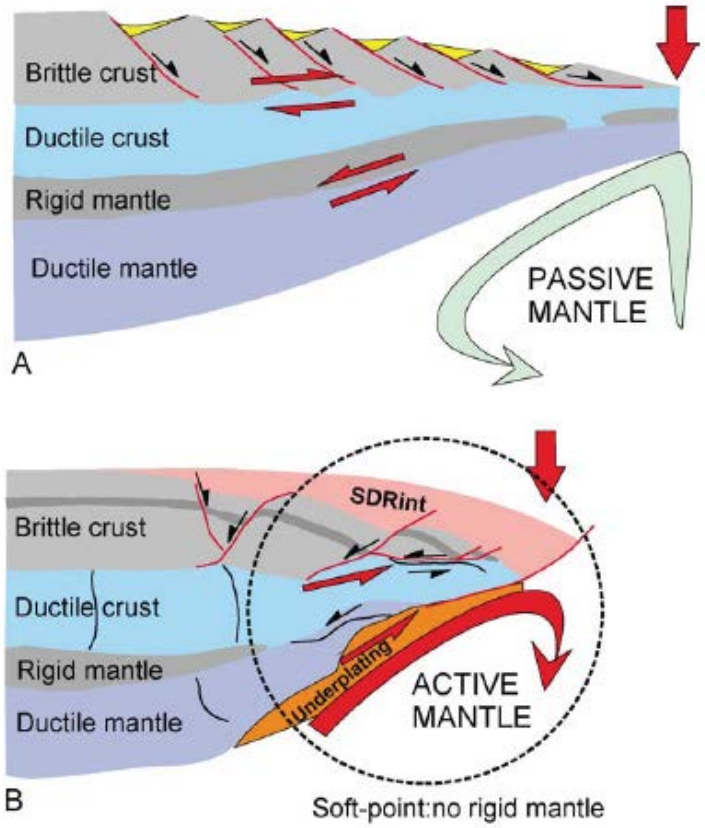

Figure 16. Représentation schématique du rôle du manteau actif par rapport à un manteau passif, qui provoque un sens de cisaillement favorable au développement de failles normales à vergence vers le continent (Geoffroy et al., *2005).*

2.4.2. Rôle de grands détachements crustaux

Le rôle de grands détachements dans l'accommodation de l'amincissement crustal, ou de grandes surfaces de décollement qui découplent la croûte cassante de la

croûte ductile ou la croûte du manteau, est suggéré par de récentes observations sismiques (Fig. 17).

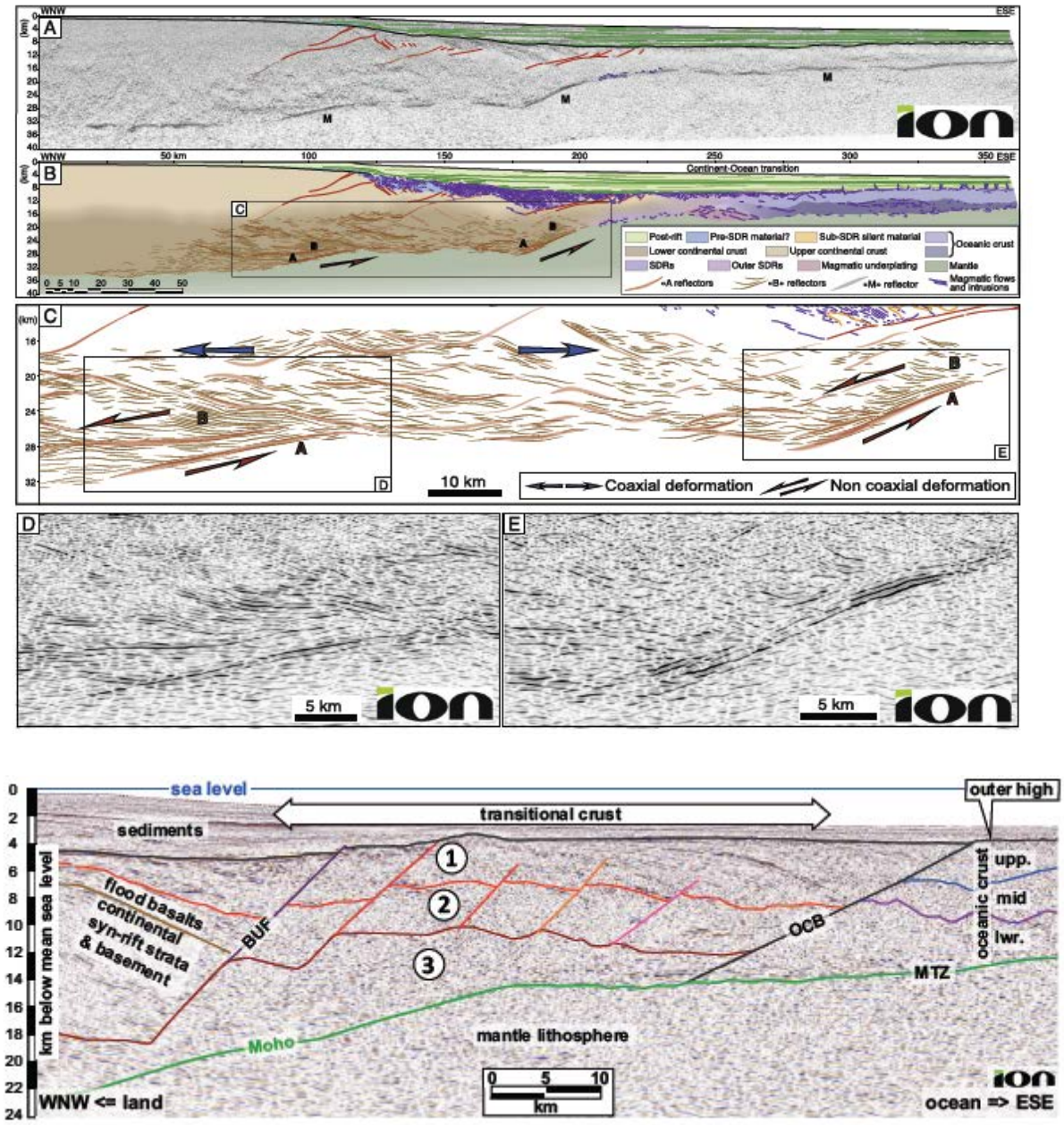

*Figure 17. Coupes sismiques interprétées à l'échelle crustale de marges volcaniques. En haut : marge volcanique Uruguayenne (*Clerc et al.*, 2015). Les auteurs mettent en évidence des zones de cisaillement dans la croûte inférieure dont le sens est compatible avec celui des failles normales qui contrôlent les SDR, en bleu. En bas : coupe sismique interprétée de la marge volcanique Est Groenlandaise (*Quirk et al.*, 2014). 1) SDR, 2) Croûte supérieure / moyenne cassante, 3) Croûte inférieure ductile. L'interface croûte cassante/ductile est interprétée comme une zone de décollement.*

La question est de savoir si les détachements sont enracinés à l'interface entre la croûte initiale et le sous-plaquage ductile (*Quirk et al.*, 2014 ; *Geoffroy et al.*,

2015), ou à des niveaux crustaux intermédiaires (*Blaich et al.,* 2011 ; *Clerc et al.,* 2015). Dans le premier cas, les détachements accommodent à la fois l'amincissement crustal et la mise en place de matériel sous-plaqué dans l'espace crée par cet amincissement, à la manière des *plutonic growth faults* documentées aux *core compexes* océaniques (*Dick et al.,* 2008 ; Fig. 18). La croûte initiale est petit à petit amincie au profit de la mise en place et de l'exhumation de matériel mafique ductile par des détachements (*Geoffroy et al.*, 2015). Les détachements ont leur *break-away* contre un bloc central continental (*Quirk et al.,* 2014 ; *Geoffroy et al.,* 2015, Fig. 18, 19) qui est progressivement démantelé par la nucléation de failles (Fig. 19), ou qui pourrait être « dilué » par des injection mafiques (Fig. 18). Le break-up surviendrait au moment où le bloc central serait complètement mafique (*Quirk et al.*, 2014). Alternativement, le manteau et la base de la croûte sont fortement couplés et la croûte inférieure *initiale* est exhumée avant la rupture du manteau (*Clerc et al.,* 2015, Fig. 17, voir aussi *Aslanian et al.,* 2009 pour un mécanisme similaire dans un segment moins volcanique de l'Atlantique Sud). Ces deux scénarios impliquent le développement de marges conjuguées symétriques, comportant chacune un détachement de vergence opposée.

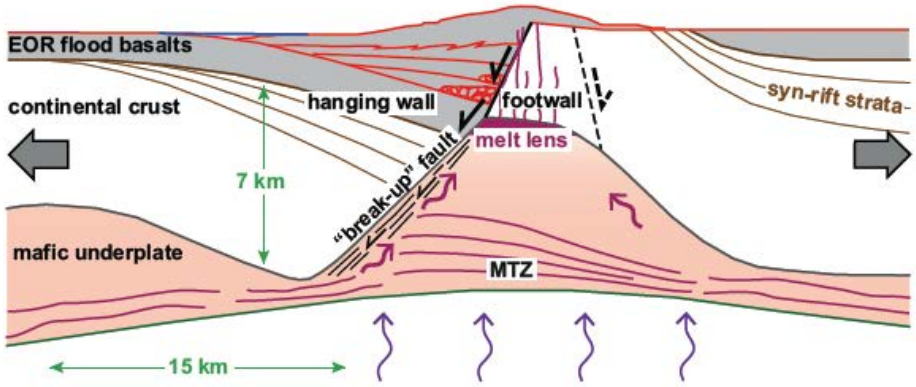

Figure 18. Schéma conceptuel de faille à croissance magmatique (Quirk et al., 2014). Le matériel mafique tend à remplacer la croûte inférieure initiale. Il est accrété dans l'espace d'accommodation crée par une faille inter-crustale qui contrôle la mise en place des SDR. Le footwall de la faille majeure, de plus en plus intrudé, constitue le lieu du futur break-up.

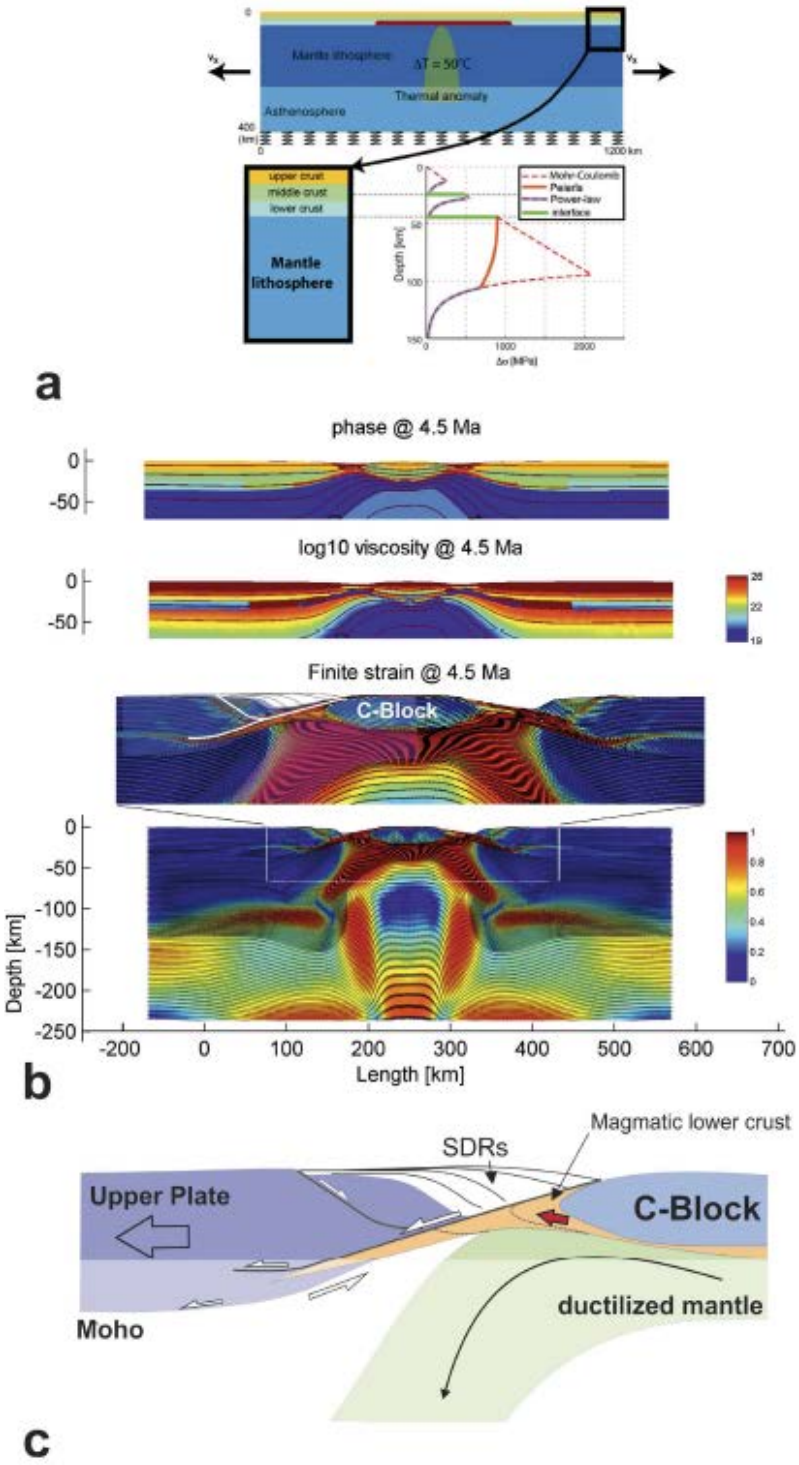

*Figure 19. Modèle numérique (a, b) et schématisation de l'évolution de deux marges volcaniques conjuguées au dessus d'un soft-point, en prenant en compte l'accrétion en surface et en profondeur de matériel magmatique, sous forme de SDR et de sous-plaquage (*Geoffroy et al., *2015). Ici, le soft point localise la déformation de manière précoce. Le strain hardening, causé par le matériel mafique progressivement sous-plaqué cause un flot mantellique divergeant vers les bords du model, ce qui a pour effet d'isoler un bloc central, et de créer un détachement en base de croûte à vergence bloc supérieure face au continent. Le sous-plaquage est accrétée à la manière de la figure 16, mais provoqué par le reflux du manteau.*

Dans le second cas, représentatif de l'Atlantique Nord, c'est un grand et unique détachement qui aminci la croûte et mène au break-up (*Blaich et al.,* 2013). Un tel mécanisme produirait deux marges conjuguées fortement asymétriques, avec la partie longue située dans le bloc supérieur du détachement (Fig. 20). Dans ce cas de figure, la marge volcanique ne serait caractérisée comme telle qu'à cause de des volumes de magmas syn-break-up, toutefois son architecture pré break-up suggère que le manteau n'a eu aucun rôle actif.

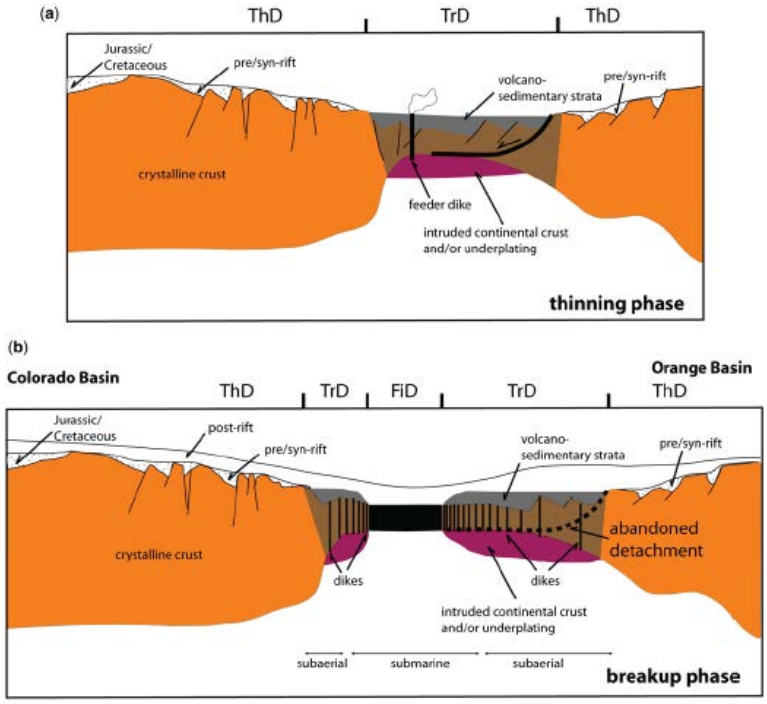

*Figure 20. Schéma conceptuel des marges Atlantiques Sud. Un grand détachement asymétrique couple le manteau et la croûte. Ce détachement est ensuite abandonné lors de la phase de break-up (*Blaich et al., *2013).*

2.4.3. Rôle de la segmentation

Nous avons évoqué le rôle de grandes structures crustales qui, avec un degré d'interaction plus ou moins prononcé avec le manteau, expliquent l'architecture observée aux marges volcaniques. Ces structures sont toujours en lien avec une production magmatique associée, que ce soit en terme de sous-plaquage dans la croûte inférieure, ou en terme d'accrétion de SDR à la surface. Il faut encore considérer le caractère fortement segmenté des marges volcaniques (e.g. *Callot et al.,* 2002). Il est aussi établi que la distribution spatiale des SDR est souvent relié aux grandes failles transformantes (i.e. *Franke et al.,* 2007 ; *Koopmann et al.,* 2014 ; Fig. 18).

L'idée est que les failles transformantes, en jouant le rôle de « barrière » à la propagation du break-up, canalisent le magma et « l'empêchent » de passer de l'autre côté du segment. En effet, on peut localement considérer que l'accommodation différentielle latérale de l'extension, résultant dans le jeu d'une faille transformante, soit équivalente à une ouverture en séquence des bassins océaniques, e.g. *Koopmann et al.* (2014) (Fig. 21). Le problème de cette approche est qu'elle considère que les transformantes sont uniquement syn-break-up. Cette idée s'oppose à la théorie des soft points qui propose des transformantes héritées de l'activité précoce du manteau au cours de l'extension. Ainsi, si la segmentation du rift semble jouer un rôle prépondérant dans le caractère volcanique ou non d'une marge, la question reste de

savoir si ces transformantes (ou, alternativement ces zones de transfert) sont ou non précoces dans le développement de la marge volcanique.

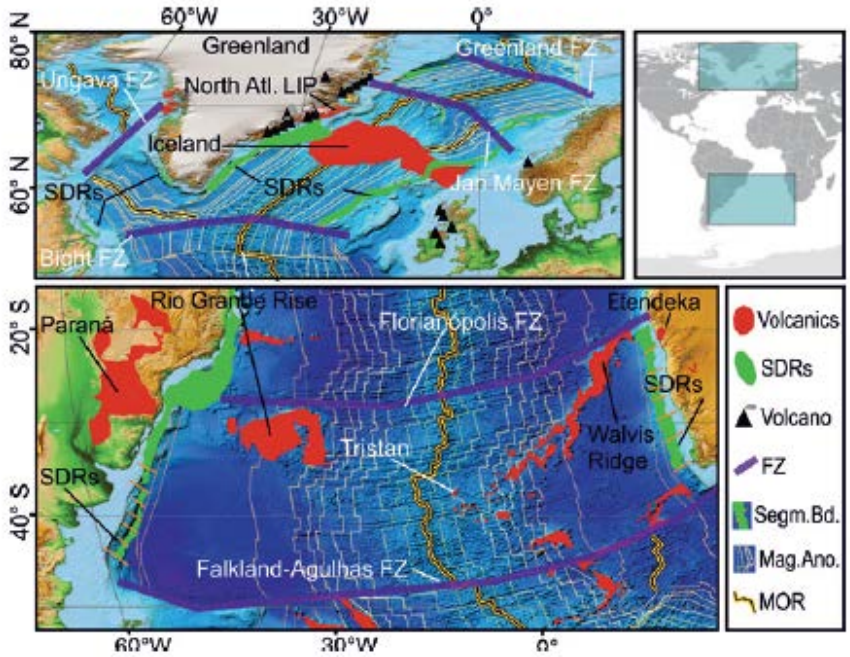

*Figure 21. Distribution du volcanisme en Atlantique, par rapports aux grandes failles transformantes (*Koopmann et al.*, 2014).*

CHAPITRE 2
-
PROBLÉMATIQUE, OBJET D'ÉTUDE ET DÉMARCHE

1. Questionnement scientifique et problématique

Effet du magmatisme dans la variabilité du style structural

Nous avons montré que les modèles qui synthétisent les observations sismiques les plus récentes prédisent la formation de marges étroites, de type *narrow rift* sensu Buck, alors que les observations d'autres segments océanisés montrent des marges asymétriques, où le couplage croûte/manteau est différent, et où la déformation a été accommodée pour partie sur une zone plus large. Une meilleure compréhension des modifications rhéologiques induites par l'ajout de matériel mafique à la croûte durant l'extension peut-être une solution pour résoudre ce paradoxe. En effet, il n'existe pas à ce jour d'étude visant à déterminer le caractère localisant ou distribuant du sous-plaquage vis-à-vis de la déformation.

Comment la modification magmatique de la croûte, au cours de l'extension, change le style structural d'une future marge ?

Amincissement lithosphérique et break-up

Nous avons montré plus dans le chapitre précédent plusieurs scénarios alternatifs pour effectuer le break-up. L'importance des détachements est suggérée, bien que rarement directement observés. Le débat porte sur leur « position » en profondeur : découplent-ils ou non la croûte du manteau? Les processus qui mènent au break-up ne font pas consensus, comme la diversité des scénarios que nous avons présentés plus haut en atteste.

Quelles structures majeures permettent à la fois d'amincir la croûte et de mener à la rupture ? Sont-ce les mêmes structures ou processus qui amincissent la croûte et le manteau lithosphérique ?

Atténuation crustale et flexure

Nous comprenons mal la signification de la flexure vers l'océan observée à terre. Y'a t-il un lien avec l'amincissement, ou plutôt avec le développement des SDR dans des parties plus distales de la marge ? Le timing de la flexure est mal compris : s'il est clair qu'elle se met en place de façon épisodique (*Lenoir et al.,* 2003, *Abdelmalak.,* 2015), voir même rapide (*Lenoir et al.,* 2003), on ne sait pas quand elle se forme par rapport au début de l'extension. Est-elle syn-rift précoce, ou syn-break-up ?

De quoi la flexure est-elle le diagnostique ? Quelle est sa signification par rapport à l'amincissement et aux SDR ?

Formation des SDR et calendrier de formation de la TOC

De même que pour la flexure, les SDR représentent un double questionnement : architectural, d'abord, avec leur lien à l'amincissement : les failles listriques qui contrôlent les SDR sont-elles des structures majeures qui accommodent à la fois l'amincissement et l'extension, et traduisent un sens de cisaillement particulier ? Ou au contraire, leur développement (surtout dans le cas de marges asymétriques) se fait de manière plus indépendante d'un style structural qui serait hérité de phases extensives antérieures à eux. Temporel ensuite, parce que comme nous l'avons montré pour la flexure, il y a une relation ambiguë entre le fait que les SDRs se développent rapidement pendant l'extension magmatique (sont-ils syn-rift ?) et le fait que certains SDR, les *outer SDR* de la figure 5 du chapitre 1, soient en contact direct avec la croûte océanique (sont-ils syn-break-up ?). Ce questionnement est majeur, ne serait-ce que parce que l'analyse par technique indirecte (gravimétrie, magnétisme) des SDR ne permet pas de distinguer l'un où l'autre cas. La figure 1 montre une carte des anomalies magnétiques au large du bassin de Vøring (*Gernigon et al.,* 2015). Les anomalies magnétiques sont bien exprimées aux alentours de la dorsale, mais deviennent brouillées à mesure que l'on se rapproche de la TOC et des SDR (Fig. 1). *Hinz et al.,* 1998 propose que ce « brouillage » est dû au caractère justement épisodique de la formation des SDR.

Quel est le calendrier de formation des SDR et comment leur formation s'agence t-elle par rapport au début et à la fin du rifting ?

Effet de la segmentation

L'effet de la segmentation sur la distribution du volcanisme syn-rift est mal connu. En effet, il n'y a pas, dans *Koopmann et al.* 2014 de distinction entre failles transformantes syn-break-up ou syn-TOC, et failles transformantes syn-rift (voir *Bellahsen et al.*, 2013a, pour une revue de ces trois types). Cela provient majoritairement du fait qu'on considère les SDR comme étant quasiment concomitants du break-up (où s'ils sont syn-rift, l'ouverture à été si rapide que cette question est éludée). Cette hypothèse est renforcée par des travaux récents de modélisation qui montrent que d'importants volumes des SDR peuvent être mis en place au break-up sans l'aide d'un manteau anormalement chaud, si la lithosphère a été amincie suffisamment lors d'épisodes tectoniques antérieurs (*Armitage et al.,* 2010). En revanche, il a été montré que certaines failles transformantes majeures peuvent être héritées des phases les plus précoces de l'extension (e.g. *Bellahsen et al.,* 2013a, *Pik et al.,* 2013).

Comment cette segmentation issue des phases précoces du rifting peut-elle jouer sur la croissance des SDR et la mise en place du sous-plaquage ?

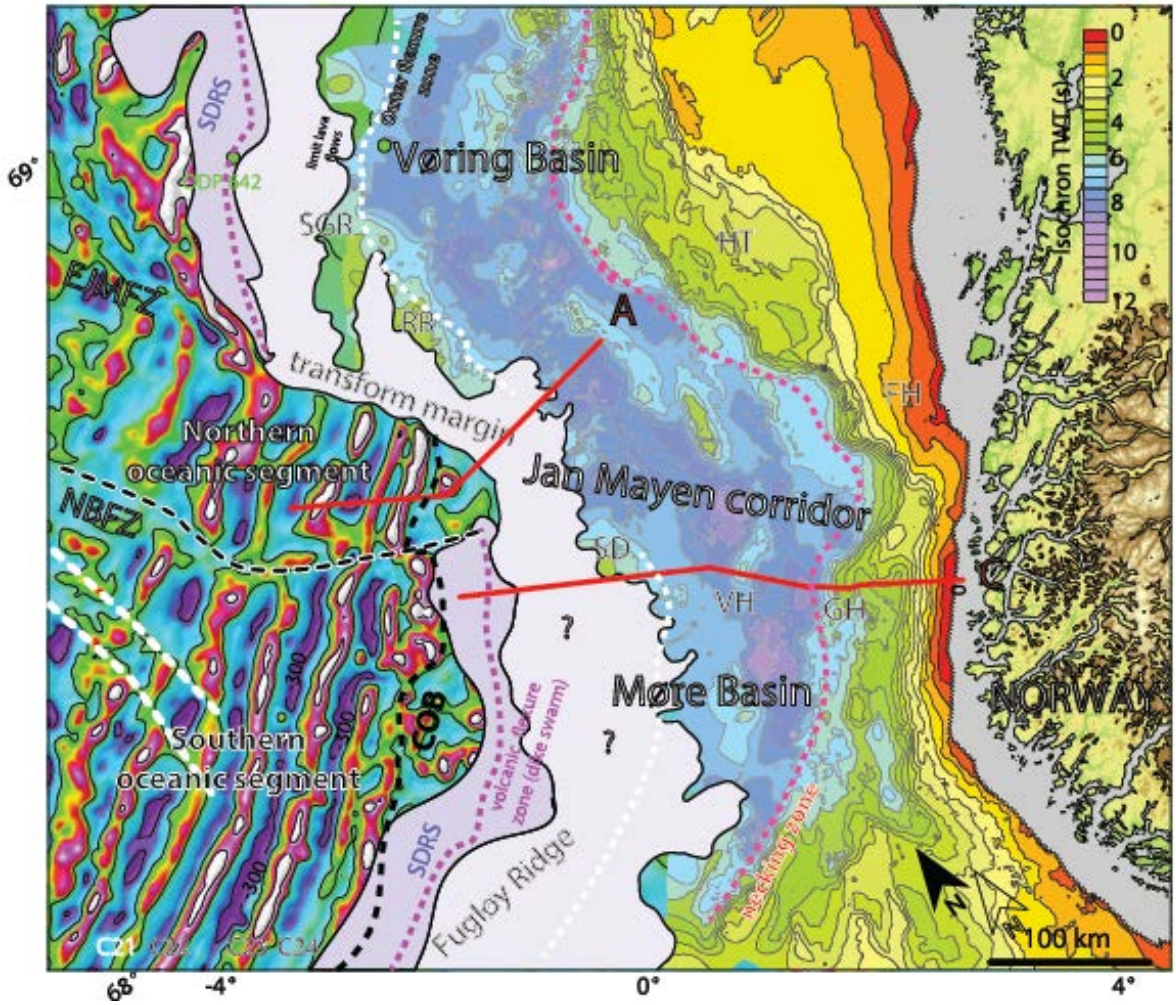

Figure 1. Carte des anomalies magnétiques le long de la marge volcanique norvégienne, Gernigon et al. *(2015). Il faut noter ici que les bandes magnétiques sont mal exprimées entre la COB (pointillés noirs) et les SDR, notamment dans le bassin de Møre.*

Effet d'un manteau

Nous avons plusieurs fois noté dans ce chapitre introductif que le rôle du manteau était complexe, et qu'il y avait ambiguïté concernant (a) son rôle dans la production des grands volumes de *flood basalts* sous forme de trapps ou de SDR et (b) son rôle mécanique dans l'expression du style structural des marges. Il y a une distinction entre la primauté du rôle de l'asthénosphère, plus ou moins chaude et active, et celle de la lithosphère, dont l'état physique plus ou moins fragile ou ductile. Nous disons que des changements d'états de ces deux parties du manteau **pourraient avoir un rôle dans la façon dont s'exprime la déformation (spatialement, temporellement, en terme de budget magmatique. Quel est-il ?**

2. La dépression des Afars

Le triangle Afar est le point triple rift-rift-rift qui sépare les plaques Nubienne, Somalienne et Arabe (Fig. 2). Cette partie documente la morphologie et l'histoire géologique de la région.

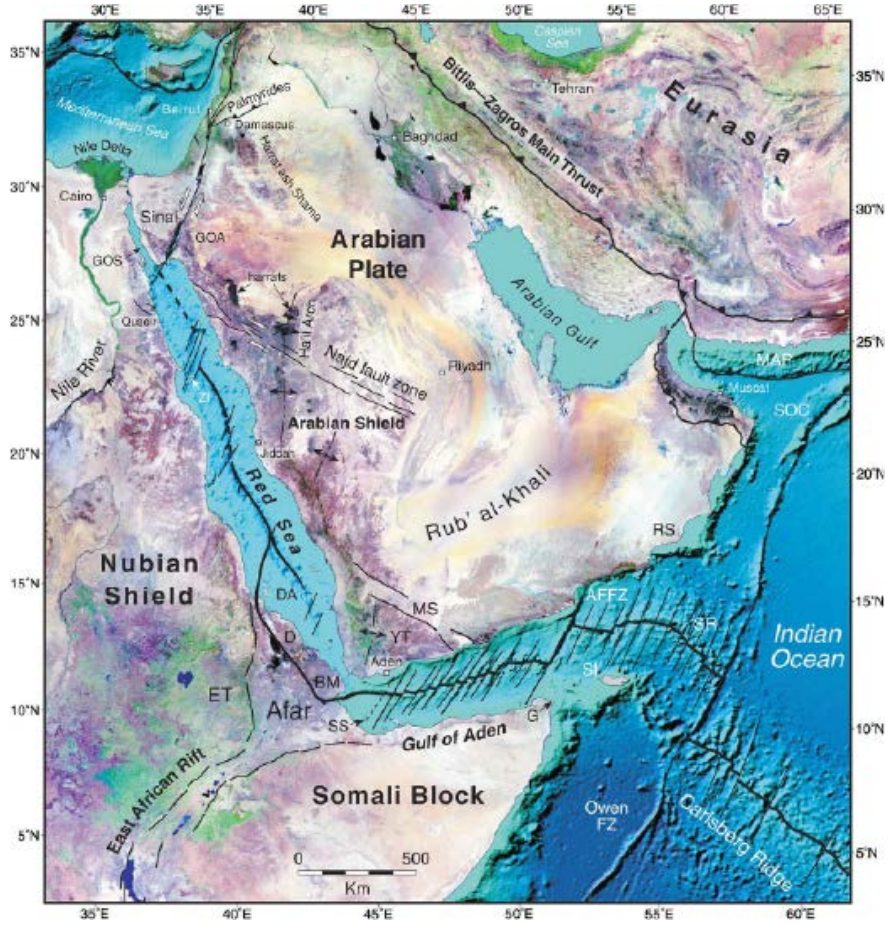

Figure 2. Image Landsat de la corne de l'Afrique et de la péninsule Arabe. Noter la direction d'ouverture NNE du Golfe d'Aden et de la Mer Rouge.

2.1. Physiographie et structures

Le triangle Afar s'étend sur une région de 200.000 km^2 bordée par des escarpements qui délimitent les plateaux éthiopiens eux même séparés par la vallée du Main Ethiopian Rift. Les blocs Ali-Sabieh et Danakil ferment respectivement la région à l'Est et au Nord-Est. L'escarpement éthiopien s'étend au Nord jusqu'en Erythrée et ferme la dépression Afar au niveau du Golfe de Zula et du bloc Danakil. Le golfe de Tadjoura s'étend vers l'Ouest depuis e Golfe d'Aden et pénètre dans la dépression par Djibouti. Il sépare les deux blocs de Danakil et d'Ali-Sabieh. Les hauts plateaux formes les épaules de la dépression Afar : hauts de 2 à 3 km, leur altitude décroît brutalement jusqu'à atteindre le niveau de la plaine en Afar. L'altitude de la dépression varie de ~600m à 0m au niveau des golfes de Zula et Tadjoura et passe sous le niveau de la mer sur le segment de l'Erta Ale (*Mohr,* 1983).

2.1.1. Les zones marginales de la dépression Afar

La dépression Afar est séparée du plateau Ethiopien par le grand Escarpement Ethiopien, orienté N-S délimitant une série de bassins marginaux appelés les grabens marginaux. Ceci constitue la marge Ouest du triangle Afar. Cette marge est formée par des blocs crustaux basculés vers le rift et érodés par un dense réseau de drainage (*Zanettin et Justin-Visentin,* 1975).

Les grabens marginaux ont une largeur d'environ 5 km pour une longueur de 30 km. Ils sont délimités par des failles normales et séparés par des zones transformantes (*Chorowicz et al.,* 1999 ; *Collet et al.,* 2000).

L'escarpement somalien délimite la marge Sud de l'Afar et est caractérisé par des blocs basculés en direction du plateau. Il n'y a pas de graben marginaux adjacents mais une forte concentration d'édifices volcaniques (Fig. 3).

L'Afar est fermé à l'Est par le bloc Danakil qui s'étend du Golfe de Tadjoura au SE au Golfe de Zula au NW. Le bloc Danakil présente une topographie légèrement asymétrique suggérant un léger basculement vers l'Est. Le bloc d'Ali-Sabieh est séparé du bloc Danakil par le Golfe de Tadjoura et est adjacent au plateau somalien via la région d'Aysha.

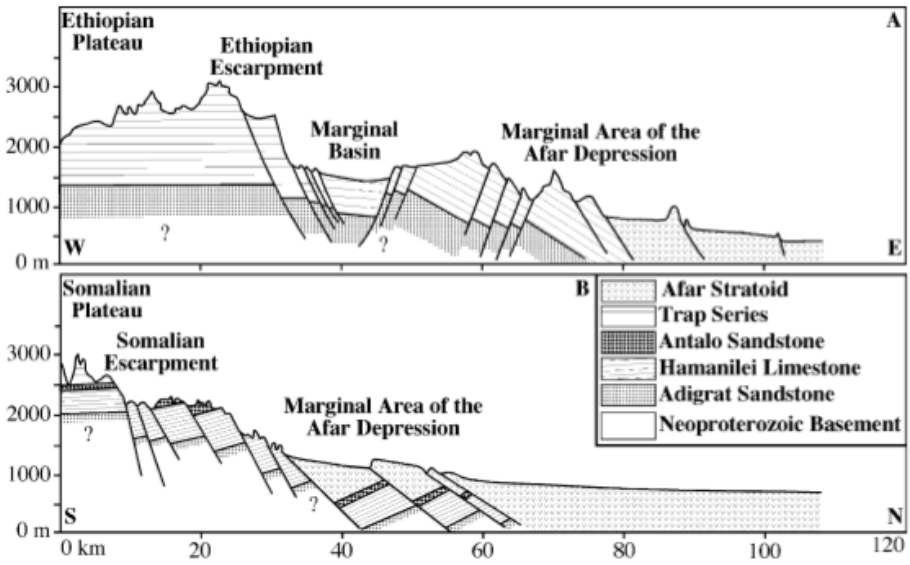

Figure 3. Coupes stylisées montrant le style structural des parties marginales (ou marges) en Afar (Beyene et Abdelsalam*, 2005). Notez la différence de pendage des blocs basculés entre la coupe W-E depuis les plateaux éthiopiens jusqu'en Afar et entre la coupe S-N depuis les plateaux somaliens. Le style structural de la marge topographique Afar évoque celui des marges volcaniques, avec des blocs basculés vers le centre du rift, alors que le côté Somalien évoque un rift non-volcanique avec une vergence opposée des blocs basculés.*

2.1.2. La partie centrale de la dépression Afar

L'Afar central est dominé par des plaines entrecoupées de horst et de grabens et quelques hauts topographiques dénotant la présence d'édifices volcaniques. Sur la base de structures tectoniques de même orientation, l'Afar est divisé en Nord Afar, ou segment Erta'Ale, qui comporte les volcans actifs de l'Erta'Ale et Alayta, et Afar Central au sud de celui-ci. La figure 4 montre un schéma structural de l'Afar et nomme les principaux segments de rift.

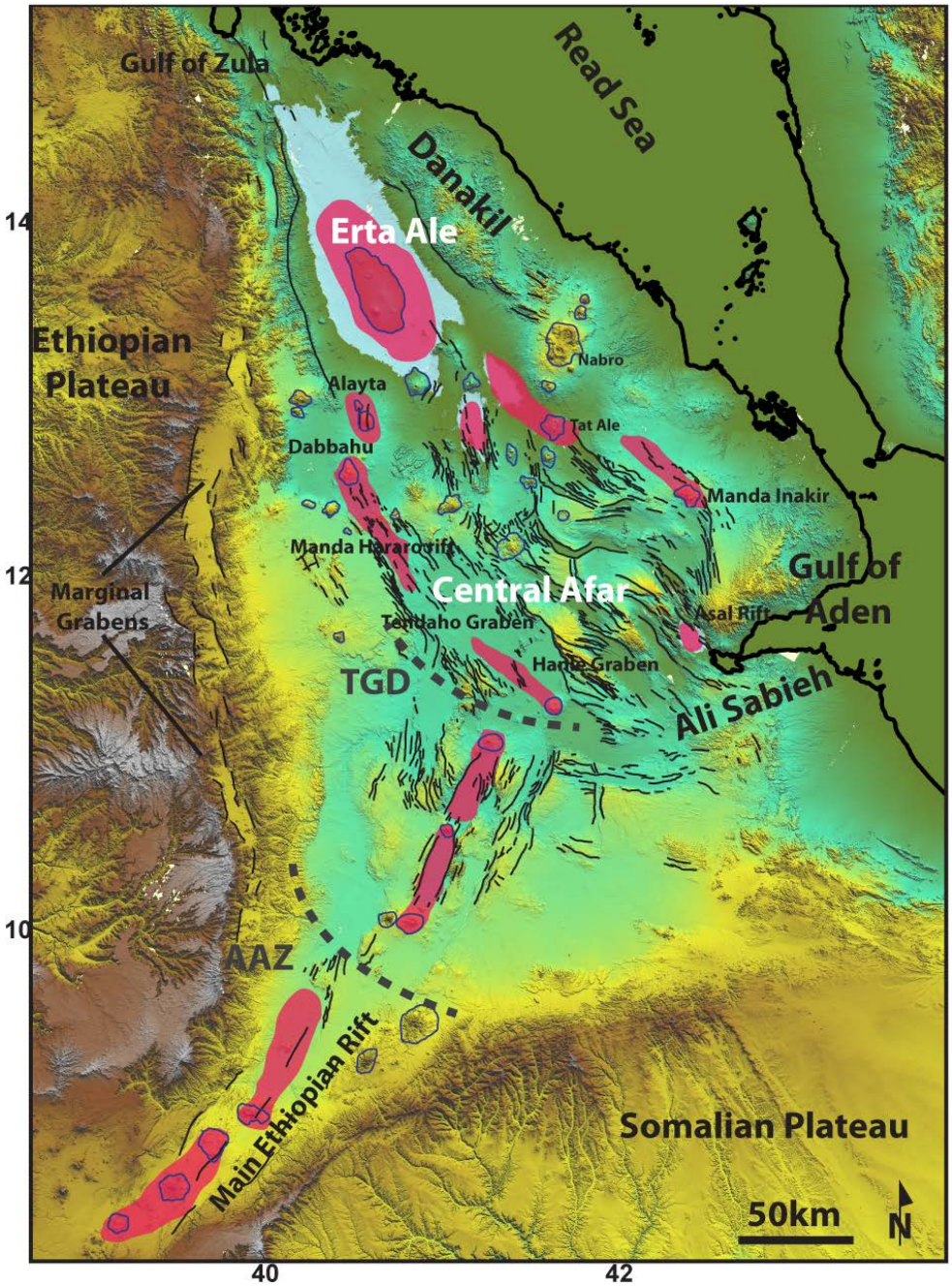

Figure 4. Schéma structural de l'Afar à partir des données topographiques SRTM90. En rouge, les segments sismiquement et volcaniquement actifs. La discontinuité Tendaho-Goba'ad (TGD) marque le changement d'orientation des structures NNW du rift Mer Rouge au Nord et NNE du Main Ethiopian Rift au Sud. La AAZ

*(Arcuate Accommodation Zone) marque le changement de pendage des failles entre l'Afar (failles vers le continent) et le MER (failles vers l'axe) (*Kidane et al., *2003). Les zones en bleu sont sous le niveau de la Mer.*

L'altitude en Afar du Nord (ou dépression des Danakils) descend à -120m au-dessous du niveau de la mer dans la zone du Dallol. Cette région comporte de grands volcans boucliers : Erta'Ale, Alayta. Le grain tectonique en Nord Afar est NNW, comme celui de la Mer Rouge. Il se subdivise en deux grains distincts : E-W en Afar Central-Est et NNW en Afar-Central-Ouest. Le grain tectonique NNW est la continuité subaérienne du rift de la Mer Rouge.

La partie Centrale-Est est délimitée par le bloc Danakil et la discontinuité Tendaho-Goba'ad (TGD) représentant la limite entre les grains tectoniques NNW-SSE et NNE-SSW. La région est dominée par une série de horsts et de grabens adjacents les uns aux autres compris entre les rifts quaternaires de Manda Hararo à l'Ouest et de Manda Inakir à l'Est.

La partie Sud-Ouest est une continuation du MER interrompue par la TGD. Elles constituée de horst et de grabens orientés N-S à NE-SW.

La partie Sud-Est ressemble au Sud-Ouest avec la seule différence que ses structures sont nettement orientées E-W.

2.2. Formations géologiques

2.2.1. Pré-rift

Les roches du socle néoprotérozoïque affleurent au Nord et au Nord-Est de l'Afar en Erythrée et en Ethiopie (Fig. 5). On les trouve aussi dans certaines parties des blocs Danakil et Ali-Sabieh. Stratigraphiquement au-dessus du socle sont déposées les roches sédimentaires mésozoïques. On les trouve sur les plateaux éthiopiens et somaliens, et ces séries consistent majoritairement en des alternances Jurassiques et crétacées de grès et de calcaires (*Varet* 1978). Ces formations anciennes ne sont jamais observées en Afar.

A la période Eocène-Oligocène, l'arrivée du panache Afar sous l'Ethiopie provoque l'éruption du LIP pour former les plateaux actuels (Fig. 5). La série basaltique et rhyolitique, ou série des Trapps, forment une pile de 500m à 2km d'épaisseur en moyenne et peuvent atteindre 3 km d'épaisseur localement (*Rochette et al.,* 1998 ; Hofmann 1997). Le volume actuel total des trapps est estimé à environ 350.000 km^3 (*Mohr,* 1983 ; *Mohr et Zanettin,* 1988) bien qu'initialement il ait pu atteindre le million de km3 (Rochette et al., 1998). Le plus gros épisode éruptif a provoqué la mise en place de la quasi-totalité de la série entre 31-29 Ma (*Hofmann et al.,* 1997, *Pik et al.,* 1998 ; *Coulié et al.,* 2003) et coïncide avec l'arrivée du panache sous l'Ethiopie. Cette série de trapps se met en place sur les séries sédimentaires et le socle au nord, et sur des basaltes pré-trapps à 45 Ma au sud de l'Ethiopie, près de la

dépression Turkana (*Berhe et al.,* 1987). L'origine des magmas des trapps est encore discutée aujourd'hui. On distingue principalement l'hypothèse de la fusion et de l'assimilation de la lithosphère par un panache ou plusieurs panaches (*Rooney et al.,* 2012, *Kieffer et al.,* 2004) de l'hypothèse de la fusion seule de la tête du panache (*Pik et al.,* 1999, 2006, in prep). Les trapps sont surimposés par des volcans-boucliers mis en place entre 30 et 10 Ma (*Kieffer et al.,* 2004). Il est important de noter qu'on n'observe pas de signes d'extension syn-trapps : ceux-ci sont déposés à plat sur les plateaux en discordance angulaire avec le Jurassique et le socle cristallin.

2.2.2. Syn-rift précoce (Miocène)

Au Miocène, l'activité volcanique décroît brutalement. Les premières formations syn-rift se mettent en place à 25-23 Ma (*Ukstins et al.,* 2002 *; Coulié et al.,* 2003) sur les plateaux sous forme de volcans-boucliers et dans le graben marginal de l'escarpement Ouest. Au même moment, les séries pré-rift sont intrudées par des porphyres acides alcalins à péralcalins mis en place à faible profondeur (< 2 km) que l'on retrouve aujourd'hui contre la marge et dans la dépression (*Varet,* 1978). Ces formations acides à 25 Ma pourraient correspondre aux grands *sills* dans lesquels les magmas éruptés sont stockés avant d'être éruptés.

Les séries volcaniques de l'Afar sont subdivisées en 3 formations : les basaltes Adolei, les rhyolites de Mablas et les basaltes de Dahla (*Barberi et al.,* 1975 *; Varet,* 1978) (Fig. 5).

Les basaltes d'Adolei sont trouvés au Nord de Tadjoura et sont datés à 22-14 Ma (*Chessex et al.,* 1975, *Barberi et al.,* 1975). Les rhyolites des Mablas sont éruptées stratigraphiquement au-dessus des basaltes d'Adolei le long de fissures N-S et sont âgées de 20 à 10 Ma *(Barberi et al.,* 1975 ; Audin et al., 2004). En discordance sur la formation des Mablas se trouvent les basaltes du Dahla datés de 7.7 à 4.8 Ma (*Audin et al.,* 2004). La mise en place de ces séries Miocènes est affectée par le jeu des failles normales. Le début de l'extension en Afar est donc daté à 25 Ma (*Barberi et al.,* 1975).

2.2.3. Syn-rift tardif (Plio-Pléistocène) : série Stratoïde

La série Stratoïde éruptée entre 4.4-1.1 Ma représente un deuxième épisode de volcanisme fissural intense (*Varet,* 1978 ; *Barberi et Santcroce,* 1980 ; *Deniel et al.,* 1994). Ces laves couvrent environ 2/3 de la surface de l'Afar et masquent souvent les structures plus anciennes (Fig. 5). Cette série est trouvée en discordance angulaire sur le Dahla. L'épaisseur maximale de la série Stratoïde est de 1.5 km dans la région de Djibouti (i.e. *Le Gall et al.,* 2011). Elle est majoritairement cachée en Afar Nord sous les laves Quaternaires et en Afar Central-Ouest le long de l'escarpement sous les plaines sédimentaires.

2.2.4. Volcanisme actuel : segments actifs

Le volcanisme depuis ~1 Ma est localisé dans les rifts axiaux et segmentés qui coupent les formations plus anciennes. Ces segments ont été très étudiés au court des dernières années car leur activité magmatique et tectonique en font des laboratoires privilégiés pour étudier les processus de déformation crustale à l'œuvre et comprendre les mécanismes de l'océanisation. Ils consistent en des zones axiales faites de coulées fissurales de basaltes associé à des produits acides. Les laves éruptées sont densément faillées. Ces segments présentent une activité sismique intense (i.e crise de 2005, *Grandin et al.,* 2010) et sont nourris par des chambres magmatiques présentes à tous les niveaux de la croûte (*Field et al.,* 2012 ; *Pagli et al.,* 2012, *Desissa et al,* 2013 ; *Medynski et al.,* 2013, 2015).

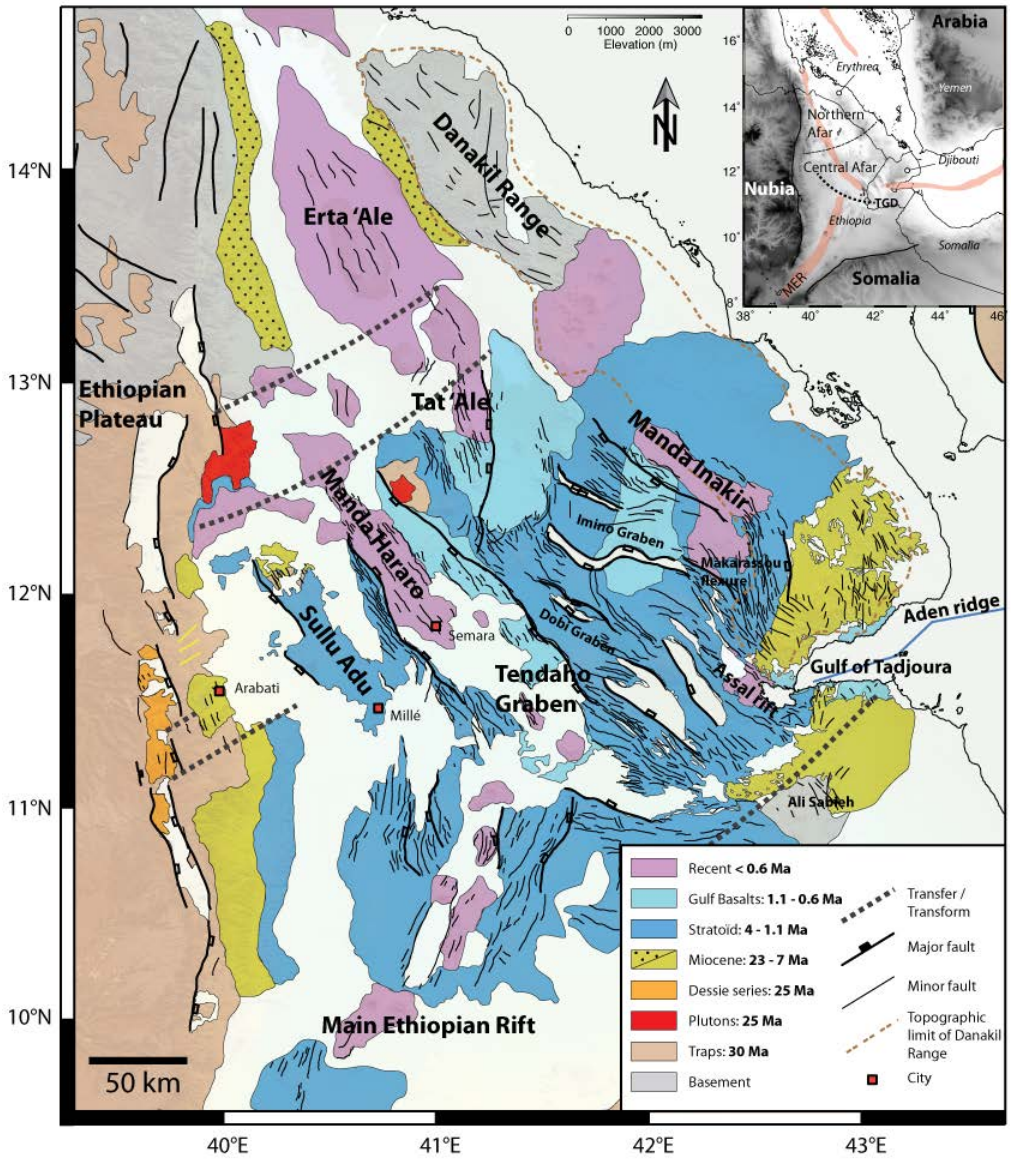

Figure 5. Carte géologique du triangle Afar (cette étude). Noter la différence entre les segments d'Afar Central et de l'Erta'Ale, situés de part et d'autre d'une zone

transformante. L'Afar Central est caractérisé par la présence de la série Stratoïde, alors que l'Erta'Ale en est dépourvu.

2.3. Nature de la lithosphère

2.3.1. L'état du manteau

Les données géologiques

Les trapps basaltiques et rhyolitiques éthiopiens épais de 2 km éruptés sur les plateaux éthiopiens et yéménites (Pik et al., 1998 ; Baker et al., 1996) aux alentours de 29-31 Ma (Hofmann et al., 1997 ; *Coulié et al*, 2003) avant le début du rifting en Mer Rouge et dans le Golfe d'Aden (*Leroy et al.,* 2012), ont fréquemment été invoqués comme témoins de l'influence du panache mantellique sous la région (Marty et al., 1996 ; Pik et al., 1999). La localisation et le nombre de ces panaches ou cellules de convections fait toujours matière à débat aujourd'hui (*Schilling et al,* 1992 ; *Marty et al.,* 1993 ; 1996 ; *Ebinger et Sleep,* 1998 ; *George et al.,* 1998 ; *Courtillot et al.,* 1999 ; *Kieffer et al,* 2004 ;; *Furman et al.,* 2006 ; *Pik et al.,* 2006 ; *Rogers et al.,* 2006 ; *Beccaluva et al.,* 2009 *; Rooney et al.,* 2012b*). Ebinger et Sleep,* 1998 suggèrent qu'un large panache s'est développé sous la plaque Africaine près de Turkana à 45 Ma avec une production de magma minimale jusqu'à ce que l'extension commence en Mer Rouge / Golfe d'Aden et que la lithosphère soit suffisamment amincie. *George et al.,* 1998 et *Roger et al.,* 2000, montrent sur des arguments pétrologiques que les laves du Kenya et de l'Ethiopie proviennent de deux panaches différents eux-mêmes enracinés au super-panache Africain. Pour *Pik et al.* (1999, 2006, in prep), le panache Afar est distinct des anomalies sous le Rift Est Africain. Il s'enracine profondément jusqu'à la transition noyau-manteau et se met en place sous l'Ethiopie à 30 Ma, provoquant l'éruption d'une LIP au dessus des magmas éruptés à 45 Ma du fait de la convection lithosphérique. Cette vue est appuyée par des études de dénudation des reliefs par thermochronologie (*Pik et al.,* 2003 ; 2008) qui corrèlent la mise en place du panache Afar avec le maintient dynamique topographique de trapps par un manteau anormalement chaud (*Pik,* 2011*). Rooney et al.,* 2012a présente des estimations de température potentielle du manteau pour 53 magmas primitifs à travers l'Ethiopie montrant que le pic actuel d'anomalie positive de température (140°C) se situe sous Djibouti. Les trapps se seraient quant à eux formés sous des conditions légèrement plus chaude (170°C) à l'Oligocène.

Les données géophysiques

Ces dernières années, des campagnes sismologiques majeures ont été réalisée en Ethiopie (*Benoit et al.,* 2006 ; *Bastow et al.,* 2011) et ont permis une meilleure compréhension de la nature du manteau et de la croûte sous l'Afar. L'imagerie par tomographie sismique a mis en évidence une anomalie négative de 3% des ondes S

étendue sur 500km sous la base de la lithosphère et prenant racine à la transition noyau-manteau (*Li et al.,* 2008 ; *Ritsema et al.,* 2011, *Mulido et Nyblade,* 2013, Fig. 6) : le super-panache africain. Ces données ont été modélisées et documentent l'uplift régional (*Moucha et Forte,* 2011) mis en évidence par la thermochronométrie U/Th-He sur les plateaux (*Pik et al.,* 2003) qui montrent un *doming* initié à partir de 30-20 Ma.

Cette anomalie régionale est en outre connectée à des anomalies moins profondes (*Bastow et al.,* 2008 ; *Benoit et al.,* 2006) à l'échelle lithosphérique. *Hammond et al.,* 2013, montre qu'à faible profondeur (<300km), ces anomalies négatives sont chenalisées en conduits qui remontent directement sous les axes quaternaires en Afar alors que la lithosphère sous-jacente aux plateaux est caractérisée par des anomalies positives (Fig.7). D'autre part, la vitesse moyenne des ondes P dans le manteau lithosphérique est de 7.2 km/s sous l'Afar, indiquant un manteau anormalement chaud (*Makris et Ginzburg*, 1987).

Les mesures d'anisotropie sismique en Ethiopie documentent les processus de déformation de la lithosphère et de fluage dans l'asthénosphère (Fig. 6). Dans le MER, l'analyse des phases SKS dans la lithosphère montre un changement d'orientation de N40° sous les bordures du rift à N10° sous les segments axiaux. Ceci est interprété comme étant causé par des intrusions magmatiques récentes (*Bastow et al.,* 2010, *Kendall et al.*, 2005, 2006). Sous la lithosphère, *Bastow et al.*, 2010, *Kendall et al.*, 2006, *Gao et al.*, 2010, observent une anisotropie N30-40° causée par l'alignement préférentiel des cristaux d'olivines et des poches de magma due au fluage subhorizontal du manteau asthénosphérique.

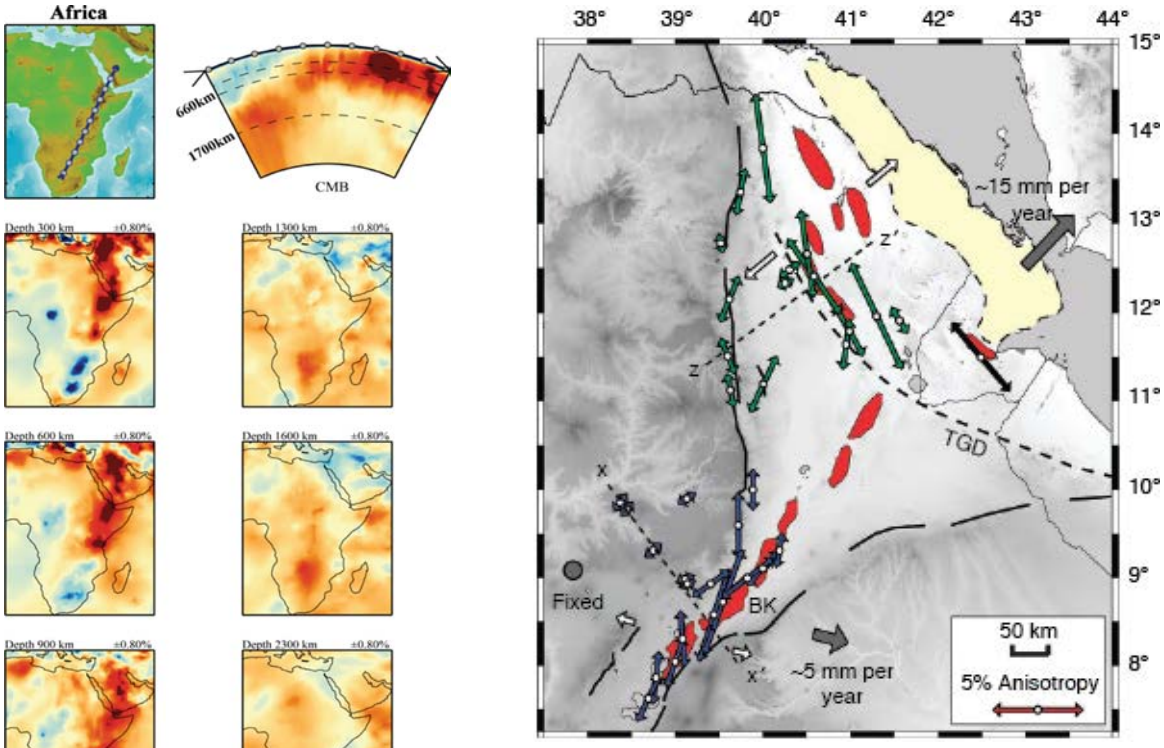

*Figure 6. a) Structure du manteau sous l'Afrique (*Li et al.*, 2008). b) Directions d'anisotropies dans la croûte (*Keir et al.*, 2011).*

2.3.2. Structure de la croûte

La structure et la nature de la croûte sous l'Afar ont été sujettes à débat depuis les 35 dernières années. La discussion a porté sur le fait de déterminer si la croûte était océanique ou s'il s'agissait de croûte continentale étirée et intrudée (croûte transitionnelle). En d'autres termes : A quel stade de maturité se trouvent les marges Afar par rapport aux MPV actuelles ?

La structure de la croûte a tout d'abord été documentée par sismique grand-angle (*Berckhemer et al.,* 1975 ; *Makris et Ginzburg*, 1987 *; Prodehl et al.,* 1997 ; *Maguire et al.,* 2006) fonctions récepteurs (*Ayale et al.,* 2004 ; *Dugda et al.,* 2005 ; *Stuart et al.,* 2006 ; *Hammond et al.,* 2011, *Reed et al.,* 2014) et gravimétrie (*Redfield et al.,* 2003 ; *Tessema et Antoine*, 2004 ; *Tiberi et al.,* 2005 ; *Mammo,* 2013).

La croûte est la plus épaisse sous le plateau éthiopien (40-45 km) et somalien (35 km). Elle s'amincit abruptement jusqu'à 15-30 km en Afar (*Maguire et al.,* 2006 ; *Stuart et al.,* 2006). Les niveaux crustaux sont les suivants dans toute l'Ethiopie : croûte inférieure à Vp = 6.7-7.0 km/s, croûte supérieure à Vp = 6.0-6.3 km/s et couverture sédimentaire et laves à Vp = 2.2-4.5 km/s (*Makris et Ginzburg,* 1987 *; Hammond et al.,* 2011). L'épaisseur de la couverture volcanique augmente à mesure que celle de la croûte diminue suggérant un lien avec l'amincissement crustal, la subsidence du bassin et le remplissage. La croûte est considérée comme étant

continentale intrudée et pas encore océanique (*Makris et Ginzburg,* 1987, *Bastow et Keir,* 2011)(Fig. 7).

En Afar central, la croûte est amincie jusqu'à 25-20 km depuis le rift de Manda Hararo jusqu'à une bande de 40km de large près du graben marginal à l'Ouest (*Hammond et al.,* 2011, Fig. 7) où *Wolfenden et al.* (2005) décrit la mise en place des basaltes du Dahla (miocènes en âge) interprétés comme étant les témoins de la localisation de l'extension lors du développement du rift sub-aérien Mer Rouge en Afar. Il reste néanmoins des zones en Afar central où la croûte reste épaisse de 30 km, notamment sous le bloc Danakil.

Sous l'Erta Ale, la croûte passe de 25 à 15 km (*Hammond et al.,* 2011). Cette variation d'épaisseur Sud-Nord est corrélée avec un changement de force de la lithosphère (Te = 60 km sous les plateaux et 9 km sous l'Afar central et ~5 km sous l'Erta Ale ; (*Ebinger et Hayward,* 1996, *Perez-Gussinyé et al.,* 2009) et avec la variation de la profondeur de la couche sismogène (25-30 km sous les plateaux à 5 km sous l'Afar *; Keir et al.,* 2009a ; *Craig et al,* 2011).

Les fonctions récepteurs renseignent également les rapports Vp/Vs moyens de la croûte. Les plateaux ont un Vp/Vs de 1.7-1.9 alors que les zones d'amincissement ont des rapports Vp/Vs = 1.9-2.1 (*Dugda et al.,* 2005 ; *Hammond et al.,* 2011). Un ratio supérieur à 1.85 ne peut pas être interprété simplement en termes de composition et nécessite une croûte intrudée de magma (i.e. *Hammond et al.,* 2011). Ceci est cohérent avec les études magnétotelluriques qui montrent des anomalies symétriques situées à 10km de profondeur correspondant à des dykes mafiques intrudés dans la croûte supérieure (*Bridges et al.,* 2012). Ces anomalies sont interprétées comme similaires à celles observées aux centres d'accrétion océaniques dans le Golfe d'Aden.

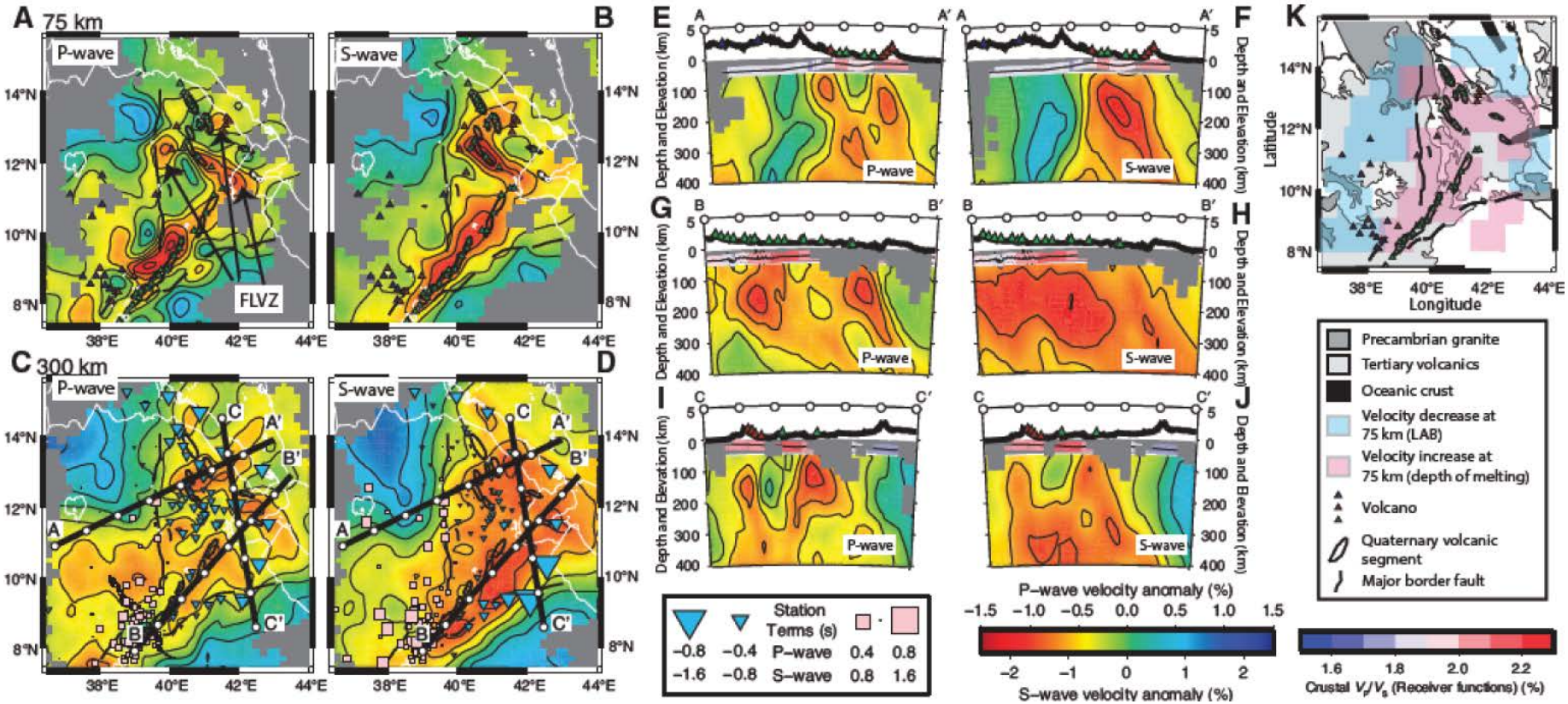
A 75 km
P-wave
FLVZ
B
S-wave
C 300 km
P-wave
D
S-wave
14°N
12°N
10°N
8°N
38°E
40°E
42°E
44°E
E
F
G
H
I
J
Depth and Elevation (km)
P-wave
S-wave
Station Terms (s)
−0.8 −0.4 P–wave 0.4 0.8
−1.6 −0.8 S–wave 0.8 1.6
P–wave velocity anomaly (%)
−1.5 −1.0 −0.5 0.0 0.5 1.0 1.5
−2 −1 0 1 2
S–wave velocity anomaly (%)
K
Latitude
Longitude
Precambrian granite
Tertiary volcanics
Oceanic crust
Velocity decrease at 75 km (LAB)
Velocity increase at 75 km (depth of melting)
Volcano
Quaternary volcanic segment
Major border fault
1.6 1.8 2.0 2.2
Crustal V_p/V_s (Receiver functions) (%)

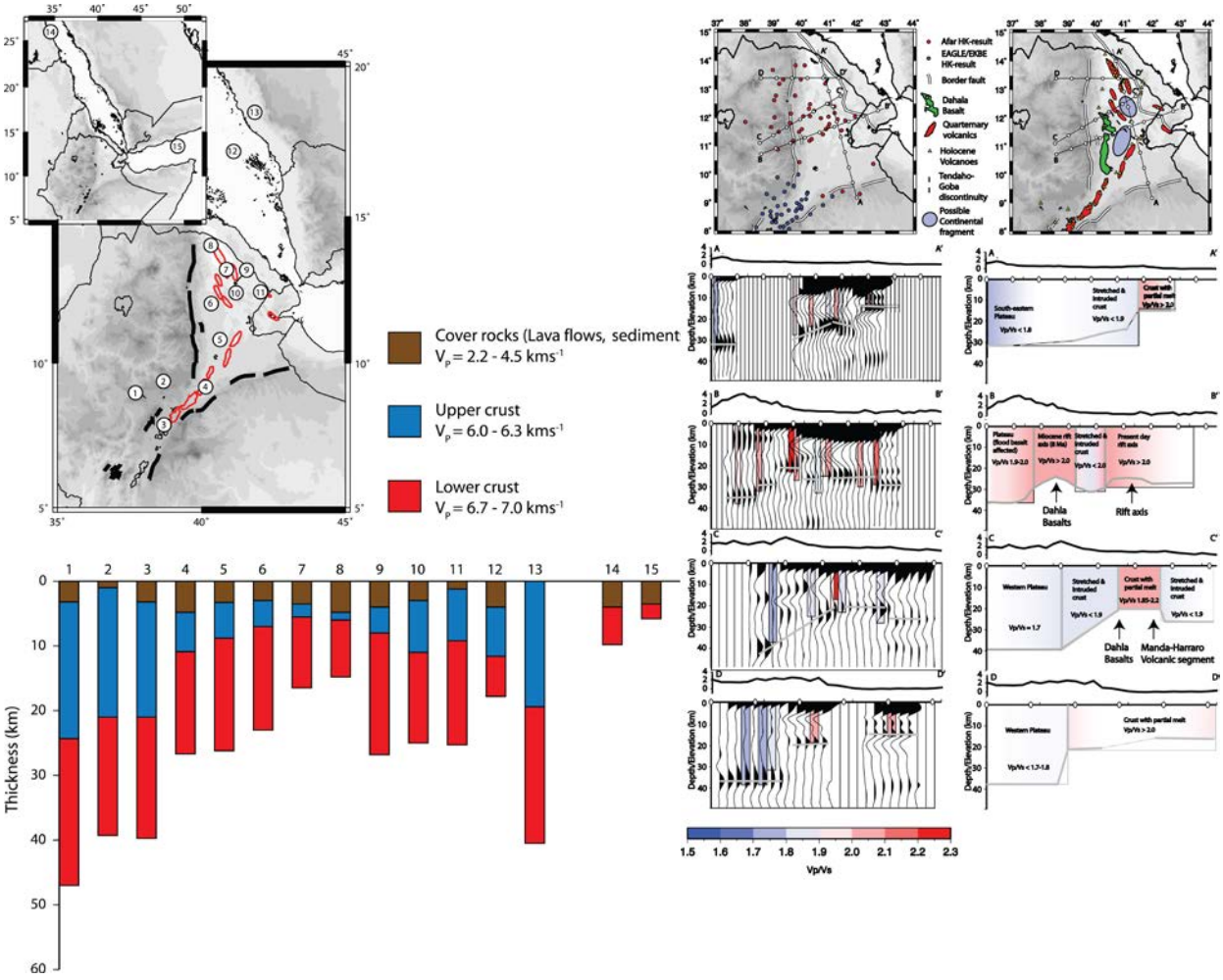

*Figure 7. Page précédente: anomalies des ondes P et S dans les premiers 400 km en profondeur montrant la chenalisation du magma sous les axes actifs (*Hammond et al.*, 2013). Panneau du bas, gauche : Epaisseurs de croûte (*Hammond et al., *2012). Noter l'amincissement préférentiel de la croûte supérieure par rapport à la croûte inférieure. Panneau du bas, droite : rapports Vp/Vs montrant la présence (rouge) ou non (bleu) de liquide dans la croûte.*

2.4. Style structural des segments de rift et développement de la TOC

Dans les marges passives volcaniques actuelles, la Transition Océan-Continent (TOC) se situe au premier ordre à l'endroit ou la croûte transitionnelle amincie et intrudée par les dykes est en contact avec la croûte océanique. Il est cependant difficile de rendre compte des processus de formation de la TOC car elle est masquée par les épais prismes de laves tholéitiiques que sont les SDR. En Afar, il est possible d'observer tous les stades de rifting de l'éruption des trapps à la formation des segments actifs. L'objectif de cette partie est de recenser ces observations.

2.4.1. Des styles structuraux contrastés

Si beaucoup d'études ont porté sur la structure du MER au sud de 9°N, peu ont documenté l'extension en Afar. *Wolfenden et al.* (2004, 2005), décrivent l'évolution tectono-magmatique de la marge Ouest du rift subaérien de la Mer Rouge (Fig. 8, gauche) : Le rifting s'initie en Afar autour de ~29 Ma avec la formation des grabens marginaux puis la déformation migre vers l'intérieur de la dépression entre 25 et 7 Ma en formant des blocs basculés par des failles à vergence vers le continent (*Black et Morton,* 1975). Les unités volcaniques de plus en plus jeunes sont disposées en discordance les unes sur les autres, témoignant des différents épisodes d'extension et de rotation des blocs crustaux. La croûte supérieure est flexurée à mesure que s'accumulent les laves éruptées à chaque épisode d'extension. Ces épanchements sont interprétés par les auteurs comme étant les analogues morphologiques des prismes de SDR imagés en sismique ou observés à terre. Pour ces auteurs, la majeure partie de l'extension lithosphérique est accommodée par injection de dykes, ceux-ci nourrissant les prismes de lave syn-rift.

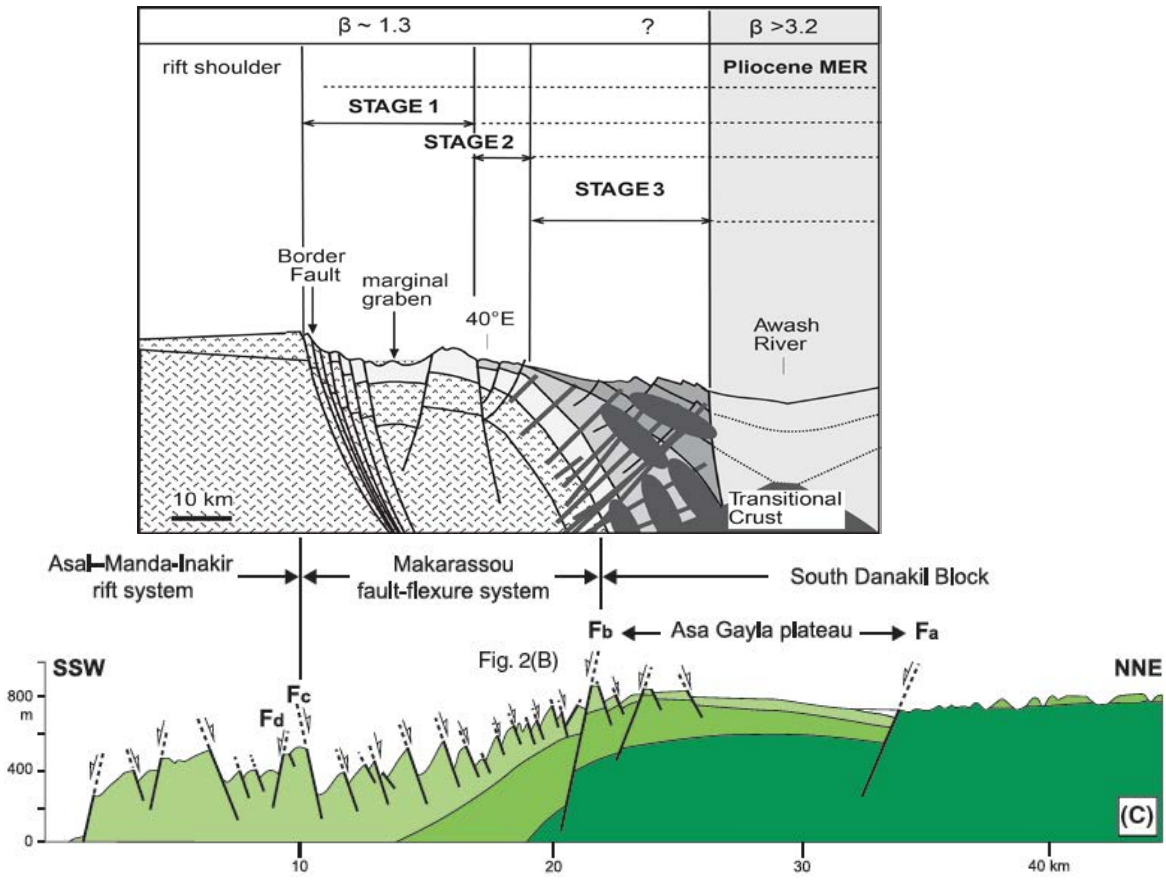

Figure 8. Haut : coupe à travers la marge Ouest, des plateaux jusqu'à la plaine d'Awash en Afar central (Wolfenden et al., *2005). Le modèle décrit une migration de la déformation depuis la faille bordière du graben jusqu'aux laves pliocènes de la série Stratoïde. La croûte supérieure est progressivement flexurée à mesure que la déformation migre. Noter que l'on a pas accès à l'histoire Pliocène du rifting dans ce*

*modèle. Bas : coupe dans le réseau de failles de Makarassou au Nord du Golfe de Tadjoura, Djibouti (*Le Gall et al., *2011). La série Stratoïde est flexurée par le jeu de failles normales à pendage vers le continent antithétique d'une grande faille bordière initiale. Le Dahla (ici d'âge 3 Ma) est déposé initialement à plat. Dans ce modèle-ci, on n'a pas accès à l'histoire ancienne du rifting, masquée par les laves Plio-Pléistocènes.*

Un phénomène similaire de flexure est observé à la marge Sud-Est à Djibouti (*Le Gall et al.* 2011). La série Stratoïde y est déformée par des failles normales à pendage NNE en direction du bloc Danakil. L'architecture des laves est celle d'un monocline flexuré en direction du centre de la dépression lors d'un épisode extensif à 3-1 Ma (Fig. 8, droite).

Alternativement, *Ghebreab et Talbot,* 2000 observent en Erythrée et sur les abords des plateaux éthiopiens dans le socle à l'affleurement des failles normales à pendage vers le continent délimitant des blocs basculés en domino (Fig. 9). Ces blocs basculés sont situés sur des détachements qui s'enracinent jusque dans la croûte moyenne et qui contrôlent l'extension du bassin de la Mer Rouge. Le système de blocs basculés et de détachements est interprétés comme s'étant développé après la flexure monoclinale des plateaux érythréens. La différence majeure avec les marges en Ethiopie se situe dans le fait que l'on n'observe pas de produits magmatiques éruptés au-dessus des trapps, suggérant que l'extension dans ce bassin se fait de manière plus amagmatique qu'en Afar Central.

Il n'y a pas de consensus aujourd'hui pour décrire le style structural de rifting précoce en Afar (voir les différences entre les figures 8 et 9). Le modèle de détachement est établi dans une zone faiblement magmatique *a priori,* et les modèles de flexure crustale sont restreints à des épisodes qui ne couvrent pas la totalité des 30 Ma de l'histoire du rifting. Il est difficile d'établir une chronologie complète des étapes de déformation car les formations syn-rift précoces sont recouvertes par les *flood basalts* de la série Stratoïde ou sont érodés, ou bien l'histoire plus tardive relative à l'ouverture de l'Afar sont inaccessibles car masquées par les dépôts alluviaux quaternaires.

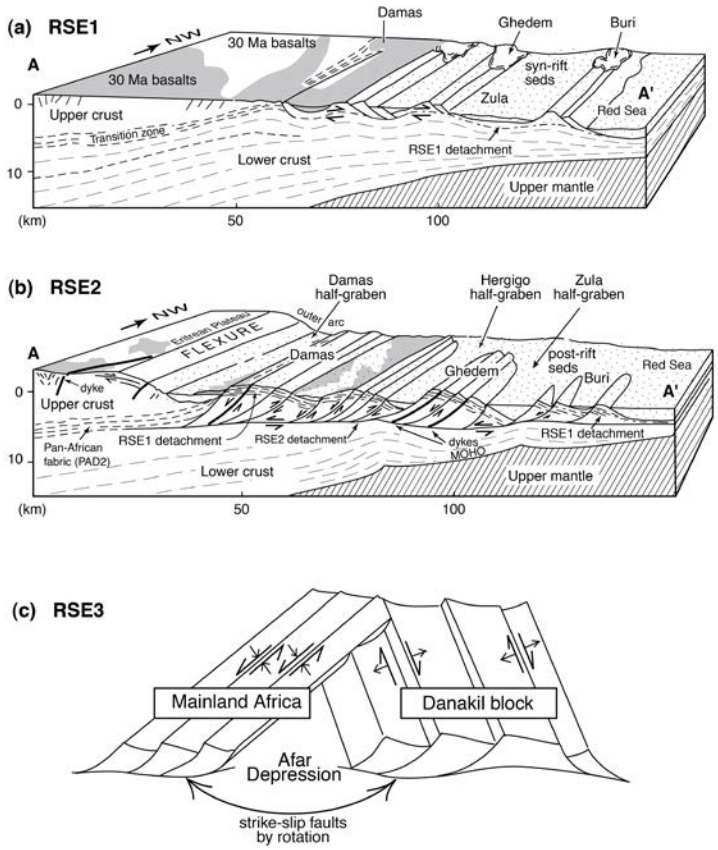

*Figure 9. Modèles structuraux de la croûte érythréenne. a) Des failles en domino se développent au dessus d'un détachement qui produit des core complexes. b) Rotation des blocs en réponse au jeu d'un second détachement à vergence opposée. Flexure monoclinale des plateaux. c) développement de failles transformantes pendant l'ouverture du bassin (*Ghebreab et Talbot, *2000).*

2.4.2. Le développement d'une TOC

La présence de croûte transitionnelle fortement intrudée sous l'Afar est un indicateur que la région se trouve proche être proche de la transition océan-continent. Les rapports Vp/Vs ≈ 2 sont caractéristiques de la présence de magma dans la croûte. Ceci est confirmé par la présence de chambres magmatiques en sub-surface (*Pagli et al.,* 2012). De plus, les épaisseurs de croûte sont incompatibles avec les taux d'extension de $\beta = 3$ prédits par les modèles de reconstruction de plaques (*Eagles et al.,* 2002 : *Redfield et al.,* 2004) et de rifting classique ($\beta = 1.7$ observés par fonction récepteur et gravimétrie). Cette incohérence apparente est interprétée comme étant due au sous-placage mafique sous la croûte qui induit un ré-épaississement pendant l'extension. Ce sous-placage correspond aux HVZ des marges volcaniques riftées.

Des études récentes (*Bastow et Keir,* 2011 ; *Keir et al.,* 2011b) mettent en évidence que l'amincissement crustal du Sud au Nord des Afars est accompagné par la mise en place de volumes basaltiques depuis le Quaternaire, notamment aux segments de l'Erta'Ale, Manda Inakir, Manda Hararo (Fig. 10). Cet épisode d'amincissement correspond selon les auteurs à un épisode récent de décompression sous la région. L'amincissement et l'extension lithosphériques sont ainsi contrôlés par l'injection de magma dans la croûte et la décompression adiabatique de celui-ci : lorsque suffisamment de magma a été intrudé et que la lithosphère a été chauffée et amincie se produit un épisode éruptif dont les flots volumineux de basaltes seraient comparables aux SDR. La croûte inférieure est alors déformée ductilement tandis que

la croûte supérieure est déformée mécaniquement par des failles. La topographie diminue du fait de la subsidence. Le modèle décrit donc :

1) une phase d'intrusion et d'extension magmatique sans amincissement. La croûte inférieure est constamment ré-épaissie et, à force d'intrusion de dykes, gagne des caractéristiques des croûtes transitionnelles observées aux marges volcaniques matures.

2) Une phase d'extrusion ou l'extension, exercée continuellement, se manifeste sous la forme de séismes et de la création de failles normales. La croûte inférieure peut s'amincir sans être ré-épaissie par la fusion partielle.

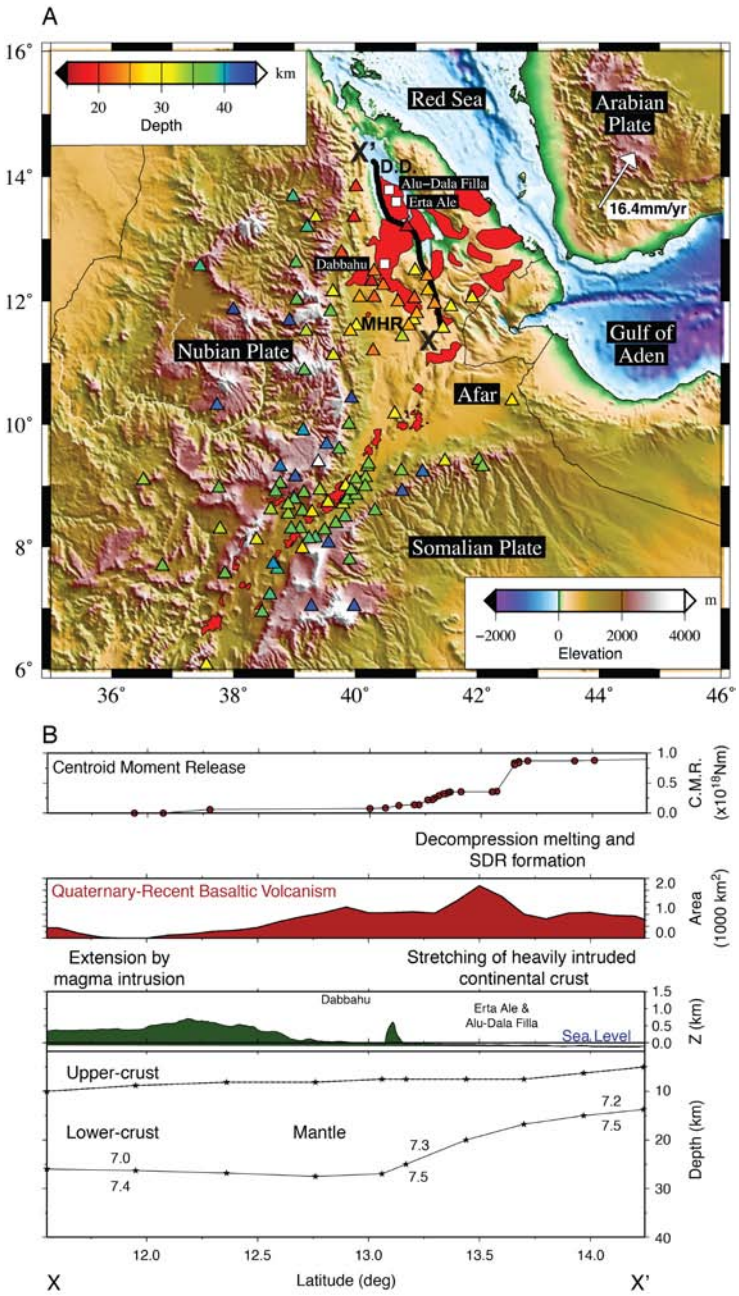

*Figure 10. (*Keir et al., *2011) A : Topographie de l'Afar. Triangle de couleur : épaisseur crustale (*Hammond et al., *2011). En rouge : volcanisme quaternaire. La ligne noire représente le profil X-X' utilisé sur la figure du bas. B : Cette figure montre l'augmentation du volume du volcanisme quaternaire exposé à la surface (en rouge), la topographie (en vert) l'augmentation vers le Nord de l'énergie relâchée par les séismes. Les épaisseurs crustales sont reportées sur le profil du bas. On notera que la croûte supérieure reste à épaisseur constante tandis que la croûte inférieure s'amincie et présente des vitesses comparables à celles d'une croûte transitionnelle.*

3. Démarche générale de la thèse

Ainsi, nous avons montré que les études les plus récentes sur l'Afar n'envisagent jamais cette zone dans un cadre global. L'Afar est étudié et décrit tantôt à l'échelle des plus petits objets qui le composent – sous l'angle de la formation de la flexure au niveau local (i.e. *Wolfenden et al.,* 2005 ; *Le Gall et al.,* 2011), ou sous celui de la formation des axes actifs discrets dans le temps et l'espace (*Field et al.,* 2012 ; *Medynski et al.,* 2013 ; 2015) ; tantôt en en se basant sur sa structure actuelle pour étudier les phénomènes de panaches mantelliques (i.e. *Montelli et al.,* 2006 ; *Li et al.,* 2008., *Hammond et al.,* 2013., *Civiero et al.,* 2015) ou la formation de la croûte transitionnelle (e.g. *Hammond et al.,* 2011) mais en laissant de côté son histoire tectono-magmatique complète. Ainsi, afin de pouvoir examiner et interpréter la formation de l'Afar en tant qu'analogue à la formation des marges volcaniques, il nécessaire de comprendre les *interactions tectono-magmatiques précoces* pendant l'histoire Mio-Pliocène du rift. Les problèmes sont les suivants :

Le calendrier de la déformation est cryptique en Afar, du fait que l'on a rarement accès à l'histoire Miocène précoce du rifting. Précisément, on ne sait pas quand et comment se fait l'amincissement crustal, et quel est son lien avec les flexures topographiques observées sur la marge ouest et à Djibouti. De fait, on ignore comment la déformation est distribuée pendant ces phases précoces.

Le lien entre cette histoire tectonique et les grands jalons de l'histoire magmatique est également mal compris. Comment le magmatisme au Miocène est-il lié aux premières phases de la divergence ? Quelle est la signification de la série Stratoïde par rapport à l'amincissement crustal observé en Afar ? Par quel biais et à quel moment du rifting la déformation et l'activité magmatique sont-elles localisées aux axes actifs ? Quelle est la signification du break-up dans ce contexte ?

Enfin, on ne connaît pas l'incidence de l'interaction du panache Afar avec la lithosphère sur cette histoire tectono-magmatique. Quel est le timing de l'amincissement lithosphérique par rapport celui de l'amincissement crustal ? Quel rôle a la lithosphère dans le développement structural du rift et dans la mise en place des grands volumes de magmas ?

Pour répondre à ces questions, nous articulerons cette thèse autour d'un segment d'importance, le segment de l'Afar Central (Fig. 5). Nous nous focaliserons dans un premier temps sur ce segment pour deux raisons : **(1)** l'Afar Central présente l'intérêt d'être cylindrique, c'est-à-dire que les structures exposées depuis le bord du plateau jusqu'à l'axe de Manda Hararo sont subparallèles (Fig. 5). Ceci est particulièrement important en contexte de point triple, puisqu'un segment cylindrique est l'assurance que les structures observées ne résultent pas d'un « mélange » entre deux rifts concurrents qui se surimposeraient l'un à l'autre. **(2)** L'Afar Central présente des zones épargnées par la série Stratoïde, et non-érodées par

les rivières qui coulent depuis les plateaux éthiopiens. Cela veut dire que les structures précoces sont accessibles à l'observation. Nous présentons une approche double centrée autour de l'Afar Central :

La première approche est une caractérisation au niveau du segment de rift cylindrique de l'Afar Central (a) du calendrier de l'extension et du style structural de la croûte, ce qui fera l'objet du **chapitre 3**, et (b) de la réponse mantellique associée à cette extension, ce qui fera l'objet du **chapitre 4**.

La seconde approche, objet du **chapitre 5**, est une contextualisation des résultats des chapitres précédents à l'échelle du système Afro-Arabe afin de documenter l'effet de la segmentation des rifts. Une fois les évolutions respectives de la croûte et du manteau documenté dans un segment accessible et unique, nous comparerons celles-ci avec des données de littérature concernant les marges volcaniques de la Mer Rouge et du Golfe d'Aden, enrichies de linedrawings de coupes sismiques non publiées. L'objectif est de vérifier dans quelle mesure nos résultats sont extrapolables à plus grande échelle et de distinguer les différences de l'Afar avec des marges volcaniques plus matures, issues d'un contexte similaire d'extension au dessus d'un point chaud.

CHAPITRE 3
-
ÉVOLUTION TECTONO-MAGMATIQUE DE L'AFAR CENTRAL

- Ce chapitre est constitué d'une publication, actuellement sous presse à *Tectonics*. -

Modes of rifting in magma-rich settings: tectono-magmatic evolution of Central Afar

Martin Stab[1,2], Nicolas Bellahsen[1], Raphaël Pik[2], Xavier Quidelleur[3,4], Dereje Ayalew[5], Sylvie Leroy[1]

[1]Sorbonne Universités, UPMC Université Paris 06, CNRS, Institut des Sciences de la Terre de Paris (iSTeP), 4 place Jussieu 75005 Paris, France
[2]CRPG, UMR 7358, CNRS, Université de Lorraine, 15 rue Notre Dame des Pauvres, BP20, 54500 Vandoeuvre-lès-Nancy, France,
[3]Univ Paris-Sud, Laboratoire GEOPS, UMR8148, Orsay, F-91405, France,
[4]CNRS, Orsay, F-91405, France,
[5]School of Earth Sciences, Addis Ababa University, Addis Ababa, Ethiopia

Corresponding author: Martin Stab, mstab@crpg.cnrs-nancy.fr, CRPG-CNRS, 15 rue Notre Dame des Pauvres, BP20, 54500 Vandœuvre-lès-Nancy

Key points

- Divergence during the Mio-Pliocene was diffuse (magmatic wide rift).
- The Central Afar lower crust experienced magma-compensated thinning.
- Shear zones at mid-crustal levels may accommodate extension.

Abstract

Recent research in Afar (northern Ethiopia) has largely focused on the formation of the present-day ocean-continent transition at active segments (e.g. Manda Hararo). However, the Oligo-Miocene history of extension, from the onset of rifting at ~25 Ma to the eruption of the massive Stratoïd flood basalts at ~ 4 Ma, remains poorly constrained. Here, we present new structural data and radiometric dating from Central Afar, obtained along a zone stretching from the undeformed Oligocene Ethiopian plateau to the Manda Hararo and Tat'Ale active volcanic segments. Basaltic and rhyolitic formations were mapped in two key areas corresponding to the proximal and distal parts of a half-rift. We present a balanced composite cross-section of Central Afar, reconstructed using our new data and previously-published geophysical data on the crustal structure. Our main findings are: 1) Extension during the Mio-Pliocene corresponds to a 'wide rift' style of rifting. 2) The lower crust has been underplated/intruded and re-thickened during rifting by magmatic injection. 3) Our restoration points to the existence of mid-crustal shear zones that have helped to distribute extension in the upper crust and to localize extension at depth in a necking zone. Moreover, we suggest that there is a close relationship between the location of a shear zone and the underplated/intruded

material. In magma-rich environments such as Central Afar, break-up should be achieved once the initial continental crust has been completely replaced by the newly, magmatically accreted crust. Consequently, and particularly in Afar, crustal thickness is not necessarily indicative of break-up but instead reflects differences in tectono-magmatic regimes.

1. Introduction

Magmatism and extensional processes are fundamental to our understanding of the formation of rift basins and their potential evolution into continental passive margins and therefore tectonic plate boundaries. Interactions between tectonics and magmatism have been investigated at all scales, from the geodynamic reconstruction of plate motions to mid-oceanic ridges. The relationship between magma supply and continental extension (rifting) has received much attention. For example, localized magmatism can help focus extension [*Buck,* 1991; *Ebinger et al.,* 2013] whereas disperse magmatism appears to distribute extension [*Corti et al.,* 2003], magma supply can facilitate rifting of the lithosphere in the absence of sufficient tectonic force [*Buck et al.,* 2004, 2010; *Buck,* 2006] and dyking and underplating appear to accommodate divergence without involving significant normal faulting [i.e. *Grandin et al.,* 2010]. Thus, tectono-magmatic interactions play a significant role in shaping rift basins and rifted passive margins. Given the various rift structures documented in the literature, it is essential to improve our understanding of rheology, i.e., the structural and thermal evolution of the lithosphere. The simple idea of stretching and thinning a lithosphere to 0 km [*McKenzie,* 1978] no longer holds as geological observations made in the past few decades have highlighted a considerable degree of complexity. Rifts may be narrow or wide and magma-poor or magma-rich, and the lithosphere may initially be thin and hot or old and cold [e.g. *Buck,* 1991, *Brun,* 1999]. While analog and numerical simulations can handle many of these rheological parameters and therefore provide important constraints on rifting processes, the effects of magma supply on rheology, and hence on the structural style of a passive margin, remain largely unknown.

Magmatism at nascent passive margins is dependent on the state of the underlying mantle. In Large Igneous Provinces (LIP), the huge eruptions of Continental Flood Basalts (CFB) are commonly related to mantle-scale thermal anomalies known as mantle plumes. The origin of mantle plumes is a subject of intense debate in the literature and will not be discussed in this paper. Nevertheless, mantle plumes are thermal anomalies, sometimes originating from the deep mantle, that trigger adiabatic melting and bring magma to the surface. The existence of such thermal anomalies may be unrelated to any other pre-existing tectonic process in continental [*Courtillot et al.,* 1999] and more often in oceanic settings [*Le Bas,* 1987]. As such, plumes could be a pre-rift feature [*Courtillot et al.,* 1999; *Hoffman et al.,*

1997] or they may be superimposed on the earlier tectonic history [*Ziegler et al.,* 2001; *Nikishin et al.,* 2002; *Ziegler and Cloething,* 2004; *Geoffroy,* 2005]. In volcanic passive margins, the eruption of massive flood-basalt prisms, tilting toward the ocean and controlled by continent-facing normal faults (the so-called seaward dipping reflectors or SDR), is related to the syn-rift, or the syn-breakup history of the margin [*Hinz,* 1981; *Mutter et al.,* 1982; *Coffin and Eldholm,* 1994; *Menzies et al.,* 2002; *Geoffroy et al.,* 2005; *Franke,* 2013; *Quirk et al.,* 2014]. This raises the question of whether magmatism during margin development necessitates the existence of a plume-type thermal anomaly or if it might instead be the consequence of processes related to lithospheric thinning, such as adiabatic decompression [*Van Wijk et al.,* 2001], small-scale convection in the mantle [*Anderson*, 1994; *Huismans et al., 2001; Ballmer et al.,* 2007], lateral rifting diachronism controlled by transform zones [*Koopmann et al.,* 2014b], pre-CFB thinning [*Armitage et al.,* 2009] or modification of the mantle's fertility by delamination [e.g. *Anderson et al.,* 2005]. A margin can sometimes be of sedimentary rather than volcanic nature, even if it is located close to a contemporaneous CFB province at the time of rifting [*Franke et al.,* 2013]. There therefore appears to be a complex spatial and temporal relationship between plume-generated magmatic provinces and volcanic passive margins, and the simple notion of purely 'active' and 'passive' rifting of *Sengör and Burke* [1978] can no longer be applied in explanations of margin formation.

Volcanic passive margins should therefore be considered in the context of their main two, closely related, features. (1) The first of these are the tectonic structures. Extension and thinning of the lithosphere is recorded by syn-rift structures, such as tilted blocks in the proximal margin and detachments in the most distal parts that, along with the SDR, form the ocean-continent transition (OCT) (*Péron-Pinvidic et al.,* 2013). These two types of structural feature are well documented at magma-poor margins and in continental rifts, and are linked to the tectonic history. (2) The second key feature of the volcanic passive margin is magmatism. Magmatic activity at volcanic passive margins is expressed by the eruption of CFB and emplacement of SDR. These are sometimes superimposed on an earlier phase of tectonic activity and associated with high velocity lower crust imaged by seismic refraction, seismology, gravimetry and magnetism [e.g., *Ahmed et al.,* 2013]. This high velocity lower crust is primarily interpreted, among other possibilities, as mafic underplating of the thinned crust [*White et al.,* 2008; *Thybo and Nielsen*; 2009; *Thybo and Artemieva,* 2013]. Extrusive and intrusive magmatism both constitute new transitional crust, which is commonly observed in geophysical studies [*Holbrook et al.,* 2001; *White et al.,* 2008; *Mjelde et al.,* 2009; *Voss et al.,* 2009; *Thybo and Nielsen,* 2009]. However, investigating the transitional crust involves further issues. First, the SDR commonly act as an observational mask in geophysics. Seismic waves are often reflected on the SDR, making it impossible to observe the underlying OCT-related structures. Second, the accretion of transition crust during rifting involves a certain degree of syn-rift

magma-compensated thinning, making it difficult to establish a sound balanced cross-section [*Geoffroy et al.,* 2005]. Thus, a current issue regarding volcanic passive margins is to be able to distinguish between tectonic stretching and thinning and magmatic underplating. Third, the rheological effects of magmatic underplating remain poorly constrained.

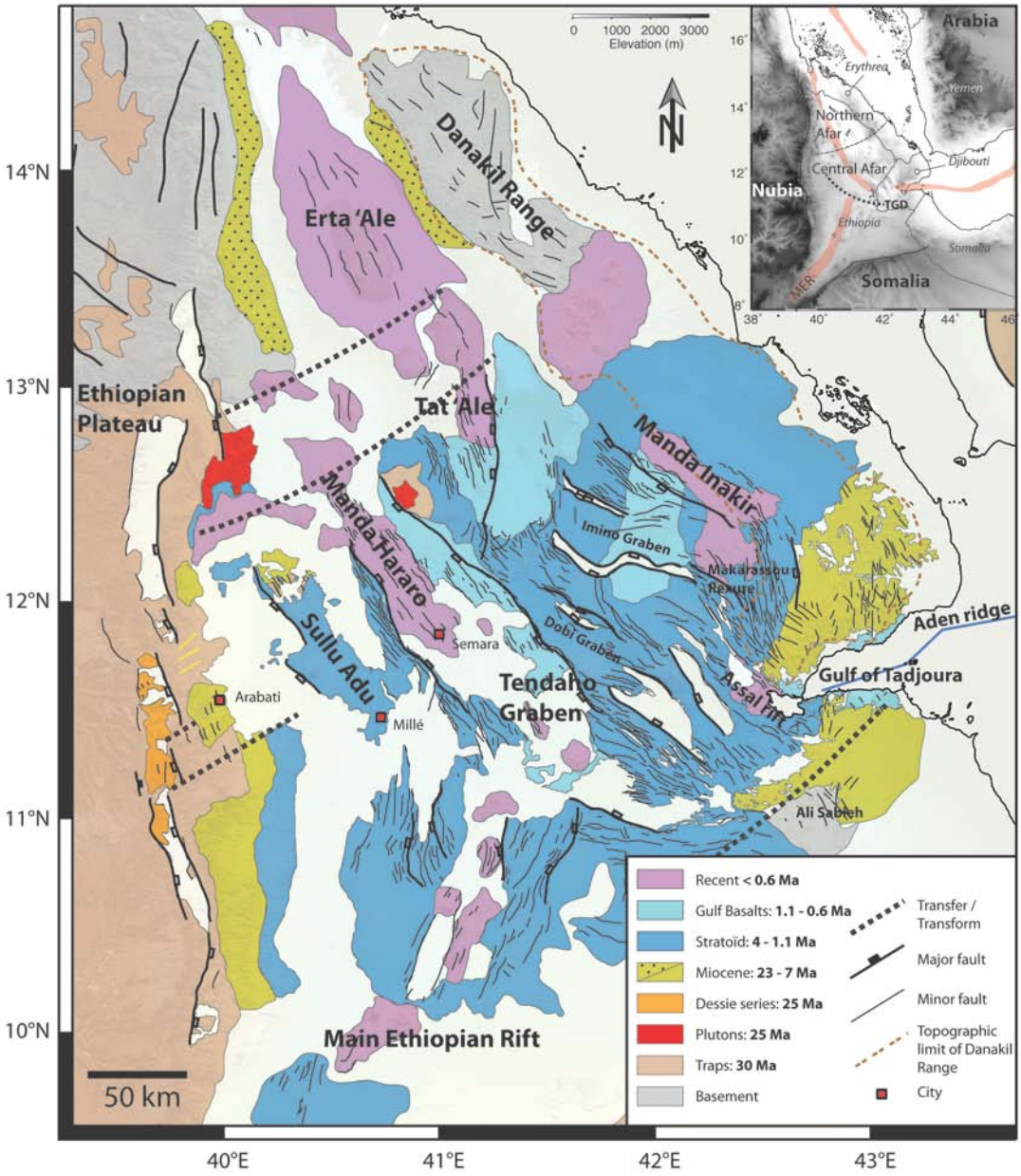

Figure 1. Structural map of the Afar Depression, modified from Varet [1978] and Wolfenden et al. [2005] for the southwestern marginal part (south of Arabati), from Le Gall et al. [2014] for Djibouti, and from Kidane et al. [2003] for Tendaho Graben. Datum: WGS84. Grey = basement rocks (undifferentiated, crystalline or cretaceous limestones). Brown = Traps series, pre-rift. Red = plutonic/ intrusive rock (Limmo massif and Affara Dara massif, see Fig. 2A). The orange unit (Dessie series) is defined as the ca. 25 Ma basaltic series found in the present-day Marginal Graben

and absent in the Afar depression, documented by Ukstins et al. [2002]. The yellow unit, labeled 'Miocene', represents the volcanic sequence described in this study, as well as other Miocene formations (e.g. the Mabla and Dahla formations, Djibouti). The dotted yellow unit in the Erta'Ale segment represents the Red Beds series [Varet, 1978], which are sedimentary deposits, possibly Miocene in age. The blue unit is the mainly basaltic Stratoïd formation whereas the light blue unit corresponds to the Gulf Basalts as redefined by Kidane et al. [2003]. Recent lavas are restricted to active segments and are shown in purple. Quaternary infill is shown white. See text for more details of the volcano-stratigraphy. The grey dotted lines are transforms. The thick dotted line is the Tendaho Goba'ad Discontinuity (TGD), which marks the change from Red Sea- oriented to MER-oriented structures [Harding et al., 1990; Hayward and Ebinger, 1996]. The thin brown double-dotted line represent the contour of the Danakil block as described in the literature [Eagles et al., 2002]. Major faults are defined as faults with throws > 100m.

To address these three key issues, we have investigated extension and magmatism in the Afar Depression - a magmatic rift that has not yet reached the break-up stage. This locality presents several advantages, in particular the fact that there are no thick volcanics masking the syn-rift structures because the rift has not yet reached break-up (although it is probably close to it; see *Hammond et al.* [2011]). The Afar Depression extends from the Ethiopian plateau to the magmatic active segments that define the plate boundary between the Nubian and Arabian plates (Fig. 1). Rifting in Afar began during the Oligocene, soon after the impingement of the Afar mantle plume and the subsequent eruption of the Ethiopian large igneous province at around 30 Ma [*Hofmann et al.,* 1997]. Seismic studies show the presence of a broad mantle anomaly rooted at the core-mantle boundary [*Ritsema and Allen*, 2003; *Simmons et al.,* 2007; *Bastow et al.,* 2008; *Li et al.,* 2008; *Ritsema et al.*, 2011], and the Afar rift is therefore considered an example of rifting following impingement of a plume-like thermal anomaly. The Afar rift system (Fig. 1) has been interpreted as an asymmetric rift, analogous to SDR, where strain and magmatism have migrated toward the rift center and play a major role in dyking [*Ebinger and Casey,* 2001; *Wolfenden et al.,* 2005], or alternatively, as a detachment-dominated rift [*Ghebreab and Talbot.* 2000; *Geoffroy et al.,* 2014]. The relationship between normal faulting, dyking and low-angle faults therefore remains unclear.

We present new structural observations and mapping, along with (U-Th-Sm)/He and K-Ar ages of the volcanic record of Central Afar. We use this new set of data alongside published geophysical data (receiver functions and wide-angle controlled source imaging) to construct a composite balanced cross-section of Central Afar, stretching from the Ethiopian Plateau in the west to the active segments of Manda Hararo and Tat'Ale (Fig. 1). We document the extension and thinning of this rift segment and then discuss their significance in the light of relevant observations

about the state of the mantle from previous studies in order to unravel the structural style of the future margin. We also discuss a number of problems concerning the distribution of volcanism in relation to rift segmentation. Finally, we compare Central Afar to other volcanic passive margins and discuss the process of SDR accretion and the significance of break-up in magma-rich settings.

2. Geological setting

2.1. Present-day extension and strain accommodation

In this paper, Central Afar is defined as the broad zone of rifting that extends from the Ethiopian plateaus to the Gulf of Tadjoura (see Fig. 1 and 2). We have named the topographic margin [e.g., *Wolfenden et al.,* 2005] the 'Western Afar'. Active volcanic segments mark the boundary between Nubia and Arabia (Fig. 1), which separated during oblique rifting in the Red Sea and Gulf of Aden, which can be linked to the convergence of Arabia on Eurasia [e.g., *Bellahsen et al.,* 2003; *ArRajehi et al.,* 2010; *Leroy et al.,* 2012; *Faccenna et al., 2013*]. GPS measurements constrain the NNE motion of Arabia with respect to Africa [*McClusky et al.,* 2010] and show that the strain shifts gradually south of 16°N from the Red Sea to the Afar and is totally accommodated in the Afar at 13°N. South of 13°N, the NW-SE-trending rift structures of the Afar are truncated by roughly N-S-trending faults of the Main Ethiopian Rift along the Tendaho Goba'ad Discontinuity (TGD) [*Harding et al.,* 1990; *Hayward and Ebinger,* 1996, see Fig. 1]. Plate reconstruction models predict a total extension factor of ß > 3 in Central and Southern Afar, assuming that the Danakil block (Fig. 1) is a separate microplate [*Eagles et al.,* 2002]. However, although the pre-rift structures are poorly documented, especially on the Danakil block, Jurassic limestones with tilts of 50-60° have been identified on the Danakil block [*Morton & Black*, 1975], suggesting high amounts of extension.

These high ß factors have been accommodated by the migration of strain from major border faults toward narrow strips of active deformation in the rift center [*Wolfenden et al.,* 2005]. Later studies have suggested that such localization, from the rift border to narrow segments controlled by dyking, can be expected when the lithosphere becomes sufficiently weak [*Corti et al.,* 2003]. In Central Afar, however, the strain is accommodated over a wide zone. *Kogan et al.* [2012] have shown that 90% of the present-day strain is accommodated over a broad strip of 175 km width. This strain pattern may be due to the presence of a weak mantle beneath the Afar [*Kogan et al.,* 2012], to complex interactions between propagating rift systems in the area [*Pagli et al.,* 2014] or to the presence of a faulting-dominated system [*Hammond et al.,* 2011*; Keir et al.,* 2013; *Pagli et al.,* 2014].

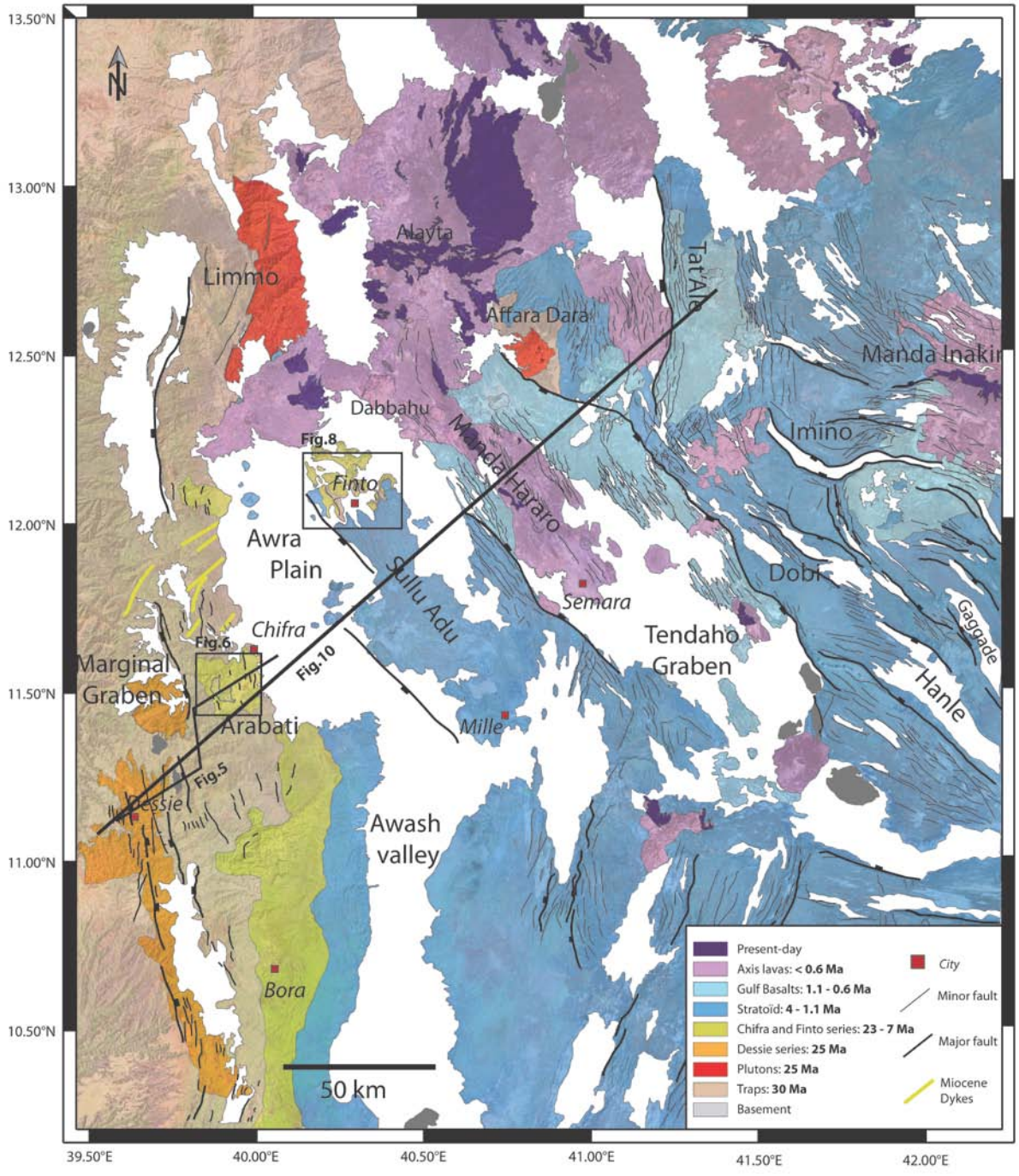
13.50°N
13.00°N
12.50°N
12.00°N
11.50°N
11.00°N
10.50°N
39.50°E
40.00°E
40.50°E
41.00°E
41.50°E
42.00°E
N
Alayta
Limmo
Affara Dara
Tat'Ale
Manda Inakir
Dabbahu
Manda Hararo
Imino
Fig.8
Finto
Awra
Plain
Sullu Adu
Semara
Dobi
Gaggade
Chifra
Fig.6
Fig.10
Tendaho
Graben
Hanle
Marginal
Graben
Arabati
Mille
Fig.5
Dessie
Awash
valley
Bora
50 km
Present-day
Axis lavas: < 0.6 Ma
Gulf Basalts: 1.1 - 0.6 Ma
Stratoïd: 4 - 1.1 Ma
Chifra and Finto series: 23 - 7 Ma
Dessie series: 25 Ma
Plutons: 25 Ma
Traps: 30 Ma
Basement
City
Minor fault
Major fault
Miocene
Dykes

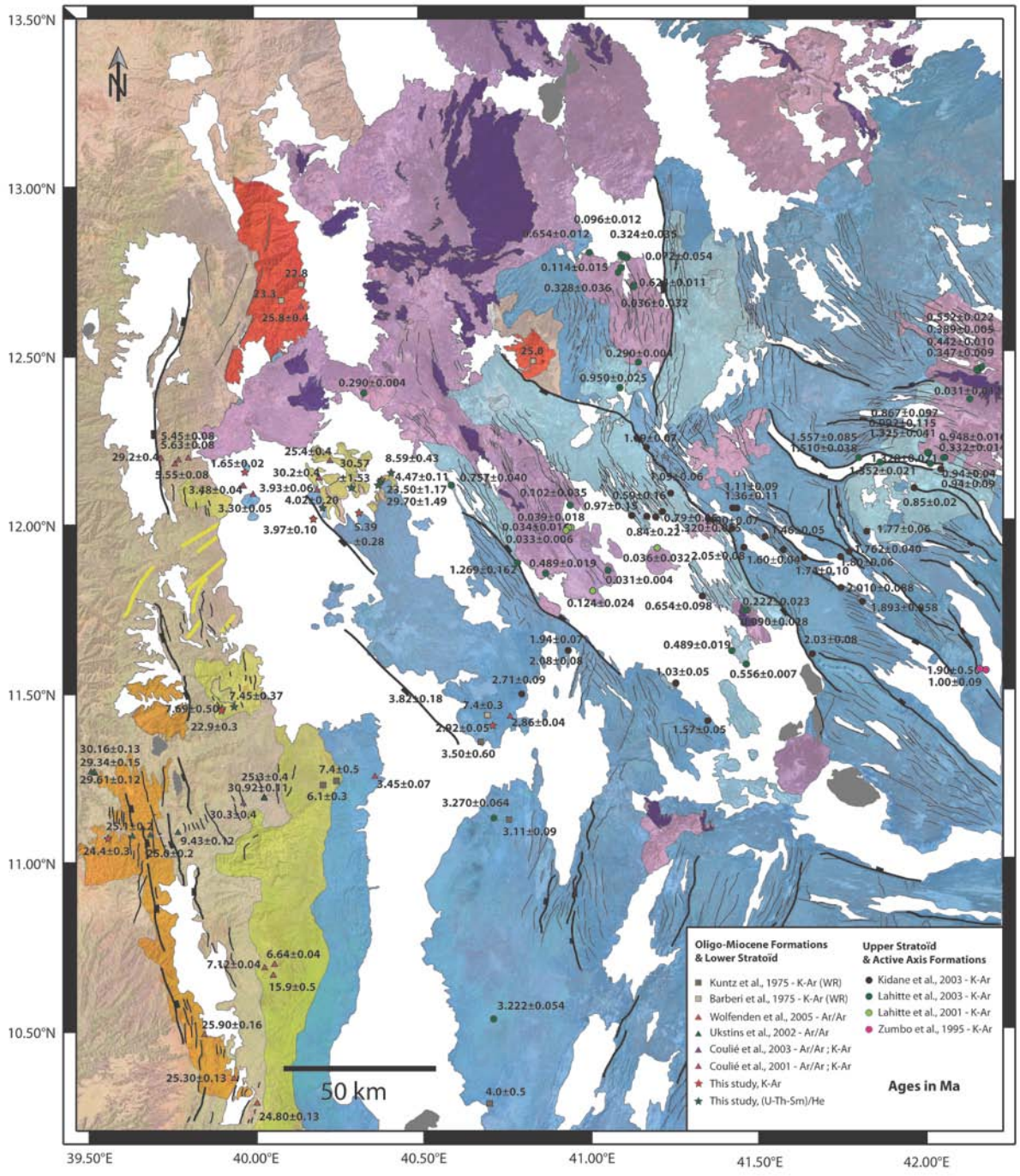

Figure 2. A. Zoom on the Central Afar, Ethiopia. Datum WGS84, projection UTM 37N. Same color code as used in Figure 1. Structures mainly trend NW-SE in the study area so the area investigated is a near-cylindrical half-rift. Black rectangles outline the two key study areas (Arabati, Fig. 6; and Sullu Adu, Fig. 8). The thin black line (labeled Fig. 5) indicates the location of the Arabati cross-section. The thick black line marks the NE-SW trending composite cross-section (Fig. 10). Note the overall SW dip of major faults. B. Compilation of age data from the literature and from this study (same area as Fig.2A). Ages (in Ma) were mostly determined by K-Ar and Ar/Ar methods, except for data from this study ((U-Th-Sm)/He and K-Ar). See legend for sources of published ages. WR = Whole Rock age (analysis was

not performed on separated minerals). Although WR ages should be treated with caution, they nevertheless show a good agreement with more recently-published data.

2.2. Mantle beneath Ethiopia

The mantle beneath Ethiopia is hotter than normal [*Benoit et al.,* 2006; *Rooney et al.,* 2012b]. Seismic tomography studies show a broad low P-wave velocity anomaly of 3% in the mantle beneath Ethiopia, which is rooted at a depth of ~500 km [*Li et al.,* 2008]. This anomaly is thought to be the expression of the Afar plume, which was responsible for the extensive magmatism during the Oligocene in Ethiopia [*Baker et al.,* 1996a, b; *Marty et al.,* 1996; *Hofmann et al.,* 1997, *Pik et al.,* 1999, 2006] and in Yemen [*Baker et al.,* 1996a,b], as well as for the dynamic topography that characterizes the Ethiopian, Somalian and Yemeni plateaus [*Daradich et al.,* 2003*; Pik et al.,* 2008; *Stamps et al.,* 2010]. This low velocity anomaly eventually connects with the Afar crust (at ~50 km depth, the limit of resolution) through narrow paths of channelization rather than a diffuse zone [*Hammond et al.*, 2013a]. This argues against the presence of a plume-head in the present day and the magma ascent is therefore best explained by passive upwelling in response to lithospheric thinning [*Rychert et al.,* 2012]. However, numerical modeling of the PT conditions necessary for the eruption of present-day basalts [*Ayalew & Gibson*, 2009; *Rooney et al.,* 2012b; *Ferguson et al.,* 2013b] has shown that the Ethiopian mantle remains hot today, with an anomaly of +150°C, and that partial melting occurs at depth of ~80 km, even though the mantle beneath Ethiopia is one of the coolest of the world's continental and oceanic magmatic provinces [*Rooney et al.,* 2012b]. The Ethiopian mantle is also characterized by some of slowest seismic velocities on Earth. P wave velocities decrease from the classic mantle velocity (Vp) of 8.0 km/s, characteristic of the MER, and then level off to a slower velocity of 7.4 km/s, characteristic of anomalously hot mantle, beneath the Afar [*Bastow & Keir*, 2011]. *Kogan et al.* [2012] have shown that a substantial part of the lithospheric strength is borne by the lithospheric mantle beneath East Africa. Long period surface wave dispersion shows that this mantle thins beneath the Afar, from 100 km under the MER to less than 30 km [*Pasyanos et al.,* 2009]. *Dugda et al.* [2007] argue for the possible absence of lithospheric mantle beneath the Afar on the basis of the absence of a lithospheric mantle lid in their observations.

2.3. Nature of the crust, magma intrusions and underplating

Debate surrounding the nature of the crust, and whether it is of stretched and intruded continental nature (transitional crust) or is already oceanic crust, has been ongoing since the early work of *Berckhemer et al.* [1975]. Magnetic anomalies analogous to those of mid-oceanic ridges have previously been observed in Afar [*Bridges et al.,* 2012], and ridge-like organization of the magmatic plumbing system, with on-axis and off-axis reservoirs, has been described in the Manda Hararo segment

[*Medynski et al.,* 2013]. Magma-assisted rifting has also been reported in the MER and Afar, where a shift occurs from fault-accommodated extension to dyke injection-accommodated extension at the active segments [*Grandin et al.,* 2010b; *Ebinger and Casey,* 2001; *Ebinger et al.,* 2005]. *Casey et al.* [2006] argues for oceanic-type extension. However, recent trace element modeling of basalts from MER Pliocene-Quaternary lavas [*Rooney et al.,* 2014a] and isotopic data from the Miocene shield on the plateau adjacent to the MER [*Rooney et al.,* 2014b] suggest that the magma associated with rifting is derived from melting of phlogopite and amphibolite-bearing mantle. Furthermore, they suggest that the oldest magnetic stripes recorded in the lavas may in fact reflect intrusions into continental crust that strike parallel to the structures and these should not be confused with oceanic-like intrusions.

Magma chambers are present at shallow depth beneath Alu Dallafilla volcano (at ~1 km depth) [*Pagli et al.,* 2012] and Dallol volcano (at 1-2 km depth) in the Erta'Ale segment, [*Nobile et al.,* 2012]. A deeper magma reservoir, containing up to 13% melt fraction and 30 km wide and 35 km deep, has been identified beneath Manda Hararo [*Desissa et al.,* 2013] (Fig. 1). Vp/Vs ratios of 1.9 to 2.1 under the Manda Hararo/Sullu Adu zone (Fig. 2) point towards the presence of partially molten mafic material in the crust [*Hammond et al., 2011*; *Dugda et al.,* 2005]. Such high ratios imply the presence of fluids that are interpreted as partial melting stored in the crust [e.g. *Ahmed et al.,* 2013; *Korostelev et al.,* 2014]. A high velocity lower crustal layer (Vp = 7.2-7.4 km/s) has been identified documented beneath the shoulder of the MER but not beneath Afar. However, the lower-crust velocity under the Afar increases from 7.0 to 7.4 beneath Erta'Ale [*Bastow and Keir,* 2011]. High velocities like these may be characteristic of mafic underplating [*Thybo and Artemieva,* 2013], but unfortunately, an insufficient number of across-strike seismic refraction profiles have been acquired to confirm the existence of a high velocity body under Afar or to constrain its spatial distribution. However, gravity modeling has shown that the crust must contain high density (3000 g/cm^3) mafic rocks in both the lower crust and the mantle in order to fit the observed prominent positive Bouguer anomalies [*Tessema and Antoine,* 2004].

2.4. Crustal thinning

The thickness of the crust has been well constrained by receiver function computations and decreases from 35-40 km under the Ethiopian plateau to ~25 km under Central Afar and ~18-15 km under Northern Afar (Erta'Ale) [*Hammond et al.,* 2011; *Reed et al.,* 2014]. *Hammond et al.* [2011] identified sparse, 30-km-thick slivers of crust under Afar (under Tendaho graben, Figs. 1 and 2, for example), which they interpreted as remnants of less-stretched continental crust. However, more recently, Reed et al. [2014] applied a correction for the strong reflective phase of quaternary sediment infill in the Tendaho Graben and concluded that was actually only 20 to 18 km thick, giving an overall thinning factor (ß) of 2.0-2.2.

The thickness of the upper crust decreases from 22-25 km under the Ethiopian plateaus [*Makris and Ginzburg*, 1987; *Maguire et al.,* 2006] to ~7 km beneath the Sullu Adu area (SW Manda Hararo, see Fig. 2) (inverse modeling of receiver function data [*Hammond et al.,* 2011]) and ~10 km under most of Central Afar (seismic refraction profiles in *Berckhemer et al.* [1975]). The lower crustal thickness seems to remain about the same beneath the plateaus and Central Afar, but thins abruptly under Erta'Ale. On the basis of modeling of dyking-accommodated extension, crustal thickness and recent volcanism, *Bastow and Keir* [2011] argued that Erta'Ale is at a more advanced stage of rifting than Central Afar.

The equivalent elastic thickness of the lithosphere under Afar is ~6 km [*Ebinger and Hayward,* 1996; *Perez-Gussinyé et al.,* 2009]. This is thought to represent the upper crust as the strength of the mantle lithosphere beneath the rifted region is negligible [*Perez-Gussinyé et al.,* 2009], or has a low thickness (with a lithospheric lid at $\leq$ 50 km depth; *Dugda et al.* [2007]). The seismogenic layer is ~7-9 km thick under Afar but 25-30 km thick under the plateaus [*Craig et al.,* 2011]. These thicknesses are consistent with those of the early magnetotelluric study of *Berktold et al.* [1975], which used the electrical properties of rocks to set the depth of brittle/ductile transition at around ~6 km under Afar after determining a mean geothermal gradient of ~60°C/km. Under the plateaus, the long-term geothermal gradient is 35-38°C/km, as constrained by U-Th/He thermochronometry [*Pik et al.,* 2003].

2.5. Stratigraphy and volcano-tectonic history

In this paper, the term syn-rift is used to describe rocks that were emplaced after the onset of extension in the area. Thus, even though the term is traditionally used to describe sequences that show syn-tectonic features (such as growth strata, extensional fans, etc.), it is used only in the temporal sense here.

Rifting in northeast Africa began during the late Eocene-early Oligocene in response to closure of the Tethyan Ocean [e.g., *Bellahsen et al.,* 2003]. Rifting began at 26 Ma in the central and southern Red Sea [*Baker et al.,* 1996a; *Ukstins et al.,* 2002], after 29 Ma in the Afar [*Ukstins et al.,* 2002; *Wolfenden et al.,* 2005] and at around 34 Ma in the Gulf of Aden [*Leroy et al.,* 2012 and references therein]. Oceanic spreading in the Gulf of Aden [*d'Acremont et al.,* 2010; *Leroy et al.,* 2012] began at around 18 Ma. Divergence between Somalia and Nubia began at around 11 Ma with the formation of a triple junction and opening of the MER [e.g., *Wolfenden et al.,* 2004; *Corti*, 2009].

A regional continental flood basalt episode occurred in the Oligocene prior to the onset of any significant extension [*Pik et al.,* 1998]. The bulk volume eruptions took place between 31 and 29 Ma [*Hofmann et al.,* 1997; *Rochette et al.,* 1998; *Coulié et al.,* 2003]. The Trap Basalt formation overlies the older Jurassic sediments and Proterozoic basement. The Traps are also found in Ethiopia and Yemen [*Baker et al.,* 1996a; *Ukstins et al.,* 2002] and are a key feature of the Ethiopian plateaus. Trap

Basalts are also found elsewhere on the Afar floor, notably in the Affara Dara massif (Fig. 1, 2.) [*Barberi et al.,* 1975; *Mohr,* 1978; *Varet,* 1978] and near the Western Escarpment [*Morton and Black,* 1975; *Ukstins et al.,* 2002; *Wolfenden et al.,* 2004, 2005]. The Traps are usually referred to as 'pre-rift' structures as they predate extension.

During the Miocene, the cessation of flood basalt eruptions signaled a decrease in volcanic activity, at the same time as or shortly after the onset of extension in the region. Volcanic activity became mostly confined to large shield volcanoes on the plateaus [*Kieffer et al.,* 2004]. In Djibouti, the Miocene lavas have been assigned to the historical Adolei, Mabla and Dahla formations [*Varet,* 1978; *Barberi et al.,* 1975; *Audin et al.,* 2004] (Fig. 1, 4A). In Central Afar, Miocene volcanics are sparser [*Ukstins et al.*, 2002; *Wolfenden et al.,* 2005; *Coulié,* 2001] (Fig. 2). The Miocene record mainly consists of silicic series and no continuous record of volcanism has been mapped. Instead, in southern Afar, the volcanic units are separated by minor (<10°) angular unconformities [*Wolfenden et al.,* 2004, 2005], indicating minor extension accommodated by faulting (see Fig. 4). Further south, where the MER overprints the Afar structures, the angular unconformities become more pronounced [*Wolfenden et al.,* 2005].

A second pulse of flood basalt eruptions occurred during the Pliocene, beginning at around 4 Ma and with peak activity at around 2 Ma. With massive basaltic fissural eruptions that spanned the Afar floor, the Stratoïd formation covers 70% of the rift surface. Above the Stratoïd formation lie the Gulf Basalts, which were emplaced between ~1.1 Ma and 0.6 Ma [*Kidane et al.,* 2003]. Unlike the rest of the Stratoïd series, the Gulf Basalts erupted along silicic centers, most notably near the major south-east-dipping fault scarps of the Tendaho and Tat'Ale grabens (Fig. 1, 2). The Gulf Basalts were first mapped and described on each side of the Gulf of Tadjoura, where the Gulf of Aden has been propagating into the Afar since around 1 Ma [*Manighetti et al.,* 1998; *Audin et al.,* 2004].

Present-day magmatism in the Afar is focused in discrete active segments. Extension is primarily accommodated by dyke injection in the crust [*Wright et al.,* 2006, *Grandin et al.,* 2010]. Morphologically, the structure of the segments resembles that of oceanic ridges [*Hayward and Ebinger,* 1996, *Medynski et al.,* 2013, 2015] but the segments have formed within a transitional crust [*Hammond et al.,* 2011]. They are therefore generally considered to be features indicative of the imminent break-up in Afar and are thought to represent the ocean-continent transition [*Medynski et al.,* 2013], which is characterized by strong segmentation, rapid emplacement, and discrete spatial distribution.

2.6. Synthesis and main objective

The Oligocene Traps and recent/active magmatic centers and faults have been comprehensively mapped and studied in the Afar [e.g., *Hofmann et al.,* 1997;

Rochette et al., 1998; *Pik et al.,* 1998, 1999, *Coulié et al.,* 2003, *Grandin et al.,* 2010; *Medynski et al.,* 2013, 2015; and references therein]. The lithospheric structure has likewise received considerable attention [*Ritsema and Allen*, 2003; *Simmons et al.,* 2007; *Bastow et al.,* 2008; *Li et al.,* 2008; *Pasyanos et al.,* 2009; *Ritsema et al.*, 2011; *Bastow and Keir,* 2011]. The Traps series have been linked to an early thermal mantle anomaly and the present-day magmatic centers have mostly been interpreted in the context of Gulf of Aden and Red Sea interactions that have taken place over the past few million years. However, the Mio-Pliocene tectonics and magmatism have received relatively little attention. Consequently, key constraints such as the amount of Cenozoic thinning/stretching and the ages and volumes of magma involved, are poorly quantified. As a result, the interactions between magmatism and tectonics could not be properly discussed so far, even though the Afar is a unique place to do so. In the following, we present our approach and the main results obtained on age constraints for magmatism and tectonic evolution.

3. Methods

3.1. Geochronology

In order to better constrain the age of the Mio-Pliocene volcanics and associated tectonic events, samples were collected between Central Afar and the Plateaus (Fig. 2b). Two methods were used to determine the geochronology: (U-Th-Sm)/He dating of zircons and apatites from rhyolites and K-Ar dating of basalt and rhyolite samples. These methods date the instantaneous cooling of the volcanics and therefore their age of emplacement.

3.1.1. K-Ar

Samples were prepared and analyzed at the GEOPS laboratory, Université Paris-Sud (Orsay, France). The Cassignol-Gillot method of K-Ar dating has already been used to determine a large span of ages in the Afar [*Lahitte et al.,* 2003a,b, *Coulié et al.,* 2003, *Kidane et al.,* 2003] and our new K-Ar ages are consistent with previously obtained Ar/Ar ages, notably those of *Ukstins et al.* [2002] and *Coulié* [2001]. The K-Ar data of this study are presented in Table 1.

After careful examination of thin sections in order to eliminate the most altered samples, rock samples were sawed, crushed and then sieved to obtain a homogenous fraction of typically 63-125 µm and 125-250 µm grain-size.

Because lava phenocrysts can crystallize prior to eruption or be inherited from the magma chamber, they may contain excess Ar that leads to erroneously old ages. Phenocrysts should therefore be discarded from the sample. Magnetic separation and heavy liquids were used to separate out the phenocrysts from the basaltic groundmass and plagioclase (in basalt) or sanidine (in rhyolite) microcrysts used for

dating. The end products of the separation process were basaltic groundmass of homogenous grain-size and a density of 3.05 to 2.95 g/cm^3, plagioclase microcrysts with densities of 2.79 to 2.75 g/cm^3 and sanidine microcrysts with densities of 2.57 to 2.54 g/cm^3. K and Ar were measured on several aliquots of each sample according to the Cassignol-Gillot technique [*Gillot and Cornette,* 1986]. K was measured by flame absorption spectrophotometry. ^{40}Ar and ^{36}Ar concentrations were measured simultaneously by mass spectrometry. The amount of radiogenic ^{40}Ar* in the sample was then obtained after correcting for atmospheric contamination using the ^{40}Ar/^{36}Ar isotopic ratio of an air pipette. Each K and Ar measurement was performed at least twice in order to ensure a relative standard deviation of less than 1% for any given sample.

The uncertainty assigned to each individual age was then calculated using:

$$\sigma_{age} = \sqrt{(\sigma_K)^2 + (\sigma_{Cal})^2 + (\sigma_{Ar*})^2} \quad [1]$$

where σ_{age} is the uncertainty in Ma, σ_K is the uncertainty in the K measurements (measurements were repeated on each aliquot until a relative standard deviation inferior to 1% was reached), σ_{Cal} is the uncertainty of the mass spectrometer calibration and is inferior to 1%, and σ_{Ar*} is the uncertainty in the determination of the quantity of atmospheric ^{40}Ar in the sample. The latter was determined by comparing the ^{40}Ar/^{36}Ar ratio of the sample with the ^{40}Ar/^{36}Ar ratio of a standard air-pipette under similar Ar pressure. Sample AF13-98 yielded more heterogeneous ages (see Table 1) than the other samples and the uncertainty reported for this sample is therefore the standard deviation of the mean age.

Table 1. K-Ar analysis.

Sample	Formation	Long.	Lat.	K (wt%)	^{40}Ar* (%)	^{40}Ar* (10^{12} at/g)	Age (Ma)	+/- (Ma)
AF12-02	Stratoid ß	40.712	11.403	1.167	7.73	3.5246	2.89	0.06
					8.84	3.5870	2.94	0.05
						Mean	**2.92**	**0.05**
AF12-06	Transform volc.ß	39.970	12.157	1.269	28.73	2.1918	1.65	0.02
					27.68	2.1879	1.65	0.02
						Mean	**1.65**	**0.02**
AF12-11	Sullu Adu ß	40.382	12.133	0.126	5.87	0.5941	4.51	0.10
					4.08	0.5817	4.41	0.12
						Mean	**4.47**	**0.11**
AF13-82	Sullu Adu ß	40.280	12.034	0.121	2.69	0.6875	5.43	0.22
				0.086	1.27	0.4776	5.31	0.42
						Mean	**5.39**	**0.28**
AF13-90	Sullu Adu ß	40.174	12.026	0.366	4.68	1.5204	**3.97**	**0.10**
AF13-98	Chifra ß	39.897	11.459	0.089	3.43	0.7669	8.23	0.27
					3.77	0.6747	7.24	0.22
					3.17	0.7109	7.63	0.26
						Mean	**7.69**	**0.50**
AF13-99	Chifra ß	39.892	11.450	0.783	36.21	18.9568	23.0	0.3
					43.45	18.7734	22.8	0.3
						Mean	**22.9**	**0.3**
AF13-102	Dessie ß	39.520	11.077	0.565	50.53	14.4679	24.4	0.3
					47.29	14.5262	24.4	0.3
						Mean	**24.4**	**0.3**

Table 1. K-Ar analyses in this study

3.1.2. (U-Th-Sm)/He

Samples were prepared at the Centre de Recherches Pétrographiques et Géochimiques and the Service d'Analyse des Roches et des Minéraux (Nancy, France), following the method described in *Pik et al.* [2003] and *Tibari et al.* [in prep]. The U-Th-Sm/He measurements are presented in Table 2. Rocks were crushed and sieved and heavy minerals were then separated by densimetry. Aliquots of three to five zircon or apatite grains were prepared and ^{4}He and U, Th, Sm concentrations were measured on each aliquot. Errors in the measured ages are equal to the reproducibility of standards [*Tibari et al.,* in prep] being 6% at a 1-sigma confidence interval. This level of precision is in agreement with those in the literature (see review in *Tibari et al.* [in prep]). The uncertainty of the U-Th-Sm/He ages is higher than it is for K-Ar, the data can still be used to identify formations of Cenozoic age. For example, an uncertainty of 6% for an age of 30 Ma (the age of the Traps in this study) will yield an error of 1.8 Ma. The ages reported in Table 2 are therefore still consistent with those documented in the literature [i.e. *Ukstins et al.,* 2002; *Coulié et*

al., 2003]. Although the (U-Th-Sm)/He method may lack the precision required to discriminate between younger formations such as the Dahla and Stratoïd, the ages obtained can be compared with the more precise K-Ar ages of the basalts. A particular advantage of the (U-Th-Sm)/He method is that zircons and apatite are typically found in acid rocks, such as rhyolites and it is therefore an ideal tool for mapping zones that contain a large abundance of acid magmatism.

Table 2. (U-Th-Sm)/He analysis.

Sample	Formation	Long.	Lat.	Phase	^{4}He (10^{-9} mol/g)	^{238}U (ppm)	^{232}Th (ppm)	^{147}Sm (ppm)	He Age (Ma)	F_T	Corrected Age (Ma)	+/- (Ma)
AF12-21	Chifra Rhy.	39.935	11.463	Zr	8.509	216.0	125.8	44.9	6.42	0.86	**7.5**	**0.4**
AF12-07	Finto Rhy.	40.379	12.127	Zr	20.961	182.3	112.1	1834.8	18.43	0.81	22.7	1.1
				Ap	2.451	10.0	39.8	2501.4	20.22	0.83	24.3	1.2
										Mean	**23.5**	**1.2**
AF12-10	Traps	40.374	12.124	Zr	8.560	51.96	45.30	55.71	25.31	0.88	28.8	1.4
				Zr	8.522	49.84	43.04	59.99	26.31	0.86	30.6	1.5
										Mean	**29.7**	**1.5**
AF12-12	Finto Rhy.	40.410	12.153	Zr	316.770	8245.51	5796.78	633.07	6.11	0.76	8.0	0.4
				Ap	14.933	387.29	270.23	951.87	6.13	0.67	9.2	0.5
										Mean	**8.6**	**0.4**
AF12-15	Sullu Adu Rhy.	40.204	12.051	Zr	3.479	163.58	99.12	29.74	3.45	0.86	4.0	0.2
				Zr	2.360	113.37	65.39	16.64	3.40	0.84	4.0	0.2
										Mean	**4.0**	**0.2**
AF13-76	Traps	40.304	12.100	Zr	14.412	75.86	88.48	22.86	27.61	0.92	29.9	1.5
				Zr	10.236	57.25	65.78	22.35	26.07	0.90	28.9	1.4
				Zr	10.381	49.79	58.07	25.90	30.30	0.92	32.9	1.6
										Mean	**30.6**	**1.5**

Table 2. (U-Th-Sm)/He analyses in this study.

3.2. Balancing cross-sections: polyphase faulting and tilted blocks

The western part of Central Afar is composed of domino-style fault blocks bound by SW-facing normal faults and tilted toward the center of the depression [*Zanettin and Justin-Visentin*, 1975]. These faults are numerous enough and have such throws that the resulting architecture is a strongly tectonized margin, with a smooth gradient in elevation from the escarpment toward the depression. The traditional method used to determine the extension factor (ß) in such environments is to calculate the amount of horizontal displacement created by the rotation of two adjacent blocks that were initially horizontal and contiguous [Le Pichon and Sibuet, 1981]:

$$\beta = \sin\theta / \sin(\theta - \phi) \qquad [2]$$

where (θ) is the fault initiation angle and (ϕ) is the amount of rotation before fault lock-up. In 'domino-models' such as this, a number of assumptions are made: (1) each

fault generation initiates at the same dip; (2) blocks do not undergo any internal deformation; (3) the difference in elevation from one tilted block to another is small enough to be neglected at a local scale (e.g., along a ~25 km long transect); and (4) the rotation of each block is identical.

However, bedding dips as high as 60° have been encountered in the Afar [*Morton and Black,* 1975]. Mohr-Coulomb theory predicts fault initiation at 60-70° dip. From this simple perspective then, extreme bedding dips of 60° would correspond to sub-horizontal fault planes and predict an infinite extension rate. Because flat or near-flat fault planes are never observed in Afar (Fig. 3A), our favored model is therefore one of polyphase faulting [*Reston*, 2005], as illustrated in Figure 3B. The method has previously been used to resolve extension discrepancy and upper/lower plate paradox issues on the Iberia-Newfoundland sedimentary passive margins [*Reston*, 2005; 2007].

In the polyphase faulting model, a first generation of faults initiates at dips of 60-70° and then rotate until fault dips of ~35° are reached (Fig. 3B). Once the first generation faults have become inactive, a second generation of faults initiates to pursue extension. These second generation faults then rotate and eventually lock-up, and the process is repeated (Fig. 3B). The extension rate obtained after n generations of faulting is much lower than that obtained from a single fault generation model (Fig. 3A). More extension is accommodated by near-flat fault planes than by a succession of steeply dipping faults

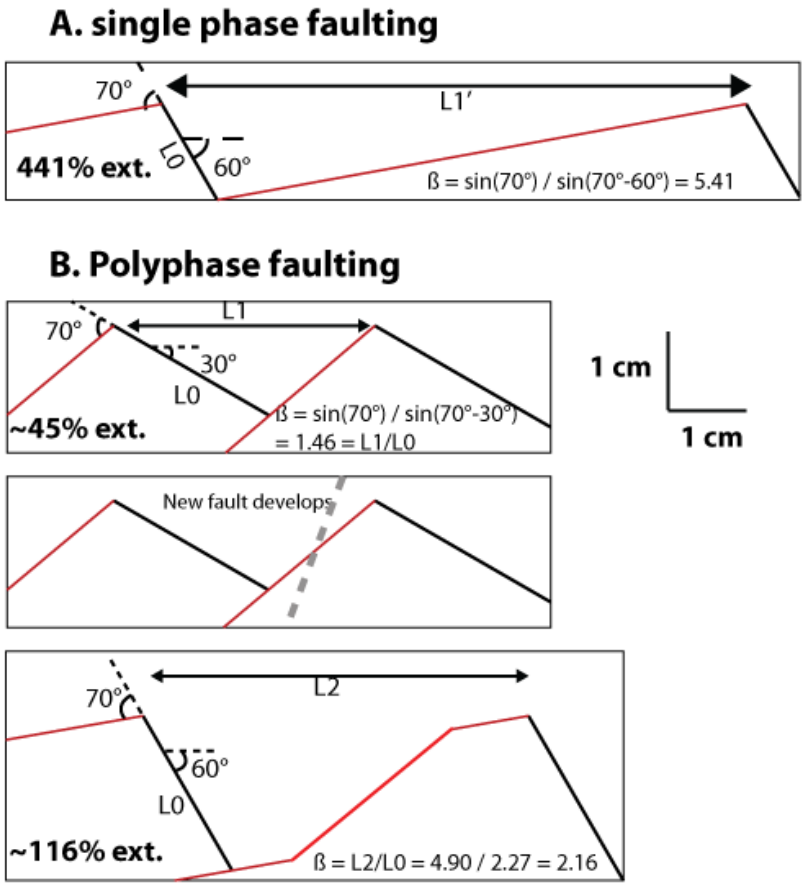

Figure 3. Surface stretching factor calculation for a single phase of faulting and for polyphase faulting bed dips of 60°. We assume a domino model with initially steep faults with dips of 70° and initial bed dips of 0°. Tilted blocks do not suffer any internal deformation and thus stress is only released by pure shear and extension is only accommodated on fault planes. Elevation differences between tilted blocks are neglected. The mathematical formula used to calculate ß is from Le Pichon and Sibuet [1981] (Equation 2 in text). A. Single faulting episode. (Conditions are such that no second-generation faults initiate during extension. Blocks are tilted from 0° to 60° and extension is accommodated on the same fault plane. The corresponding accommodated extension is 441% (ß = 5.41). Note that after rotation the fault plane is nearly flat. B. Polyphase faulting. A first generation fault rotates the beds from 0° to 30°. At this point it is more favorable for a second-generation fault to develop so the fault consequently locks-up. The second-generation fault rotates the strata from 30° to 60°. The first-generation fault planes are rotated to a nearly flat angle, whereas the second-generation fault plane dips to around 45°. The corresponding accommodated extension is 116% (ß = 2.16). The figure illustrates the impact of the number of fault generations on the surface stretching factor corresponding to observed strata dips: the greater the number of fault generations, the smaller the value of ß.

4. Results

The Central Afar study zone encompasses the northern half of the map in Figure 2, extending from the Ethiopian plateaus, across the marginal graben and through the depression (Fig. 1 and 2). Towards the south, there is a shift from the NW-SE to NNW-SSE trending structures of the Red Sea, characteristic of Central Afar, to a NNE-SSW- oriented grain that corresponds to the opening of the Main Ethiopian Rift through the Afar (Fig. 1). We therefore focus our study on a cylindrical part of the margin, where all structures strike sub-parallel to the marginal graben and Manda Hararo active segment (Fig. 2). The area was mapped using field observations, calibrated Landsat 7 composition with bands (7, 4, 1), UTM 37N projection and satellite imagery (SPOT, CNES), and aerial photographs. In this section, we will refine the chrono-stratigraphical chart and structure of the Central Afar rift by focusing on two key localities, Arabati and Sullu Adu (Fig. 2), which correspond to a proximal zone (east of the marginal graben) and a more distal zone in the depression, (west of the Manda Hararo active segment), respectively. We first present new field data and radiometric ages in an attempt to unravel the tectono-magmatic evolution. We then synthesize the results along a balanced composite cross-section in order to link surficial and deep structures.

4.1. Volcano-stratigraphy of Central Afar

A local stratigraphic chart for the Arabati and Sullu Adu areas is presented in Figures 4A and 4B. The ages obtained from K-Ar and U-Th-Sm/He techniques are presented in Table 1 and Table 2, respectively. The results are summarized in Figure 4, which shows the south-north distribution of ages along the western part of Central Afar, based on the stratigraphic charts of profiles A, B, C and D in *Wolfenden et al.* [2005] (see Fig. 2). This is compared to a west-east variation that reflects the time span of lava formations along our study profile (Fig. 2). We were able to distinguish four units, which are separated by angular unconformities.

4.1.1. Oligocene flood basalts

The Traps formation is recognizable in the Sullu Adu area by the U-Th-Sm/He ages of 29.7 ± 1.5 Ma and 30.6 ± 1.5 Ma of strongly tilted rhyolites (AF12-10 and AF13-76; Fig. 4B). These ages are in agreement with the age of *Coulié* [2001] of 30.2 ± 0.4 Ma obtained at the northernmost tip of the Sullu Adu area (Fig. 2B). Although we did not date any samples of the Traps in the Arabati area, they are most likely present below the Miocene volcanics [*Ukstins et al.,* 2002; *Wolfenden et al.,* 2005] (see below). We can correlate the Trap formation in Sullu Adu to the Trap Basalts observed elsewhere in Western Afar and on the plateaus.

4.1.2. Miocene basalts and rhyolites

The marginal graben basalts near Dessie yield a K-Ar age of 24.40 ± 0.35 Ma (sample AF13-102; Fig. 2B). We did not observe any unconformity between this formation and the underlying Traps. Given the age range and similar rock types we correlate this formation to other local marginal graben-related volcanics (Dessie and Kemise Fms.; *Wolfenden et al.,* [2005]) (Fig. 1, 2, 4). These upper Oligocene formations appear to be restricted to the present-day marginal grabens and are not found in Arabati or Sullu Adu (Fig. 2). This may suggest that the eruptions at 25 Ma were localized in a proto-marginal graben.

In contrast, early to late Miocene volcanic formations are found in both the Arabati and Sullu Adu zones. In Arabati, the age of Chifra series is bracketed between 22.9 ± 0.3 Ma (AF13-99, K-Ar) and two ages of 7.69 ± 0.50 Ma (AF13-98, K-Ar) and 7.5 ± 0.4 Ma (AF12-21, (U-Th-Sm)/He, Fig. 4B). However, as it was not possible to observe the contact between the tilted Arabati series and the Traps, the lowermost part of the series may well be older than this. A series as old as 25 Ma, i.e., as old as the basalts of the marginal graben, might therefore exist.

In Sullu Adu, the base of the Finto series has an age of 23.5 ± 1.2 Ma (AF12-07, (U-Th-Sm)/He, Fig. 8). The sample was taken from an ignimbrite layer lying conformably above a layer of green tuff. This tuff is a commonly observed stratigraphic marker throughout the area and lies unconformably above rhyolites and basalts of the Traps formation (Fig. 9). The top of the Finto series has an age of 8.6 ± 0.4 Ma (AF12-12, (U-Th-Sm)/He), but the upper limit for this series may be younger. Given the age correspondences between the two study areas, we correlate the Chifra and Finto series and argue that they erupted simultaneously.

Little to no extension appears to have occurred during the emplacement of these series as no internal unconformities were observed. Moreover, no intermediate ages (i.e., between 22 and 9 Ma) were determined within the formation. This suggests that the volcanic activity was either sparse, consisting of only two significant events, or was continuous but with relatively low volumes. This Miocene formation can be correlated to other formations found towards the south, namely the Burka, Aneno and Bercha Fms. [*Wolfenden et al.,* 2005] (Fig. 4). In these locations, the Miocene series contains several unconformities: in profile A (Fig. 4), the Burka Fm. is apparently continuous [*Wolfenden et al.,* 2005] whereas in the MER profiles B and C, a 10° discontinuity separates the ~16 Ma Aneno Fm from the ~7 Ma Bercha Fm [*Wolfenden et al.,* 2005]. In profile D this corresponds to a MER-type orientation, the Early Miocene record being truncated by three angular unconformities [*Wolfenden et al.,* 2005].

4.1.3. Pliocene flood basalts

The flat-lying Arabati and Sullu Adu series (Fig. 8) occupy the top of the volcanic record in our study areas. We dated the Sullu Adu flat-lying basaltic

formation at several places along the NE-SW Sullu Adu transect (Fig. 8) and obtained ages of 5.39 ± 0.28 Ma (AF13-82, K-Ar), 4.47 ± 0.11 Ma (AF12-11, K-Ar), 4.0 ± 0.2 Ma (AF12-15, (U-Th-Sm)/He), and 3.97 ± 0.10 Ma (AF13-90, K-Ar). *Coulié* [2001] determined a similar age of 3.93 ± 0.06 Ma for a rhyolite located further north. These results are consistent with our age of 2.92 ± 0.05 Ma (AF12-02, K-Ar) obtained south of Sullu Adu, near the Mille river (see Fig. 2B). Given these ages, we correlate the Pliocene flood basalts with the lower Stratoïd formations found elsewhere in Afar.

One sample from the Awra plain yielded an age of 1.65 ± 0.02 Ma (AF12-06, K-Ar, Fig. 2B). This upper Stratoïd age argues in favor of late uplift of the Sullu Adu area. Thus, after emplacement of the Stratoïd formation, the Sullu Adu area was uplifted while the Awra basin subsided and was filled with volcanic products until at least ~1.6 Ma.

Unfortunately, we were unable to find any suitable material with which to date the flat-lying Arabati rhyolites (Fig. 8). However, these lie flat over the tilted Miocene Chifra series in the same way as the Sullu Adu basalts lie over the tilted Finto Miocene series. We therefore correlate these two volcanic units and can infer that the Arabati rhyolites most likely have an age of between 8 and 4 Ma. Because of the occurrence of 6-Ma-old acidic rocks north of our profile (Fig. 2B), we can correlate the Arabati rhyolites with Stage 3 of *Wolfenden et al.* [2005] (see Fig. 4).

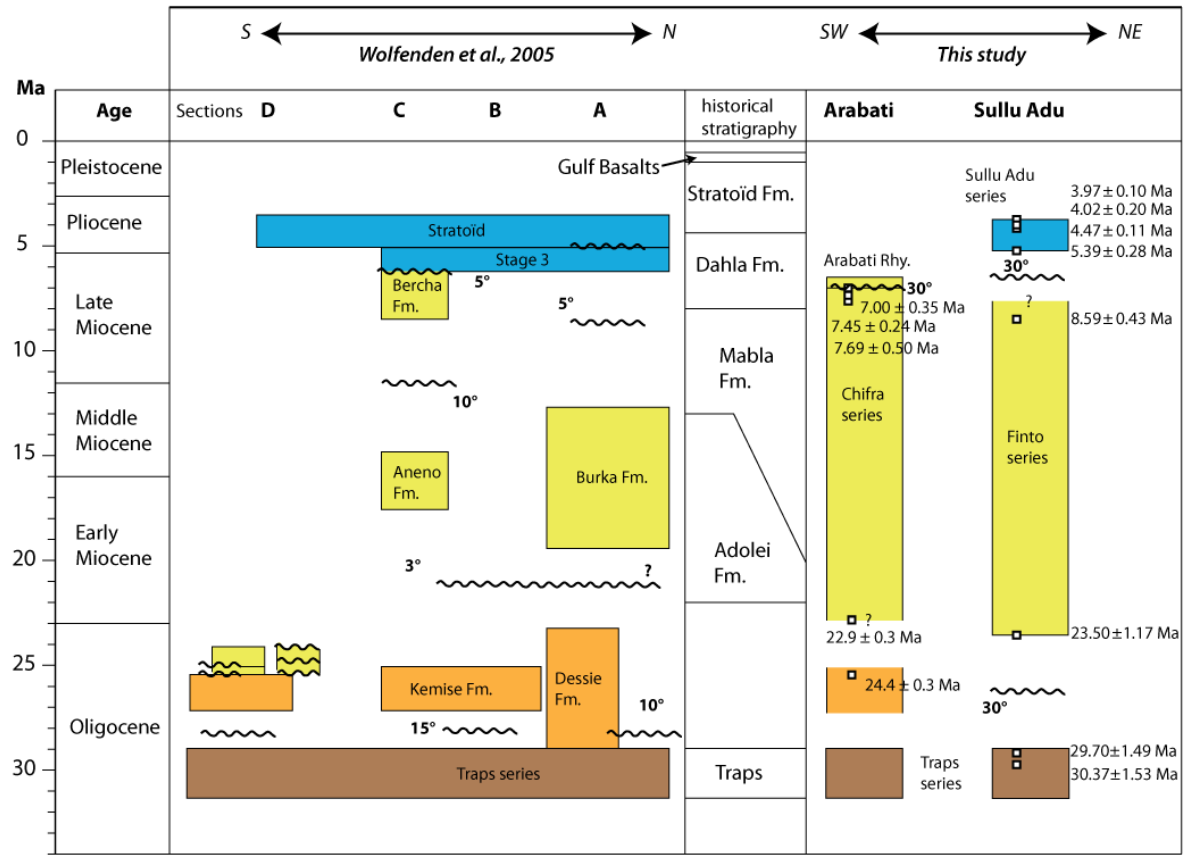

Figure 4. Volcano-stratigraphic chart of Central Afar and Djibouti. Left panel: compilation from Wolfenden et al. [2005] of local volcano-stratigraphic records mapped along four transects (A, B, C and D) that show the along-strike N-S evolution of Western Afar. The transects document the transition from N-S trending structures representative of the MER (profiles D and C), to NW-SE trending structures representative of the Red Sea tectonic grain (profiles B and A). Right panel: spatio-temporal evolution of volcano-stratigraphy along a SW-NE cross-section (see Fig. 2A) based on new age data and field observations of this study. Wavy lines represent angular unconformities. Values in degrees (°) are the difference in dip between the two discordant units. Straight contacts represent conform volcanic units. Question marks indicate inferred contacts between units (contact was not observed) (see text for more information). The (U-Th-Sm)/He and K-Ar age data of this study are shown in the right panel (in Ma, 1-sigma uncertainties; see Tables 1 and 2). For comparison, the central column shows historical formations mapped mainly in Djibouti and then extended to the rest of Afar (after Varet [1978] and references therein).

4.2. Structural features of Central Afar

4.2.1 Arabati (flexure area)

The Arabati area (Fig. 2, 5, 6A-D) is part of the flexure zone, which has been preserved from significant erosion. Further north, erosion has been more intensive and the only markers of past volcanism that remain are feeder dykes that intruded the Traps (Fig. 2). Topographically, the Arabati area remains high, with an elevation that decreases slightly, from ~2000 m to ~1500 m, in a northeastward direction (Fig. 5). The area consists of a tight network of tilted blocks with observed faults that strike between 150°N and N-S and dip WSW (Fig. 5 and 6C). The blocks tilt toward the rift center (northeastward) and the main faults are typically spaced 1 to 5 km apart (Fig. 5 and 6C, D). These observations are consistent with the description given in *Zanettin and Justin-Visentin* [1975]. The easternmost tilted blocks of Arabati are buried beneath the present-day sedimentary infill of the Awra Plain around the town of Chifra, at an elevation of ~ 900 m (Fig. 6). The area can be divided into two parts: the western side, which contains the Oligocene Traps (Fig. 5), and the eastern side, where the Miocene lavas outcrop (Fig. 5 and 6).

In the western part of the flexure area, the Traps series lies sub-horizontally in the footwall of the W-dipping marginal graben border fault (Fig. 5). The dip then increases progressively from 10°NE to 40°NE at Arabati (at 22 km on the cross-section in Fig. 5), forming a flexure. The Traps are then buried under Miocene volcanics in the eastern part of the flexure area (Fig. 5). In our balancing calculations we assume that the Traps series is 2 km thick, as is commonly reported in the literature [e.g. *Hofmann et al.,* 1997].

In the eastern flexure area, the Chifra series consists of a series of basalts, which lie below interbedded rhyolites and tuffs capped by a massive white rhyolitic unit. The dip of the Chifra series decreases from 35°NE at Arabati to 10-15°NE at the north-easternmost tip of the study area (Fig. 5, 6, and 7). The angular relationships between the Chifra series and the Traps series are unclear as no contacts were observed. However, given the smooth variation in dip between the traps to the west and the tilted Chifra series to the east, the existence of an abrupt unconformity of 30° between the two is unlikely. This suggests that either little extension occurred between the emplacements of the Traps series and Chifra series, or that tilting of the Traps to the west occurred synchronously after emplacement of the Chifra series. It is interesting to note that no thickness variations, unconformities or growth strata are observed within the Miocene series, indicating that significant deformation most likely took place after the whole unit had been emplaced.

The Arabati flat-lying rhyolites series is also observed in the eastern part of the flexure area, lying horizontally and unconformably above the 30°-dipping Arabati series (Fig. 5, 6A-B and 7). The Arabati flat-lying rhyolites are 100 m thick at most, and have been affected by a few NE-dipping normal faults (Fig. 6A- B). The total stretching factor accommodated by the Arabati flexure is ß = 1.30 (obtained by measuring the initial length of the base of the traps).

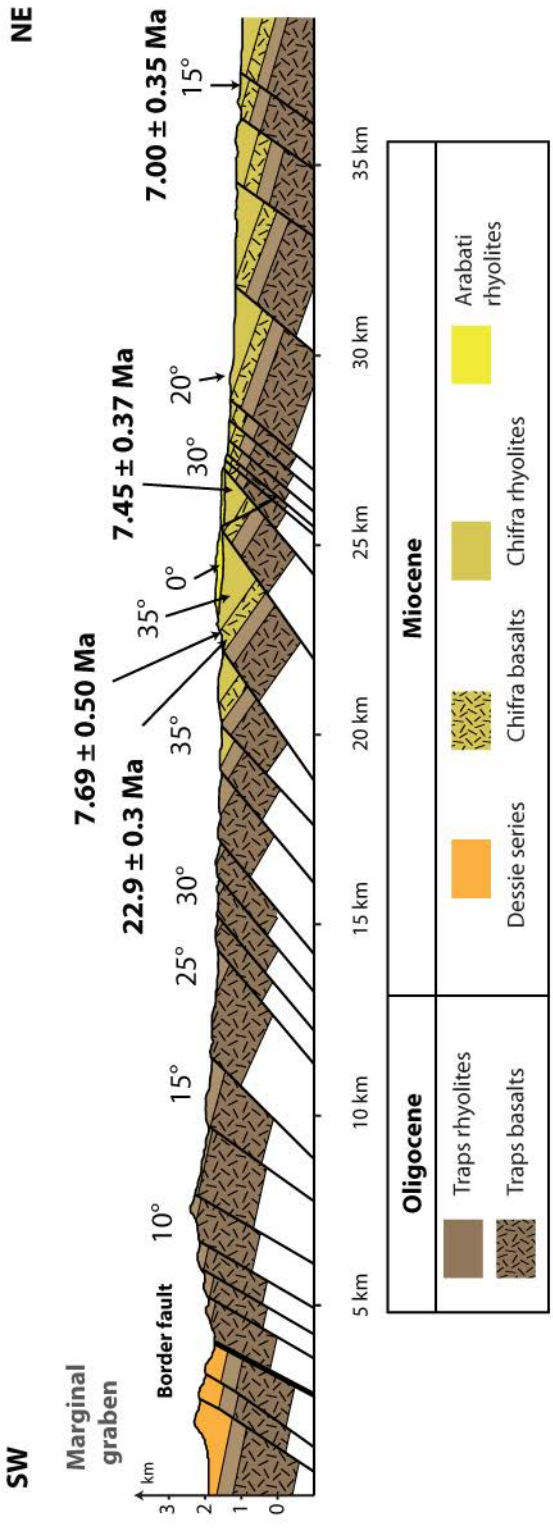

Figure 5. Cross-section from the Marginal Graben through the Arabati study zone (see Fig. 2A). The 'Western side' is the zone of Oligocene outcrops, where Trap basalts and rhyolites are found, progressively flexured toward the NE. The 'Eastern side' represents the Arabati zone, where outcropping Miocene Chifra and Arabati series lie unconformably over the Traps. Bedding dips and ages are also shown.

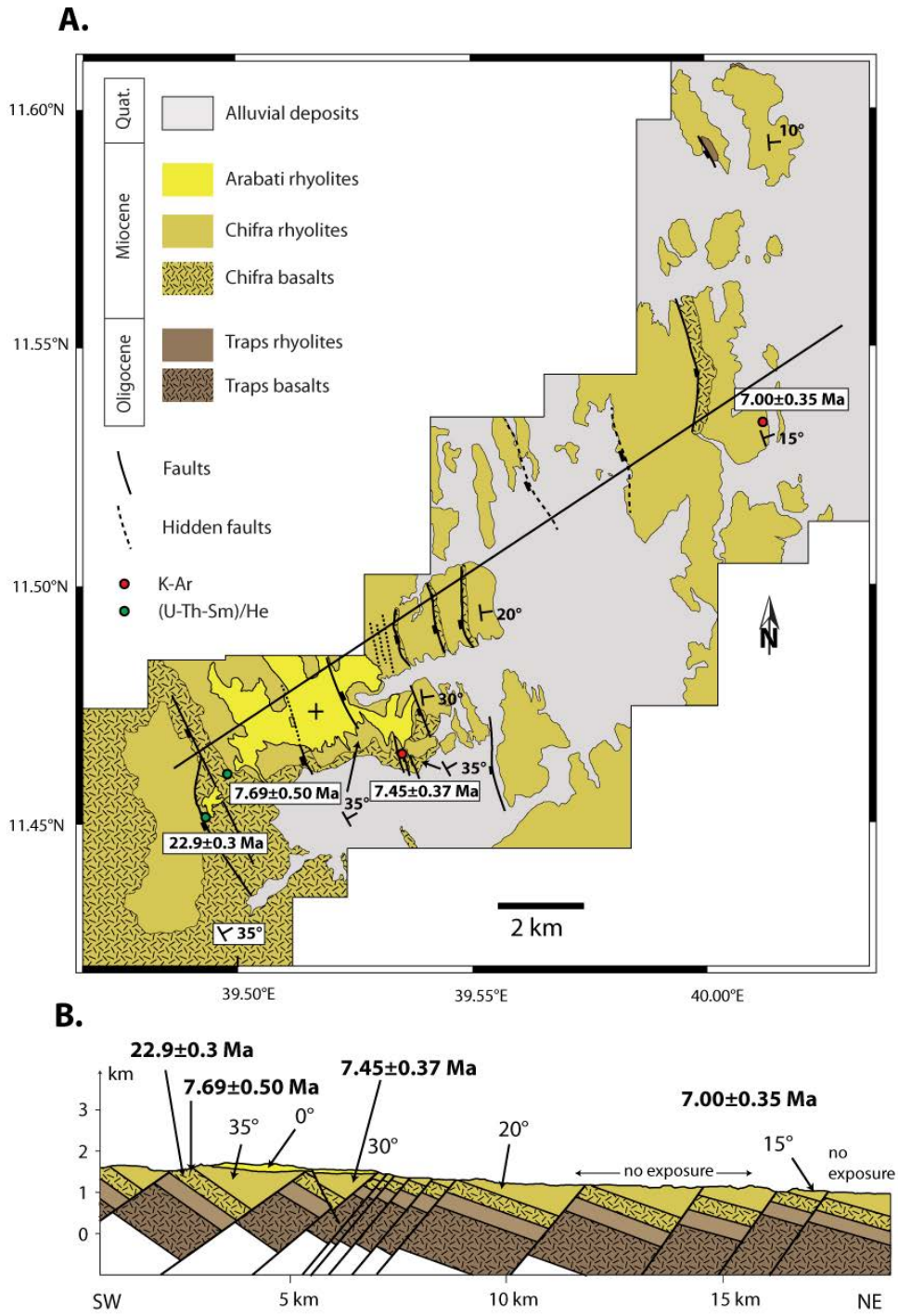

Figure 6. A. Geological map of the Arabati area, WGS84, UTM 37N, inset in Fig. 2A. Maps were constructed using SPOT and Landsat (7,4,1) images calibrated with field observations. B. Cross-section of the Arabati area, ('Eastern Side' in Fig. 5). Mapped faults are projected onto the cross-section. Emphasis is put on the angular relationship between the tilted Chifra series and the flat-lying Arabati series. The relationship with the underlying traps is unclear. Two faults were hypothesized (dotted lines, or 'hidden faults') based on the observation of topographic ridges on the satellite images.

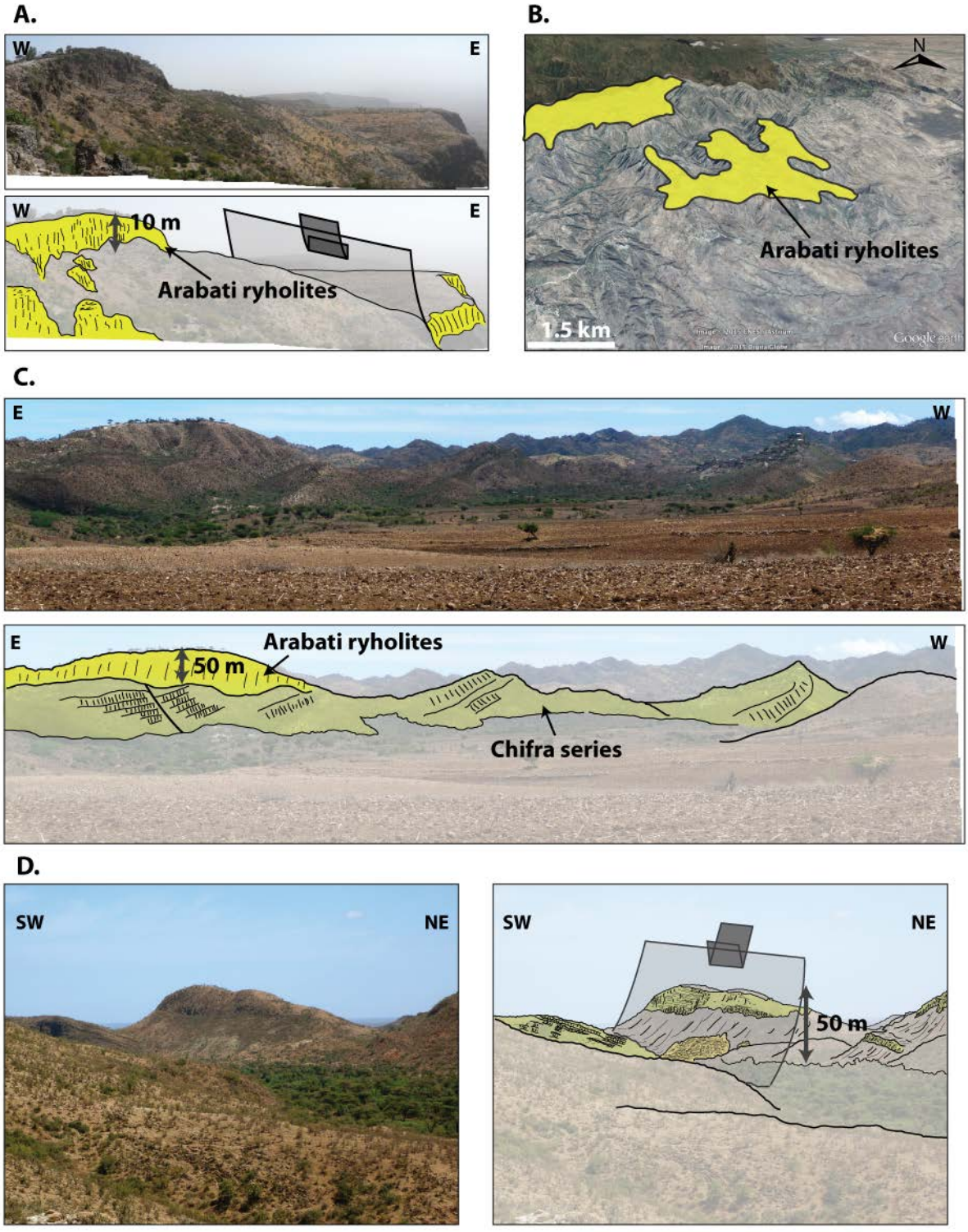

Figure 7. Field photographs of the Arabati area. A. Left: flat-lying rhyolites of the Arabati series, represented in bright yellow. The Arabati rhyolites form a flat plateau (see Fig. 6) affected by a single NE-dipping normal fault. Right: Google Earth view of the Arabati plateau (outlined in bright yellow) over the Miocene tilted blocks (uncolored). B. E-W view of the 50-m-thick Arabati rhyolites (bright yellow) lying unconformably over the tilted Chifra series (pale yellow). The tilted blocks of the Chifra series dip E-NE. C. Typical tilted block of the Chifra series. These tilted

blocks have the fault plane preserved, with a throw of at least 50m. The upper part of the series is composed of rhyolites (pale yellow) and the basal part is composed of basalts (pale yellow/orange), which outcrop in the footwall of the fault.

4.2.2. Sullu Adu (area of highly tilted blocks)

We re-mapped the area as far as the northernmost tip of the Sullu Adu range, a prominent positive topographic anomaly in the Awra basin (Fig. 2, 8). In previous mapping studies, the area was reported to be mostly covered by the Dahla Fm. [*Varet,* 1978] and was interpreted to be a proto-rift axis corresponding to an episode of localization of deformation at 8 Ma [*Audin et al.,* 2004; *Hammond et al.,* 2011]. In our mapping, however, we identified three distinct formations separated by angular unconformities (Fig. 4B, 8 and 9A-C). The youngest formation is a thin (50 m) undeformed layer of basalt that caps the tilted blocks. This flat-lying Sullu Adu basalt is the main feature observed in the Sullu Adu range (Fig. 8, 9B).

The tilted blocks are composed of the Traps and Miocene Sullu Adu series. These dip to the NE and are bound by W- to SW-dipping normal faults (Figs. 8 and 9A-C). The ~1 km spacing of the tilted blocks is tighter than it is in Arabati (Fig. 8). This most likely indicates that the crust has been thinned more here than it has in Arabati. This is consistent with the lower bulk elevation (~600m above sea level) compared to Arabati, and the Traps in this region do appear to have undergone intense deformation as they are found dipping at 60°E-NE at three localities (Figs. 8 and 9A-C). This dip direction appears to be constant over the whole area and is a key feature of the Sullu Adu area.

The Miocene series (in yellow in Figs. 8 and 9) are tilted 30° ± 5° above the traps, indicating that an episode of extension took place between the emplacement of the Traps at 30 Ma and emplacement of the Miocene series at ~27-23 Ma. This age is consistent with the period of Marginal Graben extension and volcanism. This suggests that a period of distributed stretching, from the Marginal Graben area to the present-day Central Afar area, occurred at around 25 Ma.

It is noteworthy that the bedding dips observed in the Miocene series are similar to the flexure of the Arabati area. This suggests that a second episode of stretching, which occurred after 7 Ma, was also distributed spatially and affected both areas in a comparable way. This second extensional episode ended with the emplacement of the flat-lying Sullu Adu series of the Stratoïd Fm.

One problem encountered when attempting to balance the Sullu Adu cross section (Fig. 8) was the 60° dip of the 'pre-rift' Oligocene traps (Fig. 9A, C). We followed the method described in Section 3.2, and assumed that the faulting was polyphase. In our reconstruction, the first generation of faults displaced the Traps series at around 23-25 Ma. A second generation of faults then affected the Finto series between 7 Ma and the emplacement of the Stratoïd series at 4 Ma. These later faults also affected the earlier tilted blocks, resulting in rotation of the Traps to 60°.

Our main limitation was that we were only able to map the second generation faults, i.e., the steep contacts between the traps and the younger Miocene rocks. In most cases, the first generation faults (i.e. those that only affected the Traps prior to emplacement of the Finto series) were not observed; we did not observe any flat fault planes and, moreover, anomalous contacts within the Traps series are difficult to map. The resulting geometry shows that some of the second generation faults have accommodated more displacement than others (Fig. 8). This is consistent with the large variation in the orientation of the mapped structures. From W to E, the strike of the tilted blocks changes from ~N160° to almost N-S in the vicinity of Finto and then back to N160°.

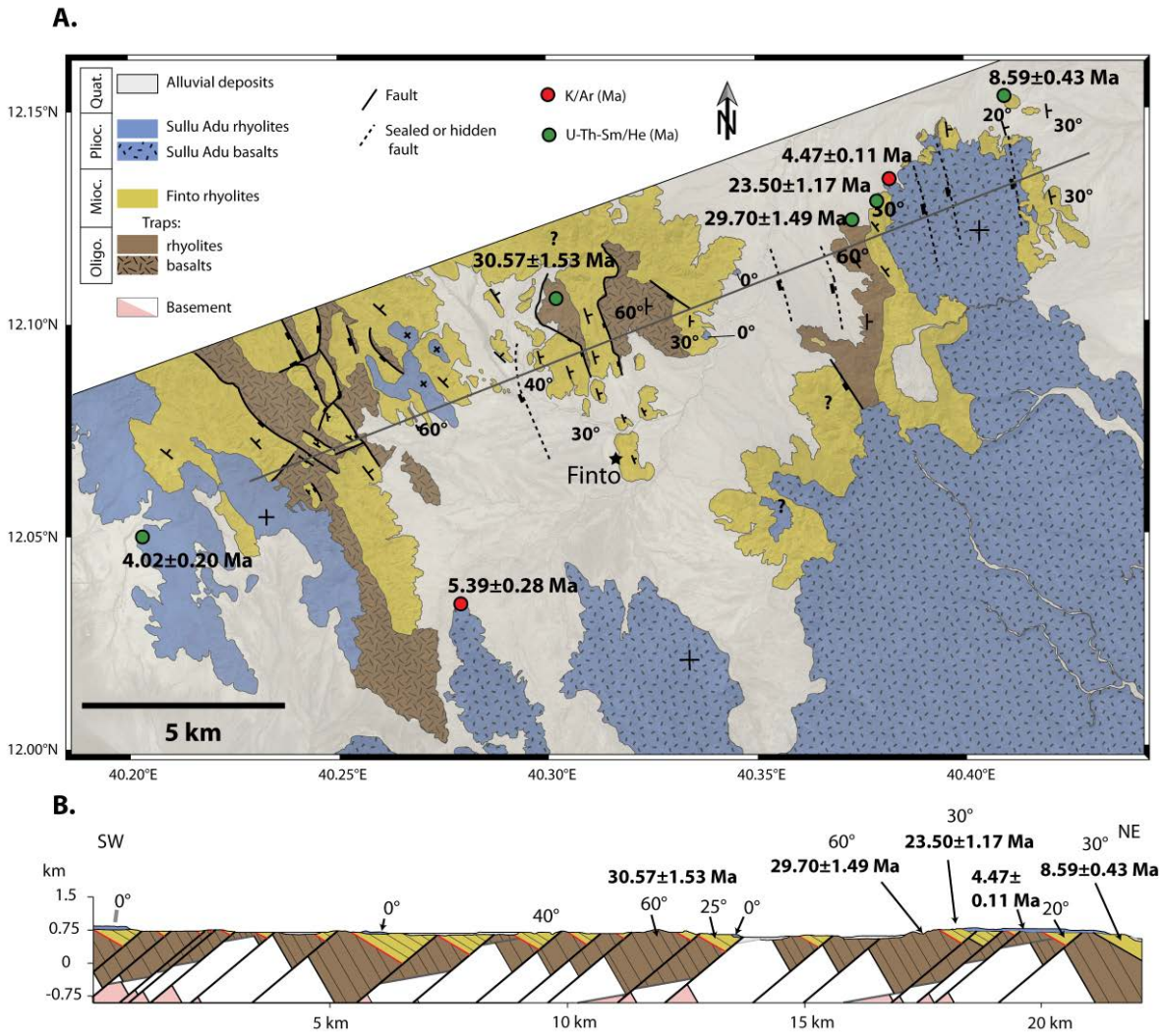

Figure 8. A. Geological map of the Sullu Adu area, WGS84, UTM 37N, inset in Fig. 2A. Map was constructed using SPOT and Landsat (7,4,1) images calibrated with field observations. A SPOT image is shown in transparency to illustrate the extent of the drainage system. The most prominent feature on the map is the flat-lying Sullu Adu basalts (blue, hatched). The rhyolitic equivalent of the Sullu Adu basalts, the Sullu Adu rhyolites (of similar age and also flat-lying) are present on the western

side of the map. B. Cross-section of the Sullu Adu area. Mapped faults are projected onto the cross-section. The reconstruction assumes that 1) all mapped faults are second-generation faults (i.e. steep faulted contacts between the Traps and the Miocene Finto series) because no flat faults were observed, 2) the throw of first-generation faults is never higher than 1.5 km so that the basement is never exposed, 3) the Sullu Adu basalts and rhyolites are strictly unaffected by any faults (see text for more information).

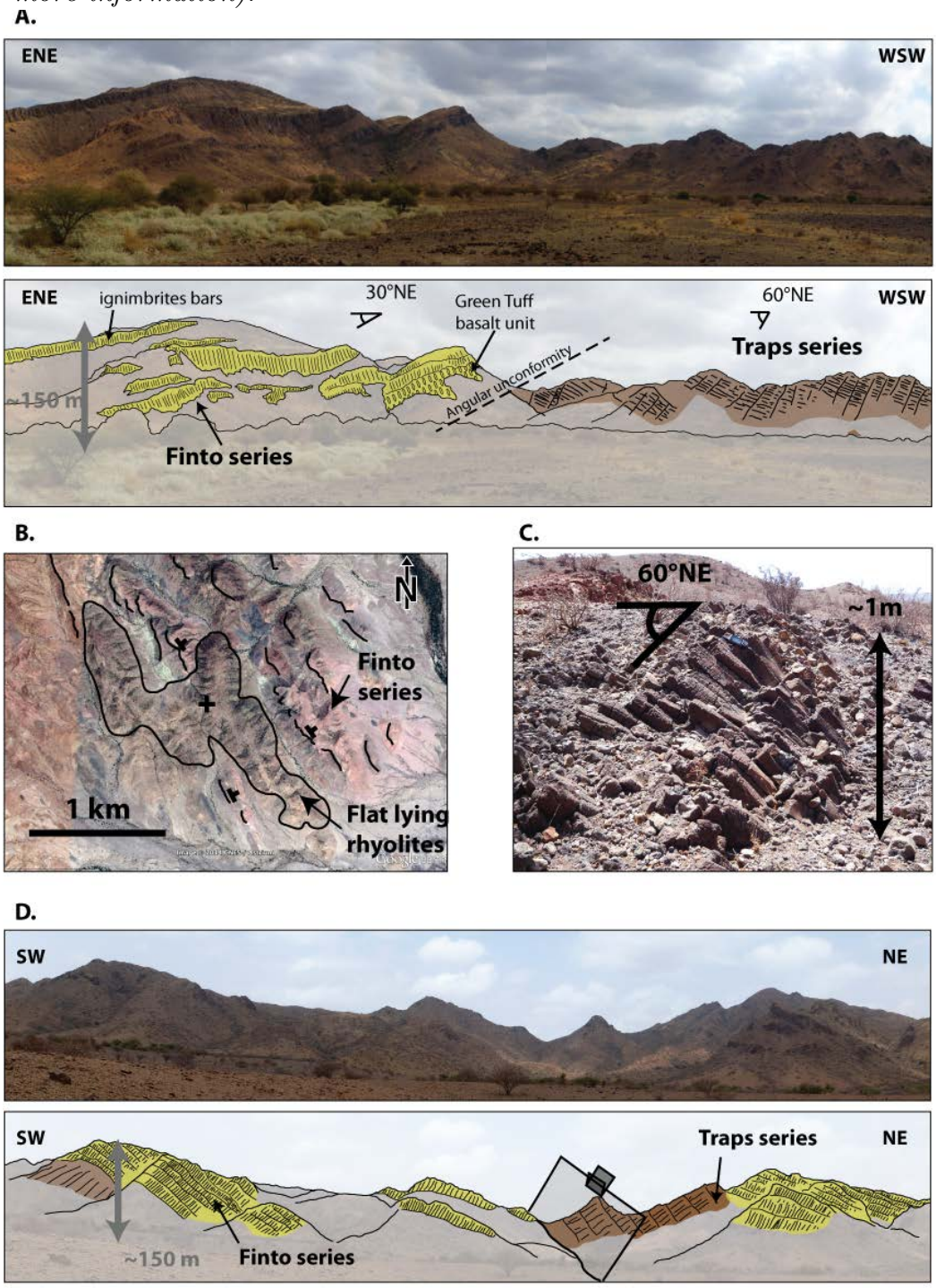

Figure 9. A. Angular unconformity between the Traps (n brown) and the Finto series (bright yellow). B. Google Earth image of the Sullu Adu flat-lying rhyolites. Although

not dated, we correlate the rhyolites of limited extent (kilometer-scale) to the acidic formation in the west of the map in Fig. 8 (because the rhyolites unconformably overlie the tilted blocks of the Finto series and are also flat lying). These structures are present throughout the studied area, suggesting that the eruption of the Sullu Adu basalts and rhyolites was widespread. C. Basaltic columns of the Trap series on which the dip of the strata (60° NE) can be measured. The columns form perpendicular to the surface of the flow, and thus flat lying flows display vertical columns. Handheld GPS device is shown for scale on the top of the columns. D. Two tilted blocks separated by a SW-dipping normal fault, a typical tectonic pattern in the Sullu Adu area. Finto series in bright yellow, Trap Basalts in brown.

4.3. Composite balanced cross-section

In this section, we present a balanced cross-section of Central Afar (see Figs. 10 and 2A for location), which we built from the sections described above (Arabati and Sullu areas; Figs. 5, 6 and 8). We then compare our calculated crustal stretching to the crustal thinning observed in geophysics. First, we present the surface extension factor for each zone (Arabati, Sullu Adu and Tendaho / Tat'Ale). These were extrapolated into tectonic 'domains' on the cross-section (Table 3; Fig. 10A). The upper crust below each domain was then balanced in order to check for consistency in the calculations assuming the conservation of area. The upper-lower crust boundary was reconstructed using the literature described in Section 2.4. Next, we balance the lower crust beneath the Awra / Sullu Adu and Tendaho domains and identify any excess lower crust beneath the cross-section, which we interpret to be syn-rift magmatic underplating, i.e., post-Traps magmatism (Fig. 10B). Finally, we propose the existence of a low-angle mid-crustal shear zone, which links the distributed stretching at the surface with the localized thinning in the lower crust. Shear zones such as this would also influence the spatial distribution of the excess lower crust (Fig. 10B).

4.3.1. Amount of extension at the surface

The first step was to estimate the surface extension factors for the different domains (Table 3, Fig. 10A). We subdivided the cross-section into several 'domains' (Fig. 10A). The length of these domains is expressed as relative length with respect to the total cross-section length (for example, the length of the Arabati domain is 13% of the total cross-section length). The Marginal Graben area experienced extension of about ß = 1.05. The Arabati area has a local extension rate of $ß_{Arabati}$ = 1.30 (see 4.2, Fig. 10 & Table 3). In Sullu Adu, ß depends on the initial dip of the faulting (Table 3), which was between 70° and 61° (Table 3). Because this variation is sizeable and because the initial dip of the faults was difficult to constrain, we chose to express the local ß for Sullu Adu with an error bar equivalent to the mean value of ß (2.50 ± 0.38; Table 3). For the Awra plain (Fig. 2), we used the same ß as for Sullu

Adu, which means that the combined length of Sullu Adu + Awra is 28% of the total length (Table 3; Fig 10A). A ß value of 2.50 ± 0.38 was eventually reached between 7 Ma (the end of Finto series emplacement) and 4 Ma (the onset of Stratoïd series emplacement). The ß for Tendaho area is the same as for Sullu Adu, multiplied by 1.07, which is the mean value of ß accommodated by the post-Stratoïd structures [*Acocella et al.,* 2008]. Thus, we obtained a ß value of 2.68 ± 0.40 for the area from Tendaho to Tat'Ale (Table 3; Fig. 10A). It was then possible to check whether the extension accommodated by faulting at the surface was equivalent to the thinning of the upper crust beneath each domain. For this, we assumed the upper-lower crust boundary to be at 15 km depth beneath Arabati and 7 km depth between Awra and Tat'Ale. [*Berktold et al.,* 1975; *Perez-Gussinyé et al.,* 2009; *Craig et al.,* 2011; *Hammond et al.,* 2011]. The upper crust beneath Awra-Sullu Adu (~590 km^2) (Fig. 10A), when balanced to a 15-km-thick pre-rift stage, displays a stretching factor of ~ 2.7, which is consistent with the calculated value of 2.5 ± 0.38 (Table 3). The upper crust beneath Tendaho-Tat'Ale (~730 km^2) displays a stretching factor of ~ 3.0, also consistent within error with the value of 2.68 ± 0.40. This means that, in the present study, the amount of extension accommodated by faulting is a good proxy for the amount of upper crustal thinning. Because we defined the base of the upper crust as the boundary between brittle and ductile behavior, the depth variation of this boundary should be temperature-dependent as well as extension-dependent. However, as our results show good agreement between surface stretching and upper crustal thinning, the depth variation over time that results from differences in heat flux can be neglected. Moreover, the effects of magma advection in the upper crust are probably also extremely local and can therefore also be neglected at this spatial scale. Thus, extension exerts the primary control on the thickness of the upper crust.

A final verification consisted of calculating the weighted mean of the sum of the initial length of the tectonic domains, weighted by the ß of each tectonic domain. This gives a virtual $ß_{WEIGHTED}$ of 1.98 ± 0.16. Of note, balancing the whole upper crust surface (~2440 km^2) back to an initial thickness of 15 km gives a ß of ~ 2.16, which is in good agreement with the model. Note however that here, ß describes the thinning of the entire cross-section and thus depends on how much undeformed length is included in the balance calculations. Thus, the 'weighted mean ß' value of ~ 2 is representative of the cross-section alone and confirms only that our surface estimations are correct. However, the 'real' ß value of ~2.7 ± 0.4 corresponds to the extension experienced in the most stretched part of Central Afar, i.e., from Sullu Adu to Tat'Ale (Fig. 2), and is comparable to other values of ß reported in the literature, notably those obtained in plate kinematics reconstructions [*Eagles et al.,* 2002; *Redfield et al.,* 2003]. Our stretching factor is however higher than the ß value of ~ 2.0 predicted by receiver functions analysis [*Hammond et al.,* 2011].

Table 3. Stretching factors.

Domain	Final Length (%)	ß (70°)	ß (65°)	ß (61°)	Mean
M.Graben	11	~1.05	~1.05	~1.05	**1.05**
Arabati[a]	13	1.3	1.3	1.3	**1.3**
Sullu Adu	28	2.13	2.50	2.88	**2.0 ± 0.4**
Tendaho / Tat'Ale	48	2.28	2.68	3.08	**2.7 ± 0.4**
$ß_{WEIGHTED}$	100	1.81	2.00	2.13	**2.0 ± 0.2**[b]
	100	/	/	/	**2.2**[c]

[a] Measured on initial length of Traps for the western side and initial length of Chifra rhyolites on the eastern side, see text.
[b] Obtained after the calculation of the weighted mean of surface ß.
[c] Obtained after the balancing of the total area of (upper crust + lower crust) - (underplating)

Table 3. Summary of local extension rates, either calculated or determined by graphical methods (for each domain), and total stretching factors, calculated as the weighted sum (ßCalculated) and deduced from the surface balancing technique (ßDrawn). Each of the 'domains' in the cross-section has a relative length and a local extension rate. For any given domain, the greater the value of ß and the greater the relative length, the more weight the domain stretching factor will carry in the total stretching factor calculated for the whole cross-section. See text for explanations of local stretching factor determinations.

4.3.2. Total thinning factor and excess lower crust

The depth of the Moho was determined by receiver functions analysis [*Hammond et al.* 2011; *Reed et al.,* 2014]. We inferred the depth of the upper/lower crust boundary by combining observations from the literature [*Berktold et al.,* 1975; *Perez-Gussinyé et al.,* 2009; *Craig et al.,* 2011; *Hammond et al.,* 2011]. The Moho depth values are projected onto the profile in Fig. 10 (location in Fig. 2A). An overall decrease in crustal thickness from ~35 km to ~20 km is shown, the 'necking' of the crust occurring under the Arabati area (Fig. 10A). We define the lower crust as the portion of crust (equivalent to a surface in cross-section) between the upper/lower crust boundary and the Moho as defined above. The lower crust has an initial thickness of 20 km (from 15 km to 35 km depth). When we balance the lower crust in Fig. 10A (~ 3350 km^2) to its initial thickness of 20 km, we obtain a mean ß factor of ~1.4, which is lower than the mean value of ~ 2 obtained for the upper crust. This means that the lower crust is too thick with respect to the upper crust, or in other words, there is an excess of lower crust beneath Central Afar. In fact, in order to

make the lower crustal thinning comparable to the upper crustal thinning, approximately 1850 km^2 must be subtracted from the lower crust. It may be necessary to assume that this excess crust was not present at the initial pre-rift stage but was instead added to the crust during rifting. Consequently, we refer to this excess lower crust as 'underplating', independent of the spatial and temporal distribution of this material during rifting. At this point, a kinematically correct although unlikely solution could be obtained by adding a uniform layer of underplating in proportions that would fit the balancing, regardless of its distribution. However, this would imply that the crustal thinning crust along the whole cross section was continuous, which is inconsistent with the crustal necking inferred from receiver functions computations [*Reed et al.,* 2014]. There must therefore have been a particular spatial and thus temporal distribution of the underplating beneath the Afar, related to the mode of crustal thinning. Moreover, part of this 'underplated' material most likely intruded the lower crust and not only stopped beneath the original Moho.

4.3.3. Structural style, mid-crustal shear zone, and underplating

Two key observations support the presence of a flat mid-crustal shear zone: (i) the uniform NE dip of tilted blocks separated by antithetic normal faulting; and (ii) the wide distribution of the domino faulting style. Because the tilted blocks achieved rotation synchronously (shortly after 7 Ma) and as all of the normal faults have similar throws (generally of 100m but occasionally up to 500m), the crustal thinning might be expected to be distributed proportionally at depth. However, seismic receiver functions reveal a necking in the western part of the cross-section. Thus, the deformation is broadly distributed at the surface (the tilted blocks occur over a ~100-km- long area) and localized within a necking zone at depth. This is consistent with the presence of a top-to-west shear-zone in the mid-crust, which is rooted towards the west in the lower crust beneath the plateau (Fig. 10B). This is also supported by detachment faulting models [*Lister and Davis,* 1989] in which thinning of the lower crust is focused on a single point whereas extension at the surface is distributed.

Moreover, in order for the two crustal layers to be stretched by the same amount, extra lower crust needs to be assigned to the cross-section. The amount of additional lower crust can be determined by comparing the $ß_{\text{UPPER CRUST}}$ to the $ß_{\text{LOWER CRUST}}$ directly below the abrupt thinning of the upper crust, and this extra lower crust does indeed fill the 'gap' left by what would be the actual thickness of the lower crust. We thus propose the existence of a flat detachment at mid-crustal level beneath the Afar, which is rooted in the lower crust in the necking zone of Arabati and which corresponds to or even controls the preferential emplacement of mafic material in the zone of abrupt thinning in order to fill the voids left in the thinned crust (the shear zone in green in Fig. 10B). Some of the largest faults would connect to the shear zone at depth (faults in green, Fig. 10B) while crosscutting older faults

(in red, Fig. 10B). This mechanism might also explain the formation of the 'active segments' of Tendaho and Tat'Ale, and this is supported by the findings of *Desissa et al.* [2013], who identified a wide zone of partial melting beneath Manda Hararo. We therefore propose that a more recent shear-zone mechanism, analogous to the first, develops and controls the localization of deformation and magmatism at depth beneath a segment.

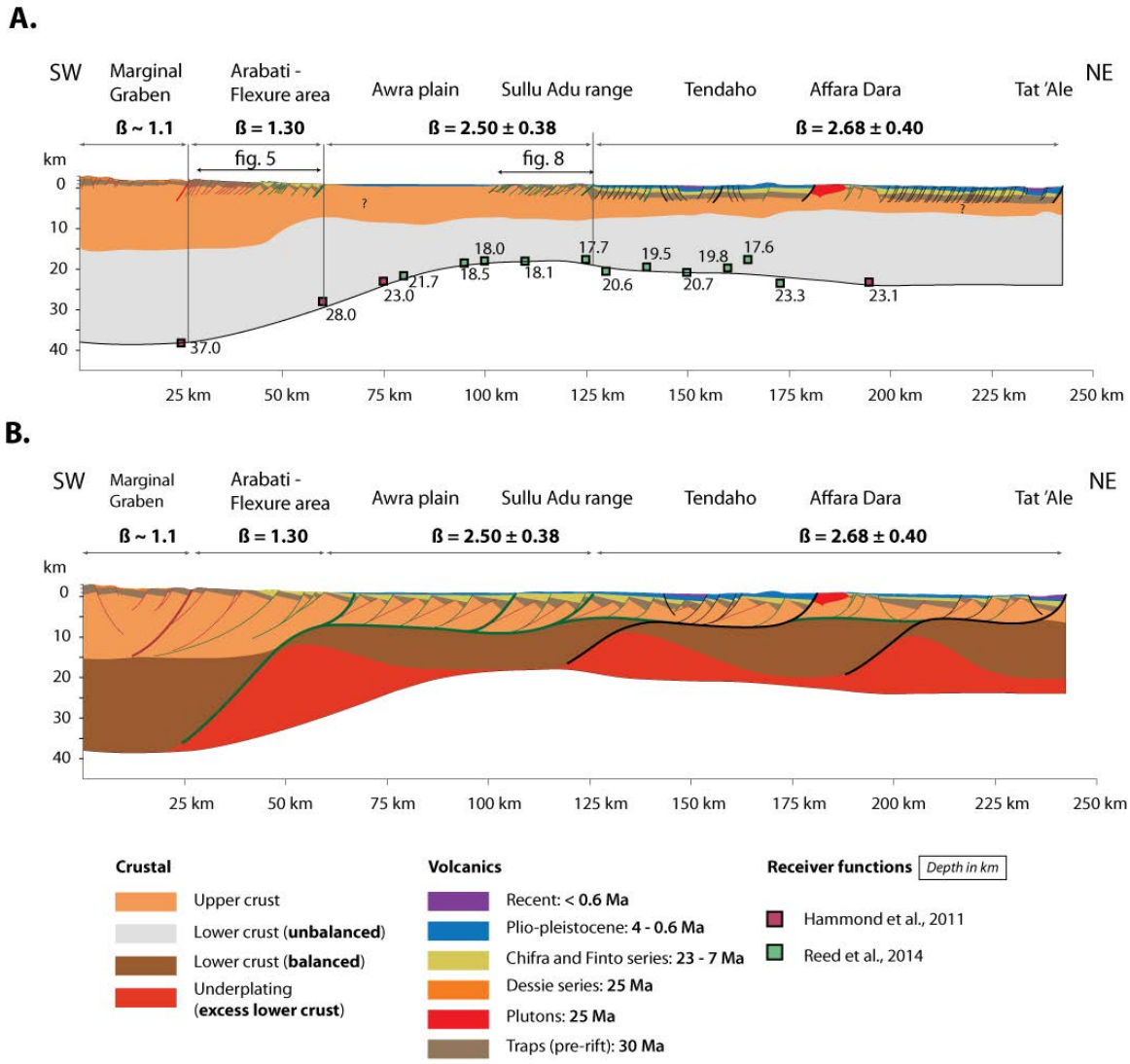

Figure 10. Composite cross-section of Central Afar constructed from field observations at Arabati and Sullu Adu and data from the literature (see text). A. Composite cross-section with no vertical exaggeration. Surface stretching factors are given for each zone. Position of the upper / lower crust boundary is based on literature. The surface (area?) of the lower crust is too large in respect to the upper crust and the section is not balanced, implying an excess of lower crust. B. Re-interpreted cross-section of Central Afar that takes into accounts underplating in the lower crust. Polyphase faulting is represented as the tectonic style of the upper crust. Second-generation faults (in green) cross-cut the older first-generation faults (red)

and are rooted on a mid-crustal shear zone that links distributed extension at the surface (upper crust) to localized deformation in the lower crust. The underplating is stored where crustal thinning has left in a 'gap' in the lower crust. The process is then repeated as third generation faults (black), absent in the Arabati and Sullu Adu areas, connect to younger shear zone beneath the Tendaho / Tat'Ale area. The three underplated bodies in this cross-section are required in order to balance the lower crust with respect to the upper crust.

This interpretation relies on the observation of W-SW dipping faults as being the major structures that accommodate extension on the long-term. Unlike *Wolfenden et al.* [2004, 2005] further south, we do not observe major E-dipping faults, except the one bounding the Tendaho graben (Figs. 1 and 2). This is either because E-dipping faults have been overprinted by Miocene W-dipping structures (which is unlikely), or because they never existed north of the Dessie-Bati accommodation zone [*Wolfenden et al.,* 2005], which separate our study area from Wolfenden's. The major E-dipping faults near Dessie (Figs 1 and 2) are located south of the accommodation zone; one of them is represented on our cross-section (Fig. 10). It is noteworthy that even though they control the topography south of the Dessie-Bati accommodation zone, they are not recognized as major structures in terms of crustal thinning in *Wolfenden et al.* [2005]. Therefore, such E-dipping faults, if they exist in our study zone, did not act as major accommodating structures, either because they were generated during the stretching phase, or because they are minor (see Figs. 5 and 10). This is compatible with the flexure we documented between the plateau and the Afar area.

It is worth noting that the wide pattern of distribution of the deformation documented in this study cannot be attributed to the presence of transfer zones. The Arabati-Chifra cross-section (Fig. 5) is located close to a minor transfer zone (Fig. 1, 2) where the marginal graben is slightly offset. However, the fault pattern we observed corresponds to a wide zone (more than 50 km, Fig. 2) compared to the width of the transfer zone and can thus be considered as representative of the rift segment. Finally, our cross-section is composite and, close to the plateau, crosses the transfer zone (the marginal graben of the cross section being south of the transfer zone and the flexure being north of it, Fig. 2, 5, 6). This has little influence on the cross-section as the structural styles are quite similar on both sides.

5. Discussion

5.1. Timing of deformation

Rifting in Central Afar from the Oligocene to the present has taken place in three main steps (Figs. 11 and 12). The first tectonic event (the stretching phase) occurred at around 25 Ma, after emplacement of the Traps at 30-29 Ma and just

prior to the onset of emplacement of the Miocene series at around 23 Ma, as observed in the Marginal Graben (Fig. 12D). In Sullu Adu, the Traps were tilted to 30°E during this first tectonic phase. Thus, the stretching was distributed over a wide area (around 100 km; Figs. 11 and 12D). In the southernmost part of Western Afar [*Wolfenden et al.,* 2005], it has been suggested that the deformation was focused on the border faults of the marginal graben between 29 and 26 Ma (Stage 1 of *Wolfenden et al.,* 2005). In our opinion, the pre-Miocene deformation in Central Afar was more widely distributed, as suggested by the succession of grabens and tilted blocks, which have recorded 0° to 30° of bed rotation locally.

The second phase of deformation (thinning phase) (Fig. 11, 12B) occurred after the emplacement of the Miocene series, which ended at about 7 Ma (marking the end of Chifra and Finto series emplacement). In both the Arabati and Sullu Adu areas, the tilting of the Miocene series can be recognized by the absence of growth strata or by variations in thickness in the hanging wall of faults, indicating that this phase of extension occurred after emplacement of the Miocene series. Moreover, we observed that the Chifra series and Finto series were synchronous and present throughout the whole of the Miocene, from ~23 Ma to ~7 Ma. During this period, the Miocene series appears to have been conform, although not continuous as no erosional surfaces were observed. However, it is possible that the oldest rocks of the unit are separated from the younger rocks by a paraconformity and that there were two distinct pulses of volcanism instead of one continuous, volume-starved series. Nevertheless, we can conclude that almost no deformation occurred in our study zone during the Miocene (Fig. 11, 12C).

In their southernmost cross-sections (see on Fig. 4B, profiles B to D), *Wolfenden et al.* [2005] found that magmatism and faulting shifted twice during the Miocene: an eastward jump occurring at 15 Ma and a second jump occurring at 8-7 Ma. This process produced younger basins towards the center of the rift. This model was supported by the early geological mapping of Afar of *Varet* [1978] in which the whole of the Sullu Adu ridge was interpreted as being of Dahla age (7.4 ± 0.3 Ma, Fig. 2B), on the basis of a single whole rock K-Ar age of *Barberi et al.* [1975]. Our observations do not support the model of progressive strain migration during the Miocene [*Wolfenden et al.,* 2005] as the Miocene series are not localized in a single narrow basin, which would have been located riftward of the proto-Marginal Graben, but are instead distributed over a large area on top of previously stretched crust (Fig. 11). Our interpretation also favors widely distributed strain during the upper Miocene/lower Pliocene second phase of deformation (5 Ma, Fig. 12B).

However, no extension is recorded in our study areas so there appears to have been a gap in extension during mid-Miocene times. As divergence did not stop between 23 and 7 Ma (as attested to in Gulf of Aden continental and oceanic records), we postulate that deformation took place further to the northeast during this time, in the southern Red Sea rift or on the Danakil block.

In the Red Sea, the main phase of rifting probably began at between 27 and 22 Ma [*Omar and Steckler,* 1995; *Hughes et al.,* 1999; *Bosworth and McClay,* 2001]. The rifting may well have started earlier than this [*Omar and Steckler,* 1995] but no evidence for significant uplift and erosion is found in the sedimentary record at this time [*Bosworth et al.,* 1998]. Moreover, the Ocean-Continent Transition in the Gulf of Aden formed at 18-20 Ma, leading to the strong localization of divergence in distal margins [*Leroy et al.,* 2004; *d'Acremont et al.,* 2006; *Leroy et al.,* 2012; *Bellahsen et al.,* 2013] (see Fig. 12C). We propose that the rifting became focused in the Red Sea at around 22 Ma and that lithospheric break-up (after the OCT formation; *Leroy et al.* [2012]) in the Gulf of Aden at 18 Ma triggered localization of the rifting in the north, i.e., along the Red Sea/Gulf of Aden connection (Fig. 12C).

From 4.0 Ma to 1.1 Ma, the Stratoïd series erupted over a large zone at the border of Western Afar (Fig. 2B), infilling the Awra basin and the more distal parts of the rift (the flat-lying Sullu Adu basalts and rhyolites, which lie horizontally above the Finto series, Fig. 5, 6, 8). Between 1.1 and 0.6 Ma, at the end of the Stratoïd emplacement (and previously included in the Stratoïd by *Varet* [1978]), a distinct mode of emplacement can be recognized [*Kidane et al.,* 2003, *Lahitte et al.*, 2003a]. The authors correlate these basalts with the 'Gulf Basalts' Fm., which outcrops around the Gulf of Tadjoura (Fig. 12A). In Central Afar, the Gulf Basalts are emplaced along massive silicic centers in the hanging wall of major west-dipping normal faults that form the easternmost border of the Tendaho Graben [*Kidane et al.,* 2003] (Fig. 1, 2) and in the major west-dipping fault that bounds the half-graben of Tat'Ale. They are also found in association with the earliest lava flows of Manda Hararo and on top of the basaltic plateaus near Manda Inakir (Fig. 2). The Gulf Basalts therefore appear to be the first geological formation in the Afar to have localized along large faults during the third phase of extension (the localizing phase) (Fig. 11). After emplacement of the Gulf Basalts (ending at 0.6 Ma), a significant amount of strain, characterized by intense dyking, localized on magmatic centers [*Wright et al.,* 2006; *Grandin et al.,* 2010; *Pagli et al.,* 2014] (Fig. 11). The distribution of the Gulf basalts therefore largely corresponds to the distribution of active volcanic segments (Figs. 11 and 12A).

Our interpretation therefore points towards widely distributed rifting during the Oligo-Miocene, both before and after the main flood basalt events (Oligocene traps and Pliocene Stratoïd series), although the mode of rifting switched from stretching to thinning during this period. During the Quaternary, the divergence became localized in the magmatic centers, although the process of localization may have started during emplacement of the Stratoïd series.

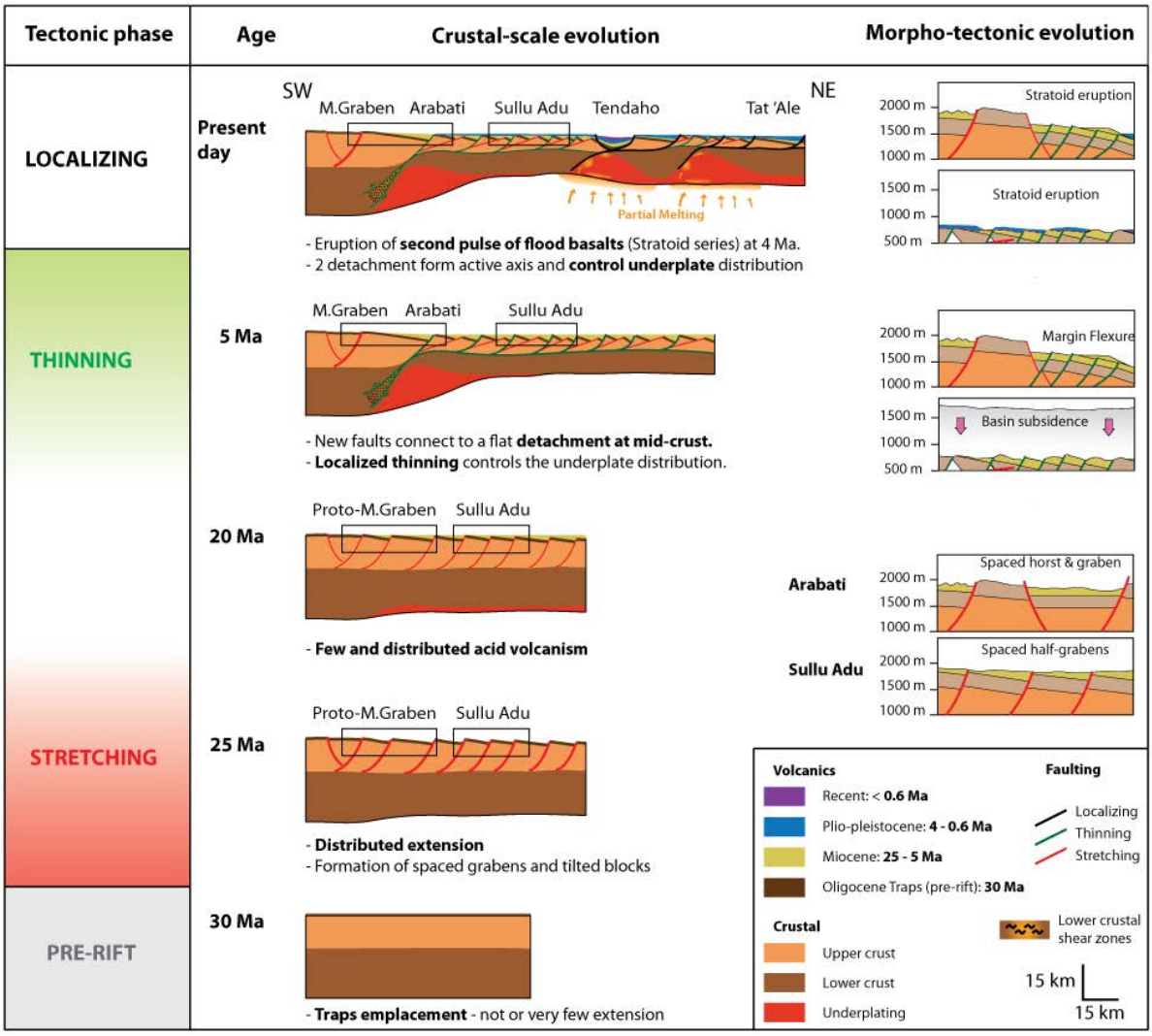

Figure 11. Volcano-tectonic evolution of Central Afar. Table figure summarizing the different tectonic phases that structured Central Afar. The Traps were emplaced at 30 Ma, during the pre-rift phase, probably in response to the thermal anomaly of the Afar plume. The emplacement was accompanied by no – or very little – extension. Rifting began between 30 and 25 Ma, prior to the onset of Miocene volcanism (in yellow), with a 'stretching' phase. The stretching affected a wide area and was characterized by strong coupling between the brittle and ductile levels of the crust: NE-dipping tilted blocks were created by the accommodation of extension on SW-dipping faults. The Afar rift was already asymmetric at this point, with numerous half-grabens. The stretching phase was followed by a period of tectonic quiescence and the eruption of sparse acidic magmas (Miocene in yellow). Between ~7 Ma and ~ 4 Ma, after the emplacement of the Miocene series and before the emplacement of the Stratoïd, a second tectonic phase - the 'thinning phase' - occurred. During this phase, the Arabati zone underwent flexure and the Sullu Adu zone started to subside in response to crustal thinning. The thinning phase was therefore a distributed mode of extension, during which time the crust was thinned and then partially re-thickened by

magmatic underplating. In our model, the normal faults of the thinning phase connect to a shear zone at depth that helped to create a necking zone in the lower crust. When tectonic activity ceased, the Stratoïd flood basalts were emplaced on top of the newly thinned Afar crust (Stratoïd volcanism from ~4 to ~0.6 Ma). This was then followed by the 'localizing phase', in which the Afar remains today. Magmatic and tectonic activity is currently focused within the active segments, in our case Manda Hararo and Tat'Ale.

5.2. Extension discrepancy and extra lower crust

Our results show that the lower crust is thicker than predicted from taking into account the surface extension calculated from the cross-section balancing of the upper crust. The amount of extension determined from surface balancing techniques when the amount of syn-rift lavas and sediments is excluded ($ß_{drawn} = 2.16$) is in agreement with the amount calculated from the local ß ($ß_{calculated} = 1.96 \pm 0.16$). This may appear to be inconsistent with a divergence model in which dyking is an important mechanism for strain accommodation. In these models, horizontal displacements are taken up by magma injection into the crust instead of displacement along normal faults [*Ebinger and Casey,* 2001; *Buck,* 2004]. Such processes are well described in the Manda Hararo active segment [e.g. *Grandin et al.,* 2010] and the Main Ethiopian Rift [see the review in *Corti et al.,* 2003] and were initially inferred to explain the most recent (< 7 Ma) formation history of Central Afar [*Wolfenden et al.*, 2005] based on the observation of feeder dykes that cross-cut the Dahla basalts. In our calculations using bedding dips, the dyke-accommodated divergence cannot be observed because dyke injection does not generate block rotation. Moreover, no dykes were found in either Arabati or Sullu Adu, making it difficult to directly quantify the amount of dyking-related divergence. Magma injection may play an important role in the accommodation of divergence [*Mohr*, 1989; *Buck*, 2004; *Keir et al.,* 2011] and can take-up up to 50% of the total divergence [*Mohr*, 1989]. However, even though this process occurs in discrete segments, there is no evidence to suggest that it is significant at the scale of a whole rift. We propose instead that most of the extension is accommodated by normal faulting at the surface. This is supported, for example, by the high density of faults (1 fault / km mapped in Sullu Adu, Fig. 8). However, we do not preclude an active role for magma in the accommodation of thinning and extension at depth, especially in the ductile lower crust.

If this is true, the stretching factor obtained in this study of ~2.7 is higher than those inferred from geophysics [e.g., *Hammond et al.,* 2011]. It is closer to the estimation of *Eagles et al.,* [2002], who provide a reconstruction of the Danakil block position with respect to Nubia and an estimation of its pole of rotation, and predicts a total extension rate of ß > 3 in Central and Southern Afar. However, geodynamic reconstructions such as this do not take into account the fact that the Danakil block

experienced extension (Fig. 12C), with bedding dips as high a 60° encountered in the pre-rift rocks [*Morton and Black,* 1975], and the block should not therefore be treated as a single rigid block. Further evidence comes from dykes that intrude the Jurassic limestones. Moreover, recent (< 2 Ma) tectonic individuation of the Danakil Block (Fig. 1) [*Le Gall et al.,* 2011] took place with the reactivation of inherited faults, which affected the Miocene Mabla formation. Several episodes of extension may therefore have affected the block since the Oligocene.

Our structural model for the Afar rift with extra lower crust was developed in order to explain the fact that the upper crust suffered a higher amount of stretching and thinning than the lower crust. This is rarely the case along non-volcanic rifted margins, as the amount of extension calculated from fault displacements in seismic reflection profiles (which provide an approximate estimate of the stretching factor of the upper brittle crust) is always lower than the stretching factor for the whole crust [*Driscoll and Karner,* 1998]. The likeliest explanation for this discrepancy is depth-dependent stretching [*Royden and Keen,* 1980; *Davis and Kusznir,* 2004], which may involve preferential extension of the lower crust through lower crustal flow while brittle faulting of the upper crust remains minimal [*Weinberg et al.,* 2007; *Blaich et al.,* 2008]. Alternatively, the discrepancy could be an artifact of the difficulty in determining the total amount of extension from several generations of faults (sequential faulting, *Reston* [2005, 2007]; *Ranero and Perez-Gussinyé* [2010]). In Afar, the problem is the opposite – there is apparently more extension in the upper crust than in the lower crust. Whether or not depth-dependent stretching due to lower crustal flow is a phenomenon at play in the Afar, our interpretation does not change. If depth-dependent stretching has been a factor in the Afar, then the lower crust would be even more thinned than the upper crust, and thus the thick lower crust would be even more at odds and there would be even more excess lower crust. A final issue concerning lower crustal flow is the possibility of lower crustal material being transported over long distances, which would make it difficult to perform proper area balancing. It could even be argued that the lower crust may be transported out of the cross-section, thus inducing a bias in the lower-crust surface estimation used for balancing. However, our 'weighted check' (see subsection 4.3.1) demonstrates that both the initial and underplated volumes have been conserved during rifting. This can be explained by the fact that we consider a relatively long cross-section (250 km), so that even if material has been transported through flow, the material has stayed within the cross-section and has been taken into account in our model.

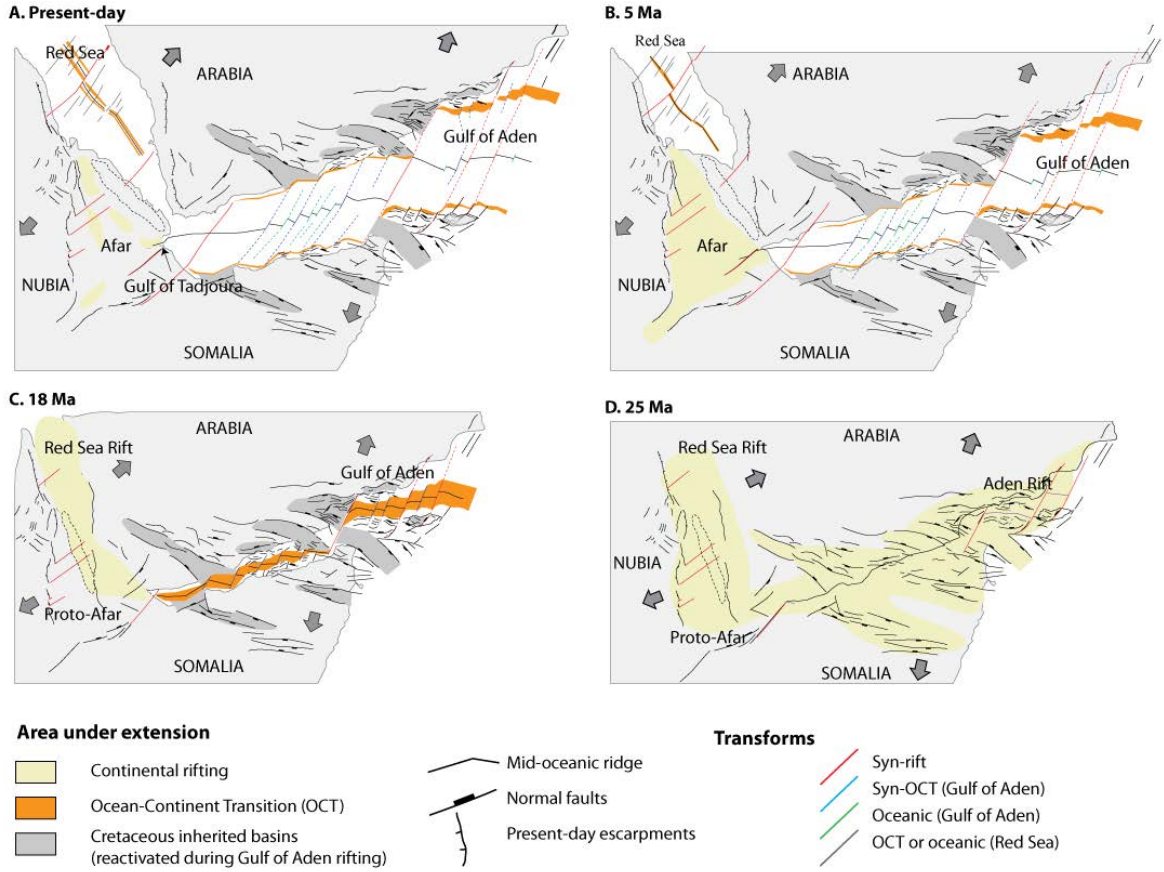

Figure 12. Geodynamic reconstruction of the movements of Nubia and Arabia during the last 25 Ma. At 25 Ma, rifting began simultaneously in the Red Sea and Afar and was already active in the Gulf of Aden. Extension in Afar was accommodated over a wide zone. At ~18 Ma, divergence in the Gulf of Aden was focused at the Ocean-Continent Transition [e.g. d'Acremont et al., 2005; Leroy et al., 2012], which could have potentially triggered localization in a narrower area, possibly in the highly deformed Danakil block as no extension was recorded in Central Afar. At 5 Ma, oceanic spreading was active in both the Gulf of Aden and Red Sea. Rifting in Afar was once again widely distributed, remaining so until recently. In the present-day, divergence in Afar is taken up by localized active segments. Areas in yellow mark the zones of accommodation of divergence, whereas those in light grey mark those that have become inactive. The OCT is marked in orange, and the dark grey areas represent inherited Cretaceous rift basins that were re-activated during rifting in the Gulf of Aden. The main escarpments are shown for clarity. Structural map of the Gulf of Aden is from Leroy et al. [2012] and references therein. Gulf of Aden transform timing is from Bellahsen et al. [2013]

5.3. Magma-compensated crustal thinning during rifting

Our interpretation of this excess lower crust is that the crust has experienced magma-compensated thinning achieved by underplating/intrusion, as is frequently observed along volcanic passive rifted margins [e.g., *Geoffroy*, 2005*; Thybo and*

Artemieva, 2013] and continental magmatic rifts such as the Baikal Rift [*Thybo and Nielsen*, 2009] and the East African Rift System [*MacKenzie et al.,* 2005; *Maguire et al.,* 2006]. Magma-compensated thinning is frequently associated with the presence of high velocity bodies at the base of the lower crust. Seismic refraction profiles across the Main Ethiopian Rift (MER) have imaged a 10 km-thick layer with a crustal velocity of Vp = 7.4 to 7.7 km/s [*MacKenzie et al.,* 2005, *Maguire et al.,* 2006]. In this case, the presence of mafic material that has been added to the base of the lower crust is supported by the existence of a reflective P-wave interface above the Moho [*Maguire et al.,* 2006], which the authors interpret as the top of the high velocity body. In Central Afar, *Hammond et al.* [2011] modeled the Vp of the lower crust with receiver functions and determined values of 6.9 to 7.2 km/s. *Bastow and Keir* [2011] report lower crustal P-wave velocities of 7.0 to 7.5 km/s beneath the Afar. Whether lower crustal layers characterized by P-wave velocities such as those described above are of magmatic origin or whether they correspond to metamorphozed basement rocks is an issue that is still under debate [*Gernigon et al.,* 2004; *Thybo and Artemieva,* 2013]. The P-wave velocities of the lower crust beneath the Afar range from 7.0 to 7.5 km/s [*Bastow and Keir,* 2011] and might therefore correspond to magmatic underplating. However, these values are restricted to the axial zones of the Afar and cannot alone account for magmatic underplating because the present-day elevated temperatures recorded in these segments could lower the P velocities. Even though these velocities are lower than in the MER, they are comparable those of other underplated bodies such as the Vøring High in the North Atlantic, which ranges from 6.9 to 7.3 km/s [*Mjelde et al.,* 2009].

Furthermore, Vp/Vs of between 1.9 and 2.2 are found in Central Afar [*Hammond et al.,* 2011] and are consistent with the presence of mafic material/injected crust. However, zones of Vp/Vs = 1.9 are found between Western Afar and Sullu Adu, which are volcanically inactive at present. This suggests that the high ratio might be better explained by mafic material whose high Vp signature would increase that of the initial continental crust. In contrast, the ratio of > 2 below Tendaho and Manda Hararo would be best explained by a mixture of mafic underplating and present-day partial melting. Another important characteristic of the Central Afar crust is the presence of positive Bouguer anomalies that are accounted for by adding high density material (d = 3000 g/cm^3) to the lower crust [*Tessema and Antoine,* 2004].

All of these observations strengthen a hypothesis that involves the addition of mafic material to the crust during crustal stretching. A common alternative interpretation for the underplating is that it could be either serpentinized mantle or high-grade metamorphic rock [e.g., *Gernigon et al.,* 2004]. Serpentinized mantle can display a broad range of Vp values, from 5 km/s to 7.5 km/s with Vp/Vs > 1.8 [*O'Reilly et al.,* 1996] similar to those observed beneath Afar. However, serpentinization is expected when the crust has been extensively stretched and

thinned [*Péron-Pinvidic and Manatschal,* 2009] thereby allowing fluids to percolate through an exhumed lithospheric mantle. Such a process seems unlikely given the ~5-10 km thickness of the upper crust [*Hammond et al.,* 2011].

The data discussed above does not allow us to completely discard the hypothesis of metamorphic rocks being part of the underplating. However, the fact that a certain volume of the lower crust must have been re-added to compensate for the thinning favors magmatic production of volumes that did not exist prior to extension (as metamorphism does not create new magma). In addition, Vp/Vs > 1.8 points towards an ultramafic origin for the underplating (Fig. 10).

Finally, this point of view is supported by the fact that underplating of magmatic origin is usually linked to the eruption of the large volumes of basaltic and sometimes rhyolitic lavas that are characteristic of Large Igneous Provinces across the world [*Cox,* 1980]. The volume of this underplating may be several orders of magnitude greater than the volume of the surface volcanics [*Cox*, 1993]. When a mantle source rock is partially melted and fractionated to produce basaltic liquids, some of the initial volume is retained in the form of olivine, plagioclase and clinopyroxene-bearing cumulates. *Cox* [1980] states that only the plagioclase-bearing cumulates (gabbros) have a crustal character and are therefore associated with crustal underplating. The remaining olivine and pyroxene-rich cumulates are the ultramafic products of primary source rock differentiation and are considered to be mantle rocks. The mass fraction ratio of gabbroic cumulates over erupted liquid is at least ~0.5, which means that at least half of the volume erupted has been retained at the base of the crust. This should be considered a minimum ratio, however, because it assumes that all of the available liquid has been erupted (if this were not the case, the ratio would be higher than 0.5).

Further evidence for important volumes of underplating is the presence of rhyolitic products at the surface. *Cox* [1993] suggests that 6 to 10 times this volume may be present as cumulates in the deep crust. These cumulates could be the source rock of the rhyolites (with the rhyolites derived from the fusion of any basalt in the lower crust), or be gabbroic cumulates formed from fractional crystallization of primitive mantle liquids (of picritic composition) or could even be cumulates formed by melting and re-crystallization of the basalts themselves [*Cox,* 1993]. This subtlety precludes any proper estimate of the amount of underplating because it assumes that the volume of cumulates, basalts and rhyolites derived from original mantle source rock melting and the amount of rhyolite derived from re-melting of the already differentiated basalt are both known. In our cross-section, we suggest that a large volume of underplated material is stored at the base of crust (Fig. 10 and 11). Given the ~1 km-thick pile of mostly acidic Miocene volcanism of over ~200 km length in the cross-section, plus the ~1 km-thick pile of Stratoïd basalts a number of acidic centers [*Varet,* 1978] spread over 120 km (excluding the Awra plain beneath which the Stratoïd is present in the form of basaltic edifices and sparse acidic flows; Fig. 2,

8 and *Coulié* [2001]), and another ~1 km of recent axial flows restricted to an area of around 20 km length, the extruded post-Traps magmas should cover an area of ~340 km^2. In contrast, the section balancing predicts a surface area of 1850 km^2 of underplated bodies (in red in Figs. 10 and 11). This therefore yields an underplated/erupted area ratio of ~5.4, which is in agreement with the interpretations of *Cox* [1993].

5.4. Mid-crustal shear zone model

The first model of crustal attenuation by polyphase faulting (i.e., several generations of faults) for the Afar margin is from *Morton and Black* [1975]. The model was developed in order to provide constraints on how much extension the Afar floor underwent in order to facilitate Arabian-African reconstruction. The model was developed after observation of pre-Miocene rocks outcropping along Western Afar and on the Danakil Block. The original hypothesis was that the Afar floor was entirely covered with oceanic floor and thus the presence of silicic outcrops in the depression was problematic [*Morton and Black,* 1975]. The model was an attempt to link the thickness of the crust to the horizontal displacement deduced from bed dips. They recognized the riftward tilting blocks and postulated they were regularly spaced and then computed the effect of several generations of faults on the extension factor. For simplicity, they assumed a purely geometric model with planar faults, that none of the divergence was accommodated by dyking and that all the strain was pure shear, i.e., that deformation was progressively taken up through ductile deformation so that there was no *décollement* or major asymmetric shear zone located at depth [*Morton and Black,* 1975]. Up to here, the approach of *Morton and Black* [1975] is similar to our own (see section 3). However, in using the seismic refraction profiles of *Berckhemer et al.* [1975], *Mohr* [1983] argued in favor of a *décollement* mechanism, through which the upper brittle crust is decoupled from the ductile lower crust. Differential thinning between the upper crustal layer (Vp = 6.0 – 6.1 km/s), which thins from 12 km under Addis Ababa to 4 km under Mille, and the lower crustal layer (Vp = 6.6 – 6.7), which thins from 30 km under Addis Ababa to 18 km under Mille, certainly occurs (Fig. 2). Thus, the upper crust has a ß of ~3 whereas the lower crust a ß of ~1.7. However, contrary to the remarks of *Mohr* [1983], second generation faults are indeed observed [*Rooney et al.* 2013]. This last observation supports our model of polyphase faulting. Thus, the model of *Morton and Black* [1975] lacks a feature that could explain both the necking of the crust at depth and the spatial distribution of the tilted blocks at the surface. As suggested by *Mohr* [1983], a shear zone (or décollement) at mid-crustal level might be a possible solution. Mid-crustal shear zones have already been directly observed in the northernmost part of Afar by *Ghebreab and Talbot* [2000] on the Eritrean Plateaus and in the neighboring Gulf of Zula. In particular, they observed tilted blocks that had been dissected by seaward-dipping normal faults rooted in an inferred top-to-the-east shear zone. According to

the authors, the extension exploited an inherited Pan-African low-angle fabric which represented an incipient detachment zone. During a second phase of extension, landward normal faults cross-cut the pre-existing detachment at the surface in a domino fashion and are rooted in an inferred second detachment at depth with top-to-the-west orientation. The Eritrean escarpment was therefore proposed to consist of a monoclinal flexure due to the second detachment. The seaward-dipping blocks of Eritrea were interpreted by *Ghebreab and Talbot* [2000] to be the equivalent of onshore SDR observed at the Disko flexure in west Greenland [*Geoffroy et al.,* 1998].

The models of SDR formation above a mid-crustal shear zone are consistent with our interpretations in Central Afar. In our model, we infer the presence of a shear zone in order to fit the deep crustal necking to the widely distributed surface extension so that our cross-section is balanced. There is however an important difference between our interpretation and the 'classical' view of syn-tectonic SDR formation. Our observations show that the main stretching and thinning episodes took place in between magmatic pulses (Fig. 11). We documented 1) an Oligocene pre-rift magmatic pulse (the Trap Basalts) followed by a stretching phase, 2) a protracted Miocene acidic magmatic phase followed by an episode of thinning and underplating, and 3) a second major magmatic pulse (the Pliocene Stratoïd), later followed by a localizing phase. Consequently, the eruption of the Stratoïd basalts, which are a characteristic feature of the wide and thick Central Afar segment, occurred over a crustal layer that had previously been intensively thinned and subsequently re-thickened. In our chronology, the magmatic compensation for the thinning is sequential: we did not observe any syn-volcanic thinning or stretching. Thus, from a chronological point of view, the crust is 're-thickened' after an extension phase. This may appear to be at odds with observations made at other onshore volcanic passive margins, such as the SE Afar rift in Djibouti [*Geoffroy et al.,* 2014]. Here, syn-tectonic prisms of 8 Ma to 2 Ma age (stage partly intermediate between Fig. 12B-C) are thought to be controlled by rollover faults that are rooted in a detachment at depth that controls the location of future break-up. It is important to specify that this is a recent feature, younger than 2 Ma, linked to the propagation of the Aden ridge into Afar [*Geoffroy et al.*, 2014]. Features such as the rollover faults may be hidden below the volcanics of the Manda Hararo magmatic center (Fig.1, 2). Although we do not directly observe this kind of detachment system, our model contains the same kind of feature beneath the Manda Hararo axis, with a break-away located at Affara Dara, where the pre-rift rocks outcrop (Figs. 1, 2, 10B).

In our mid-crustal shear zone model, the location of detachments rooted in the lower crust (i.e. the locus of maximum thinning) exerts a strong control on the distribution of underplating. Extra lower crust is added at the footwalls of detachments where the lower crust is thinnest, i.e. where the pressure gradients are most favorable for ascending mafic material. Comparable mechanisms have been described for megamullions at slow-spreading ridges, where core complex-like

detachments are interpreted as non-conservative faults because magmatic material is continuously stored at the base of the detachment footwall and are preferentially underplated, like plutons, during amagmatic periods [*Dick et al.,* 2008]. These faults are thus termed 'plutonic growth faults' by the authors.

5.5. A 'magmatic wide-rift' during the Mio-Pliocene

GPS measurements in the MER and Central Afar have revealed that, despite relative localization of strain in the active volcanic segments, the distribution of deformation was accommodated within a zone that widens gradually from the Southern MER (~6 km) to the Afar (175 km) [*Kogan et al.,* 2012]. Deformation in Afar is thus distributed over a length that exceeds the lithosphere thickness. This corresponds to the definition of a 'wide rift' [*Buck,* 1991; *Brun*, 1999]. Wide rifting has occurred in natural extensional settings such as the Basin and Range province [*Lister and Davis,* 1989]. *Kogan et al.* [2012] related the increasing size of the actively extending zone from the MER to Afar to a reduction in the integrated lithosphere strength, as modeled by *Stamps et al.* [2010], and to the thinning of the lithospheric mantle under Afar [*Pasyanos et al.,* 2009]. They suggested that the disappearance of the strong lithospheric mantle enhanced the gradual widening of the zone of strain accommodation. The presence of hot mantle beneath Afar was reported in the early work of *Makris and Ginzburg* [1987] and later in *Bastow et al.* [2008] (and references therein). More recently, *Stork et al.* [2013] and *Corbeau et al.* [2014] showed the presence of a low velocity mantle (P-waves velocities of 7.2 ± 0.4 km/s) beneath a zone encompassing the western flexure to Manda Hararo. This may indicate a weakening of the uppermost mantle and, since low lithospheric mantle strength due to mantle thinning can trigger delocalization [e.g. *Sokoutis et al.,* 2007], could thus explain the delocalizing pattern observed by *Kogan et al.* [2012]. In contrast, *Reed et al.* [2014] found that crustal thinning in the area adjacent to the Tendaho Graben was not focused under the graben but was instead quite diffuse. They suggested that most of the extension was diffusely accommodated by the ductile lower crust and that the lower crust is decoupled from the brittle upper crust, a parameter that may enhance delocalizing [*Davis and Kusznir,* 2004; *Reed et al.,* 2014].

We propose that this 'wide rift' strain pattern, characteristic of magmatically weakened lithosphere and crust, was already present in early Miocene times, i.e., during the early rifting. This means that the mantle was already hot at the beginning of rifting, still under the influence of the mantle thermal anomaly that was responsible for the eruption of the Traps at 30 Ma. Our aim is not to discuss the provenance of such a thermal anomaly (e.g., a mantle plume), but to highlight the fact that the temperature effect and the subsequent mantle thermal erosion and weakening has had an effect on the structural style of Afar since the early history of rifting, and that this effect is recorded in the distribution of Miocene and Pliocene faults and volcanic sequences.

In Iceland, rollover structures have formed during the last 12 Ma. These tectono-magmatic structures were underlain by shallow magma chambers at different places within a large zone about 200 km wide and were triggered by the decoupling of the upper crust from the lower crust [*Bourgeois et al.,* 2005]. Moreover, this strain distribution tends to disappear away from the sustained temperature anomaly of the mantle, i.e., the Icelandic plume. This is consistent with our model of a mid-crustal detachment above the thermal anomaly, this detachment being rooted in the lower crust in a more localized fashion beneath the Plateau, away from the thermal anomaly.

The novelty of our model is that it combines this 'magmatically-enhanced wide rifting' mode with localized necking at depth. It does not therefore oppose a mechanism of dyke injection that localizes strain in the rift center into narrow magmatic segments [e.g., *Ebinger et al.,* 2005 and references therein]. It instead suggests that such processes may have been active during earlier rifting and distributed the strain over a wide zone.

5.6. Segmentation and Seaward Dipping Reflector (SDR) formation

As described in *Bastow and Keir* [2011], the wide and thick Central Afar rift segment and the narrow and thin Northern Afar Erta'Ale segment experienced different amounts of magma eruption in relation to stretching and thinning. For Central Afar, we have shown in this study that extension has been accommodated over a wide zone as it has in other volcanic settings with a magmatic wide rifting mode, such as Iceland. Furthermore, Central Afar has experienced intense volcanism with the eruption of the Stratoïd flood basalts at 4 Ma. In northern Afar (Erta'Ale segment), the crust has been thinned to ~15 km and the Stratoïd series is absent. Instead, a Miocene sedimentary infill has accumulated in the subsiding basin. Between these two provinces, a NE-SW transfer zone has developed (Fig. 1).

Along the North and South Atlantic margins, the emplacement of the SDR occurred in close relationship with major syn-rift transfer faults and thus the observed along-strike variation in breakup-related magmatism appears to have been controlled by the rift segmentation [*Franke et al.,* 2007; *Elliott and Parson,* 2008]. Numerical simulations in *Koopmann et al.* [2014b] show that a delay in the opening of a rift segment bound by a transfer fault zone can explain the difference in SDR volume on either side of the transfer fault zone. Furthermore numerical modeling [*Armitage et al.* 2009] has shown that SDR volumes observed in the Atlantic required not only a thermal anomaly, but also a previously thinned lithosphere in order to be erupted.

This suggests that the presence of the Stratoïd in Central Afar and its absence in northern Afar is closely related to the two rift segment morphologies. Although we cannot tell whether the segmentation influenced the magmatism or if the major transfer zones were the result of the distribution of pre-existing partial-melting

sources in the mantle, it appears that the two are strongly linked. *Bastow and Keir* [2011] stated that the northern Afar is closest to break-up because it is thinner, however, we suggest in this study that break-up in Afar is not necessarily a function of the apparent thickness of the crust. The northern Afar has not experienced the same amount of magmatism and underplating as Central Afar. Furthermore, the mantle temperature anomaly was most likely lower in northern Afar than in Central Afar and the mode of rifting is appears to have been different as a result.

5.7. Comparison with Volcanic Passive Margins

The model presented here has several implications for the formation of volcanic margins. In Figure 13, we compare our Central Afar cross-section to a section of the Pelotas margin in the South Atlantic [*Stica et al.,* 2014]. The thinning of SDR formation at the Pelotas margin, though unclear, appears to have been syn-rift, coeval with the first rifting phase of thinning and followed by a phase of sag-like accommodation of lava weight [*Stica et al.,* 2014]. The overall thickness of the SDR is several tens of kilometers whereas in Central Afar it is only few km thick (Figs. 5, 6, 8). This is likely due to the fact that Central Afar has not yet reached the break-up stage. If magma decompression is enhanced by a thin lithosphere, as suggested by the eruption of the Stratoïd above a thin crust (Figs. 10, 11), then the complete removal of the initial crustal thickness should provoke another, break-up-related, pulse of magmatism which would cover up the pre-existing tilted-blocks. In our view, SDR development is controlled by two parameters: 1) the intensity of magma decompression, which is probably enhanced by thinning of the crust (with maximum thinning experienced during break-up; see Section 5.6, above); and 2) mantle temperature. *Rooney et al.* [2012] showed that the Ethiopian Large Igneous Province (LIP) has a lower mantle potential temperature (Tp) than any other LIP. A Tp anomaly of +170°C characterizes the Oligocene flood basalt, whereas the Tp anomaly of <10 Myr old lavas in Djibouti is only +140°C [*Rooney et al.,* 2012]. The recent lavas at Manda Hararo exhibit a Tp anomaly of +150°C [*Ferguson et al.,* 2013]. Although hotter than normal asthenospheric mantle (Tp = 1350 ± 50 °C, *Herzberg et al.* [2007]), the Tp recorded in the Afar lavas are still some 100°C lower than in the North Atlantic Province [*Rooney et al.,* 2012]. Even though crustal thinning has been shown to be the primary control on massive SDR emplacement along the North Atlantic margins [*Armitage et al.,* 2009], it is likely that a low Tp would have had an effect on the volumes of magma produced and erupted. In Afar, we suggest that the Stratoïd to recent lava series are equivalent to SDR or proto-SDR (blue and purple units in Figs. 1, 2, 8 and 10) as they thicken towards and into the active magmatic segment (i.e., the rift center). Of note, these (proto)-SDR are emplaced over an already thinned and intruded/underplated crust.

An important question raised by examining the Pelotas margin in Figure 13 is the temporal relationship between the SDR emplacement and the first oceanic crust.

Towards the ocean, the most recent layers of the SDR fan lie on oceanic crust, which means that the youngest part of the SDR fan is post break-up (or syn-break-up), emplaced after (or during) the formation of the first oceanic crust (Fig. 13). This implies that break-up sometimes occurs during the SDR emplacement, some of the layers being syn-rift, others being post-rift. In our schematic cross-section (Fig. 13), it appears that the place where the lower crust is the youngest (i.e. thinned and re-thickened by underplating during rifting) corresponds to the thinnest part of the upper crust, where most of the material is erupted volcanics. In this particular view, the break-up consists of the complete removal of the upper crust, which would then be replaced by volcanic material. Successive re-thickening by mafic material would then modify the lower crust in the same way that the initial pre-rift lower crust was thinned to 0 km and then replaced by new syn-rift accreted lower crust, analogous to the transitional crust described in many models [e.g. *Menzies et al.,* 2002; *White et al.,* 2008; *Franke,* 2013]. We suggest that in this type of magma-rich environment, break-up can be defined as the complete removal of the upper crust, marking a lateral transition from 'continental upper crust and continental lower crust' to 'surface volcanics and newly accreted gabbroic lower crust', the latter constituting the continent-ocean transition. This would be consistent with the model of magma-assisted extensional growth presented in the study of *Quirk et al.* [2014]. Here, a high quality seismic line from East Greenland was used to observe the transitional crust beneath the SDR. The SDR were observed in a 50-km-wide band between the continental slope and the oceanic crust, underlain by a narrow necking zone. The transitional SDR-bearing crust (identified using magnetic and gravimetric profiles) is composed of around 4 km of volcanics forming the SDR fans, 4 to 6 km of faulted mid-crust, and 2 to 5.5 km of lower crust, which correlates with mafic underplating towards the continent [*Quirk et al.,* 2014]. The SDR fans begin in the hanging wall of a major landward dipping fault. The continental upper crust disappears on the footwall of this fault. The fault then flattens and is rooted in the lower crust. The authors interpret this ~160 km long structure as being the last syn-rift fault as it marks the outer limit of the continental crust, and they therefore referred to it as 'Break-up Fault' [*Quirk et al.,* 2014]. The outer limit of the transitional SDR domain is marked by a second major fault – referred to as 'Ocean Continent Boundary' – that separates the SDR from 'normally' structured oceanic crust [*Quirk et al.,* 2014]. According to their observations and to the magnetic and gravimetric inversion data of *Voss et al.* [2009], the lower crust of the transitional domain has the same composition as both the continental underplating and the oceanic crust.

Despite the similarities between Central Afar and the present-day volcanic passive margins of Pelotas and East Greenland, there are some important differences. The first is that the length of the half-margin appears to be narrower for the two present-day rifted margins. The transitional crust zone is also narrow in East Greenland (~50 km; [*Quirk et al.,* 2014]), which infers localized rifting. This is

consistent with volcanic passive margin formation models that predict a narrow margin as a result of localized extension [e.g. *Callot et al.,* 2001; 2002, and references therein]. In these models, the rapid necking of a strong, four-layered lithosphere is achieved by incorporating a weak zone in the mantle, corresponding to a thermal anomaly [*Callot et al.,* 2001]. These thermal anomalies, or soft points [*Geoffroy,* 2001], are assumed to be persistent zones of localized partial melting in the mantle that act as local rheological weaknesses. They favor the localization of the break-up zone and drive the segmentation of the future margin [*Callot et al.,* 2002]. However, the models do not consider the possibility that a broad zone of the mantle may be anomalously hot, which would have an effect on the distribution of the deformation (see Section 5.5, A 'Magmatic wide-rift' during the Mio-Pliocene). Although our results do not allow us to predict the future zone of breakup or the geometry of any transitional domain, the widely distributed strain in Central Afar 'half-margin' might be attributed to rheological modification due to the absence of 'normal' brittle lithospheric mantle and an elevated Moho temperature.

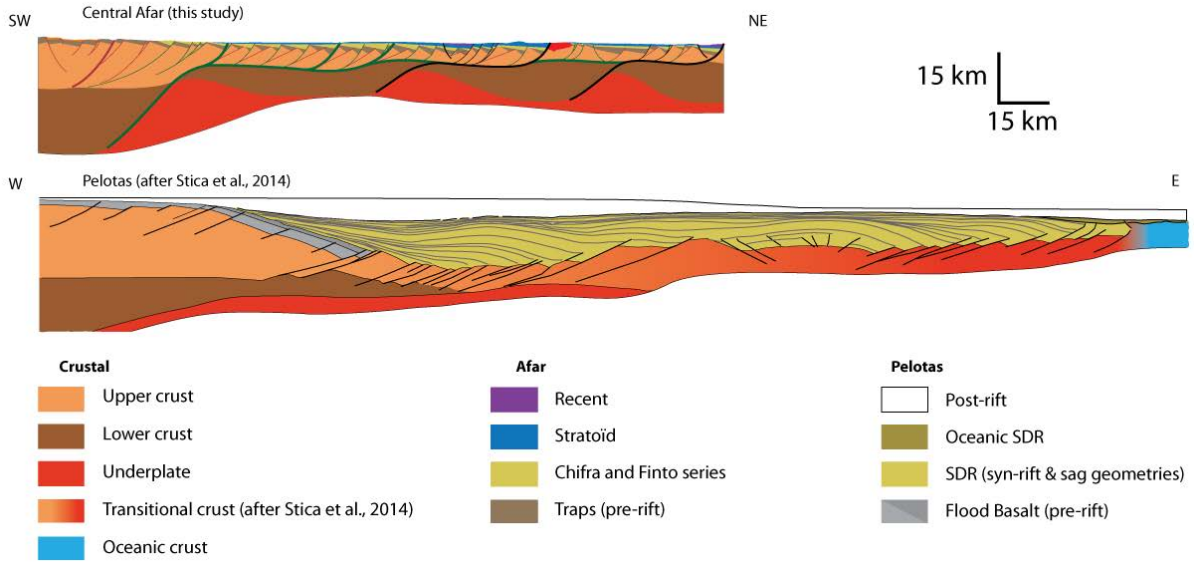

Figure 13. Comparison of the Central Afar half-rift presented in this study and an interpreted seismic line of the Pelotas basin (modified from Stica et al., [2014]).

Another difference is the size of the underplating beneath the Pelotas margin compared to Central Afar (Fig. 13). In Pelotas, the underplated layer seems to be too thin to compensate for the amount of erupted SDR. One possible reason for this is that the required volume of mafic material left over after SDR differentiation is hard to estimate. In Section 5.3, estimation of cumulate volumes was seen to be closely tied to the composition of extruded lavas. If the minimum underplating/erupted lava ratio of ~ 0.5 of *Cox* [1993] is correct for primitive basalts, then the amount of underplating present below the Pelotas margin in Fig.13 may well be correct.

However, if there are more-evolved lavas, such as rhyolites, present in the SDR, then this ratio should be considerably higher [*Cox*, 1993]. If so, the thinness of the underplated layer might instead be explained by a ductile nature of the underplating. In this case, lateral mass movements enhanced by ductile flow could displace the underplating and thus lead to an apparent deficit in the volume budget along strike.

6. Conclusions

In this contribution we have refined the volcanic stratigraphy of Central Afar and re-mapped certain key areas along a transect that stretches from the Ethiopian plateau to the Manda Hararo active rift axis. We show that extension was accommodated over a wide zone during the early Miocene rifting and that extension remained diffuse until the recent formation of an active volcanic axis (<1 Ma). We also demonstrate that the tectono-magmatic evolution of the Central Afar was marked by two flood basalt pulses (at 30 Ma and 4 Ma) each followed by a tectonic phase (stretching, thinning and localizing). Long periods of tectonic quiescence are characterized by 'starved' volcanism with the emplacement of rhyolitic series during the Miocene (23 Ma – 7 Ma). This apparent gap in the extension record implies that extension must have been at play elsewhere on the Danakil block (and southern red Sea), which can no longer be considered as an undeformed, steady micro-continent.

The crust has experienced much more thinning than is usually documented by geophysical studies in this area. Our restorations suggest that thinning of the Afar crust has been compensated for by magma intrusion and underplating. We argue in favor of a shear zone at mid-crustal levels with a top-to-west sense of shear on which landward-dipping continental faults are rooted. Such a structure explains both the distributed fault pattern in the upper crust and the localization of crustal thinning into a narrow necking zone at depth. The presence of crustal underplating is predicted by our restorations. This underplating would be distributed in the lower crust but mostly below the deep root of the detachments. Moreover, the predicted volume of underplated material is consistent with the volume of the lava series erupted at the surface.

Once the crust had been sufficiently thinned (although its thickness was partially maintained by magma addition), the Stratoïd flood basalt pulse occurred, which was possibly analogous to SDR. We have called this particular tectono-magmatic style of rifting 'magmatic wide-rifting' and we link it to the effect of mantle temperature and magma on the lithospheric rheology. In the case of Central Afar, both factors prevent localization of deformation: thermal attenuation and weakening of the lithospheric mantle coupled with weak and thick lower crust during extension led to a distributed mode of rifting.

The difference between the wide, magma-rich, thick crust Central Afar segment and the narrow, thin and relatively magma-poor Northern Afar Erta'Ale segment is probably due to differences in magma supply. Both segments are probably

close to break-up and apparent crustal thickness cannot be used to predict the location and timing of break-up.

The implications of our findings are that volcanic rifted margins are not necessarily narrow and that the wide rift mode can occur and be maintained during most of the history of rifting until the area proceeds to break-up. Eruption of large magma volumes (such as SDR) is not necessarily synchronous with the lithospheric thinning, but may rather intrude into and erupt over an already thinned lithosphere.

Acknowledgements

The various structural and radiometric data used to produce the maps and cross-section in this article are all presented in the figures and tables. This work was financially supported by the 'Actions Marges' program and by TOTAL. For their help on the field, we would like to thank the Afar local government and the Ministry of Mines of Semara. The authors thank Bouchaïb Tibari (CRPG) for technical assistance with (U-Th-Sm)/He analyses, Gilles Peltzer (UCLA) for providing Landsat imagery, Alain Rabaute (UPMC) for his help with the SIG mapping and Cécile Doubre (EOST) for useful discussions. We acknowledge Claudio Faccenna and Derek Keir for editorial handling along with Julie Rowland and one anonymous reviewer for their critical reading and comments, which were of great help in improving the quality of the manuscript. We finally warmly thank Alice Williams for providing many useful corrections to the English. This is CRPG contribution n° 2404.

CHAPITRE 4
-
ÉVOLUTION DES RÉGIMES DE FUSION MANTELLIQUE EN RÉPONSE A L'EXTENSION

- Article en préparation pour soumission à *Geochemistry, Geophysics, Geosystems.* -

Dans le chapitre précédent, nous avons documenté les différentes phases d'extension et d'amincissement crustal en nous basant sur des arguments structuraux. Nous avons montré que l'amincissement crustal se produisait de manière tardive entre 7 et 5 Ma par rapport au début du rifting (29-26 Ma), mais avant la mise en place des premières coulées de la Série Stratoïde, trouvée à Sullu Adu (~ 4 Ma).

Dans ce chapitre, l'objectif et d'étudier la réponse mantellique associée à cette extension crustale. Nous préciserons l'évolution du manteau lithosphérique par rapport à l'extension, et dans quelle mesure celle-ci est influencée par le panache Afar.

Notre approche sera donc pétro-géochimique. Nous utiliserons les compositions en éléments majeurs et traces dans les liquides basaltiques émis en surface à chaque étape de déformation crustale en nous basant sur le calendrier établi dans le chapitre précédant. Notre objectif est d'interpréter ces signatures spécifiques en terme de processus de fusion partielle (ou « régime mantellique »). Que peuvent-elles nous apprendre sur la profondeur (P) du manteau qui fond, sa température (T) et la quantité (F) de magmas produits ?

Toutefois, le régime mantellique n'est pas le seul paramètre capable d'influencer les signature géochimiques des laves : pour les éléments traces et les Terres Rares (REE) elles peuvent varier indépendamment de celui-ci en fonction de la chimie de la source qui les a produit. Aussi faut-il s'assurer que tous les basaltes que nous comparerons entre eux proviennent de la même source.

Pour ce faire, nous nous basons sur des travaux complémentaires à cette étude de *Pik, Stab et al.* (in prep) qui documentent, sur une grande partie des échantillons utilisés dans ce chapitre, les compositions isotopiques (Sr-Nd-Pb), et réinterprètent le jeu de données des laves des plateaux, de l'Afar et du Main Ethiopian Rift depuis les Trapps jusqu'à l'actuel. Les résultats principaux de cette étude sont que :

- (1) les basaltes syn-rift de la marge W-Afar, ceux d'Afar Central et ceux du MER expriment une signature isotopique identique à de celle des Trapps High-Ti

pré-rift (Fig. I), qui est interprétée comme étant la signature du panache Afar (modifiée par une composante de contamination crustale mineure)

- (2) la signature isotopique radiogénique en Pb de toutes les laves régionales est interprétée comme étant issue du manteau lithosphérique sous-continental (en suivant l'interprétation des travaux précédents de *Baker et al.* (1996) ; *Pik et al.* (1999) ; *Bertrand et al.* (2003) ; *Lucassen et al.* (2008) ; et à l'inverse des réservoirs interprétés par *Schilling et al.* (1992) ; *Deniel et al.* (1994) ; *Rooney et al.* (2012)).

- (3) cette réinterprétation permet de proposer un modèle de distribution et d'évolution des sources mantelliques au cours de l'extension en bon accord avec la segmentation et les conclusions des chapitres 3, 4 et 5 de cette thèse, qui met en évidence l'influence du Panache Afar sur l'évolution de l'Afar Central (Fig. II).

Pour construire notre chronologie évolutive du manteau, tous les échantillons discutés dans ce chapitre proviennent donc bien d'une même source mantellique.

*Figure I. Ci-contre, page de droite. Evolution des signatures isotopiques des laves de la marge W-Afar et Afar Central au cours de l'extension (*Pik, Stab, et al., *in prep.). Le code de couleurs pour les laves correspond au composant principal impliqué : rouge = panache Afar ; jaune = lithosphere continentale ; orange : mélange entre le panache Afar et la lithosphère continentale ; vert : Depleted Morb Mantle. Les deux poles du panache Afar (HT1 et HT2,* Pik et al., *1999) et les deux poles presents dans la lithosphere continentale (;* Shaw et al., *2007 ;* Lucassen et al., *2008) sont distingués avec des carré rouges et jaunes respectivement. Les points noirs représentent des incréments de 10 % le long des courbes de mélange reliant les pôles. Les points jaune à cercle marron correspondent aux compositions isotopiques des péridotites du manteau lithosphérique des plaques Africaine et Arabe qui montre une signature essentiellement appauvrie.*

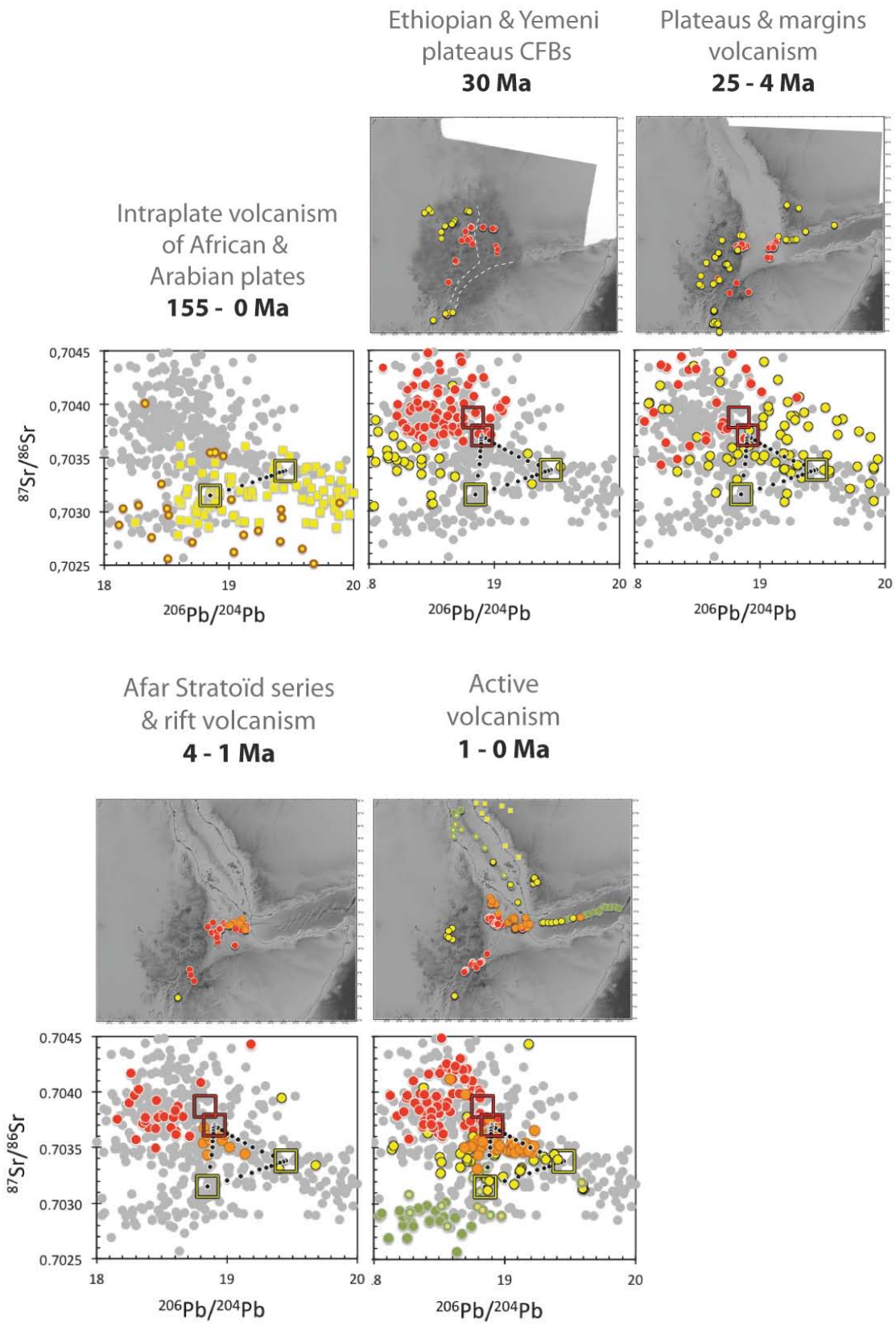
Ethiopian & Yemeni plateaus CFBs
30 Ma
Plateaus & margins volcanism
25 - 4 Ma
Intraplate volcanism of African & Arabian plates
155 - 0 Ma
Afar Stratoïd series & rift volcanism
4 - 1 Ma
Active volcanism
1 - 0 Ma
87Sr/86Sr
206Pb/204Pb
0,7045
0,7040
0,7035
0,7030
0,7025
18
19
20

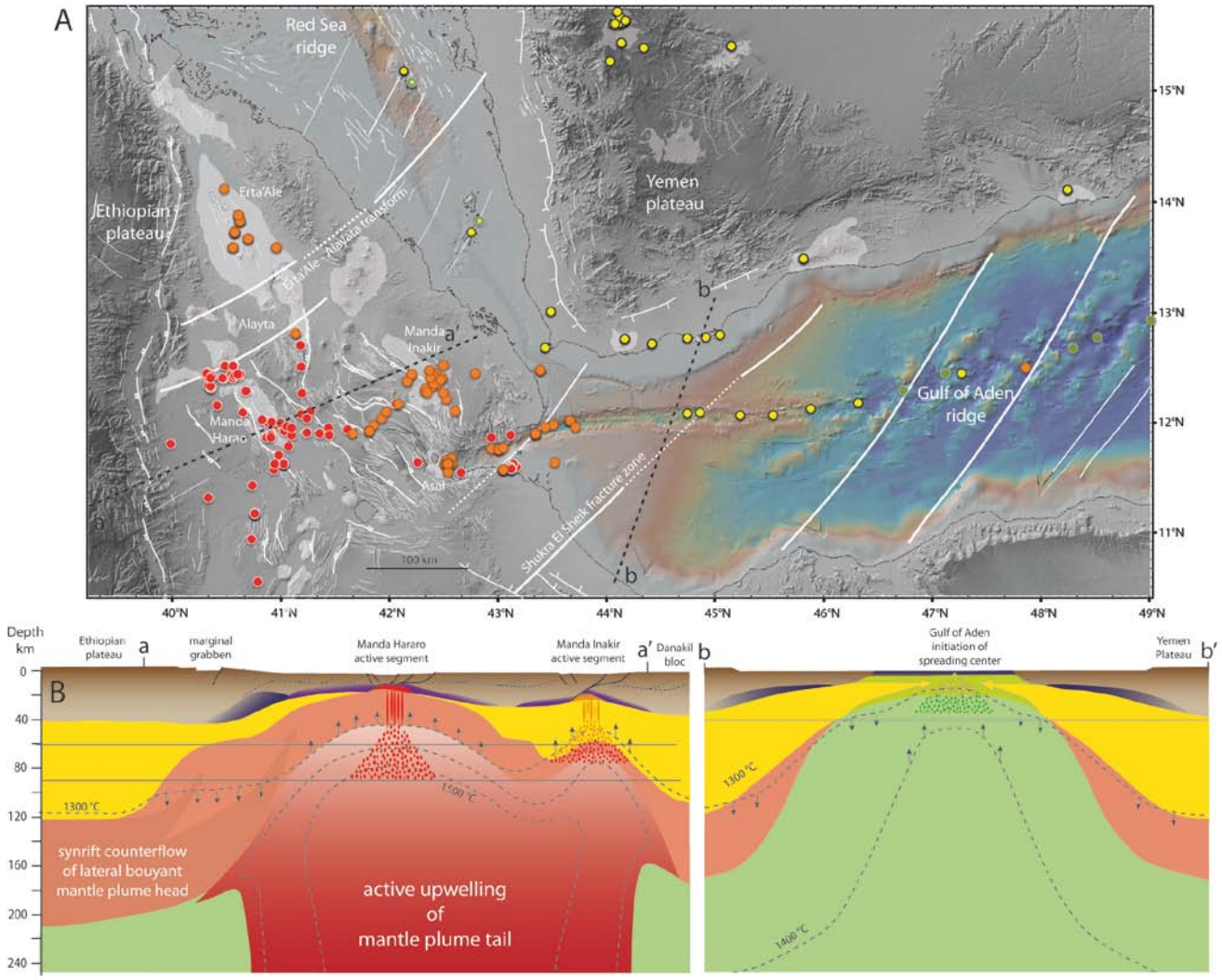

*Figure II. A : répartition spatiale des signatures isotopiques des laves de la province volcanique Afar (*Pik, Stab, et al., *in prep.). Le code de couleur est le même que sur la figure I. Structure d'après* Stab et al., *(in prep., chapitre 5). B : modèle de l'état du manteau sous la province volcanique basé sur l'interprétation des signatures isotopiques (figure I) des laves, ainsi que les profondeurs et températures de fusion (*Rooney et al., *2012 ;* Ferguson et al., *2013 ;* Stab et al., *in prep., Chapitre 4). Les signatures isotopiques identiques pour les trapps, la marge W-Afar, l'Afar Central et le MER (points rouges sur la figure I) impliquent que le matériel mantellique issu du panache Afar a continuellement participé à la genèse des laves à l'apex de la tête du panache, dans la zone centrale du dôme soulevé, là où la future marge volcanique va se développer (coupe a-a'). Dans cette zone, la lithosphère continentale ne participe jamais à la fusion, ce qui contraste avec les zones latérales où pendant la mise en place des trapps LT, et plus tard lors de la localisation des volcans boucliers sur les plateaux, elle domine. Pour être en accord avec les données P, T et F (*Stab et al., *in prep, chapitre 4) il faut envisager que cette fusion du matériel du panache s'effectue au cours du rifting (25-7 Ma) par refroidissement progressif et fluage latéral de la tête impactée à l'Oligocène (qui est représenté par du matériel mantellique plus*

"flottable"). Grâce à ce fluage latéral et à l'érosion thermique du manteau lithosphérique, la tête du panache va très tôt dans l'histoire de l'Afar Central remplacer le manteau lithosphérique dans cette zone, menant probablement à un break-up mantellique avant le break-up crustal (similaire au marges de type II de Huismans et Beaumont, *2014). La deuxième coupe (b-b'), perpendiculaire au Golfe d'Aden, représente le phénomène inverse avec la participation actuelle du manteau lithosphérique dans la genèse des basaltes à l'axe de la dorsale jusque vers 46°E, alors que d'après les anomalies magnétiques le break-up crustal à eu lieu il y plusieurs Ma (*Leroy et al., *2012). Ceci met en évidence le sous-placage probable de manteau lithosphérique sous la marge et ceci jusqu'à l'axe du rift pendant et après le break-up lors de l'installation du système de spreading (marges de type I-C de* Huismans et Beaumont, *2014). Il faut noter aussi le fluage latéral possible de ce même matériel dans le compartiment océanisé depuis 18 Ma de l'autre coté de la zone de fracture de Shukra El Sheik, et l'anomalie topographique et volcanique que ceci engendre grâce à la fusion d'un manteau lithosphérique continental probablement très fusible.*

Mantle melting regime and lithospheric thinning constrained by basalts geochemistry at the Central Afar nascent volcanic passive margin

Martin Stab[1,2], Raphaël Pik[2], Nicolas Bellahsen[1], Sylvie Leroy[1], Dereje Ayalew[3]

[1] Sorbonne Universités, UPMC Univ Paris 06, CNRS, Institut des Sciences de la Terre de Paris (iSTeP), 4 place Jussieu 75005 Paris, France
[2] CRPG UMR 7358 CNRS, Université de Lorraine, 15 rue Notre Dame des Pauvres, BP20, 54500 Vandoeuvre-lès-Nancy, France,
[3] School of Earth Sciences, Addis Ababa University, Addis Ababa, Ethiopia

Corresponding author: Martin Stab, mstab@crpg.cnrs-nancy.fr, CRPG-CNRS, 15 rue Notre Dame des Pauvres, BP20, 54500 Vandoeuvre-lès-Nancy

Abstract

The conditions under which the mantle melts (i.e. pressure, temperature, extent of melting) during the formation of a volcanic passive margin are fundamental parameters that should be taken into account in order to understand how the mantle is thinned prior to break-up, and how the ocean-continent transition formed. However, the syn-rift lavas, which are principal markers of the aforementioned processes, are usually inaccessible because located several kilometers underwater and sediments. In this paper, we provide new data on the syn-rift history of extension of a nascent offshore volcanic passive margin, Central Afar, to better constrain these melting conditions. We carry out a geochemical study of the depth and extent of melting that formed primitive basalts associated with each step of extension. We use fractional-crystallization corrected elements suchs as $Fe_{7.3}$ and $(Sm/Yb)_{n,7.3}$ (depth proxies) and $Na_{7.3}$, $Ti_{7.3}$, $(La/Sm)_{n,7.3}$ (extent of melting proxies) to determine the evolution of the mantle during rifting. We then compare these proxies to the equilibrium pressure and temperature of formation of these magmas. Our main findings are that the lithospheric mantle was brutally thinned after the continental flood basalt (CFB) emplacement at 30 Ma, due to the thermal erosion induced by the Afar plume impingement and localized mantle anisotropy associated to the large volumes of CFB extracted. The melting conditions were sustained during the Late Oligocene to Early Miocene, where the mantle experiences a post-Traps cooling. The lithospheric mantle is again thinned – probably during or shortly after the main crustal thinning event at ~7 Ma. This thinning occurred prior to the Stratoïd flood basalt eruption at 4 Ma, which records a corresponding geochemical signature (lid effect) that is strongly associated with previously thinned zones in the crust. The

mantle is again hot (T_P > 1500°C) during the active axis emplacement in Afar, suggesting a plume stem, which in turn is absent from the Main Ethiopian Rift.

1. Introduction

The knowledge of the interplays between tectonic extension and mantle melting is fundamental to understand the formation of volcanic passive margins – and their relationship with hot mantle plumes. Indeed, volcanic passive margins can form where the mantle temperature is elevated during extension or break-up [*White and Mckenzie*, 1989] and where spreading rate was elevated [*Bown and White,* 1995]. They were therefore generally associated to the break-up of the lithosphere above oceanic hot-spots [*Campbell,* 2007; *Armitage et al.,* 2010]. However, it has been shown that this simple relationship is not straightforward. The lateral variations in the volume of syn-rift magmatism is sometimes inconsistent with the proximity to a volcanic province [e.g. *Franke et al.,* 2007], some hotspots postdate the first oceanic crust initiation [e.g. *Menzies et al.,* 2002]; Furthermore, flood volcanism (expressed either by continental flood-basalts or CFB and by seaward-dipping reflectors or SDR) is not restricted to break-up and can occur at the pre-rift and the pre-to syn-rift transition stages [*Menzies et al.,* 2002]. More recently, it has been shown that the way the lithosphere has been thinned prior to a thermal anomaly impingement had a considerable influence on the volumes of magma produced, and thus the volcanic nature of the margin [*Armitage et al.,* 2009, 2010]. If the lithosphere is thick, the thermal anomaly cool down and do not produce syn-rift or syn-break-up magmas [*Armitage et al.,* 2009]. If it is thin, important volumes of magma are produced, even if the spreading rate is low [*Armitage et al.,* 2009]. This shows the importance of building a sound temporal frame for crustal/lithosphere deformation and mantle activity. Therefore, knowledge of the melting conditions (depth and extent of melting, potential temperature, etc.) during the syn-rift period of time at volcanic margins can provide insights on the geodynamic processes. The syn-rift lava record at volcanic passive margins take the form of the voluminous magmatic wedges, called seaward-dipping reflectors (or SDR) [*Menzies et al.,* 2002; *Geoffroy et al.,* 2005; *Quirk et al.,* 2014]. These wedges syn-tectonic growth is controlled by major listric continentward dipping normal faults [i.e. *Clerc et al.,* 2015]. Although there were significant improvement on the SDR structures made in the past years thanks to new high quality seismic refraction lines [e.g. *Quirk et al.,* 2014; *Clerc et al.,* 2015], little is known about the state of the mantle at the moment of eruption because the only available geochemical data come from sparse IODP drilling [see *Franke et al.,* 2013 for a review].

The Central Afar and Main Ethiopian Rift (MER) in Ethiopia are ideal areas to study the lithospheric extension/melting interactions. It forms the northern tip of the East African Rift system that eventually connects in a triple rift junction with the Red Sea and the Gulf of Aden [*Wolfenden et al.,* 2004]. It presents the unique

opportunity of studying a magmatic evolution in the frame of a well-constrained rifting history [*Stab et al.,* 2015]. Magmatism was active for the last 30 Ma and both rifts (Afar and MER) began to open after the Afar plume impingement and the Traps eruption at 30 Ma. The hot Afar plume thermally eroded the lithosphere [*Ebinger and Sleep,* 1998], so that the Central Afar and the MER developed above an extensively thinned [*Dugda et al.,* 2007; *Pasyanos et al.,* 2009] and weak [*Stamps et al.,* 2010] lithosphere. The MER is a classical case of narrow-rifting [*Buck,* 1991] where extension has been localized in a ~30 km wide valley [*Corti,* 2003], presumably due to Neoproterozoic sutures [*Keranen et al.,* 2009]. Conversely, Central Afar has experienced a protracted period of wide rifting, where extension was distributed, with discrete stretching and thinning episodes punctuated by magmatic activity [*Stab et al.,* 2015].

Most past studies that intended to constrain the Ethiopian melting regimes were focused either on the Oligocene Traps basalts and aimed to better understand the manner flood basalts derived from a deep, primitive, mantle plume source [*Mohr and Zanettin,* 1988; *Pik et al.,* 1998; 1999; 2006; *George and Rogers,* 2002; *Kieffer et al.,* 2004; *Beccaluva et al.,* 2009] or where focused on the tectono-magmatically active segments – whether to highlight the plume-like origin of those rocks [*Barrat et al.,* 2003; *Pik et al.,* 2006, in prep; *Rooney et al.,* 2013] or to constrain the hot and deep origin of these lavas [*Ferguson et al.,* 2013; *Pinzuti et al.,* 2013].

Although those studies provided pertinent insights into the mechanism of rifting in Ethiopia, they all suffer from considering only the very beginning of it (30 Ma traps) and the very end (present-day lavas). For instance, *Armitage et al.* [2015] modeled the continuous extension of the Afar region, taking into account only the pre-rift and present-day situation. The syn-rift magmatic history is poorly documented although it can have major implications to understand the crust/mantle interactions and the development of the future volcanic margin. Furthermore, it is widely accepted that the lithosphere beneath Ethiopia has been thinned [i.e. *Pasyanos et al.,* 2009; *Rychert et al.,* 2012], but little is known about the timing of this thinning [*Stab et al.,* 2015]. Constraining this process would help understanding the tectono-magmatic relationships.

This study is an attempt to fill this time gap. We bring new data about syn-rift lava series that cover the major steps of extension, along with the younger and extensive Stratoïd series that covers the major part of the area [i.e. *Barberi and Santacroce,* 1980; *Wolfenden et al.,* 2005; *Stab et al.,* 2015]. We combine those with available literature data to provide a complete temporal framework relevant for Central Afar. The magmatic evolution of Central Afar, from the Oligocene Traps is compared to the Main Ethiopian Rift, which evolution since the last 30 Ma has been markedly different. The interactions between the crustal extension and mantle thinning and magmatic activity will be discussed. Eventually, we will try to answer the following questions: how does the mantle melt during the syn-rift history of the

region? What is the significance of the Stratoïd in the Central Afar context? What are the links between mantle regime and accommodation of extension? Is Central Afar far from break-up [i.e. *Hayward and Ebinger,* 1996; *Bastow and Keir,* 2011]?

2. Context

2.1. Geological settings

The Traps were erupted at ca. 30 Ma [*Hofmann et al.,* 1997; *Rochette et al.,* 1998*; Coulié et al.,* 2003] prior to the beginning of extension, which started in the MER in between 20 – 10 Ma, in a diachronous way [*Wolfenden et al.,* 2004; *Bonini et al.,* 2005; *Pik et al.,* 2008]. Extension started earlier in Afar between 29 and 26 Ma [*Ukstins et al.,* 2002; *Wolfenden et al.,* 2005; *Stab et al.,* 2015]. The opening of the MER accommodates the divergence between Somalia and Nubia, whereas extension in Afar, Red Sea and Gulf of Aden accommodates the divergence between Arabia and Somalia/Nubia. At the present days, these plates are diverging with a slow velocity: 20 to 15 mm/yr directed N45° for Afar [*McClusky et al.,* 2010] and 6-7 mm/yr directed N100° for the MER [*Fernandes et al.,* 2004].

The Central Afar and MER rifts have developed with markedly opposed structural styles. The MER is a localized narrow-rift, where the crust has stretched in a > 100-80 km wide zone [sensu *Buck,* 1991], although it has been deformed over a hot lower crust and a thin and weak mantle lithosphere [see the review in *Corti,* 2003], which should enhance distribution of the deformation in a 'wide-rift' [Buck, 1991, Buck et al., 1999]. This is explained by the reactivation of previous Neoproterozoic sutures [*Keranen et al.,* 2009], which can cause localization of the deformation despite a weak rheological layering [*Sokoutis et al.,* 2007]. In contrast, the Afar rift is segmented from south to north [*Hayward and Ebinger,* 1996]. The Central Afar has been deformed over a wide area [*Kogan et al.,* 2012], at least since the early Miocene [*Stab et al.,* 2015]. Its crust is apparently thick [*Hammond et al.,* 2011], but has been heavily underplated during rifting [*Stab et al.,* 2015]. Northern Afar (Erta'Ale) segment is in turn much narrower and with thinner crust [*Makris and Ginzburg*, 1987; *Bastow and Keir,* 2011]. It has been proposed that the northern segments are closer to break-up than the Central part [*Bastow and Keir,* 2011], because the crust is here apparently thinner and the length and width of the active segments (narrow Erta'Ale vs. much wider Tendaho, Dobi graben, etc.) resemble more those of oceanic spreading centers [*Hayward and Ebinger,* 1996]. However, the 'replacement' of stretched and thinned continental crust by mafic material, underplated and extruded, leading to a proto-oceanic mafic lower crust, has been proposed as a break-up mechanism [*Quirk et al.,* 2014]. This requires a heavily thinned crust [*Quirk et al.,* 2014] and growth-faults to accommodate cooling melts,

such as detachments [*Dick et al.,* 2008; *Quirk et al.,* 2014]. This mechanism may be at play in Central Afar [*Stab et al.,* 2015].

2.2. Magmatic series

The Traps consist of a ~500 to 2000 m thick pile of bi-modal lavas [*Mohr and Zanettin,* 1988; *Pik et al.,* 1998*; Ayalew et al.,* 2002], emplaced by fissures fed by dykes [*Mège and Korme*, 2004]. The Traps mafic lavas are High-Titanium (HT) picrites to the southeast and Low-Titanium (LT) in the northwest of the Ethiopian plateaus [*Pik et al.,* 1998]. The 500m thick Traps rhyolites are the differentiation products of the basaltic melts [*Ayalew et al.,* 2002]. They are interpreted as originating from the fusion of primitive mantle material, as they have elevated $^{3}He/^{4}He$ ratios up to 20 R/Ra [*Marty et al,* 1996, *Pik et al.,* 2006] and solar-like $^{21}Ne/^{22}Ne$ down to 0.034 [*Halldórsson et al.,* 2014]. This primitive material was likely upwelled by the Afar plume [*Li et al.,* 2008*; Ritsema et al.,* 2011]. The HT basalts are indeed produced by a hot mantle [*Rooney et al.,* 2012], characteristic of other CFB worldwide [i.e. *Cox,* 1980; *Fram and Lesher,* 1997].

The Dessie basalts series [*Stab et al.,* 2015] are 26 to 24 Ma old basalts found mainly in the marginal graben along the western Afar margin [*Ukstins et al.,* 2002; *Wolfenden et al.,* 2005; *Stab et al.,* 2015], although they are found on some tilted blocks eastward of the marginal graben [*Ukstins et al.*, 2002; *Stab et al.,* 2015]. They consist of ~500 to 800 m of erupted basalts. They are directly emplaced after the initiation of rifting and therefore are the first 'syn-rift' series. These series are of particular importance from a geodynamic point of view, because they are the only basalts that follow one major stretching episode in Central Afar, dated between 29 and 26 Ma [*Stab et al.,* 2015].

The Dahla (and Mabla) series subsequently follow the Dessie series and are emplaced between 20-15 Ma up to 5-7 Ma [*Deniel et al.,* 1994]. The temporal limits of this geological formation vary according to the location: The Dahla basalts s.s. are restricted to the 9-4 Ma period of time in Djibouti [*Deniel et al.,* 1994] and the Mabla series is 20-9 Ma [*Le Gall et al.,* 2010], while on the western side of the rift, correlations are less straightforward due to many internal unconformities [see *Wolfenden et al.,* 2005]. These series are bi-modal in Djibouti, with numerous occurrences of mafic products [Deniel et al., 1994] and a pile thickness of some 200 m [*Daoud et al.,* 2010] to 1 km [*Le Gall et al.,* 2011], whereas it is more silicic in northern Central Afar, characterized by few volumes of rhyolites, punctually erupted within a timespan from 23 Ma to 7 Ma [*Stab et al.,* 2015]. Although the pre-Dahla tectonic history is hard to constrain [i.e. *Le Gall et al.,* 2011], the Dahla series in Central Afar predate or are coeval with a phase of crustal thinning that thinned the crust to its present-day thickness [*Stab et al.,* 2015].

The Stratoïd is a pulse of flood basalts [*Barberi et al.,* 1972; *Barberi and Santacroce,* 1980] that covers ~70% of the Afar flood [*Varet,* 1978], although its

presence is restricted to Central Afar and is absent from the northern side of the main transform that separates central Afar from the Erta'Ale segment in northern Afar. It reaches the thickness of at least 1000 m, although its base has never been observed [*Barberi and Santacroce,* 1980]. Its eruption occurred between 4 Ma and 1 Ma [*Barberi et al.,* 1975] with a peak activity at 2 Ma – which defines the transition from Lower to Upper Stratoïd [*Kidane et al.,* 2003]. They were classically interpreted as the beginning of oceanic floor spreading [*Barberi and Santacroce,* 1980] although they have enriched REE pattern [*Deniel et al.,* 1994] and overly a crust that is of continental nature [*Hammond et al.,* 2011]. These series are an important tectono-magmatic milestone, because it is currently unclear if the Stratoïd emplacement was synchronous of significant crustal or lithospheric extension. In Central Afar, there is a lack of field relationship (such as syn-tectonic structures) to answer this question [see *Kidane et al.,* 2003; *Acocella et al.,* 2008], although syn-tectonic wedges are observed in Djibouti [*Geoffroy et al.,* 2014], which is a distinctive characteristic of volcanic margins [*Quirk et al.,* 2014; *Clerc et al.,* 2015]. It has been suggested that Stratoïd could represent an equivalent to SDR [*Stab et al.,* 2015], as they are emplaced above previously thinned crust, which is a prerequisite to syn-break-up eruption of SDR [*Armitage et al.,* 2009].

The Ethiopian lithosphere has been thinned since the Oligocene, probably in response of the thermal erosion generated by the Afar plume and by tectonic stretching. The lithospheric mantle extends from 30 to 80 km depth beneath he Ethiopian plateaus [*Dugda et al.,* 2007; *Rychert et al.,* 2012] and is much thinner beneath Central Afar: it extends from 20 to 30 km depth [*Dugda et al.,* 2007], or even thinner – perhaps absent [*Pasyanos et al.,* 2009]. The mantle temperature have cooled from ~ 1550 °C to 1450 °C from the Oligocene to present-day [*Rooney et al.,* 2012; *Ferguson et al.,* 2013] in Central Afar. This is attributed to the cooling of the plume head and the switch form active upwelling to passive decompression melting [*Rychert et al.,* 2012; *Hammond et al.,* 2013]. In contrast, the MER lithospheric mantle is probably as thin as the Afar one [*Keranen et al.,* 2009], although less hot, with a temperature close to the temperature of the ambient MORB mantle [*Rooney et al.,* 2012].

3. Rationale, dataset and methods

3.1. Rationale

The aim of this study is to document the melting regimes during the syn-rift period, from 26 to 1 Ma. To do so, the strategy is to compare the syn-rift Afar margin lavas to two other end members: the Traps basalts that bear the signature of initial pre-rift plume impingement and the recent MER lavas that represent a typical case of narrow-rifting, in a less-magmatic context and a 'simple' context of mantle

cooling since the last 30 Ma [*Ayalew and Gibson*, 2009]. Another constrain is to be able to compare the evolution of mantle activity with the evolution of crustal deformation as the extension of the margin proceeded. The data used in this paper must fit a well-defined profile of a complete rift segment, going from the pre-rift plateau through active segments. For this, we use the Sullu Adu – Manda Hararo rift segment of *Stab et al.* [2015], which has well-defined tectonic phases from 29 Ma to present-day. The 20-7 Ma period of time is represented by silicic lavas, and therefore not suitable for the methods used in this paper. We thus implement the Djiboutian Dahla series to this study.

There exist much data in the literature concerning Traps and recent lavas, and these are used as pre-rift and present-day conditions in studies that track the time evolution of melting conditions [*Ferguson et al.,* 2013; *Armitage et al.,* 2015]. The Dahla and Stratoïd [*Deniel et al.,* 1994; *Daoud et al.,* unpublished data] have never been implemented in such studies, most likely because of the wide spatial scatter of the available data. Indeed, so far the Stratoïd was documented only near Djibouti [*Deniel et al.,* 1994], or at the junction between the MER and the Central Afar [*Hart et al.,* 1989]. In this continental environment, such scatter is likely to bring up heterogeneities that can be erroneously interpreted. The Dahla was originally described in Djibouti [*Barberi et al.,* 1975], and only chrono-stratigraphic attempts were made to link the western Afar margin's rocks to the Dahla series [*Wolfenden et al.,* 2005]. The same applies to the Dessie series [*Ukstins et al.,* 2002; *Wolfenden et al.,* 2005; *Stab et al.,* 2015]. In other words, those volcano-stratigraphic markers where used to constrain the crustal tectonics of the region, but never in terms of mantle melting conditions.

3.2. Dataset and methods

We measured 58 new data of major and trace elements on aphyric basalts, from the Dessie, Dahla and Stratoïd series (Table 1). Recent lavas from Tendaho graben and Tat'Ale segment are documented as well, because they provide insights on the spatial variations of melting regimes at the present days. The new Stratoïd samples come from both sides of the Manda Hararo and Tendaho segments, so that they make an effective spatial junction between the samples of *Hart et al.* [1989] and *Deniel et al.* [1994]. New samples from the Gulf Basalt series [1.1 – 0.6 Ma, *Kidane et al.,* 2003] are added to the dataset, because they correspond to a phase of relocalization of the deformation [*Stab et al.,* 2015]. In line with these new data, previous data were used. Traps are HT2 samples from Pik et al. [1998]. Existing Dahla samples are taken from *Barrat et al.* [1993], *Deniel et al.* [1994] and *Daoud et al.,* unpublished data. They mainly cover the Djiboutian side of the rift. Manda Hararo on-axis [*Barrat et al.,* 2003; *Ferguson et al.,* 2013; *Medynski et al.,* 2013], off-axis [*Ferguson et al.,* 2013; *Medynski et al.,* 2015], and Main Ethiopian Rift [*Rooney et al.,* 2011] samples are the recent lavas erupted at axial zones.

As shown elsewhere [e.g. *Klein and Langmuir,* 1992; *Pinzuti et al.,* 2013], major elements such as Na, Ti, Fe in line with light and heavy rare earth elements (La/Sm, Sm/Yb) can be efficiently used as proxies for depth and extent of melting. To properly extract this particular signal from the geochemical signature of the lavas two conditions must be matched.

(1) We must avoid any effect of source variation when using trace element and rare earth elements. We thus based on the work of [*Pik et al.,* in prep] whose compilation and reinterpretation of the isotopic (Pb-Sr-Nd) systematics of Afar allowed redefining the mantle source(s) of magmatism. We chose rocks that thus have the same source than the traps HT2, which are interpreted to best represent the superficial expression of the Afar plume [*Pik et al.,* in prep].

(2) We must consider only primitive samples, and correct their elemental compositions from the fractional crystallization. Samples were sawed and crushed to avoid marks of alteration and phenocrystals. We then selected the most primitive (MgO > 4%, SiO_2 < 52%) and aphyric basalts so that our measurements reflect the composition of the liquid with minimum effect of phenocrystals accumulation. Major and trace elements were measured at SARM (Service d'Analyse des Roches et des Minéraux), Nancy on ICP-AES and ICP-MS respectively. Correction form fractional crystallization is detailed in the following section.

4. Fractional crystallization

4.1 Major elements

The evolution on major elements vs. MgO diagrams (Fig. 1) of all three groups distinguished in this study (HT2 traps, Syn-rift Afar margin lavas and MER lavas) reflects processes of low-pressure magma differentiation. This has been documented by various past studies [i.e. *Barberi and Santacroce,* 1980; *Pik et al.,* 1998; *Hart et al.,* 1989; Deniel et al., 1994; etc.] Indeed, the variations of major oxides in the liquid do reflect the progressive removal of the assemblage ol±cpx+pl (respectively olivine, clinopyroxene and plagioclase) from basaltic melts prior to their eruption. MgO is taken here as a differentiation index because it is the most relevant for mafic liquids that contain SiO_2 < 53 wt. % and MgO > 4 wt.% (Fig. 1). Please refer to Appendix A for more precise representation of all groups considered in this study.

HT2 traps are characterized by MgO content generally higher than 10 wt.% and are the most primitive lavas in the considered dataset. FeO* (total Fe expressed as Fe^{2+}, FeO* = 0.9 Fe_2O_3*), Na_2O, TiO_2, CaO and Al_2O_3 increase with MgO decrease, showing the effect of fractional crystallization. The absence of brutal kink in the trend suggests that mostly olivine fractionates between 16 wt.% and 7 wt.% MgO. However, lower values in SiO_2, Na_2O, below 14 wt.% MgO (Fig. 1) show that the most primitive samples may have accumulated olivine as phenocrystals (Na_2O

and K_2O are incompatible with olivine). It seems however that initial Na_2O concentrations for high MgO contents increase from the Traps toward the MER end-member, indicative of lower extent of melting [*Klein and Langmuir*, 1987]. CaO and FeO* are high in HT2 traps and samples fall on the subtraction line of olivine. As already demonstrated by *Pik et al.* [1998], HT2 traps have elevated TiO_2 of 3.92-4.62 wt.% compared to other samples (Fig. 1). This high value of TiO_2 and the fact that HT2 traps display the highest FeO* of all samples indicate that traps may originate from a deeper region in the mantle than the rest of the Oligocene to present-day lavas [*Langmuir et al.,* 1993]. This is commonly found in OIB, where it has been shown that high FeO* melts cannot be generated by initial low FeO* melts, typical of MORB for instance [*Putirka,* 2008]. The MER lavas have low FeO*, which in turns constitute a 'low-depth' endmember (Fig. 1). The Oligocene to Pliocene Afar margin syn-rift lavas (Dessie, Dahla, Stratoïd) show FeO* spans generally closer to that of the MER (Fig. 1), while the most recent on-axis Manda Hararo lavas have FeO* contents comparable to that of the Traps (Fig. 1).

The Afar lavas (Dessie, Dahla, Stratoïd and recent) are generally more evolved than the HT2 traps: most of the samples display 4–7 wt.% MgO while the most primitive lavas reach 10 wt.% MgO. These lavas rapid increase of FeO* and decrease of Al_2O_3 and CaO vs. MgO, is reflective of cpx+pl fractionation (Fig. 1) as Al_2O_3 and CaO are compatible in these phases. There is a general kink for most of the trend around 7.3 wt.% MgO, where the slope is rapidly increasing (Fig. 1). Such a kink is characteristic of the entrance of plagioclase into the crystallizing assemblage. Indeed, plagioclase and clinopyroxene consume CaO and Al_2O_3, which would become compatible and be subtracted from the liquid. In turn, FeO* is compatible in olivine and clinopyroxene but is incompatible in plagioclase, so that when plagioclase enters the fractionating assemblage, FeO* increases more rapidly in the liquid. Then, FeO* seems to decrease at MgO $<$ 5.0-4.5 wt.% which indicates that the most evolved samples may have crystallized Fe-Ti oxides (Fig. 1). Na_2O diagrams shows that Afar lavas and HT2 traps follow very close trends, because Na_2O is not fractionated by olivine, clinopyroxene or plagioclase.

The recent lavas of the MER are more primitive than the one from Afar, with a range of 7.0-9.0 wt.% MgO. They follow the same trend than the Afar lavas in TiO_2, CaO and Al_2O_3 where they seem to have fractionated the same ol-cpx-pl assemblage. They display lower FeO* than the recent on-axis Afar lavas for the same values of MgO. They also exhibit lower FeO* than Stratoïd and Dahla, although it is not clear at this point if they follow the same liquid line of descent (LLD) or not. They have however higher Na_2O (2.6-3.5 wt. %) at equal MgO concentration (Fig. 3) indicating an overall lower degree of melting [e.g. *Langmuir et al.,* 1992].

4.2. Trace elements

Light to heavy rare earth elements (REE) behave as incompatible elements during crystallization processes and thus have their concentration increase with decreasing MgO wt. %. Our dataset unsurprisingly reflects this trend, as it is shown on variations diagrams in Appendix B.

More interesting are the variations of La/Sm and Sm/Yb ratios (all values normalized to chondrites after *Sun and McDonough* [1989]). Indeed, LREE are more affected by differentiation than HREE (Fig. 2A). This is because the most incompatible REE exhibit a partition coefficient between liquid and clinopyroxene (close form 10^{-2} – 10^{-1} [i.e. for Lanthanum, *Irving and Frey,* 1984; *Hack et al.,* 1994]) about 3-4 order of magnitude higher than for olivine or plagioclase. As such, the La/Sm ratio is expected to fractionate during differentiation. It is noteworthy that this effect is rarely taken into account in most studies. However our data demonstrate that there is a slight dependency of LREE concentration vs. MgO, that will be further corrected using power law equations to allow more precise investigation of magma groups differences using La/Sm and Sm/Yb (see below; Fig. 2B).

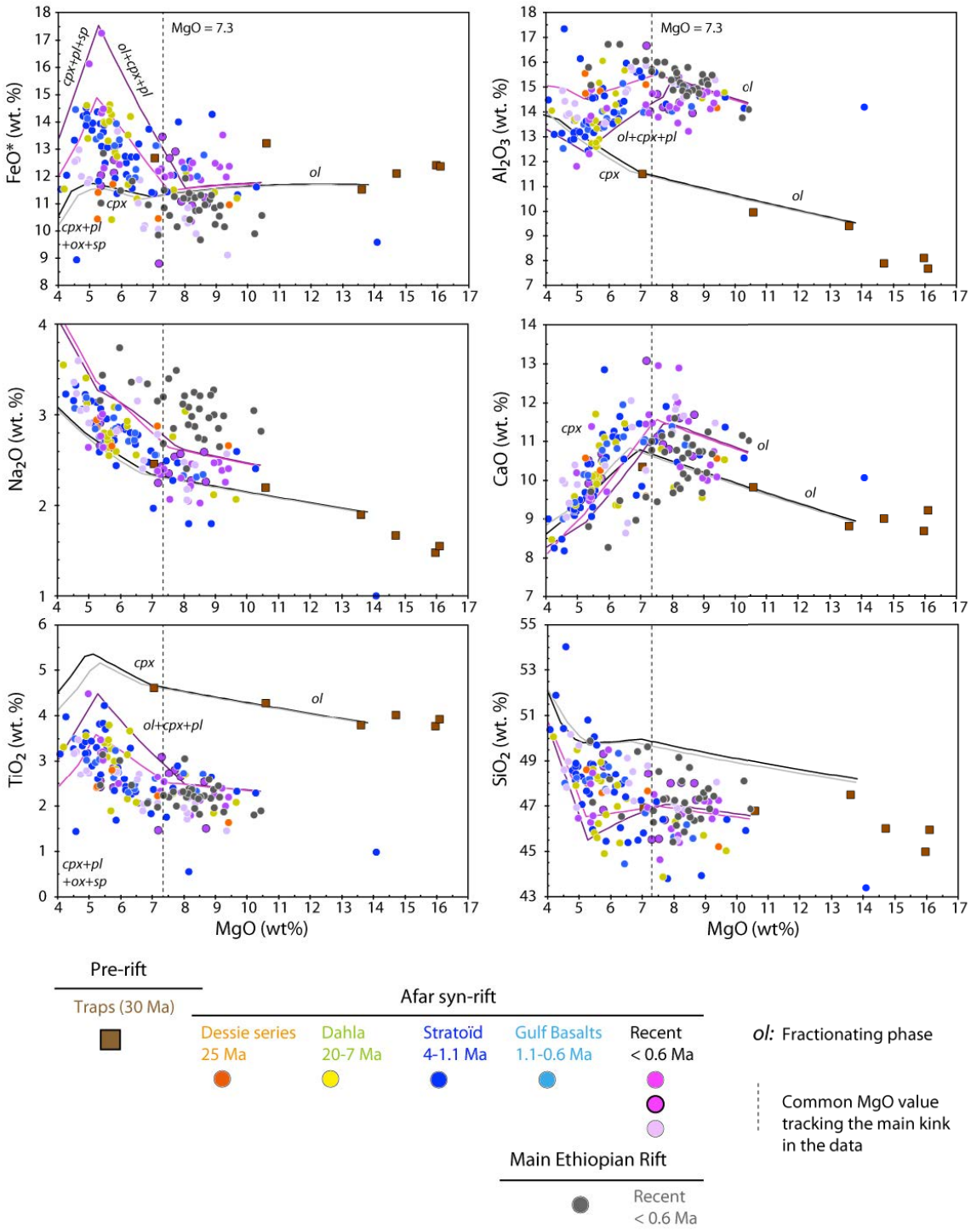

Figure 1. Major oxides variations against MgO. LLDs calculated with MELTS [Ghiorso and Sack, 1995; Gualda et al., 2012a] are also shown as examples to help identifying the fractionating phases. Note that HT2 traps and syn-rift Miocene-to-recent rocks are well separated into two groups. The first is derived from the most primitive melts whereas the second group reflects differentiation of more evolved magmas. The main difference is that syn-rift group has fractionated along the olivine-clinopyroxene-plagioclase cotectic whereas the traps have not experienced plagioclase fractionation For each magma groups, the following starting compositions

have been used: ***E38*** *[HT2 traps,* Pik et al. *1998] has relatively* ***high*** *MgO, FeO*, TiO_2, and* ***low*** *Al_2O_3, Na_2O and CaO.* ***E21*** *(Stratoïd, this study) has* ***high*** *FeO*, Al_2O_3, Na_2O, CaO and* ***intermediate*** *TiO_2, K_2O and P_2O_5 and* ***low*** *MgO.*

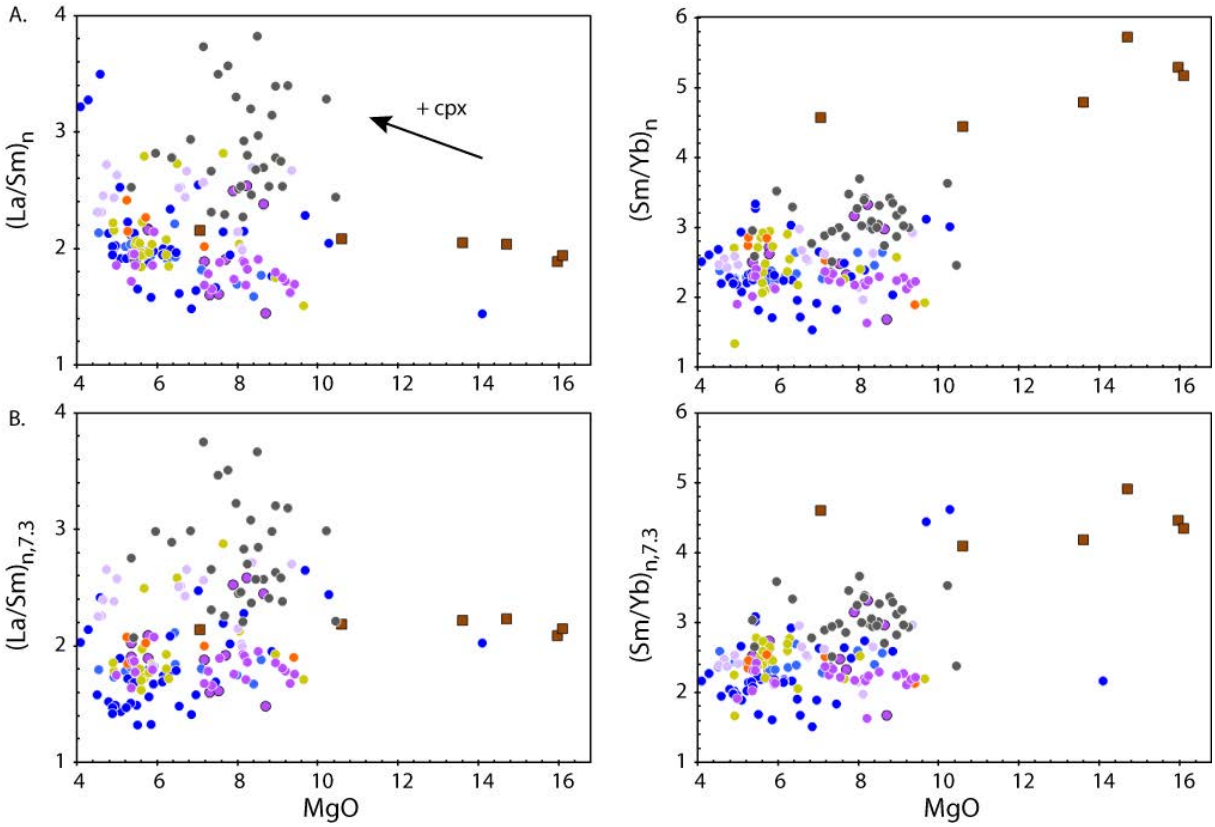

Figure 2. A. $(La/Sm)_n$ and $(Sm/Yb)_n$ covariations with decreasing MgO. Note that LREE increase with differenciation whereas HREE are not. This is mainly due to clinopyroxene removal from the liquid, as LREE (elements from Lanthanium to Samarium) have a higher partition coefficient in clinopyroxene than HREE (Samarium to Lutetium). With respect to that, La/Sm should slightly increase during fractional crystallization while Sm/Yb should stay constant. B. Ratio corrected for low-pressure fractionation. Note that the dependency to MgO has been suppressed. Also, corrected data is less scattered than uncorrected one. Note however that two samples from the Stratoïd series exhibit a very high Sm/Yb after correction. These may be outliers, however there are no reasons whatsoever not to consider these as authentic.

4.3. Liquid lines of descent (LLD) calculation

We test the hypothesis of fractionating assemblage using the rhyolite-MELTS code [*Ghiorso and Sack,* 1995; *Gualda et al.,* 2012a] to calculate the compositions of the residual liquids during differentiation (liquid lines of descent, or LLD). We did isobaric fractionate crystallization runs of the most primitive samples selected as

parental liquids, at various pressure (P = 1–4 kbar, i.e. ~3 km to ~ 12 km) and water content (1000-4000 ppm H_2O; significant range for Afar basalts, as in *Schilling et al.* [1992] and *Pinzuti et al.* [2013]) with fO_2 = QFM (Quartz-Fayalite-Magnetite, relevant for upper crustal processes). The aim was to simulate the two main trends in the data: **trend A: high** FeO*, Al_2O_3, CaO with low TiO_2, and **trend B: low** FeO*, Al_2O_3, CaO, with **high** TiO_2.

The results mainly show that the entering of cpx + pl in the fractionating assemblage is controlled by A) pressure and H_2O content: wet liquids fractionate those phases at lower MgO content whereas fractionation at greater depth allows cpx + pl to crystallize at higher MgO content (Fig. 3). B) Starting composition. The E38 model predicts ol, then ol + cpx fractionation at MgO 6.5-8.5 wt.% (+ opx for the 4kbar runs), with pl entering the assemblage at very low MgO (< 3 wt.%). On the other hand, models with less primitive starting compositions (E21, 0402) predict fractionation of ol, then ol + cpx + pl (cpx + pl for 4kbar runs) at MgO 6.0-7.7 wt.%.

As a result, the E38 model fit satisfactorily the HT2 traps compositions in all major oxides except for K_2O for which data are too scattered. In turn, E21 and 0402 models (alternatively E21and JV240 for K_2O) bracket the Afar and MER samples in most major oxides. Those lavas plot above all three computed LLD in CaO vs. MgO diagram (Fig. 1), which suggests a minor contribution from accumulated plagioclase crystals. MER lavas are richer in Na_2O than what is predicted by the E21 model, indicating that their parental magma was richer than the Afar lavas and the HT2 traps.

4.4. Correction of low-pressure fractional crystallization

Only few of the basalts of this study can be considered primitive (with MgO > 7 wt. %) and the major part of Stratoïd samples are not. We correct this effect by projecting the data for major and trace elements to a common value of wt. % MgO. Classically, the common value is MgO 8% for MORBS because it supposes that basalts only experienced olivine fractionation at MgO concentrations above 8% MgO [*Klein and Langmuir*, 1987, 1989; *Langmuir et al.,* 1993]. However, according to equilibrium thermodynamics used in MELTS [*Ghiorso and Sack,* 1995; *Gualda et al.,* 2012a], cpx and pl can fractionate at different values (between 6% and 9%) depending on the amount of water and on the pressure, as we show in the above subsection. There are two approaches to correct to a common MgO value. One is to make a linear regression through the apparent trend of the data when the eruption context is complex [i.e. *Wang et al.,* 2002]. This approach considers that LLD calculation is hardly meaningful because lavas erupted in intraplate settings would often have assimilated crustal component at various extent [*Wang et al.,* 2002]. The second approach is to calculate theoretical LLD during fractional crystallization for different settings. We believe the second approach is useful for two reasons. First,

modeling LLDs helps to find the kinks in the series. Looking only at the apparent trends can work well enough, but some groups (i.e. MER or on-axis / off-axis) do not display breaks clearly. It is noticeable that, for these data, the modeled kinks with MELTS and the observed ones in actual trends are equivalent, at about MgO ~7.3 % instead of 8% (Appendix A). Second, trends in our data are to the first order sub-parallel to the calculated LLD, i.e. for FeO*, Al_2O_3, Na_2O, CaO and sometimes crosscut the LLD, as for TiO_2, SiO_2. This makes sense given the large spatial and time span we considered: our dataset comprises 30 Ma to 0 Ma rocks that were erupted in a geodynamically active region. This also means that fractional crystallization is the governing process over assimilation or contamination. Thus, we chose in this paper to proceed as in *Pinzuti et al.* [2013] and use the mean slopes of the LLD to correct the data back to 7.3 wt.% MgO. Details are given in Appendix B. We calculated major oxides corrected to 7.3 wt.% MgO as:

$$Ox_{7.3} = Ox + a \cdot (7.3 - MgO) \quad (1)$$

With 'a' the mean slope of the LLDs. We also corrected trace elements to 7.3 wt.% MgO. HT2 traps were corrected using the E38 model, whereas MER and Afar lavas were corrected using the mean slope of E21 and 0402 models. Trace elements correction were performed using a power law relationship which gave the best fit, as:

$$REE_{n,7.3} = REE_n \cdot (\frac{7.3}{MgO})^a \quad (2)$$

Where 'a' is the power-law coefficient and subscript n indicate normalization to chondrites [*Sun and McDonough,* 1989].

5. Fe-Na-Ti systematics of initial magmas

For each series, we used the equations above (Appendix A) to calculate $Fe_{7.3}$ from FeO*, $Na_{7.3}$ from Na_2O and $Ti_{7.3}$ from TiO_2. Applying this correction effectively suppresses the effects of low-pressure fractionation (Fig. 3). It means that every variation can be genuinely attributed to melting processes. On figure 4, the data define a trend comprised between the HT2 Traps (mean $Fe_{7.3}$ = 12.02 ± 0.70 wt.%, $Na/Ti_{7.3}$ = 0.47 ± 0.05), which are the lower end the trend; and the MER lavas (mean $Fe_{7.3}$ = 10.56 ± 0.65 wt.% and $Na/Ti_{7.3}$ = 1.39 ± 0.19), which is the higher end of the trend. Dessie series (mean $Fe_{7.3}$ = 11;05 ± 0.61 wt.% and $Na/Ti_{7.3}$ = 1.27 ± 0.22) and Dahla series ($Fe_{7.3}$ = 11.25 ± 1.00 wt.% and $Na/Ti_{7.3}$ = 1.25 ± 0.34) define fields of intermediary values (Fig. 4). The Stratoïd is the only formation that is offset from that main trend (mean $Fe_{7.3}$ = 10.86 ± 0.87 wt.% and $Na/Ti_{7.3}$ = 1.15 ± 0.28) toward the low Na/Ti and low Fe quadrant (Fig. 4). Finally, the present-day axial lavas are segregated into two well defined groups (Fig. 4): the on-axis lavas

($Fe_{7.3}$ = 11.71 ± 0/77 wt.% and $Na/Ti_{7.3}$ = 1.05 ± 0.11) resemble the initial Traps (Fig. 4), whereas the off-axis lavas (mean $Fe_{7.3}$ = 9.47 ± 0.95 wt.% and $Na/Ti_{7.3}$ = 1.14 ± 0.23) display a more MER-like signature (Fig. 4). All error bars are the 1-sigma standard deviation from the mean.

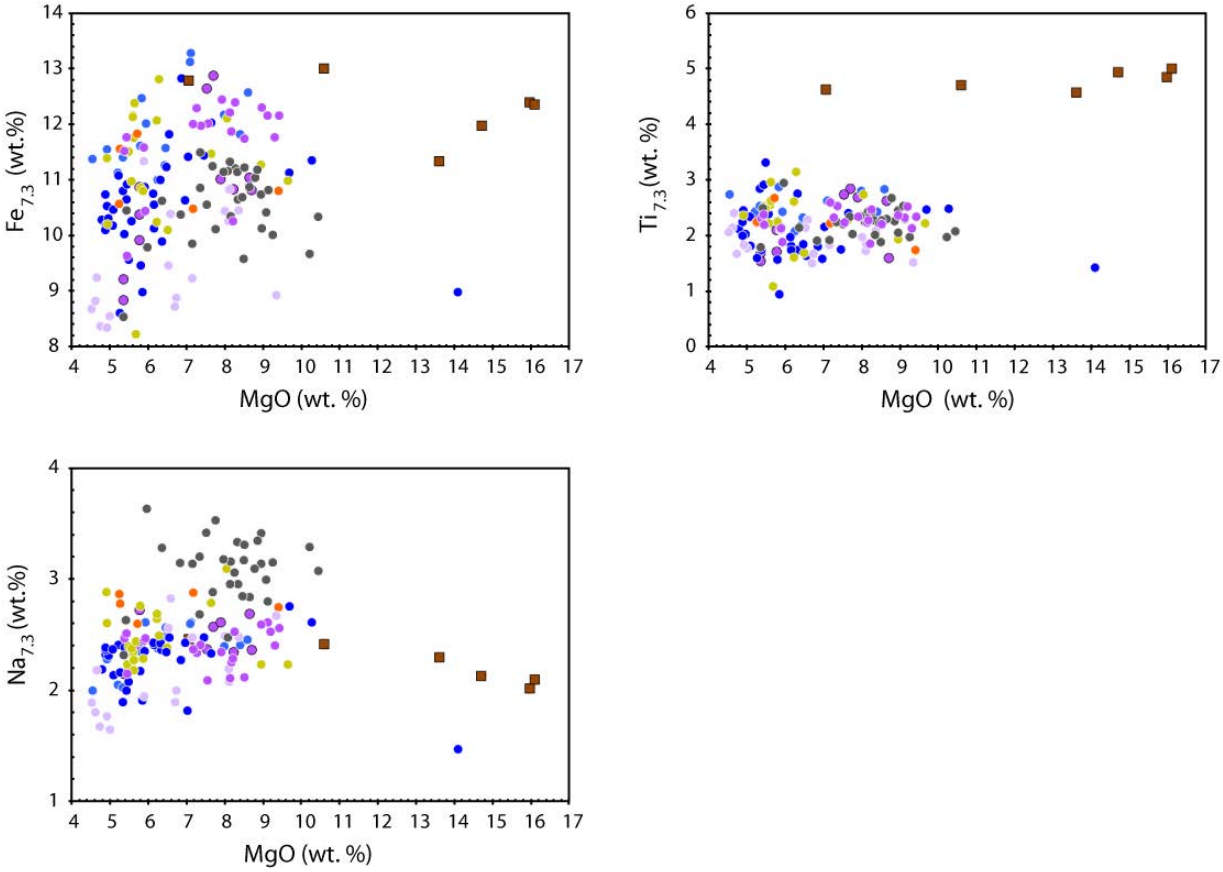

Fig. 3. Plots of corrected Fe, Na and Ti against MgO. Note. All three oxides show no relationship with decreasing MgO.

In this systematics, increasing Fe signifies an increase in depth of melting [e.g. *Klein and Langmuir,* 1989; *Pinzuti et al.,* 2013] and is often used to infer mantle potential temperature (T_P) [*Wang et al.,* 2002]. The reason is that Kd of Mg and Fe between olivine and melt decrease primarily with increasing temperature along the solidus so that melts are enriched in olivine components at higher pressures [*Langmuir et al.,* 1993]. Na and Ti are moderately incompatible elements during melting of mantle peridotite. They are primarily hosted in cpx, so that the ratio $(Na/Ti)_{7.3}$ and $D^{cpx/liq}(Na) < D^{cpx/liq}(Ti)$, so that, low $(Na/Ti)_{7.3}$ values indicate a high degree of partial melting [i.e. review in *Langmuir et al.,* 1993]. $D^{cpx/liq}(Na)$ also increase with increasing pressure of melting, so that the ratio is to some extent correlated to $Fe_{7.3}$ [*Putirka,* 1999]. To a first order, there seems to be a general correlation between increasing pressure ($Fe_{7.3}$) and extent of melting $(Na/Ti)_{7.3}$ as shown on Fig. 4, which is expected due to the pressure-dependence of both proxies.

However, the Stratoïd displays a shift toward low $Fe_{7.3}$ and low $(Na/Ti)_{7.3}$, which means an increase of extent of melting at the expense of the pressure of melting, which decreases.

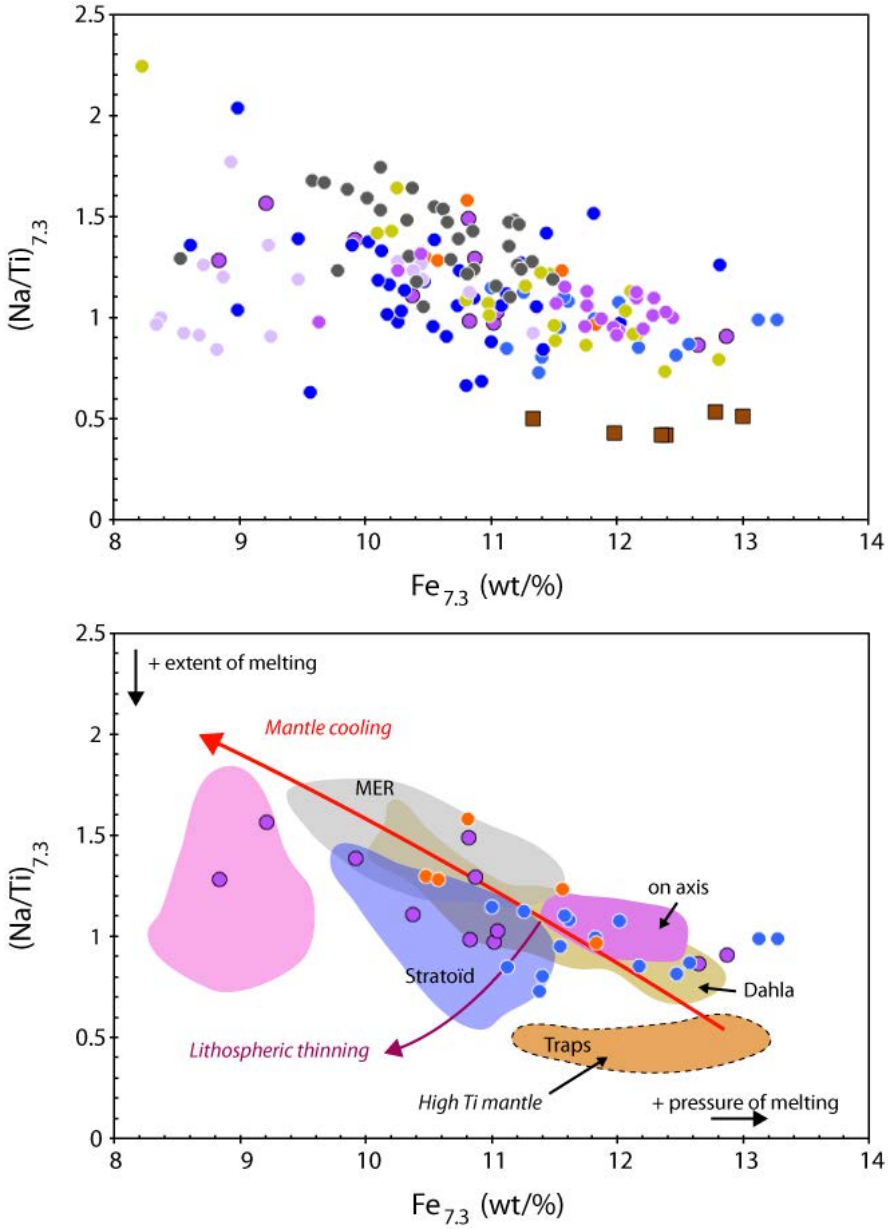

Figure 4. $(Na/Ti)_{7.3}$ plotted against $Fe_{7.3}$. Upper panel shows data, lower panel show fields in which the bulk of each series falls into. Series with few data point are represented above those fields to highlight their behavior. On this diagram, $(Na/Ti)_{7.3}$ ratio works as an ratio of incompatible elements, whose variation depicts difference in extent of melting, whereas $Fe_{7.3}$ is the proxy for pressure of melting.

6. REE systematics of initial magmas

REE ratios are correlated to MgO content, so that we need to correct them (as explained in 4.2). Corrected to 7.3 wt.% MgO LREE and HREE systematics [ratio are chondrites-normalized after *Sun and McDonough,* 1995] are similar to the first order to $Fe_{7.3}$ and $Na_{7.3}$ systematics. On Fig. 6, we show the variations of $(La/Sm)_{n,7.3}$ vs. $(Sm/Yb)_{n,7.3}$. $(La/Sm)_{n,7.3}$ is used a proxy for the extent of melting (F). The REE have distribution coefficient decreasing from the heaviest element (Lu) to the lightest (La), so that, as $D^{solid/liquid}(La) < D^{solid/liquid}(Sm)$; an elevated $(La/Sm)_{n,7.3}$ ratio corresponds to a small extent of melting, because the higher the incompatibility of an element, the higher its concentration in the liquid. LREE are generally incompatible with every common mineral phase in the mantle. However, HREE have gradually higher partition coefficient with garnet, so that $D^{garnet/liquid}(Sm) < D^{garnet/liquid}(Yb)$. In the case of a garnet-bearing source, the most heavy REE (Yb here) will be retained in the source's garnets, while the lightest (Sm here) will be fractionated into the melts, and this will yield an elevated $(Sm/Yb)_{n,7.3}$ ratio in the liquid. In order to express the REE signature in terms of variations of source mineralogy and extent of melting, we modeled non-modal equilibrium melting of garnet-bearing peridotite. We varied the quantity of garnet in the source by diluting it with olivine, as done in *Jourdan et al.* [2007]. Source concentrations, mineralogy and melting modes are given in Fig. 6 caption.

The HT2 Traps display the most prominent garnet signature of the whole dataset (Fig. 5, mean $(La/Sm)_{n,7.3} = 2.15 \pm 0.04$ and mean $(Sm/Yb)_{n,7.3} = 4.50 \pm 0.26$). This is consistent with the high value of $Fe_{7.3} = 12.02 \pm 0.70$ wt.%. The rest of the data, i.e. Afar and MER lavas form a trend of various $(La/Sm)_{n,7.3}$ with only little changes in $(Sm/Yb)_{n,7.3}$. The MER field is at the high $(La/Sm)_{n,7.3}$ / high $(Sm/Yb)_{n,7.3}$ end (Fig. 5), thus defining the low F endmember.

The Dessie series (mean $(La/Sm)_{n,7.3} = 1.89 \pm 0.08$ and $(Sm/Yb)_{n,7.3} = 2.23 \pm 0.09$) and Dahla series (mean $(La/Sm)_{n,7.3} = 1.94 \pm 0.30$ and $(Sm/Yb)_{n,7.3} = 2.37 \pm 0.38$) display an homogenous field with F similar to the Traps value (Fig. 5). The Stratoïd series (mean $(La/Sm)_{n,7.3} = 1.61 \pm 0.34$ and $(Sm/Yb)_{n,7.3} = 2.16 \pm 0.52$) form the higher end of the trend with the most elevated F and the lowest garnet content (Fig. 5). The most recent rocks then have signatures closer to that of the early syn-rift lavas: The Gulf Basalts series (mean $(La/Sm)_{n,7.3} = 1.74 \pm 0.09$ and $(Sm/Yb)_{n,7.3} = 2.49 \pm 0.13$) and the on-axis (mean $(La/Sm)_{n,7.3} = 1.86 \pm 0.24$ and $(Sm/Yb)_{n,7.3} = 2.33 \pm 0.34$) plot in a well-defined field (Fig. 5). The off-axis lavas (mean $(La/Sm)_{n,7.3} = 2.38 \pm 0.27$ and $(Sm/Yb)_{n,7.3} = 2.44 \pm 0.29$) fall closer to the MER endmember (Fig. 5).

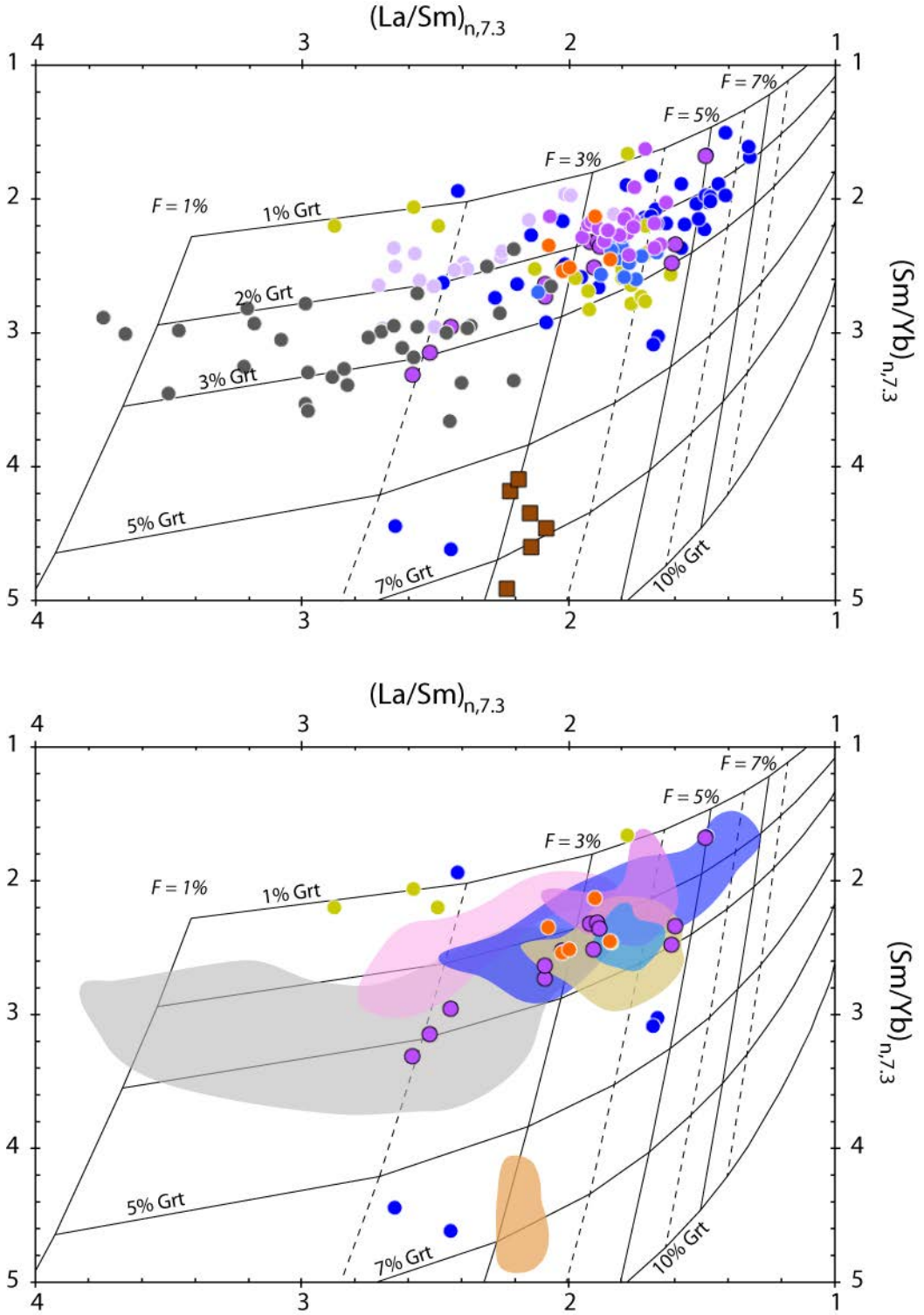

Figure 5. $(La/Sm)_{n,7.3}$ vs. $(Sm/Yb)_{n,7.3}$ ratio of our dataset. Melting model is non-modal batch melting of a lherzolitic mantle source. Modal compositions is a garnet lherzolite with modal 61% Ol, 20% Opx, 9% Cpx, 10% Grt. Garnet is then removed and replaced with olivine. REE contents are those of the primitive mantle (PM) from Sun and McDonough [1989] with La = 0.687 ppm, Sm = 0.444 ppm, Yb = 0.49 ppm. Melting modes are after Winter [2001] with Ol = 16, Opx = -12%, Cpx = 81%, Grt = 15%. Partition coefficients are from McDade et al. [2003] (see Appendix C).

7. Thermobarometry of primary magmas

We used major elements thermobarometry to determine the P-T conditions of the most primitive samples in the dataset. This has been done using the equations from *Lee et al.* [2009] that link P and T to the primary liquids compositions (i.e. the first liquids directly in equilibrium with the melting mantle). Primary liquids compositions are inferred from the most primitive samples (MgO > 8 wt. %) to be certain that only olivine was the fractionating phase. Then olivine was added (Si, Mg, Fe and O) back into the primitive basaltic liquid until it is in equilibrium with Fo_{90}, which is the average forsterite composition of the mantle. The major oxides concentrations of the primary liquids are then converted to molecular species with 8-oxygens basis to account for the chemical interactions that occur between silica and the other major components [*Ghiorso et al.,* 1983; *Lee et al.,* 2009]. Doing so allows to better capture the effect of chemical activities, which are important as this thermobarometer is mainly based onto silica activity [*Lee et al.,* 2009].

Pressure and temperatures are representative (for each data point) of the average conditions in the melting column: they are the average parameters of all the aggregated melts produced along a polybaric melting path [*Lee et al.,* 2009]. Mantle potential temperature (or T_P) [*McKenzie and Bickle*, 1988; *Katz et al.,* 2003] is classically inferred from the PT conditions of the primary melts by back-calculating along a melting adiabat until the solidus is reached. T_P is then the temperature the mantle would have if it were decompressed along a solid adiabat up to the surface (see Fig. 6). In this study, this estimation is performed qualitatively.

To a first order, the Afar lavas seem to have been generated deeper in the mantle and at more elevated temperatures than the MER lavas (Fig. 6). Indeed, the MER primary magmas plot on a lower trend than the Afar lavas. For example, at the temperature of 1560°C, the MER melts are offset from 0.2 to 0.8 GPa lower than the Dahla, Tendaho and Off-axis melts.

Even though there are no samples plotting on the solidus, one can see on figure 7 that the MER trend is 'bent' toward the solidus at lower P and T, with a T_P of ~1520°C. This is consistent with the low $Fe_{7.3}$ and high $(Na/Ti)_{7.3}$ of the MER lavas (Fig. 6). Despite the fact that only one sample from the Dessie series was suitable for inversion, it is noteworthy that it plots on the same trend than the MER lavas, suggesting similar tectonic environment at the time of eruption.

The 'Afar trend' displays an overall high potential temperature (T_P = 1620°C; close to that of the traps), in agreement with Fe-Na-Ti systematics (Fig. 4) and with previous studies [*Ferguson et al.,* 2013] and is segmented in different groups. The on-axis and Gulf primary melts constitute the 'hot and deep' end of the trend, while the Tendaho and Manda Hararo off-axis plot on the 'cold and shallow' end (Fig. 6). This segregation is consistent with previous studies [e.g. *Medynski et al.,* 2015] that inferred a shallower origin for the off-axis volcanism derived melts. The Dahla and

Stratoïd seem to have intermediate values, although little can be said due to the lack of data.

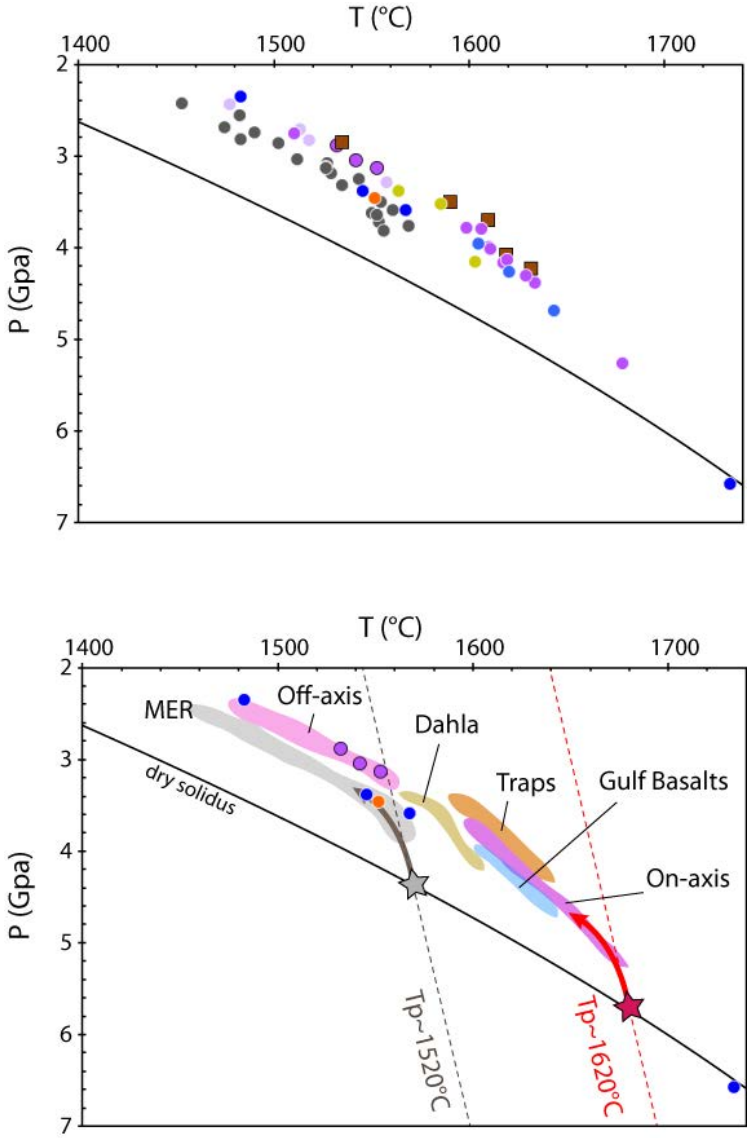

Figure 6. P-T conditions of primary melts. Stratoïd (blue), Dessie (orange), and Tendaho (dark circle with purple heart) are shown over colored fields for clarity. Mantle potential temperatures (dotted lines) and dry solidus of fertile peridotite are from [Katz et al., 2003]. The melting adiabats (colored arrows) are schematized by graphically extrapolating the trends onto the solidus (grey and red stars). Note the Traps, trending above other Afar magmas.

It is difficult with the data shown on figure 6 to know if the Traps are fully part of the Afar trend, or if they plot slightly above it, possibly intersecting the solidus at greater depth and temperature. In that case, the traps primary magmas would form the 'head' of the trend.

To test this hypothesis, we used the software MEGAPRIMELT3 (or Primelt) [*Herbzerg and Asimow,* 2008; 2015] to directly calculate the potential temperature

from the primary compositions. Contrary to the thermobarometer of *Lee et al.* [2009], Primelt uses a semi-forward model to infer the melt fraction F needed to produce a primary melt in equilibrium with the mantle.

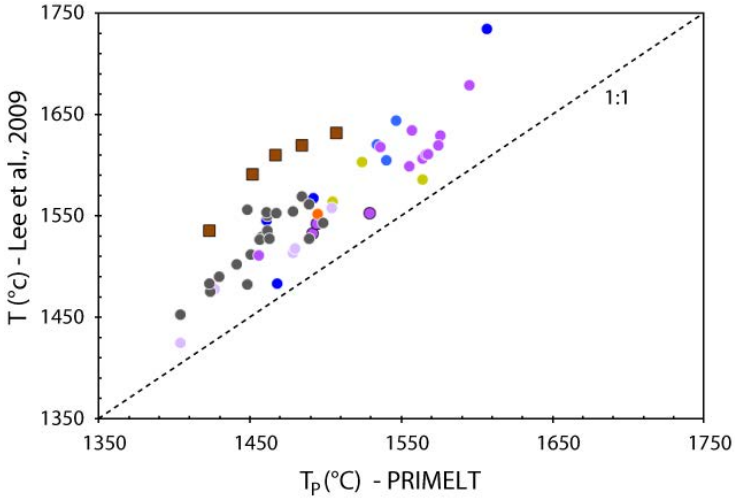

Figure 7. T (Lee) vs. T_P (Primelt). Note the shift toward lower potential temperatures of the traps primary magmas.

Surprisingly, for a same range of temperature calculated after *Lee et al.* [2009], the traps primary magmas have a much lower potential temperature than the on-axis, Gulf and Dahla basalts. The difference is up to $\Delta T_P = 100°C$ (Fig. 7). This has been previously documented by *Rooney et al.* [2012] that obtained T_P from 1430 to 1470°C on the same samples, but obtained significantly higher temperatures for traps samples closer to the center of Afar, or on the Yemeni plateaus (T_P as high as 1520°C). Those higher temperatures are in good agreement with those obtained in this study for the 'Afar trend', i.e. T_P ~[1530-1590°C].

8. Discussion

8.1. Significance of the P-T results

The potential temperatures estimated for the MER and the Traps (with PRIMELT) and the recent Afar rocks are in good agreement with what has been previously documented in the literature. The traps record an elevated $T_P = 1450°C$ using PRIMELT (fig. 8), slightly higher than the estimation of *Beccaluva et al.* [2009] of T_P ~1350-1400°C that used the SiO_2-MgO thermobarometer in *Albarede.* [1992], but in accordance with the T_P = 1430-1470 °C in *Rooney et al.* [2012] that used the same technique as in this study. These ranges of T_P are some 100-150°C above the 'normal' mantle potential temperature of 1350±50°C [*Herzberg et al.,* 2007; *Ono et al.,* 2008] consistent with a mantle plume origin [*Rooney et al.,* 2012].

The T_P recorded by the MER lavas are the lowest, which is consistent with low F, Grt, $Fe_{7.3}$ and $(Na/Ti)_{7.3}$ (Figs. 5 and 6). We found in this study a mean T_P of ~1400

°C for axial samples in the MER, with lower mean pressures of 90-105 km. *Ayalew and Gibson* [2009] found a T_P of 1350°C for the MER lavas as being the best fit for their rare earth inversion modeling, with 7% partial melting and melting starting between 130-100 km (4.3-3.3 GPa) and stopping at 53 km (1.8 GPa), which they interpreted as the base of the rigid lithosphere [*Ayalew and Gibson*, 2009]. *Rooney et al.* [2012] found T_P = 1400°C – 1430°C, which is expected because in this study, the same dataset were used for this region.

For Manda Hararo lavas (along with Gulf Basalts and some Dessie samples), the potential temperatures calculated with PRIMELT are significantly higher than those calculated in other studies. For instance, *Ferguson et al.* [2013] use a REE inversion model and predicted T_P = 1450°C. *Armitage et al.* [2015] fits the REE profiles of several active segments in Afar (Erta'Ale, Assal and Manda Hararo) with a TP of 1450°C as well. The only difference between those two studies is that a thick mantle lid (80-90 km) is required in *Fergusson et al.* [2013], whereas a thinner lid (50 km) consistent with seismic observations [*Rychert et al.,* 2012] is obtained by *Armitage et al.* [2015] using hydrous melting of the mantle.

One direct possibility to explain this counter-intuitive result is that the recent and Gulf basalts lavas have fractionated along ol+cpx cotectic, which would have yielded higher FeO* in the liquids. This would yield artificially higher P and T [*Herzberg and Asimow,* 2008; *Lee et al.,* 2009]. However, LLD calculations performed with MELTS (shown in Appendix A) seem to invalidate this hypothesis, as olivine is always the only phase on the liquidus.

Instead, our preferred interpretation is that the higher T_P calculated with PRIMELT may be explained by the use of a different technique: instead of a REE model, we used a major elements-based model, REE models are largely dependent upon the initial composition of the mantle. For instance, we use a set of peridotites that become gradually depleted in garnet (from 7% to 2%) and with 9% clinopyroxene, whereas the source peridotite in *Ferguson et al.* [2013] has 7% clinopyroxene and 11.5% garnet. Simple batch melting of this composition would be unable to fit our data, as it would produce melts far too enriched in HREE. Instead, *Ferguson et al.* [2013] uses a polybaric model in which the mantle is also able to melt in the spinel stability field, which yields less HREE in the modeled melts. For this reason, our F and P cannot be directly comparable to theirs. For the following discussion of this study, this is however not a problem because we choose to investigate the full range of magmatic episodes with the same approach. Therefore, whatever the veracity of the mantle Tp calculated with this approach, the relative values of the Tp between the various lava series and the Traps/MER end-members will be meaningful. It should be however acknowledged that the choice of partition coefficients and initial mantle lithologies (and concentrations) can make an important difference in the obtained results, and makes comparison between two different studies using different technique somewhat cumbersome. For instance, the use of

REE that have poorly constrained partition coefficient can heavily change F and Grt: $(Dy/Yb)_N$, (equivalent of Sm/Yb, that better capture the effect of garnet) used in *Armitage et al.* [2015] is dependent of K_{Dy}, which varies from 1.06 [*McKenzie and O'Nions*, 1991] to 4.13 [*Hauri et al.,* 1994].

The P-T conditions calculated in this study with the thermobarometer of *Lee et al.* [2009] always produces higher T_P than with PRIMELT (Fig. 8). Indeed, the 'MER trend' of figure 7 corresponds to a T_P of ~1520°C (against 1400°C for PRIMELT) and the Traps and Afar trend seem to cross the solidus at T_P ~1600°C instead of (1450-1550°C). Nonetheless, this systematic offset toward higher values is not a problem in our case. First, because these estimations suffer the lack of samples that fall on the solidus, so that we only have a partial idea of what the actual T_P is. Second, because the trends on figure 7 provide an idea of the extent of the melting columns. Indeed, all the data on figure 7 define an array of decreasing P with decreasing T. This is because it defines a melting adiabat [see *Lee et al.* 2009], which means that this array is due to the nature of partial melting itself.

One issue about these arrays is to know if each data point is representative of a given melting column – as it is frequently hypothesized while studying a very large dataset on wide regions i.e. the Indian Ocean MORB [e.g. *Lee et al.,* 2009], or if the array itself defines the melting column beneath a given region. The second case is common in intraplate settings, because in such locations well-defined magmatic series are often sampled [as in *Wang et al.,* 2002; *Lee et al.,* 2009].

8.2. P-T conditions of the mantle

In this frame, the Traps series correspond to the products of the mantle melting at the highest potential temperature, because it trends above the other series in the P-T space (Fig. 7). This is consistent with a high garnet signature (Fig. 6) and high majors elements contents (Fig. 5), which means that the Traps correspond to a hot mantle-endmember. Conversely, the MER field falls beneath the other series in the P-T space, consistent with a cold mantle-endmember (Fig. 5, 6, 7). The difference between the cold and shallow off-axis and the hot and deep on-axis Manda Hararo magmas is interpreted as being the result of the melting of different part of the melting column (Fig. 7), which would yield both contrasted Grt, $Fe_{7.3}$ and $(Na/Ti)_{7.3}$ (Figs. 5 and 6) and contrasted T_P estimates [Fig. 7, as in *Herzberg and Gazel,* 2009]. Eventually, the off-axis record PT conditions more similar to the MER while the on-axis lavas resemble the Traps.

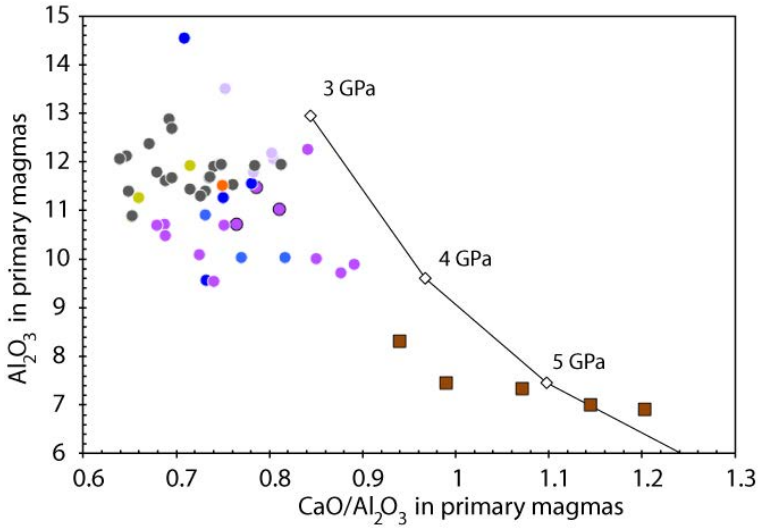

Figure 8. Al_2O_3 vs. CaO/Al_2O_3 in primary magmas, calculated for the most primitive samples after Lee et al. [2009]. Diamonds labeled with pressure in GPa and solid lines are the liquidus melts compositions of lherzolite KLB-1, calculated from the expressions in Herzberg and Zhang [1996].

This systematics is further supported by the Al_2O_3 vs. CaO/Al_2O_3 values of the primary magmas compositions (Fig. 8). Melting experiments of lherzolite have shown that melts produced under high pressures have high CaO and low Al_2O_3 [*Herzberg and Zhang,* 1996]. This is because a high pressure, clinopyroxene tends to dissolve into garnet, increasing the proportion of CaO in both garnet and cpx, which is reflected in the liquid. On the contrary, Al_2O_3 decrease with pressure because garnet stability field gradually expands, reducing the capacity of melts to dissolve garnet, which is the primary Al_2O_3 bearing mineral (spinel is, at pressures < 2 GPa). In our data, the Traps plot near the 5 GPa lherzolite melt and axial recent lavas are likely issued from pressure 3.5 GPa. MER display the lower pressures of ~3 GPa. The Afar primary magmas have pressure of equilibration intermediary between those of the MER and of the Traps (Fig. 8). Therefore, the observed trend of the traps, i.e. plotting above the recent Afar lavas, on Fig. 6 f *Lee et al.* [2009], can be interpreted as a higher T_P trend, consistent with $Fe_{7.3}$, $(Na/Ti)_{7.3}$ Grt%, and primary CaO/Al_2O_3 vs. Al_2O_3 advocate for a deeper origin of the Traps (Figs 4, 5 and 8).

We can now build a framework that reconciles the basalts-derived proxies ($Fe_{7.3}$, $Na/Ti_{7.3}$, F, Grt) and P-T estimates together. **(a)** The Traps, generated at great depth (Figs 4, 5, 6, 8) and temperature (Figs. 4, 6), and therefore at great T_P = 1550°C-1600°C [accounting a 100°C offset in Fig. 6, and the data in *Rooney et al.,* 2012]. **(b)** The recent MER lavas, generated at lower depth (Figs. 4, 5, 6 and 8), lower temperature (Figs. 4, 6, 7) and thus inferior T_P = 1400°C, [1520°C- 100°C on Fig. 6; Fig. 7; *Rooney et al.,* 2012] slightly above the normal asthenosphere. **(c)** The Afar recent lavas are generated at high depth and temperature, similar to that of the Traps, (Fig. 6), despite slightly lower P, T, T_P. (Figs 4, 5, 6, 8). Like the Traps (Fig.

7), the most recent Afar lavas sharply record the effect of the shape of the melting column, with major on- and off-axis differences (Fig. 4, 5, 6, 7, 8). **(d)** The early syn-rift melting regime is characterized by lower temperatures and pressures than the Traps immediately after the Dessie series emplacement. However, the extent of melting is similar until the Stratoïd emplacement. **(e)** The Stratoïd records the lowest pressures, but the highest extent of melting.

8.3. Mantle cooling vs. lithospheric thinning

The shift from the high P-T Traps to the low P-T Main Ethiopian Rift is consistent with a decrease in the mantle T_P and a decrease in Grt and $Fe_{7.3}$ (Figs. 11, 12). This relationship between those parameters resembles the 'global trend' documented at mid-oceanic ridges [*Klein and Langmuir*, 1987, 1989; *Langmuir et al.,* 1993]. The 'global trend' consists in a co-variation of P and F proxies accordingly to the mantle potential temperature: the higher T_P, the hotter the adiabat, and the higher P and F proxies recorded by basalts [*Planck and Langmuir,* 1992; *Langmuir et al.,* 1993]. We call this type of variation a (-P-F), which simply signifies that pressure and extent of melting are reduced accordingly with T_P. This overall 'mantle cooling' effect is effectively recorded by most of the lavas emitted within the Ethiopian province at all stages of rifting (Fig. 11).

The Stratoïd however is singular and exhibit the lowest pressure of melting and the highest extent of melting of the whole dataset (Figs. 11 and 12). Therefore, there is a correlation of the type (-P +F) focused in time, between 4 and 2 Ma. It has been shown that lithospheric variations alone could account for the major part in the anti correlation observed between the P and F proxies found in OIB [*Humphreys and Niu,* 2009; *Niu et al.,* 2011]. They hence introduced the notion of 'lid effect' [*Humphreys and Niu,* 2009; *Niu et al.,* 2011; *Guo et al.*, 2014]. The mantle lithosphere would in this model act as a thermo-mechanical boundary layer that 'stops' melting at a final depth P_F. An important lid would reduce the vertical range of decompression ($P = P_0 - P_F$), which is proportional to the extent of melting. Therefore, a thin lid, as under mid-oceanic ridges, yields an elevated F with a moderate P, whereas a more important lid would increase P by setting P_F at deeper ranges, whereas F is proportionally reduced [*Humphreys and Niu,* 2009; *Niu et al.,* 2011]. We thus suggest that the 'initial signal', which would be the 'mantle cooling' signal in this case, has been overprinted by the 'lithospheric thinning signal' at the time of the Stratoïd eruption. It is even possible to add a temporal framework: the lithospheric lid must necessarily have been thinned prior to the Stratoïd eruption and could not have been synchronous with it, like the Traps. The reason is the following: the Traps were erupted in a short timespan [~1 Ma, *Coulié et al.,* 2003], with an initial thermal erosion of the lithosphere [*Rychert et al.,* 2012]. However, the lid effect [*Niu et al.,* 2011] signal has not been recorded in the sense that the immediately following Dessie basalts (25 Ma) fall on a 'mantle cooling' trend (Fig. 11). We

suggest that the early 'mantle cooling' signal was stronger than the lithospheric thinning, precisely because of the amplitude of the plume's thermal anomaly. Conversely, later on, at the time of the Stratoïd emplacement (4-2Ma), the lid effect dominates, because the lithosphere has been thinned enough prior to its eruption. This is consistent with the timing of the crustal 'thinning phase' in *Stab et al.* [2015].

It is interesting to note that the localized volcanism emplaced after the Stratoïd, i.e. from the Gulf Basalts and forth, do not bear the lid effect signature. Instead, they display a (+P-F) type of correlation. +P is obvious since Grt and $Fe_{7.3}$ content of those lavas are higher than during the Stratoïd event (Fig. 11). The extent of melting decreases back to the bulk 'Afar value' in the case of the on-axis lavas, or to MER-like values for off-axis lavas, as previously noted (Fig. 11). We call this re-increase of P proxies with complex 'shape' effect reflected by off vs. on-axis signatures, the 'localization' signature.

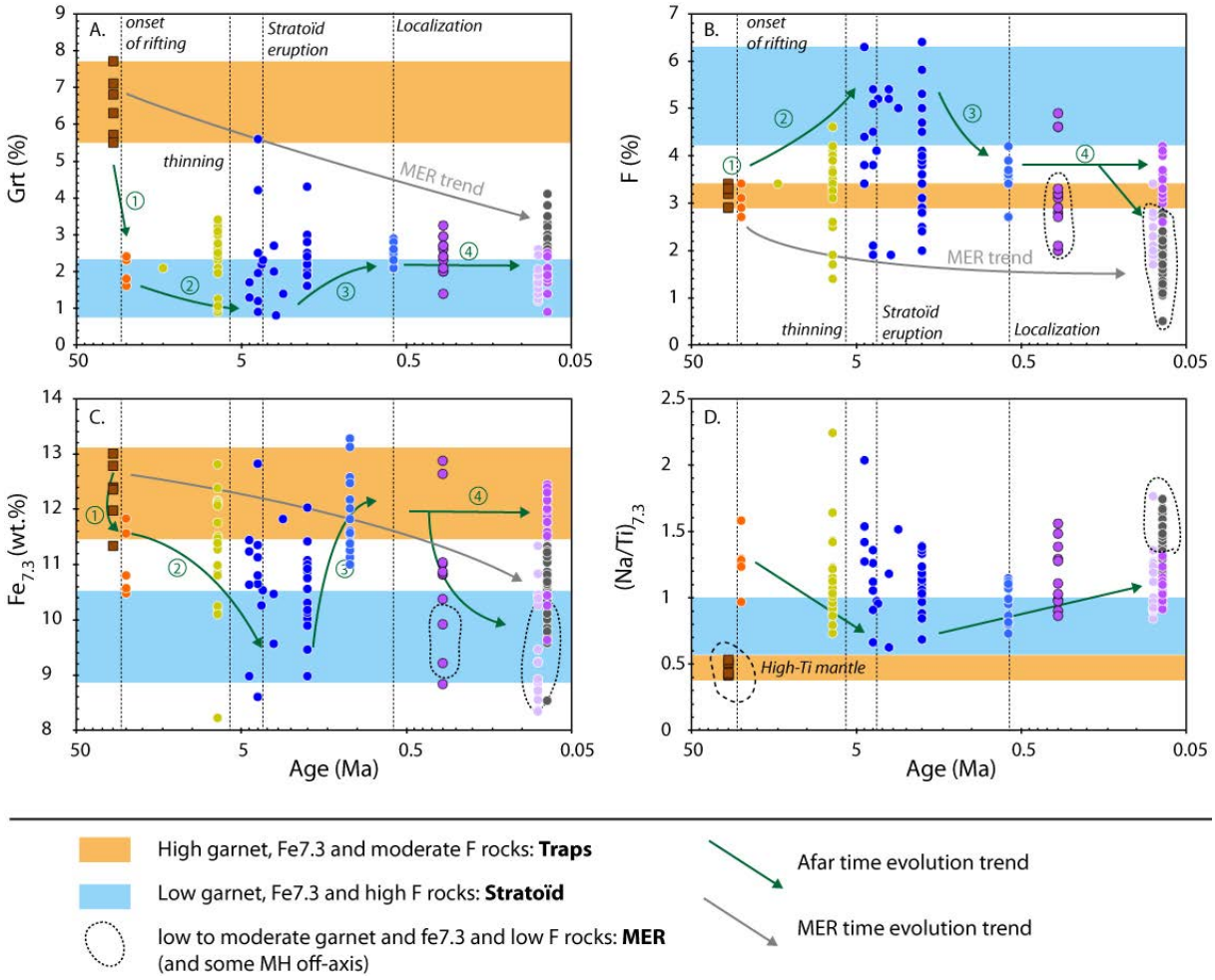

Figure 11. Time evolution of melting parameters. Both Afar and MER follow an overall 'mantle cooling' trend. In the case of the Afar, the abrupt initial lithospheric thinning is recorded between the Traps and the Dessie basalts emplacement. It is attributed to the thermal erosion of the lithospheric mantle due to the Afar plume. A genuine 'lithospheric thinning' signal is recorded during the Stratoïd emplacement, in

line with a major tectonic phase observed at the outcrop between 7 and 5 Ma [Stab et al., 2015], which suggests this thinning is of tectonic nature. The recent lavas of Afar reflect the effect of the shape of the column melt (see text).

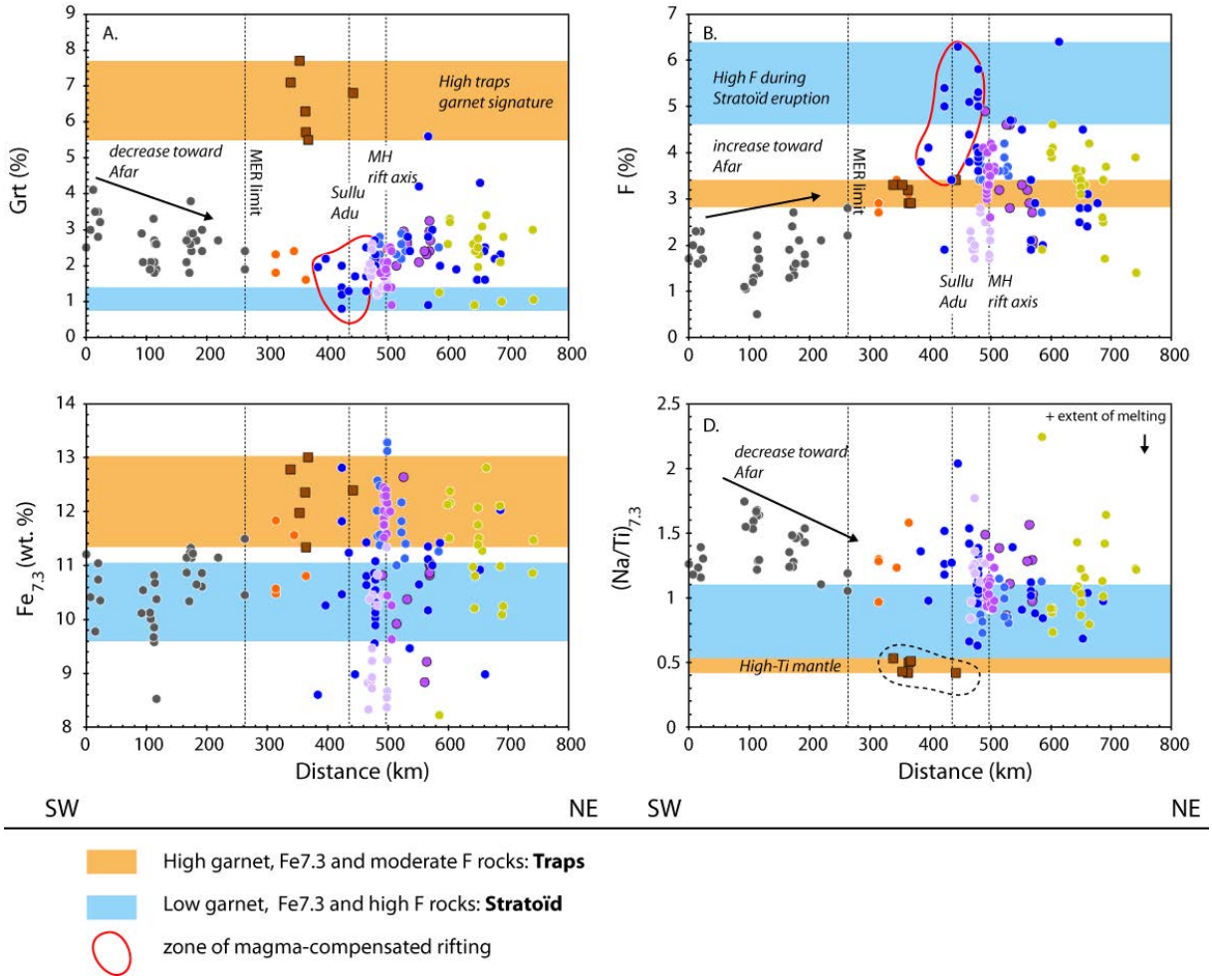

Figure 12. Spatial evolution of melting parameters along a regional transect, going form the MER to the NE tip of Djibouti. Maximum values of extent of melting are recorded near the Sullu Adu / Manda Hararo zone, along with the lowest depth of melting. The Stratoïd records the strongest 'lid effect' at this location (see text). Furthermore, the recent lavas of the MER have a signature resembling the recent Afar toward the Sullu Adu / Manda Hararo area. This indicates that the present-day channelization is favored by f the thinning episode recorded in the Stratoïd lavas.

8.4. Evolution of the melting regime

30 Ma: emplacement of pre-extension CFB, concomitant with lithospheric thinning

The 30 Ma Traps record a deep signature, with the most elevated Grt value coupled to high $Fe_{7.3}$ (Fig. 11, 12). This is coeval with the thermic erosion that reduced the thickness of the lithosphere from an initial value of 100-125 km [*Dugda et al.*, 2007] to the present day 75-80 km [*Rychert et al.*, 2012] found under the plateaus

(Fig. 13). This is equivalent to a $ß_{LITH} = 2$, taking into account an initial lithospheric thickness of 120 km. The signature of this process is still expressed by melt-related SKS anisotropy of the mantle [*Kendall et al.,* 2005] that record parallel-to-structures preferred orientation of anisotropy, explained by the upwelling of the mantle. *White and McKenzie* [1989] first attribute the high magnesian and alkaline nature of the erupted basalts in Ethiopia to high mantle temperature provoked by a decompression of anomalously hot asthenospheric mantle, due to lithospheric stretching. In turn, *Buck* [2004] predicts that a high magma input can facilitate lithospheric deformation when tectonic forces are insufficient. Therefore, thermal weakening and lithospheric stretching certainly are echoing processes, the first enhancing the latter and vice-versa. This phenomenon, which is maximum at the apex of the plume head, may act as the principal localizing parameter of the future volcanic margin.

29-7 Ma: crustal extension with sustained mantle regime

After the Traps eruption, the mantle rapidly acquired melting conditions that were held until the eruption of the Stratoïd (Fig. 11, 12). The syn-rift lavas of the Afar margin record a drop in the pressure of melting that rapidly occurred after 30 Ma, right after the Afar plume impingement and the traps eruption [*Pik et al.,* 1998; *Coulié et al.,* 2003] (Fig. 11, 13). The thermal weakening of the mantle mentioned earlier probably played a major role in rift initiation [*White and McKenzie,* 1989; *Buck,* 2004]. The average depth of melting was thus shallow and remained more or less constant from 29-7 Ma since the beginning of crustal extension (between 29 and 26 Ma [*Wolfenden et al* 2005; *Stab et al.,* 2015]). It suggests that the melting regime was sustained by a combination of decompression melting and cooling. The original 'mantle plume' signature is preserved during this time period, as shown by isotopic signatures of the basalts since the Oligocene [*Pik et al.,* in prep]. We interpret this as the cooling plume head being channelized in an extending zone of the lithosphere extremely focused below Central Afar and its margins (Fig. 13). Thus, there exist a close relationship and interplay between the apex of the plume head, the most uplifted part of the Ethiopian dome, the preferential zone of CFBs magma extrusion in the mantle and crust, and the extending zone that will form the future volcanic margin (Fig. 13). The 'original' structure of the mantle plume likely evolved from a large plume head to much narrower channelization systems soon after extension begun (Fig. 13). This change was probably enhanced by slab pull forces that drive Arabia away from Africa [*Faccenna et al.,* 2013]. Moreover, the extent of partial melting through time is remarkably constant during the early phases of syn-rift magmatism (Fig. 13), although some high-F basalts during the Dahla emplacement are found on the Djiboutian side of the rift (Fig. 12). This is in agreement with an unequal repartition of the extruded volumes within Central Afar: on the western part of Central Afar, there is less than 1 km of rhyolitic lavas [*Stab et al.,* 2015], whereas

the Mabla and de Dahla (20 Ma to 7 Ma) can be locally much thicker. [*Barberi et al.,* 1975; *Varet*, 1978; *Hart et al.,* 1989; *Deniel et al.,* 1994; *Le Gall et al.,* 2011].

This period of sustained mantle conditions is bracketed by two phases of crustal extension: **(1)** a first stretching phase (Fig. 13) at ~29 Ma in the Afar [*Ukstins et al.,* 2002; *Wolfenden et al.,* 2005; *Stab et al.,* 2015] by an episode of crustal stretching of moderate amplitude ($ß_{CRUST}$ = 1.2-1.3) [*Morton and Black,* 1975, *Wolfenden et al.,* 2005; *Stab et al.*, 2015], distributed over a wide area [*Stab et al.,* 2015]. **(2)** A major thinning event at ~7 Ma (Fig. 3) [*Stab et al.,* 2015], which yielded an associated $ß_{CRUST}$ = 2 for this tectonic phase (total $ß_{CRUST}$ ~2.7 without counting the underplating). This underlines a process close of the 'depth-dependent stretching' [*Davis and Kusznir,* 2004], where the lithosphere and the crust are not stretched and thinned at the same amount in the same time.

4-1 Ma: building of the SDR (Stratoïd)

The Stratoïd mode, timing of emplacement and spatial repartition share some characteristics with the wedges of SDR found at mature volcanic passive margins. First, the emplacement of the Stratoïd required a thinned lithosphere (Figs. 11, 12, 13) and occurred over a thinned crust [*Stab et al.,* 2015]. Such thinning likely produced a decompression pulse. This is in line with the most recent modeling studies that predict the emission of important volumes of magma during the break-up if the lithosphere has been previously thinned [*Armitage et al.,* 2010]. This decompression may have been driven by preferential zones of lithospheric thinning, as attested by the local maximum of the 'lid effect' (Fig. 12). Indeed, the zone of lowest %Grt and highest %F is located within the Stratoïd series emplaced between Sullu Adu and Manda Hararo (Fig. 12) which may have been preferentially underplated during the Miocene [*Stab et al.,* 2015].

Second, the Stratoïd has been emplaced over a short timespan: the maximum emission occurred between 2-1 Ma [*Kidane et al.,* 2003]. It is difficult to constrain the exact timing of emplacement of the SDR offshore because of the lack of datings; however, their internal structure suggests an episodic emplacement [*Franke et al.,* 2007], as do their lack of development of magnetic anomaly [*Hinz et al.,* 1999]. In Eastern Greenland however, the flexured lavas flow expressed in onshore SDR were emplaced in ~2 Ma [*Lenoir et al.,* 2003]. This is consistent with an overall timespan of ~1 Ma for the Stratoïd. Furthermore, the thickness of the Stratoïd (which is about 1 km thick locally) is inferior to the 4-15 km frequently observed at mature margins. In this frame, the Stratoïd would constitute the first episodic pulse of a fully developed SDR (its lowermost flows), rapidly emplaced in ~1 Ma prior to break-up.

Third, the Stratoïd spatial distribution tightly linked to the presence of the transform that separates the Central Afar from the Erta'Ale segment [*Stab et al.,* 2015]. A relationship between SDR and segmentation is documented at many volcanic passive margins elsewhere [e.g. *Koopmann et al.,* 2014]. It is worth noting

that this flood basalt pulse occurs during or right after the onset of the Ocean-Continent Transition in the Red Sea, around 5 Ma [*Davison et al.,* 1994]. It is possible that both the 7 Ma crustal thinning in Central Afar and the lithospheric break-up in the Red Sea provoked favorable conditions for the anomalous asthenosphere to melt. Indeed, the contrast between the thinned oceanic crust and lithosphere in the Red Sea and the thinned continental lithosphere with underplated crust beneath Central Afar may have enhanced convection cells that would have acted as channelization path for fusible mantle material. *Franke et al.* [2007] has suggested that transfer zones act as stopping barriers, thus restricting the SDR distribution in zones of preferential thinning. In Afar, such a zone could correspond to the Sullu Adu / Manda Hararo segment [*Stab et al.,* 2015].

0.6 Ma onward: localization of the plume stem

At 0.6 Ma, both extension and mantle melting are localized beneath active segments [e.g. *Ebinger et al.,* 2008; *Grandin et al.,* 2010; *Medynski et al.,* 2013; 2015]. (Fig. 13).

We propose that a hot plume stem generated the recent Manda Hararo on- and off-axis lavas. This explains why the mantle is again hot and melts at higher pressure than during the Stratoïd episode [Fig. 8 and *Ferguson et al.,* 2013; *Armitage et al.,* 2015], with temperature suggesting mantle plumes [*Rooney et al.,* 2012] whereas it is much colder beneath the MER [Fig. 8 and *Rooney et al.,* 2012, *Ayalew and Gibson,* 2009], with lower %F (Fig. 11, 12). In this view, the plume stem would feed the nascent volcanic margin once the 'fossil' plume material had cooled down and was reworked by the different tectonic phases. This plume stem would thus be the remnant of the original plume that connects with the low velocity anomaly located deeper in the mantle [*Hammond et al.,* 2013], and would localize melting where the lithosphere has been previously thinned and the crust underplated [Fig. 12, as in Rychert et al., 2012]. Indeed, the geochemical signature of 're-localization' in the recent rocks appear to be maximum beneath Central Afar nowadays, and is progressively diluted as one get closer to the MER (Fig. 12). *Rychert et al.* [2012] suggests that the thermal structure beneath Ethiopia corresponds rather to a passive mantle upwelling than to a classically pictured mantle plume. We advocate for the latter, given the high temperatures and pressures expressed by the < 0.6 Ma basalts, although this plume stem should be connected to a deeper thermal anomaly. This is supported by the fact that the on-axis lavas display similar Grt contents than the older syn-rift lavas, but a higher $Fe_{7.3}$. This can be interpreted as higher starting pressure of melting after 0.6 Ma, but with the bulk of the melting region taking place above the spinel-garnet transition.

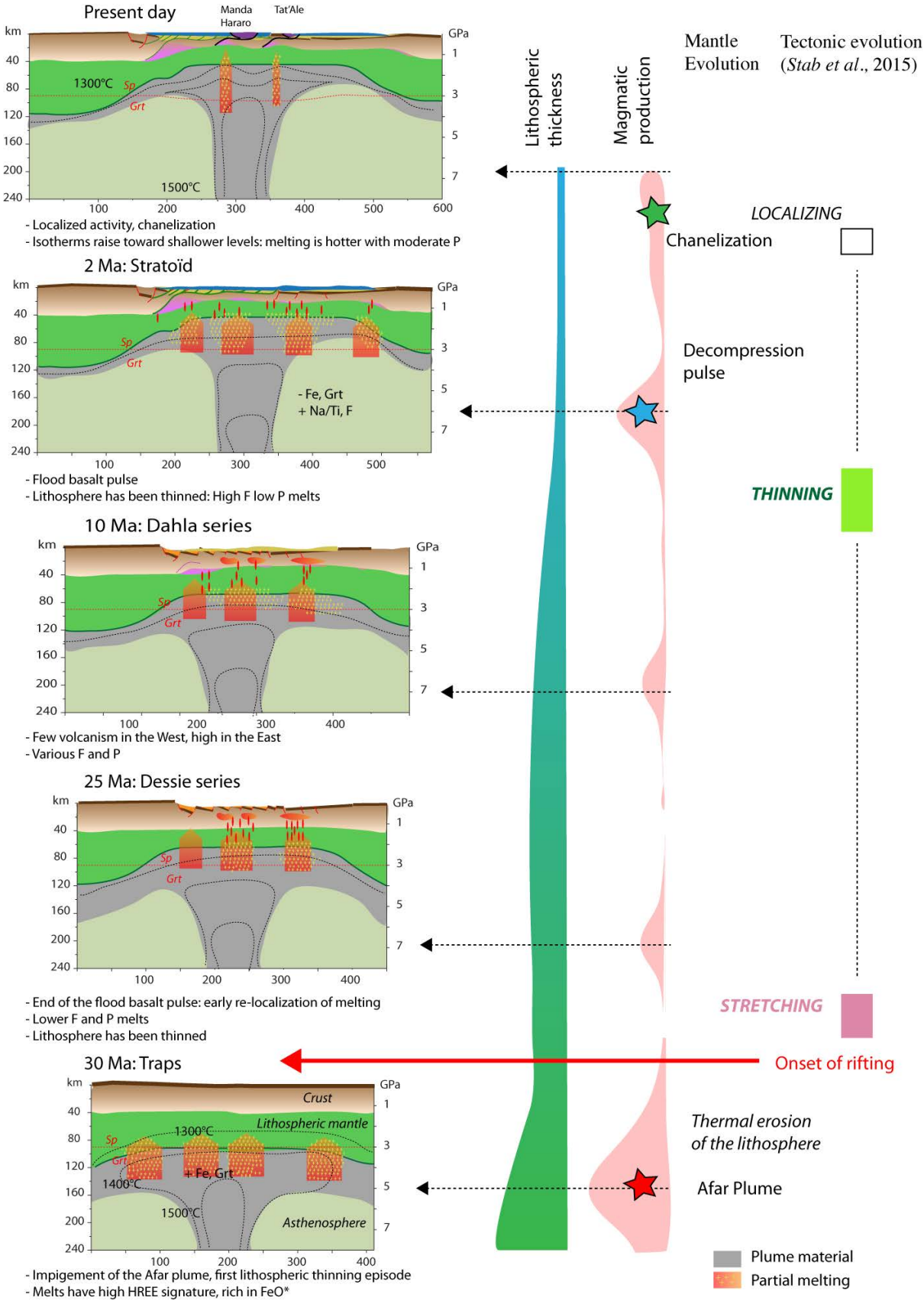

Figure 13. Time evolution of the mantle regime (this study) and the crust [after Stab et al., 2015].

9. Conclusion

In this contribution, we present an integrated geochemical study of a complete volcano-stratigraphic record of the Ethiopian province. We provide constraints on the mantle melting regimes during the syn-rift history of extension of this nascent volcanic passive margin. We show that the lithospheric mantle experienced the combined effect of post-plume cooling, but also thinning during the Miocene. Mantle cooling is expressed by the late Oligocene to early Miocene lavas erupted in the Marginal Graben and in Djibouti. This effect is protracted and bracketed in time by two crustal extensional episodes. Mantle cooling is accompanied by the rapid post-plume channelization of the plume head into narrower zones, which perhaps helped focus extension at the future volcanic margins location. Lithospheric thinning signature is found in the Stratoïd series, whose emplacement is controlled by rift segmentation and characterized by a rapid episodic decompression pulse. These post-thinning volumes thus share analogies with the SDR sequences observed at mature volcanic margins ocean-continent transition, which are emplaced in tight link to major transform zones in episodic, rapid, flood-like eruptions. Immediately following this major decompression, the magmatic activity became focused at the active segments, where narrower melting columns root in the deeper plume remnants, but the bulk of the partial melting being located at depth inferior to garnet-spinel transition. The mantle potential temperature is elevated during this relocalization phase, which leads us to argue in favor of a plume stem activity, instead of purely passive adiabatic decompression characteristic of mid-oceanic ridges.

Appendix.

A. LLD determination for major elements

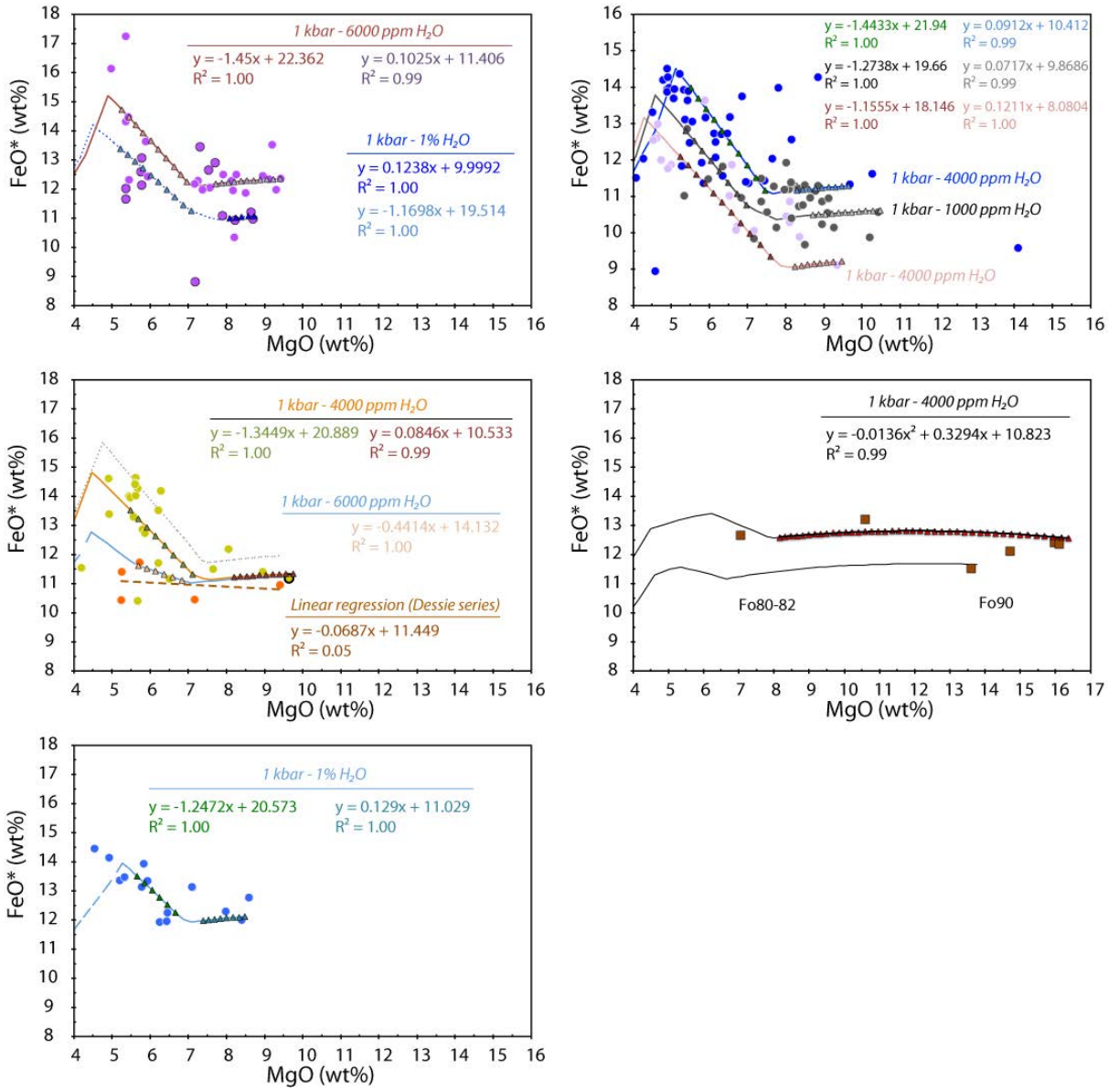

Figure A1. FeO against MgO variation for each series. LLD with specific amount of water and pressure are shown.*

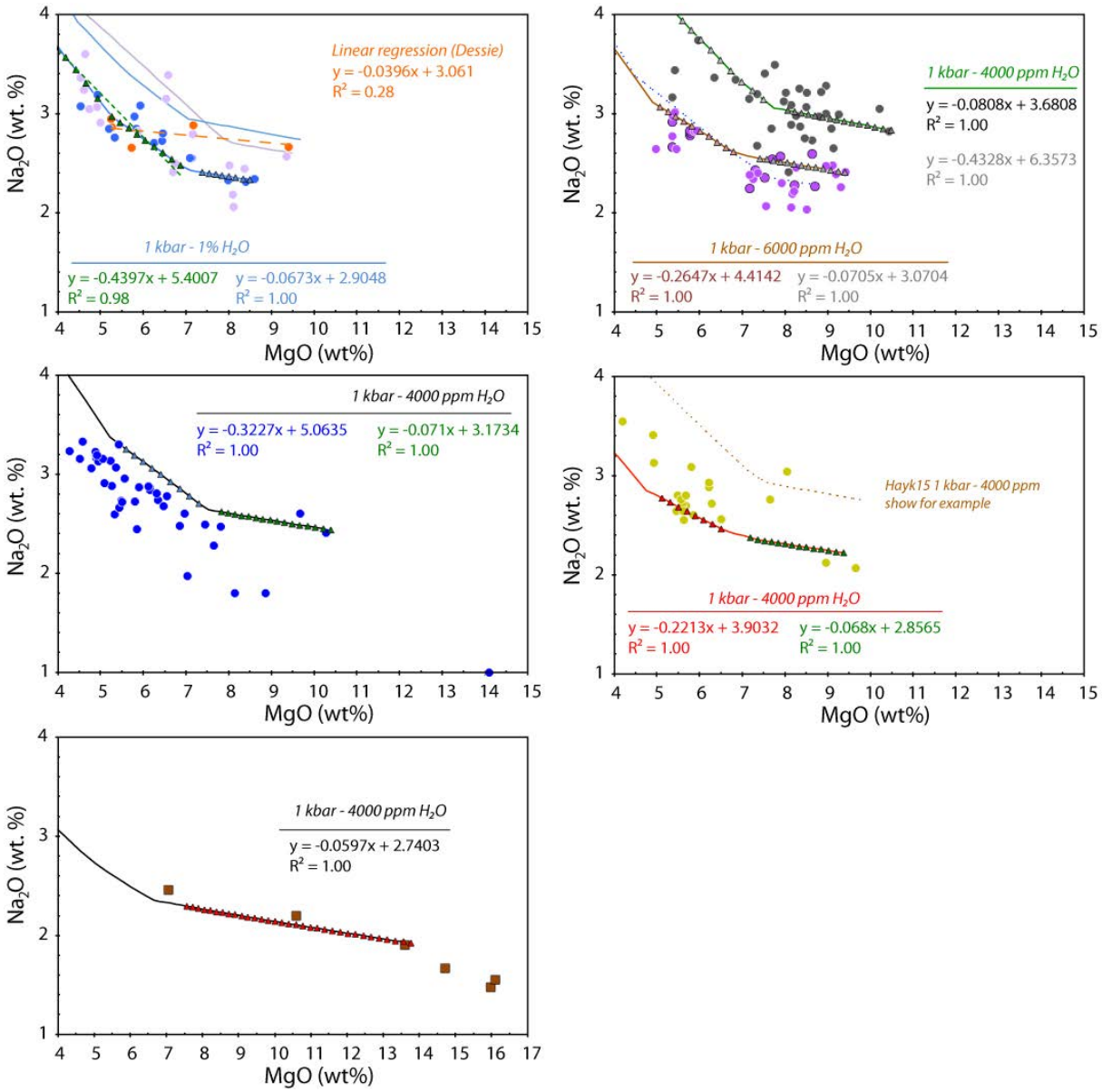

Figure A2. Na_2O against MgO variation for each series. LLD with specific amount of water and pressure are shown.

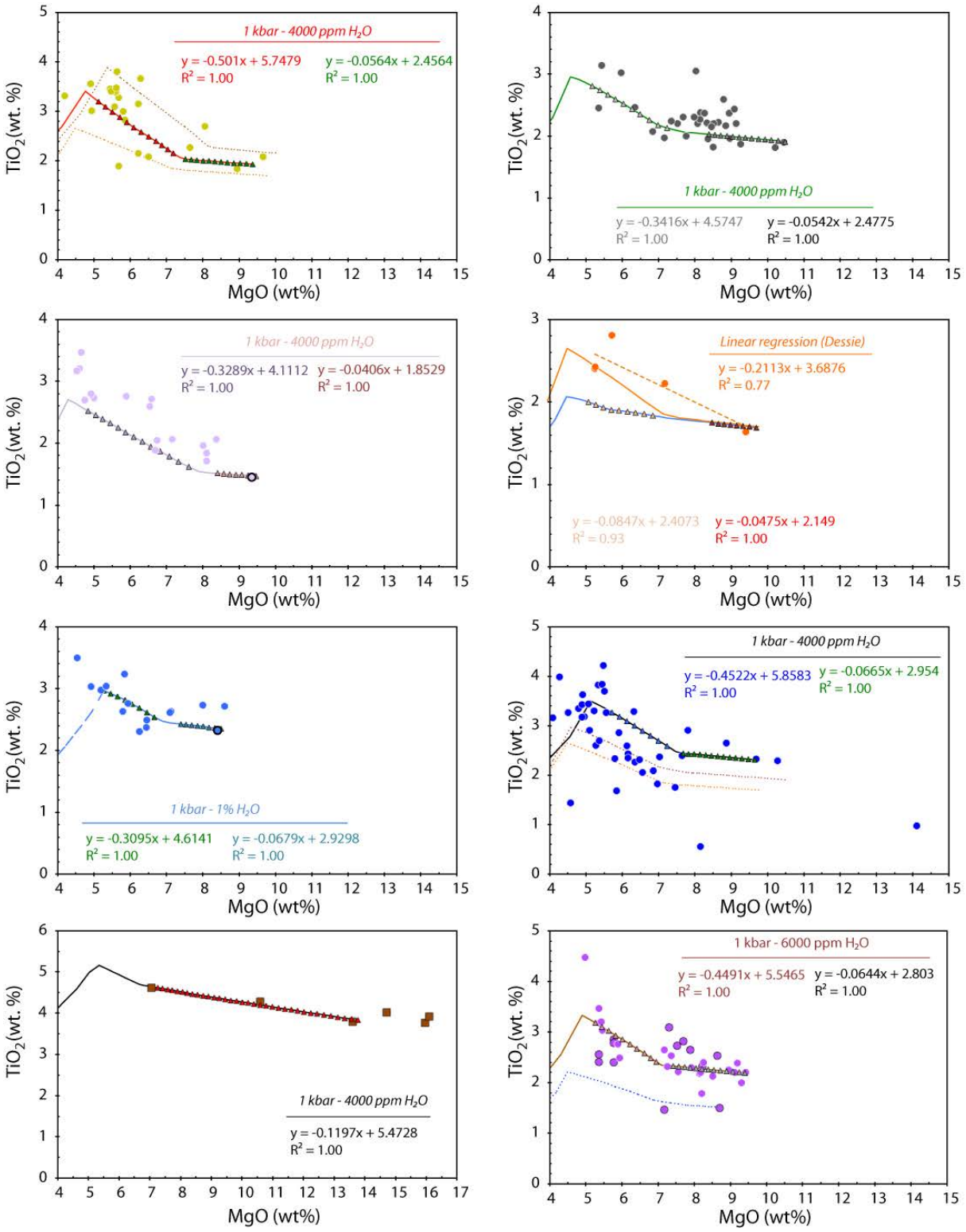

Figure A3. TiO_2 against MgO variation for each series. LLD with specific amount of water and pressure are shown.

B. LLD determination for trace elements

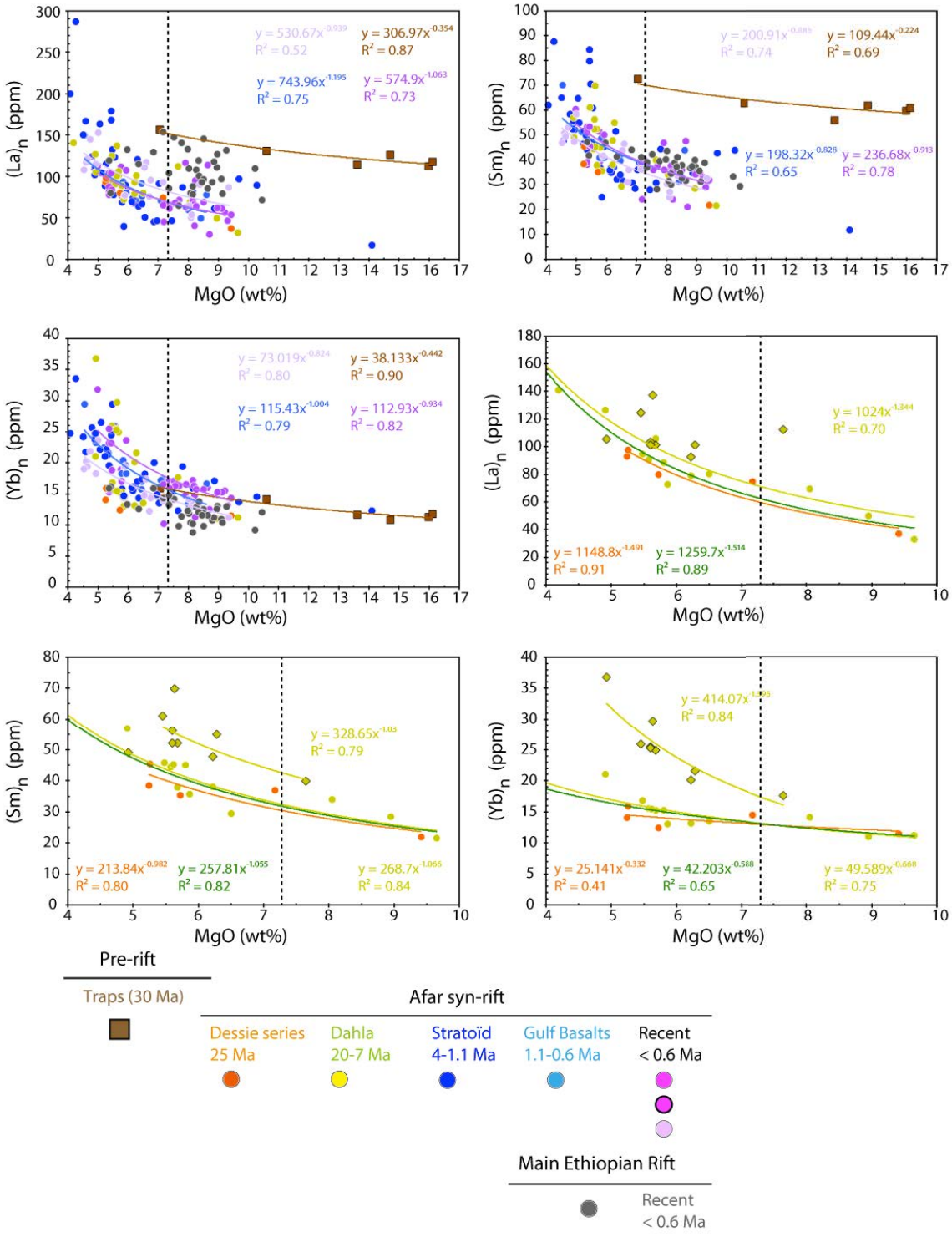

Figure B1. Trace elements variations for each series.

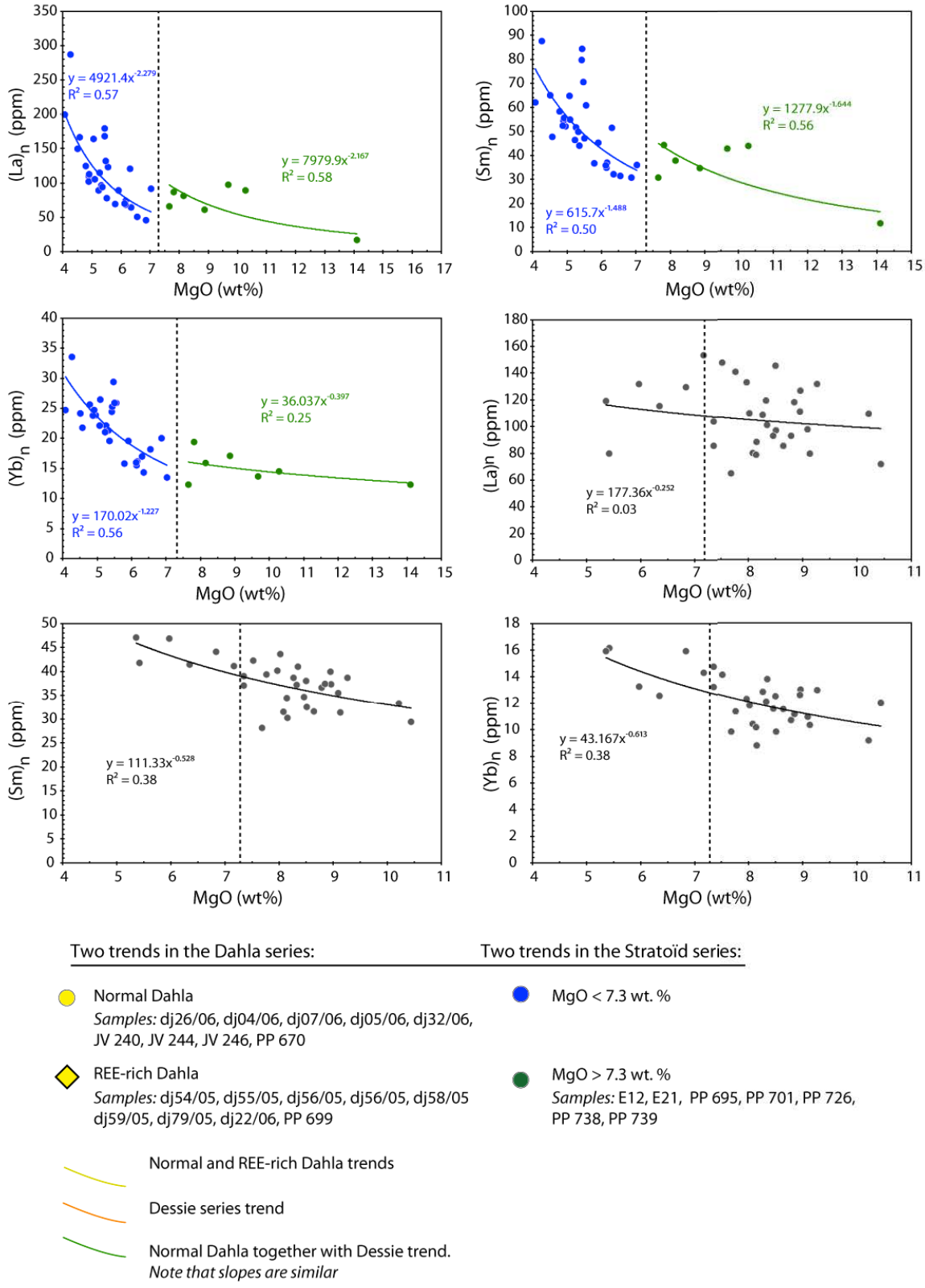

Figure B1. Continued.

C. Non-modal batch melting of lherzolite peridotite

We used non modal batch melting equations to model pooled melts derived from a lherzolitic source. Equation used is.

$$\frac{C_L}{C_0} = \frac{1}{F(1-P)+D}$$

Where C_L is the trace element concentration in the liquid, C_0 is the trace element concentration in the source, F is the extent of melting, D is the trace element partition coefficient in the source and P the congruence parameter that accounts for the fact minerals do not enter in the melt in the same proportions (i.e clinopyroxenes melt more rapidly than olivines and thus have a higher P).

The average partition coefficient of a trace element X between the liquid and the peridotite is calculated as follows:

$$D = \sum_i m_i K_i^{X/L}$$

Where m_i is the modal proportion (mass %) of the mineral phase i, and $K_i^{X/L}$ is the partition coefficient of the element X between the mineral phase i and the liquid.

The congruence coefficient is calculated as

$$P = \sum_i p_i K_i^{X/L}$$

Where p_i is the proportion in which the phase i enters the liquid.

K and p values used in this study are summarized in this table:

Mineral	**modal**	**p**	**K (La)**	**K (Sm)**	**K (Yb)**
Ol	0.61 + Δ[a]	0.16	0.00000082	0.00032	0.0096
Opx	0.20	-0.12	0.0008	0.0251	0.047
Cpx	0.09	0.81	0.071	0.459	0.76
Grt	0.10 - Δ[a]	0.15	0.001	0.21	4.18

[a]: the value Δ represent the amount of garnet diluted by olivine to model progressive shallowing of the melting region.

Graphical determination of F and Grt

For each data point, we plotted a melting curve that passes through the data by modifying only the mean partition coefficient (D), which reflects the amount of garnet in the source. The error associated to this 'modeled garnet content' estimation is the point size, because it depends on the way the curve intersects with a given point. F was then associated to a pair of (La/Sm) and (Sm/Yb) with a precision of 0.1 %. This method must not be seen as an absolute way to constrain source composition because it relies on some heavy assumptions:
a) Melting is strict batch melting. Batch melting gives a satisfactory approximation of the compositions of pooled melts that would mix as partial melting proceeds. However, it neglects more complex aspects. b) La, Sm and Yb initial concentration in the peridotite are set constant, independently of the amount of garnet in the source. This is a very partial hypothesis but is has the advantage of being easy to model. c) Garnet content is diluted with olivine only, and the content of clinopyroxene stays unchanged. This simulates reduction of fertility caused by repeated melting of the same mantle material, as depicted by Pb and Sr isotopes [*Pik et al.,* in prep]. d) Melting occurs at a discrete depth (i.e isobaric), pictured by %Grt. In nature, melting occurs in a column of mantle comprised between an initial and a final depth of melting. This means that the parameters that we constrain as %F and %Grt are more a graphical representation of a change of variables than absolute constraints of source peridotite compositions. %Grt thus represents only a relative 'garnet-number' meaningful in the frame of the batch-melting model. The fact that %Grt happen to be very low (2-3% for most of the samples) most likely means that for the concerned lavas, melting occurred mostly above the garnet-spinel transition and only sampled a small portion of the deeper garnet-bearing mantle. Despite those considerations, those newly %F and %Grt are self-consistent and can be compared to other parameters.

CHAPITRE 5
-
INFLUENCE DE LA SEGMENTATION SYN-RIFT SUR LA DISTRIBUTION DU MAGMATISME ET DU STYLE STRUCTURAL

- Article en préparation pour une soumission à *Terra Nova.* -

Nous avons montré que la déformation est accommodée de façon distribuée en Afar Central depuis la fin de l'Oligocène et pendant le Miocène, donnant ainsi à ce segment de rift sa morphologie actuelle très large. Nous suggérions que la différence de morphologie entre l'Afar Central (segment large avec une croûte ré-épaissie) et le segment de l'Erta'Ale (segment plus étroit avec une croûte plus mince) était du à une différence d'accommodation de l'extension. Cette différence est exprimée par l'existence d'une zone transformante qui sépare les deux segments de rift. De plus, nous évoquions la possibilité que cette même zone transformante ait pu restreindre la mise en place plus tardive de la série Stratoïde à 4 Ma au segment de l'Afar Central. Dans le chapitre 4, nous avons montré que la mise en place de cette série Stratoïde ne succédait pas seulement à une phase d'amincissement crustal, mais enregistrait également une forte signature d'amincissement du manteau lithosphérique (le manteau fond alors en réponse à cet amincissement). Cela impliquerait que la zone transformante qui sépare l'Afar Central de l'Erta'Ale contrôlerait à la fois l'amincissement crustal et lithosphérique, mais aussi le régime de fusion partielle dans manteau.

Nous avions évoqué dans le chapitre 1 le caractère fortement segmenté des marges volcaniques (*Gac et Geoffroy,* 2009) et l'influence des zones transformantes dans la distribution spatiale des SDR lors du break-up (e.g. *Koopmann et al.,* 2014). Dans ce chapitre 5, nous étudierons la distribution de la déformation et du magmatisme à l'échelle de l'Afar, du Sud Mer Rouge et du Golfe d'Aden, que nous mettrons en relation avec les grandes zones transformantes qui structurent ces rifts actuellement afin de voir si la segmentation est une caractéristique acquise pendant les phases les plus précoces de la divergence.

Early syn-rift segmentation control on the Cenozoic tectono-magmatic evolution of the Afar-Red Sea-Gulf of Aden system

Martin Stab[1,2], Sylvie Leroy[1], Nicolas Bellahsen[1], Raphaël Pik[2], Dereje Ayalew[3], Khaled Khanbari[4]

[1]Sorbonne Universités, UPMC Univ Paris 06, CNRS, Institut des Sciences de la Terre de Paris (iSTeP), 4 place Jussieu 75005 Paris, France
[2]CRPG UMR 7358 CNRS, Université de Lorraine, 15 rue Notre Dame des Pauvres, BP20, 54500 Vandoeuvre-lès-Nancy, France,
[3]School of Earth Sciences, Addis Ababa University, Addis Ababa, Ethiopia,
[4]Yemen Remote Sensing Center and Department of Earth and Environmental Science Sana'a University, Yemen

Corresponding author: Martin Stab, mstab@crpg.cnrs-nancy.fr, CRPG-CNRS, 15 rue Notre Dame des Pauvres, BP20, 54500 Vandoeuvre-lès-Nancy

Abstract

The complex and diachronous Afro-Arabian rift system is an ideal location to study how the pre-, syn- and post-tectonic volcanism affect the rifted margins systems, and what are their relationships with the rift segmentation. However, if past studies were focused at particular rift segments, no attempt was made so far to reconcile them into a single comprehensive geodynamical model. We present interpretations of seismic profiles offshore the Eritrea-Yemeni margins in the Red Sea and Yemeni margin in the Gulf of Aden and reassess the regional geodynamic evolution. Emphasis is put on the role of two major transform zones, Erta'Ale-Alayta and Shukra-El-Sheik, in structuring the volcanic and faulting patterns at those rifts. We show that those transform zones not only control the present-day rifts organization, but also were active since the beginning of rifting in Oligocene times, influencing development of rift asymmetry and creating margins displaying various diagnostic elements of volcanic passive margins.

1. Introduction

Onshore and offshore syn-rift magmatism, expressed as SDR (seaward-dipping reflectors), is a diagnostic feature of the volcanic rifted margins (e.g., Menzies et al., 2002). The SDR have been frequently associated to Large Igneous Provinces (LIP) worldwide, i.e., to the presence of a hot thermal anomaly in the mantle, which could have the capacity of triggering, or influencing the plate extension processes (e.g. White and McKenzie, 1989). However, a tight correlation also exists between the SDR distribution in space and time and the rift segmentation (Franke et al., 2007,

2013; Koopmann et al., 2014). More precisely, it has been demonstrated that the development of transform/transfer zones accommodate distinct structural styles (e.g., for the Gulf of Aden, Leroy et al., 2012; Pik et al., 2013; Bellahsen et al., 2013a). In particular, it has been shown that the main fractures zones in the Gulf of Aden are syn-rift structures (Leroy et al., 2012; Bellahsen et al., 2013a). Such features can also induce delay, and differences in volumes, of erupted magmas during rifting (Koopmann et al., 2014). Moreover, difference in crustal thinning in a given region can have a major influence on the amount of magma erupted during rifting (e.g., Armitage et al., 2010). In this frame, it is critical to better understand how the deformation is spatially distributed at passive margins in volcanic provinces in relationship with the initial mantle temperature anomaly.

The Afro-Arabia rift system, which has been influenced by the Afar plume during the Oligocene (Hofmann et al 1997), is therefore a suitable place to document the aforementioned processes. Indeed, despite a synchronous early Oligocene opening, this system produced passive margins that are volcanic at different degrees and displays local variations of the structural style (Leroy et al 2010; 2012). So far, the structural and magmatic characteristics of each rift segment in Ethiopia (Stab et al., in press), Eritrea (Savoyat et al 1998) and Yemen (Davison et al, 1994) have been widely discussed. However, there is no attempt to reconcile those rift systems in a single comprehensive model that would account for the early syn-rift segmentation, although it has a great implication on the timing of deformation and the way to lead to break-up. For instance, Stab et al. (2015) have suggested that the difference in width and crustal thickness between the Erta'Ale and Central Afar was related to major rift transform zones, which also appears to control the post-thinning flood basalt distribution in the area (Stab et al., in prep). Given the contrasted styles of rifting documented in the Afro-Arabian system (i.e. Davison et al., 1994; Savoyat et al., 1998; Ghebreab and Talbot, 2000; Stab et al., 2015), a confrontation of this hypothesis to a more regional scale is required.

In this paper we examine seismic cross sections (Fig. 1 for the location) of the Eritrean – Yemeni margins (Figs. 2 and 3) and the Yemeni Gulf of Aden margin (Fig. 4). These results are confronted to literature data in order to build a chronological and geodynamical model, which emphasizes the role of transform zones during rifting.

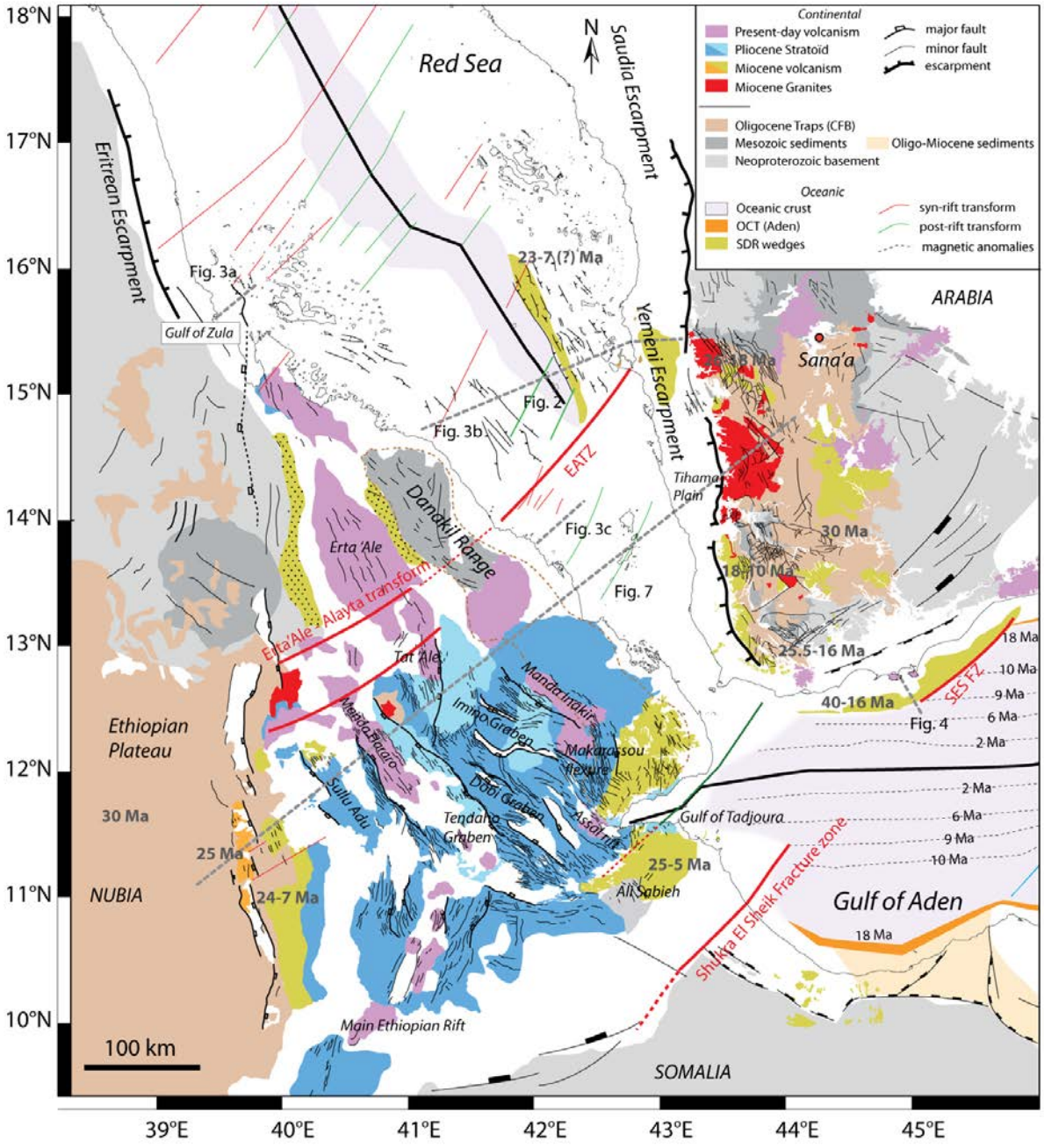

Figure 1. Geological map of the Afro-arabian rift system, encompassing the Afar rift and the Yemen margins. The Afar geology is from Stab et al., 2015, while the Yemen geology is after the geological map of Yemen (Geological survey and Mineral Resource board). Emphasis is put on the yellow color, indicating Miocene volcanism, which can be onshore as in Central Afar and in Djibouti, or offshore as SDR along the Yemeni margins. Ocean-continent transition, magnetic anomalies and transform faults in the Gulf of Aden are taken and modified from Leroy et al., 2012. Transform faults in the Red Sea are taken from Savoyat et al. *(1998). SDR in the Gulf of Aden are from Tard et al, (1991). Volcanism and faults in Somalia are from* Ali *(2015). SDR in the Red Sea are identified in this study. Note the presence of the Stratoïd*

flood basalt in Central Afar (in blue), while it is absent from northern Afar (Erta'Ale segment) and Yemen.

2. The diachronous evolution of the Afro-Arabia rift system

Oligocene Traps were erupted on a regional scale (Fig. 1; Baker et al., 1996, Pik et al., 1998, Coulié et al., 2003) due to Afar plume impingement at ~30 Ma in Ethiopia (Hofmann et al., 1997) and slightly later in Yemen at 29-26 Ma (Zumbo et al., 1995; Baker et al., 1996). This flood basalt episode was coeval with the beginning of extension in the Gulf of Aden at ~34 Ma (Leroy et al., 2012; Robinet et al., 2013; Pik et al. 2013). In Afar, Oligocene Traps predate an early extensional phase between 29 and 26 Ma (e.g. Wolfenden et al., 2005; Stab et al., 2015).

Miocene volcanism mostly affected the Yemeni margins and Djibouti, whereas it was sparser in Eritrea and Afar (Fig. 1). At the western margin of Central Afar in comparison, few volumes were erupted between 25 and 7 Ma (Stab et al., 2015). In Eritrea, no volcanism is recognized to post-date the Traps (Ghebreab and Talbot, 2000).

In Yemen, magmatic activity decreased after the Oligocene Traps peak activity and ceased at Early Miocene times. This Miocene activity is synchronous on both Red Sea and Gulf of Aden margins with: (i) along the Red Sea rift, the emplacement of basaltic dyke swarms at 25.5 and 18-16 Ma (Zumbo et al., 1995) and lava wedges beneath the Tihama plain between 30 and 16 Ma (Davison et al., 1994); and (ii) along the Gulf of Aden margin, the emplacement of up to 5 km thick syn-tectonic SDR between 40 and 16 Ma (Tard et al., 1991) (Fig.1). The main continental extension phase along both the Red Sea and Gulf of Aden margins is coeval with this volcanic activity. Along the future Red Sea, this is constrained by the stratigraphic relationships between onshore tilted blocks of 26-18 Ma and intruded granites of 22-21 Ma (Huchon et al., 1991; Baker et al., 1996; Geoffroy et al., 1998). This phase is also coeval with rapid regional uplift at 20-25 Ma of the Yemeni plateau (Menzies et al., 1992).

During the Pliocene, a widespread crustal thinning episode occurred in Central Afar (Stab et al., 2015). In Djibouti, extension affected the Dahla basalts (Geoffroy et al., 2014) before 5 Ma. The Stratoïd flood basalts were then erupted in Central Afar at 4.5-0.5 Ma (Fig. 1; Barberi et al, 1975). The oceanic spreading begun at ~6 Ma in the vicinity of the Aden city (Fournier et al, 2010; Leroy et al 2012) even though it begun earlier at around 18 Ma in the east of the Shukra el Sheik fracture zone (Fig1; Leroy et al 2012) as well in the easternmost Gulf of Aden (d'Acremont et al., 2006; 2010; Leroy et al., 2004; 2012).

Quaternary volcanics are concentrated at discrete tectono-volcanic rift segments in Afar (i.e. Manda Hararo, Medynski et al., 2013, 2015; see Fig. 1), whereas in Yemen they constitute active volcanic fields, although unrelated to any extensional structures (Fig. 1; Leroy et al 2010b; Korostelev et al., 2014; 2015).

It is noteworthy that the complete pile of volcanics observed in Central Afar and in Djibouti is of comparable thickness (2 km of Traps, ~1km of Miocene syn-rift, 1 km of Stratoïd), than the thickness of the SDR offshore Yemen (Tard et al., 1991).

This complex diachronous history is also characterized by a strong segmentation (Fig. 1) that is thought to be early-syn rift. The Erta'Ale – Alayta transform zone (Fig. 1) separates the northern Erta'Ale segment from the Central Afar segment (e.g., *Stab et al.*, 2015). The tectonic evolution of the Erta'Ale segment is unclear, although the sedimentary infill (the so called Red beds (*Varet*, 1978, Fig. 1) is thought to be Miocene in age, which suggests that the opening of this segment was synchronous to the main extensional phase. The Shukra-El-Sheik fracture zone (SESFZ) bounds the edge the Gulf of Aden volcanic margin (Fig. 1), and perhaps affected the distribution of the volcanism in Djibouti, before becoming inactive at 9 Ma.

3. Seismic cross-sections

3.1. Southern Red Sea (Eritrean – Yemeni conjugate margins)

The Eritrean-Yemeni margins are examined with three seismic cross-sections (Fig. 2). The geological formations of these cross-sections (Desset, Amber, Habab) are recognized after the seismic facies analyses of the nearby Thio-1 well data (Fig. 1) (Savoyat et al., 1989).

Geological units

The most significant feature of the Eritrean margin is the prominent post-tectonic 2 km thick Late Miocene to Pliocene Desset Fm. (Fig. 2), which consists of sand-shale infill, later covered by the post-rift Dunishub Fm. (Fig. 2). The Desset Fm. has strong internal reflectors that are good stratigraphic markers. This stage marks an important subsidence in the basin. The immediately underlying Amber Fm. salt (Fig. 2A-B) is Messinian in age (Savoyat et al., 1998) and easily identified thanks to its strong basal reflections, chaotic internal structures and halokinetic related structures. The same formations are observable at the Yemeni margin. Although there is a lack of well calibrations, first-order recognition of these formations is the geometrical relationships between salt diapirs and the overlying units.

Many continentward faults cut the reflection of the Habab Fm (Fig. 2A) showing that the main phase of deformation took place between 27 and 23 Ma (calibration in Thio-1 well, see Savoyat et al., 1989). The fluviatil Habab Fm. is characterized by thicker reflections than the Desset Fm. The Habab Fm. also displays syn-tectonic thicknesses variations (Fig. 2A), which means that it is syn-rift. Some strong and sharp reflections may suggest sills at the easternmost part of the basin although neither edifices nor structures are directly observed (Fig. 2A).

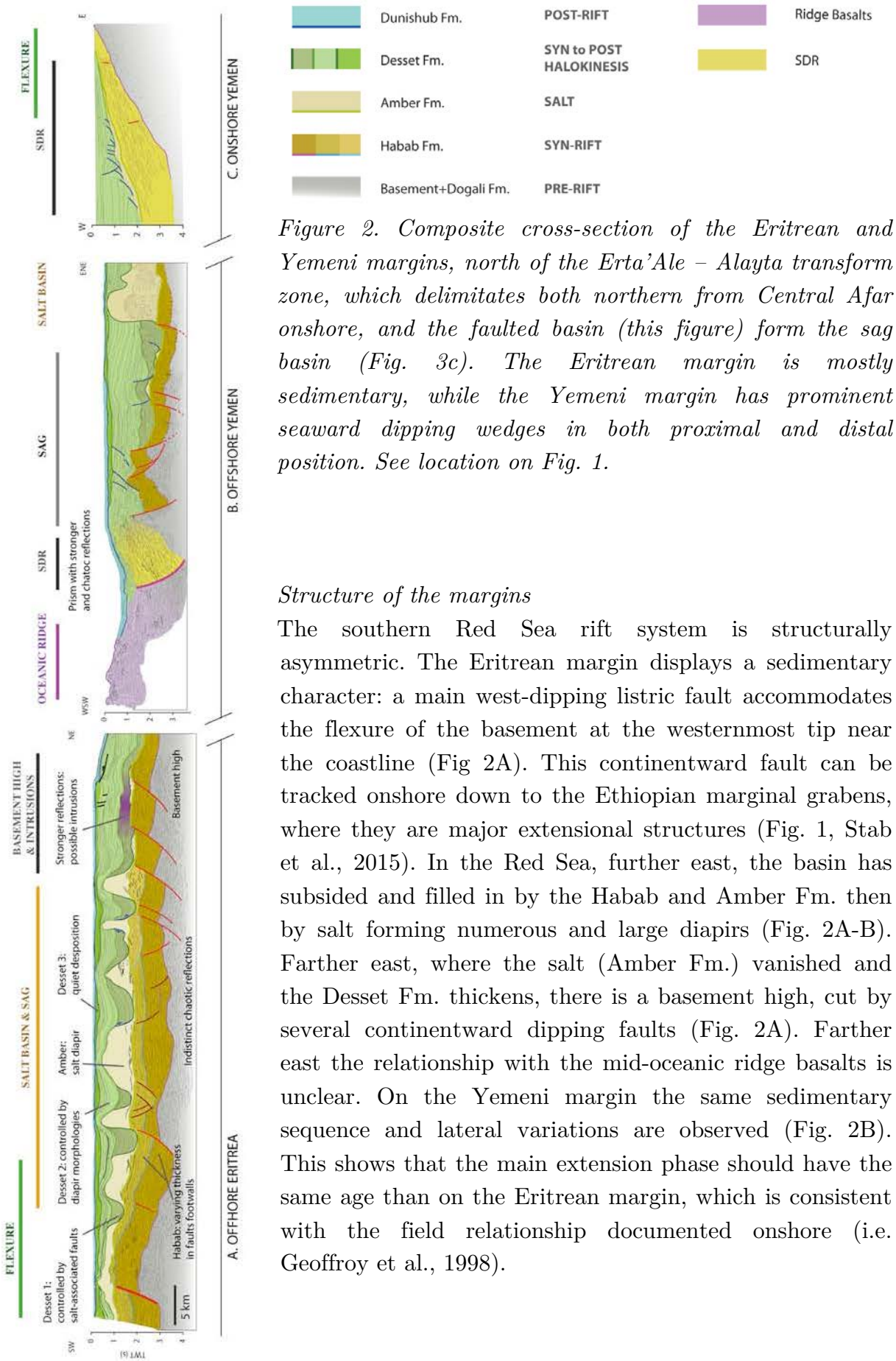

Figure 2. Composite cross-section of the Eritrean and Yemeni margins, north of the Erta'Ale – Alayta transform zone, which delimitates both northern from Central Afar onshore, and the faulted basin (this figure) form the sag basin (Fig. 3c). The Eritrean margin is mostly sedimentary, while the Yemeni margin has prominent seaward dipping wedges in both proximal and distal position. See location on Fig. 1.

Structure of the margins

The southern Red Sea rift system is structurally asymmetric. The Eritrean margin displays a sedimentary character: a main west-dipping listric fault accommodates the flexure of the basement at the westernmost tip near the coastline (Fig 2A). This continentward fault can be tracked onshore down to the Ethiopian marginal grabens, where they are major extensional structures (Fig. 1, Stab et al., 2015). In the Red Sea, further east, the basin has subsided and filled in by the Habab and Amber Fm. then by salt forming numerous and large diapirs (Fig. 2A-B). Farther east, where the salt (Amber Fm.) vanished and the Desset Fm. thickens, there is a basement high, cut by several continentward dipping faults (Fig. 2A). Farther east the relationship with the mid-oceanic ridge basalts is unclear. On the Yemeni margin the same sedimentary sequence and lateral variations are observed (Fig. 2B). This shows that the main extension phase should have the same age than on the Eritrean margin, which is consistent with the field relationship documented onshore (i.e. Geoffroy et al., 1998).

The Yemeni margin, however, displays a more volcanic character (Fig. 2B-C). Indeed, a 2-2.5s (twt) wedge of seaward dipping reflectors is identified on a basement high (Fig. 2B). It appears to be controlled by a listric continentward dipping fault (or discontinuity, Fig. 2B). This allows bracketing the age of the wedge in between 23 Ma and 7 Ma (end of the Desset Fm. deposit). In this view, the first 'oceanic' magnetic anomaly may postdate the first reflectors associated with the mid-oceanic ridges basalts. Onshore the Yemeni margin, a flexured volcanic wedge is found, which predates the Amber salt, as the base of Amber Fm. overlies the lavas flows (Fig. 2C).

The influence of the Erta'Ale – Alayta transform zone (EATZ) on the structural style

The extensional structural style changes across the EATZ from a flexural basin with tilted blocks of Hababb Fm. in the north (Figs 3A-B) to a 'sag-like' basin to the south formed during the early Miocene (Fig. 3C). As shown of figure 1, the EATZ can be tracked onshore as the transform zone separating the Central Afar rift from the Erta'Ale segment, much narrower with no Mio-Pliocene volcanics (Fig. 1). We explicitly name it a 'transform fault zone' because it is related to an early syn-rift fault that initiated during the Miocene, prior or coeval to the Hababb Fm. deposit (Fig. 3C). The EATZ trends is parallel to the divergence, which suggests that it probably used a pre-existing basement shear zone or weakness to nucleate (as do the Type 1-C in the classification of Bellahsen et al., 2013a) instead of being related to an older extensional structure, as it is observed at the non-volcanic margin of the Gulf of Aden in Socotra island (Denèle et al., 2012; Bellahsen et al., 2013a; Pik et al., 2013).

Although it is uneasy to locate the base of the Hababb Fm. in this southern area, it is noticeable that the uppermost reflectors of the Hababb Fm. are not disturbed (Fig. 3C), suggesting little – or no extension induced by faulting during the Miocene, but rather a subsiding sag-like basin. A slight, broad amplitude basement height variation at the eastern part of the basin, suggests gentle faulting prior to Hababb Fm. deposition or possibly occurring at Early Miocene times (Fig. 3C).

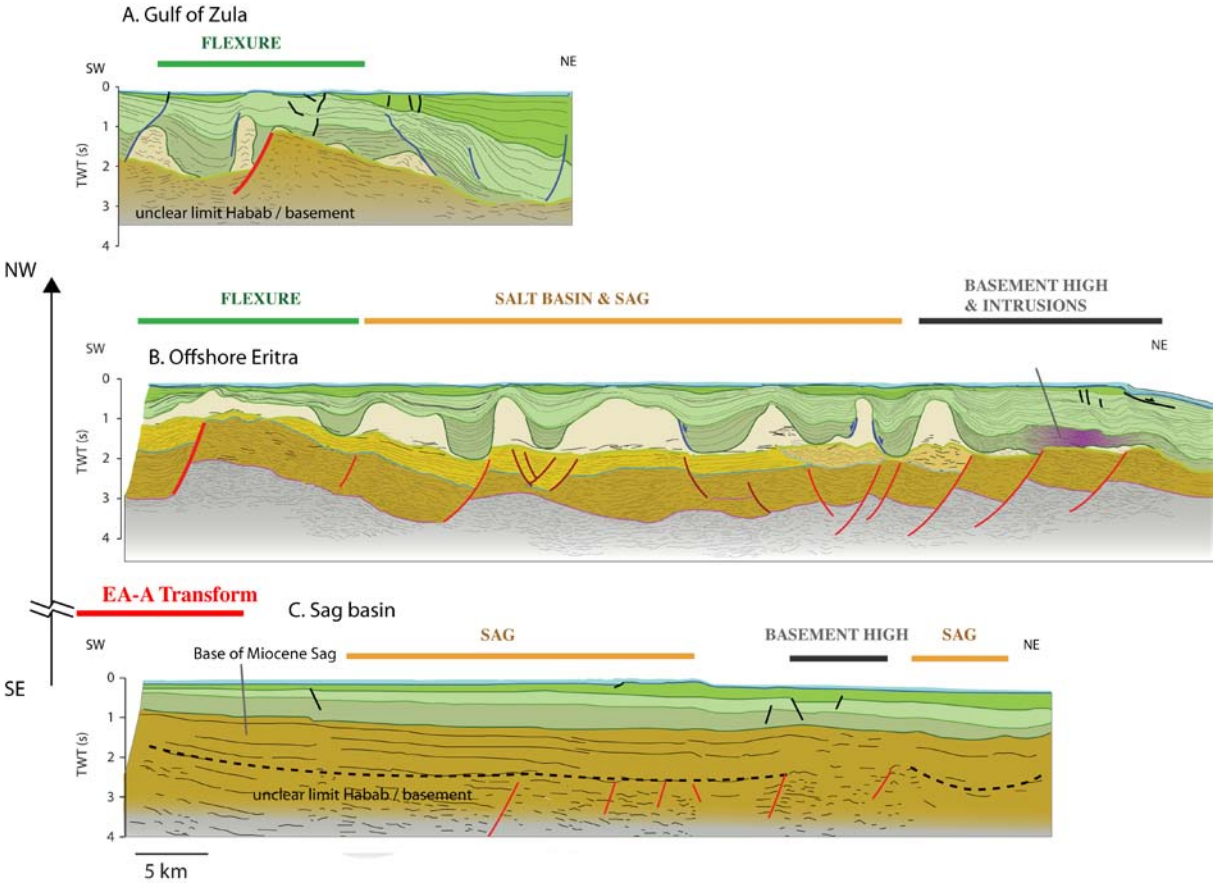

Figure 3. Structure and infilling of the Eritrean margin from Northwest to Southeast. Same legend than figure 2. (A) Flexured basement at the proximal margin near the Gulf of Zula. Note the major continentward dipping fault, which may be a continuation of the onshore marginal graben in Eritrea and Ethiopia. (B) Flexured basement in the proximal margin, with the subsiding basin northeastward. The Amber salt formation forms diapirs that affect the overlying sediments. Further east in the most distal position, there is a basement high cut by continentward dipping normal faults. The salt almost disappears as the late Miocene Desset formation thickens. (C) Subsiding sag basin south of the Erta'Ale-Alayta transform. The reflectors are mostly undisturbed and no salt is found here. Some small faults cut the basement.

3.2. The Gulf of Aden volcanic margin offshore Yemen and the SESFZ

The volcanic margin of the Gulf of Aden (Tard et al., 1991; Leroy et al., 2012; Ahmed et al., 2013) corresponds to the Yemeni margin between 44.5°E and 45.4°E. The margin is characterized by the presence of several prisms of SDR, displaying internal progressive unconformities, with increasing thickness toward basement highs (Fig. 4). These have been interpreted as the result of magma flow eruption during listric faulting (Tard et al., 1991). The prisms can be subdivided on the basis on internal onlaps (Fig. 4), with the relatively youngest one being directly in contact to the sills of the oceanic crust. As in Yemen, the first magnetic anomalies are 9 Ma old (Leroy et al., 2012, Fig. 1), while the topflows of the SDR were dated at ~16 Ma

(Tard et al., 1991). This time gap is illustrated by the SDR positions mapped by Tard et al. (1991) and the magnetic anomalies on Fig. 1.

The SDR are sparse east of the Shukra-El-Sheik fracture zone (Fig. 1), which indicates that this structure was exerted a control on the distribution of the syn-tectonic volcanism during the Miocene. It is therefore a first order parallel-to-divergence feature, which indicates that it was an active syn-rift type 1-C transform fault during the Miocene, as proposed by Bellahsen et al. (2013a). The Shukra-El-Sheik transform zone became an inactive fracture zone at around 6 Ma, which is shown by development of well-expressed magnetic anomalies, unaffected by the SESFZ (Fig. 1).

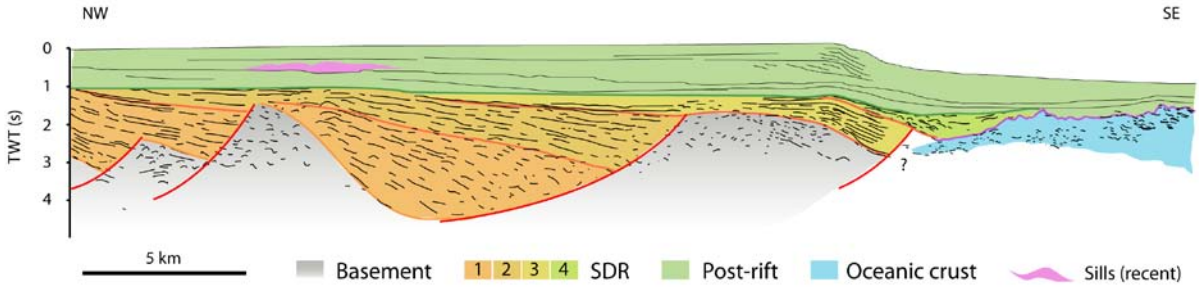

Figure 4. Volcanic margin on the Yemeni side in the Gulf of Aden. The syn-tectonic units are arranged in seaward dipping reflectors of basalts and volcanic ashes, with the top being dated at 16 Ma (Tard et al., 1991). The wedges are controlled by continentward dipping normal faults. The different shades of orange to yellow color indicate internal angular unconformities, which suggests that volcanism and deformation migrated oceanward at the time of the wedge emplacement. The topmost part (light green) of the SDR is doubtlessly syn-break up due to its structural contact with the oceanic crust (in blue). The whole margin is overlain by a carbonate prograding platform (Tard et al., 1991).

4. Tectono-volcanic evolutionary model of the Afro-Arabia rifts system

Through this integrated interpretation of seismic profiles combined with our field and geochemistry works (Stab et al., 2015; Stab et al, in prep), we highlighted the importance of the two major transform zones, Shukra-El-Sheikh (SESFZ) and Erta'Ale-Alayta (EATZ). Those two transforms, active during the syn-rift period of time, played a major role throughout the whole volcano-tectonic history of the region (Figs. 5 and 6).

Since 25 Ma, they controlled the distribution of faulting during the early syn-rift period of time; bounding an early sag-basin, which is distinct from other tectonized areas located further east in the Red Sea and Gulf of Aden incipient rifts (Fig. 5D). This happened although the extension was distributed (Fig. 5D). Furthermore, at the same time, the associated syn-tectonic volcanism distribution

appeared to be already controlled by the transforms fault zones, which delimitate the zones of SDR building (Fig. 6D).

At 18 Ma, SESFZ acted as propagation barrier to the formation of the OCT in the eastern-most Gulf of Aden (Fig. 5C), while the Djiboutian volcanism distribution was restricted to the south of the EATZ (Fig. 6C). Volcanism and deformation were more focused, probably in response of the localization of extension during the OCT formation in the Gulf of Aden (i.e. Stab et al., 2015) leading to the creation of flexured, volcanic proto-margins (Fig. 6C; Wolfenden et al, 2005, Bosworth et al., 2005).

At 5 Ma, the EATZ separated the highly stretched Central Afar from the much narrower Erta'Ale segment (Fig. 5B). This could suggest that the transform also played some role in the lack of volcanism at the Erta'Ale to the north (Fig. 6B). Onshore, this transform fault zone prevented the Red Sea OCT to develop into the sag basin, in which the Desset Fm. was deposited, undisturbed by faulting (Figs. 3, 5B and 6B). Instead, the deformation was focused further west in Afar (Fig. 5B).

Past 5 Ma, the Stratoïd series were emplaced strictly south of the EATZ (Fig. 6A), which underlines the latter's proactive role in the post-thinning evolution of Afar. At present day, the active tectono-volcanic active segments in Afar develop with respect to the pre-existing segmentation (Fig. 5A, 6A). The regional tectonic setting is modified by the propagation of the Gulf of Aden ridge into Afar in the Gulf of Tadjoura and the Assal rifts (Fig. 1, Manighetti et al., 1998; Kidane et al., 2003). This propagation induces that the SESFZ is cut by the active oceanic ridge and ceased to act as a barrier (Fig. 5A).

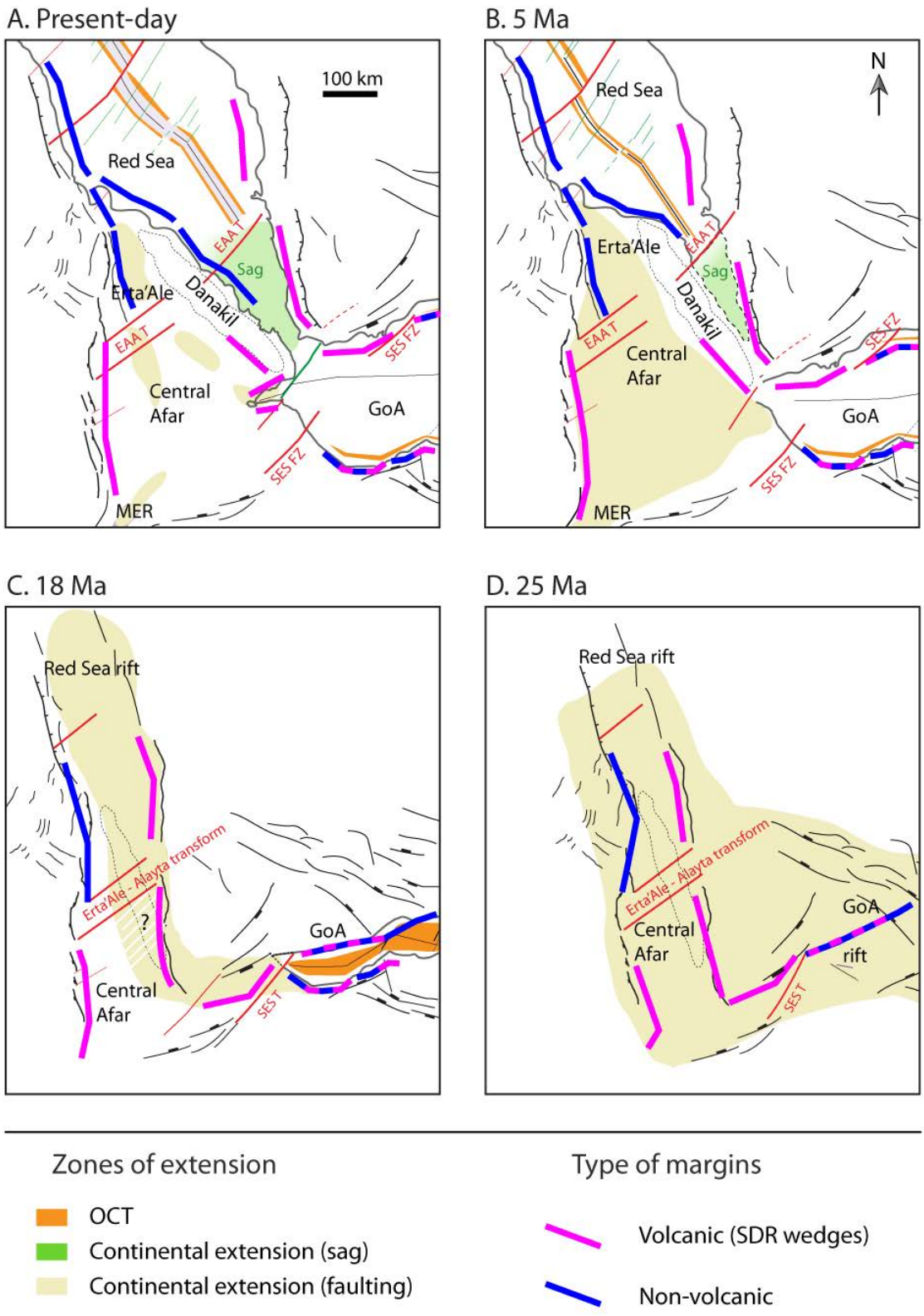

Figure 5. Tectonic evolution of the Afro-Arabian rift system. Areas in yellow represent the continental regions under extension. Oceanic spreading is represented by OCT and ridge axis (on panels A, B and C). Volcanic and non-volcanic distinction is based on the presence of lavas as the dominant syn-rift lithologies. Note that the Danakil block is considered stretched.

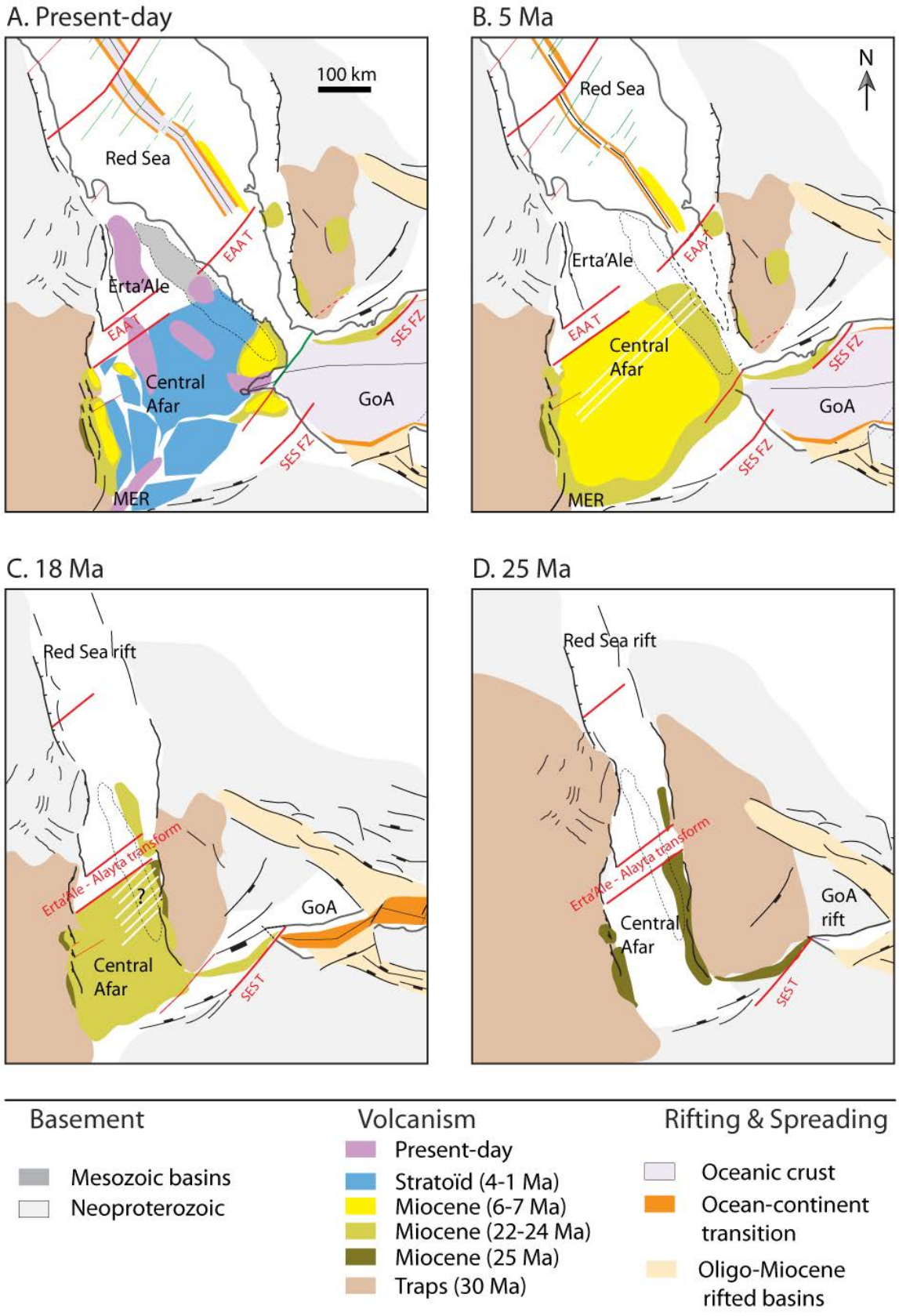

Figure 6. Volcanic evolution of the Afro-Arabian rift system.

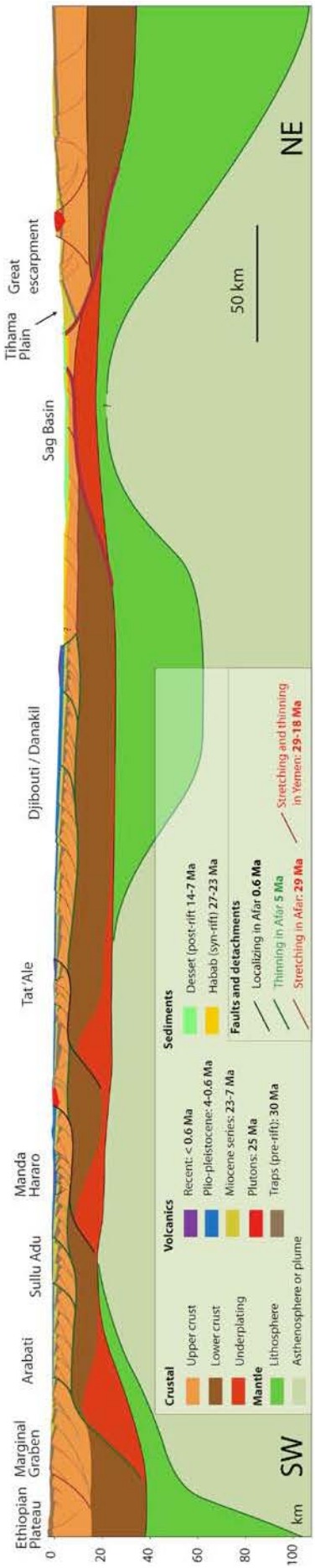

Figure 7. Synthetic cross-section, which its location is indicated on figure 1. Red faults represent the extension step described on Fig.5C-D and 6C-D, from 25 Ma to 18 Ma. Green faults (detachment) represent the thinning step that occurred prior to the Stratoïd series eruption.

5. An asymmetric rift system

Despite its complex evolution, the Afro-Arabian rift system can be described as asymmetric conjugate volcanic rifts and margins, where the structural style, timing of extension and distribution of volcanism, are controlled by the early syn-rift segmentation (Figs. 1, 5 and 6). On figure 7, we show a synthetic crustal transect across the conjugate margins. The two margins probably began to rift symmetrically (as hypothesized on figures 5 and 6). However, the transform zones rapidly segregated the distribution of erupted, and maybe intruded magma, which would have had an effect on the structural style and the length of the future margins. Strikingly, the 'Afar basin' margin became much longer than the Red Sea and the Gulf of Aden margins (Fig. 1 and 7). This fact is coincident with the presence of huge volumes of post-tectonic volcanism (i.e. the Stratoïd series), while the other volcanic margins of the area are composed of mainly syn-tectonic volcanism. This exemplifies the fact that, while volcanics distribution is controlled by the rift segmentation, the presence (Yemeni margin, Fig. 7) or absence of lithospheric mantle (Afar margin, Fig. 7) beneath the rift zone also has an impact on how deformation is accommodated (Fig. 7). The question is to know whether the presence or absence of underplating is the cause of the contrasted width differences between Yemen and Afar, or if the mantle mainly controls this difference in structural style.

The answer is ambiguous, because great volumes of magmatic underplating (and extrusions) may come either from the mantle lithospheric removal (i.e. Armitage et al., 2010; Stab et al., in prep.), or from a higher mantle temperature, allowing it to melts deeper and at greater extent without the need of lithospheric thinning (as for the Traps, e.g. Stab et al., 2015, in prep). More geochemical analysis from the Yemeni SDR would certainly be required to solve this. However, sandbox analogue experiments have shown that a weak anomaly in the mantle tends to distribute the deformation, whereas it would rather localize it when located in the lower crust (Sokoutis et al., 2007). This suggests that mantle removal exerts a first order control on the widening of the margins. In the case of the Afar-Yemen margins, the Traps likely thermally eroded the lithosphere prior to extension (i.e. Stab et al., in prep).
In this regard, the initial position of the Afar plume head would have triggered wide rifting above it, and narrower rifting away from it. Perhaps this is also true for the other rifts segments such as the Erta'Ale (Fig. 1) or the volcanic margin of Yemen (Figs. 1 and 4). In this case, the early syn-rift segmentation would certainly play a great role in channelizing the thermal weakening caused by the plume head.

6. Conclusion

In this study, we re-assessed the distribution of syn-tectonic and inter-tectonic volcanics distribution in the Afro-Arabia rift system. The re-interpretation of existing seismic data along with unpublished seismic lines allowed us to build a comprehensive geodynamic model of the region that emphasizes the importance of the early syn-rift transform fault zones. We found that the EATZ and SESFZ, which shapes the present-day Afro-Arabia geological map, were active since the earliest phase of extension. They controlled the emplacement of volcanics immediately after the Traps eruption, which had the effect of triggering differential crustal thinning and enhancing margins asymmetry at the latest stages of extension. Our findings have implications on the notion of SDR building at volcanic passive margins. It is widely accepted that during the break-up of continental lithosphere, the building of voluminous SDR wedges is controlled by major transform faults (i.e. Franke et al., 2007; 2013; Koopmann et al., 2014). Here, we outline the potential of old transform fault zones, pre-existing from the earliest stages of continental extension, in controlling the development of proto-SDR and the preferential areas of crustal thinning, which in turn could trigger the eruption of more volumes of lava. The same transform fault zones then influence the repartition of incipient oceanic crust when the lithospheric conditions are favorable for its emplacement.

Acknowledgments

This project was funded by the Actions Marges program (Total-CNRS-INSU-IFREMER-BRGM). We thank Total for funding the PhD thesis of Martin Stab.

CHAPITRE 6
-
DISCUSSION GÉNÉRALE

1. Synthèse des résultats principaux

Evolution tectono-magmatique de l'Afar Central

Notre travail de cartographie de détail de deux zones clefs en Afar Central a permis de montrer que ce segment de rift ne correspondait pas à une succession de « bassins » volcaniques de plus en plus jeune vers l'axe (comme proposé par *Wolfenden et al.* (2005)), mais en réalité à une succession depuis les plateaux éthiopiens jusqu'à l'axe de Manda Hararo de blocs de plus en plus basculés (flexure d'Arabati) jusqu'à des blocs hyper-basculés (60°) en partie plus distale (Sullu Adu). La vergence de ces blocs basculés est toujours en direction du centre du rift, ce qui est caractéristique des marges volcaniques. La datation de ces blocs basculés a mis en évidence la présence des Trapps pré-rift à la base de certains de ces blocs. Cela montre que les volumes de magma émis sont beaucoup moins importants que prévus sur les bords de l'Afar Central (car les séries volcaniques au dessus des trapps sont très fines), et que la croûte est étirée de façon importante, et pas seulement flexurée (*Stab et al.,* in press).

L'observation de discordances angulaires synchrones à la fois en position proximale (Arabati) et distale (Sullu Adu), d'amplitudes comparables montre que la déformation en surface s'accommode depuis la fin de l'Oligocène et pendant le Miocène sur de larges zones, de façon diffuse. C'est donc un 'wide rift' magmatique pendant cette période, au sens où la zone de déformation de surface excède l'épaisseur de la lithosphère (e.g. *Buck,* 1991). Ce mode d'extension commence à 29-26 Ma avec une première phase extensive qui affecte les Trapps avant la mise en place des séries Miocène. La datations des laves post-Trapps au sein des blocs basculés a Arabati et Sullu Adu montre met en évidence une mise en place entre 24-7 Ma. Celles-ci sont basculées en même temps par une phase d'amincissement crustal à 7-5 Ma, elle est aussi très distribuée, qui signe la fin du mode d'extension « wide rift ». Cette seconde phase pré-date la série Stratoïde, puisqu'elle n'affecte pas les basaltes supérieurs de Sullu Adu datés entre 4.5-4 Ma. Le premier marqueur de la localisation de la déformation en surface est la mise en place des Gulf Basalts, qui sont associées à de grandes failles à pendage sud-ouest et bordent les axes actifs de Manda Hararo et Tat'Ale. Ceci se produit à ~1.1 Ma, plus tôt que la formation desdits axes actifs.

Nous avons caractérisé avec précision les phases extensives en Afar Central, en calculant les taux d'extension (ß) associés à chaque étape. Pour ce faire, nous avons

utilisé un modèle d'extension polyphasé (*polyphase faulting*) qui permet de reproduire les structures observées en surface en respectant le pendage des failles vers le continent, caractéristiques de l'Afar. Nous avons montré que c'est après la seconde phase que la croûte a été amincie jusqu'à son épaisseur actuelle –précisément parce que le taux d'extension exprimé est dès lors maximal. Elle est également synchrone du développement de la flexure observée sur la marge topographique de l'Afar. Cela précise le lien entre les flexures continentales observées à d'autres endroits et l'amincissement crustal.

Ce travail de détermination de la chronologie des événements tectoniques et magmatiques en surface nous permet de produire une coupe équilibrée synthétique de l'Afar Central afin d'examiner le lien entre amincissement et extension en surface – ce qui constitue la première tentative de la sorte à ce jour. L'équilibrage de cette coupe synthétique implique la présence de volume de croûte additionnelle, que nous proposons être de nature mafique, sous-plaquée pendant le rifting. En effet, la croûte continentale sous l'Afar Central est épaisse, malgré d'importants taux d'extension en surface (ß = 3). Il nous semble de plus que notre étude constitue le premier essai de détermination quantitative de ce phénomène. La présence d'important volumes de nature mafique sous plaqués et/ou intrudés dans la croûte est cohérent avec la dominance de laves siliceuses en surface ; l'éruption d'un volume donné de rhyolites et d'ignimbrites requiert en effet la présence de presque un ordre de grandeur supplémentaire de cumulat gabbroïque sous-plaqué ou injecté (*Cox,* 1993). L'équilibrage de la coupe de l'Afar Central requiert également que ce sous-placage soit préférentiellement distribué là où la croûte a été préférentiellement amincie.

L'extension crustale est accommodée de façon diffuse à la surface, alors qu'il semble y avoir un *necking* en profondeur (*Reed et al.,* 2014). Le jeu de détachements en profondeur pourrait expliquer une telle différence de distribution. La présence de ces détachements (que nous supposons être actifs à la transition cassant-ductile) est compatible avec le fait que les failles que l'on a déterminé en cartographie ont toutes une orientation similaire (i.e. pendage vers le continent), suggérant un sens de cisaillement unique « top-vers-le-SW ».

Evolution des régimes de fusion du manteau au cours de l'extension

Nos nouvelles mesure isotopiques Sr-Nd-Pb des laves d'Afar Central, intégrées dans une base de données régionale des laves Miocène et Pliocène nous ont permis de clarifier l'évolution des sources du magmatisme au cours de l'extension. Nous avons montré que l'ensemble des basaltes mis en place en Afar Central depuis l'Oligocène a une signature isotopique qui correspond à celle des Trapps HT2, modulée à des degrés mineurs par une composante de contamination crustale. Cela montre que c'est le même matériel mantellique qui est chenalisé sous l'Afar Central depuis l'Oligocène. En revanche, les autres segments de l'Afar (l'Erta'Ale et Assal) ont enregistré une

signature isotopique qui traduit encore une interaction avec le manteau lithosphérique originel (*Pik et al.,* in prep).

Une fois la source du volcanisme pré-rift et syn-rift en Afar Central identifiée, nous avons pu réinterpréter les variations de compositions enregistrées par les liquides émis en surface comme résultant d'une évolution du régime mantellique, c'est-à-dire, de la profondeur (P) et du taux de fusion partielle (F). A cette fin, nous avons enrichi la base de donnée géochimique existante dans la littérature de nouvelles mesures, notamment des laves émises au début de l'extension à 25 Ma et de la série Stratoïde – qui constituaient les jalons manquants dans les modèles d'évolution du manteau antérieurs. Nous avons utilisé une méthode de correction des données qui permet de s'affranchir de l'effet de la cristallisation fractionnée des liquides magmatiques dans la croûte (qui a pour effet de modifier les compositions élémentaires indépendamment de P et F). La nouveauté de notre approche réside dans le fait que nous avons appliqué cette correction aux éléments traces comme aux majeurs, ce qui est rarement réalisé dans la littérature.

Nos données corrigées montrent que l'évolution des profondeurs et taux de fusion est liée aux phases tectoniques enregistrées par la croûte (*Stab et al.,* in prep-a). Le manteau sous l'Afar a été brutalement aminci pendant la mise en place des Trapps avant le début de l'extension crustale. En effet, les Trapps sont issus de la fusion d'un manteau profond (~5 GPa), soumis à une importante température potentielle (~1600°C) de type point chaud.

Après le début de l'extension crustale, le manteau aminci est progressivement refroidi et la zone de fusion partielle chenalisée sous le rift. Les basaltes de Dessié, première formation à être mise en place après le début du rifting à 25 Ma, enregistrent en effet des conditions de pression de fusion partielle réduites. Ce régime magmatique dure jusqu'à la phase d'amincissement crustal (évoquée plus haut) entre 7 et 5 Ma. Il est associé à la mise en place en surface de faibles volumes de laves différentiées sur la partie Ouest de l'Afar Central tandis qu'à Djibouti, les séries des basaltes du Dahla atteignent des épaisseurs de l'ordre du kilomètre localement.

L'amincissement crustal que nous avons mis en évidence en Afar Central est vraisemblablement concomitant d'une phase d'amincissement lithosphérique qui a lieu après la mise en place du Dahla (7 Ma) et juste avant l'éruption de la série Stratoïde (4 Ma). En effet, la série Stratoïde enregistre un signal d'amincissement lithosphérique prononcé, traduit par une anti-corrélation entre les proxies de taux et de profondeur de fusion partielle, où « *lid effect* ». Cela met en évidence un lien contingent entre l'amincissement crustal d'une part, et l'amincissement lithosphérique d'autre part. Ce dernier semble de plus avoir été une condition préalable à la mise en place de ce second pulse de *flood basalts*. Ainsi, bien que le manteau lithosphérique ait été passivement refroidi, son amincissement a certainement permis de générer les volumes de laves massifs de la série Stratoïde via des processus de décompression.

La phase crustale de localisation post-Stratoïde évoquée plus haut est coïncidente avec une ré-augmentation de la température potentielle du manteau (T_P >1500°C) et un ré-approfondissement de la colonne de fusion à l'époque de la mise en place des Gulf Basalts puis des axes actifs. Cela suggère l'existence d'une « queue de panache » fortement chenalisée et localisée (du fait de sa température élevée), qui vient réalimenter la future marge volcanique après que le manteau lithosphérique sous-jacent ait été pratiquement éliminé. Il est possible que cette queue de panache se soit mise en place du fait du précédent épisode de décompression : les mouvements ascendants dans l'asthénosphère lors de l'éruption de la série Stratoïde ont pu « tirer » ce qui restait de la queue du panache, laquelle commencerait à fondre en affectant préférentiellement les zones du rift les plus faibles, potentiellement celles qui avaient été les plus amincis et sous-plaquées. Cette anomalie est absente de sous le Main Ethiopian Rift, dont le manteau est plus froid et est affecté de taux de fusion moindres.

Influence de la segmentation des rifts sur le magmatisme et l'extension

Nous avons mis en évidence une distribution hétérogène dans l'espace et dans le temps du magmatisme et de la déformation, notamment entre les segments d'Afar Central, de l'Erta'Ale (chapitre 3) et du Main Ethiopian Rift (chapitre 4). Nous suggérions un contrôle possible de la segmentation sur les différences d'accommodation de la divergence *depuis le début* du rifting, et potentiellement jusqu'au *break-up* dans le chapitre 3 ; Mais peut-être aussi sur le magmatisme et l'amincissement lithosphérique dans le chapitre 4. Afin de tester ces hypothèses, nous avons mené une étude structurale régionale de l'Afar, la Mer Rouge et du Golfe d'Aden afin de préciser le rôle de ces grandes zones transformantes dans la structuration du rift et la distribution des SDR (*Stab et al.,* in prep-b). Nous avons intégré l'interprétation de coupes sismiques des marges continentales en Sud Mer Rouge et dans le Golfe d'Aden à une revue bibliographique de l'histoire de l'extension régionale. Nous avons mis en lumière que la zone transformante qui sépare l'Afar Central du segment Erta'Ale (*Erta'Ale-Alayta transform zone*) avait une prolongation en Mer Rouge. Celle-ci sépare une zone tectonisée au Nord, où les sédiments syn-rift fluviatiles d'âge 27-23 Ma sont basculés par des failles normales, d'un bassin de type « sag » au Sud, où ces mêmes sédiments ne sont pas perturbés par la tectonique. Plus à l'Est, dans le Golfe d'Aden, nous montrons qu'une deuxième zone transformante majeure Shukra-El-Sheik, contrôle la répartition spatiale de SDR syn-tectoniques. Ces deux zones transformantes ont donc un impact non seulement sur la propagation du break-up en Mer Rouge et dans le Golfe d'Aden, mais sont actives depuis le début de l'extension. Elles séparent des zones où l'extension s'est accommodée de façon localisée (Mer Rouge, Golfe d'Aden) et où se sont mis en place des prismes de SDR syn-tectoniques et probablement syn-amincissement, d'une zone intermédiaire (Afar Central / bassin sag) où au contraire, la majeure partie du

volcanisme syn-rift se met en place à la suite d'une phase d'amincissement majeure, distribuée sur une zone plus diffuse.

2. Accommodation de la déformation et signification du sous-plaquage

L'hypothèse que les marges volcaniques se forment à partir de rifts nécessairement très étroits semble avoir la faveur de la littérature, tout simplement parce qu'il est communément admis que les marges passives volcaniques possèdent des zones de necking courtes (~50-100 km), (e.g. *Callot,* 2001, *Geoffroy et al.,* 2005 ; *Franke,* 2013) immédiatement adjacentes aux SDR et à la croûte océanique. Or cette interprétation pose problème pour deux raisons. La première est que les études de sismique réflexion les plus récentes semblent montrer que la croûte continentale initiale ne disparaît pas brutalement sous les SDR au profit d'une croûte océanique nouvelle, mais est plutôt amincie, transitionnelle et progressivement intrudée par du matériel mafique au cours de l'extension (*Quirk et al.,* 2014 ; *Geoffroy et al.,* 2015). La seconde raison est qu'il est paradoxal de considérer nécessairement que le magma soit un facteur localisant pour déformation. Il est vrai qu'une poche de magma, ou une anomalie thermique localisée dans la croûte ou le manteau a pour effet de concentrer l'extension à l'aplomb de cette dernière (i.e. *Corti et al.,* 2003 ; *Buck et al.,* 2004). En revanche, le magmatisme est associé a des températures élevées dans le manteau, et un manteau plus chaud aura plutôt tendance à « affaiblir » la rhéologie de la zone et de permettre l'extension sur une zone plus diffuse (e.g., *Buck,* 1999). Enfin, le manteau fond de manière extensive dans les rifts et marges volcaniques, produisant de grands volumes magmatiques intrudés, extrudés, ou sous-plaqués à la croûte. Or, l'effet sur la rhéologie de l'ajout d'un matériau mafique plus ou moins chaud dans la croûte inférieure (sous-plaquage) est mal connu.

La structure et la segmentation du rift Afar apportent une réponse. L'Afar Central, d'une part, est un cas où la déformation a été accommodée de façon diffuse pendant la quasi-totalité de l'histoire extensive. On peut considérer que la croûte sous-jacente y a été considérablement ré-épaissie (sur la base d'arguments structuraux et géochimiques), et sans doute également considérablement modifiée par du matériel mafique. Au nord de la transformante Erta'Ale-Alayta, le segment Afar Nord est très étroit, et en comparaison, bien moins riche en magma (pas de Stratoïde). Au premier ordre, on peut établir un lien factuel entre délocalisation de la déformation et magmatisme. Cela se vérifie également au niveau de la marge volcanique de la Mer Rouge au Yémen, où le rift est étroit et comporte, sinon d'important volumes *extrudés* (sous forme de SDR et dykes), peu de volumes *sous-plaqués* (le *Low Velocity Body* dans *Ahmed et al.,* 2013). La marge volcanique de Pelotas (au large de l'Uruguay, *Stica et al.,* 2014) est un cas emblématique

puisqu'elle est très courte, mais présente aussi un rapport de volumes *sous-plaqués / extrudés* faible.

La limite de cette analyse réside peut-être dans la différence entre les moyens « directs » d'identification du sous-plaquage aux marges actuelles et le modèle telle qu'on l'a déterminé pour l'Afar Central dans cette thèse. Dans le premier cas, c'est la détermination de corps ayant des propriétés gravimétriques et magnétiques différentes de celle de la croûte continentale qui est interprétée comme du sous-plaquage (fort rapport Vp/Vs, densité supérieure à 2900 g/cm^3). Dans le cas de l'Afar Central développé dans cette thèse, nous nous basons sur une interprétation de résultats d'équilibrage de coupe.

Or, certains corps sous-plaqués aux marges volcaniques actuelles pourraient-être d'origine métamorphique et non magmatique. En effet, la croûte inférieure ancienne comporte des granulites, qui, en quantité suffisante, peuvent modifier les caractéristiques géophysiques de la croûte et les faire ressembler à celles d'une croûte sous-plaquée par le magmatisme (i.e. *Gernigon et al.,* 2004). Ceci nous pousserait à surestimer les volumes de sous-plaquage. De même, l'estimation des volumes de sous-plaquage proposée dans cette thèse dépend en premier lieu de la compréhension que nous avons de l'épaisseur de la coûte continentale, notamment la croûte supérieure. Nous postulons que la croûte continentale amincie est « purement » continentale, en nous basant sur l'analyse de fonctions récepteurs (*Hammond et al.,* 2011), et donc sur les vitesses sismiques modélisées de cette croûte. Or, il est possible que la croûte supérieure soit très modifiée par le magmatisme : on ne sait pas à ce jour différencier les vitesses sismiques caractéristiques d'une croûte modifiée par une certaine quantité de dykes d'une croûte supérieure non modifiée comportant en surface quelques kilomètres d'épaisseur de formations volcaniques. Cela impliquerait que nous mésestimions l'amincissement crustal réel et donc les volumes de sous-plaquage syn-rift.

Toutefois, il faut souligner que ces biais « techniques » induits par les modes d'identification des volumes sous-plaqués induisent des erreurs qui pourraient être à même de renforcer notre hypothèse. En effet, si les marges volcaniques « courtes » telles qu'évoquées plus haut contiennent une part de roches métamorphiques en lieu et place de sous-plaquage magmatique, et que l'Afar Central se trouve avoir une croûte plus modifiée (plus injectée de magma) que la géophysique ne permet de le voir, alors l'hypothèse que plus la marge est longue, plus elle est sous-plaquée est d'autant plus vraie.

L'idée que la présence de sous-plaquage soit associée à une déformation crustale délocalisée est à contre-courant de celle défendue par les modélisateurs (e.g. *Lavier et Manatschal,* 2006). En effet, la rhéologie d'un matériau mafique refroidi dans les conditions de pression et température de la croûte est cassante, ce qui a la propriété de promouvoir la localisation de la déformation (*Buck*, 1991 ; *Brun,* 1999). Cette propriété est d'ordinaire invoquée pour expliquer le fait que beaucoup de

marges volcaniques se soient formées à partir de rifts étroits (e.g. *Geoffroy et al.,* 2005). Or, les modèles de formation des marges volcaniques sont tous basés sur le fait qu'il doit exister une faiblesse lithosphérique initiale très localisée dans le manteau (*Callot et al.,* 2001, 2002 : *Geoffroy et al.,* 2015), ce qui en soit est déjà un facteur extrêmement localisant (*Buck,* 1991 ; *Corti et al.,* 2003). Il est possible qu'en Afar Central, le sous-plaquage soit ajouté à la croûte de manière prolongée avant et pendant la Stratoïde et de fait, resterait suffisamment chaud pour entretenir un effet délocalisant.

De plus, les marges modélisées sur la base d'une faiblesse rhéologique située dans le manteau sont très symétriques, ce qui est en accord avec les morphologies observées dans les marges volcaniques courtes de l'Atlantique Sud par exemple (e.g. *Geoffroy et al.,* 2015) En revanche, nous montrons que le système Afro-Arabe est très asymétrique (chapitre 5), ce qui est lié à la façon dont la segmentation précoce des rifts distribue le magma en surface – et de fait, en profondeur. (chapitre 4).

Une dernière possibilité est que le sous-plaquage en Afar Central ne soit pas une cause de la distribution de la déformation crustale, mais une conséquence du conrôle exercé par le manteau chaud et l'apex de la tête du panache (chapitre 4). Si l'on postule que la mise en place de la plus volumineuse partie de sous-plaquage est liée à l'éruption de la Stratoïde, qui est post-amincissement majeur, alors cela veut dire que la phase d'amincissement entre 7 et 5 Ma *n'a pas besoin* de sous-plaquage pour être très distribué. Il faut alors imaginer une rhéologie délocalisante qui pourrait-être due à un manteau sous continental très peu rigide (voir les expériences analogiques dans *Sokoutis et al.,* 2007) ou très aminci (comme suggéré dans *Kogan et al.,* 2012). Cette hypothèse trouve la faveur des données de géochimie présentée dans cette thèse, qui montrent un rapide amincissement du manteau lithosphérique peu après l'éruption des Trapps, *avant* le début du rifting.

En résumé, l'affaiblissement et l'amincissement du manteau lithosphérique initial par la tête du panache (manteau anormalement chaud) avant le début de l'extension induisent une déformation crustale distribuée et beaucoup de sous-plaquage, lequel, s'il est mis en place de façon suffisamment prolongée, participerait à la délocalisation.

3. Amincissement crustal et break-up

Le manque d'imagerie fait qu'on ignore comment se produit précisément le necking crustal aux marges volcaniques. On comprend mal le lien entre les SDR qui sont des structures d'extension et l'amincissement crustal, et notamment, comment ces structures mènent au break-up (e.g. exhumation de la croûte inférieure, *Blaich et al.,* 2013 ; ou isolation d'un bloc central, *Geoffroy et al.,* 2015).

Il existe de plus en plus de preuves qui démontrent que les SDR (et les monoclinaux des flexures à terre) sont mis en place le long de failles normales à pendage vers le continent et le fait que ces derniers soient des objets syn-tectoniques

fait consensus. En effet, il est fréquent que l'imagerie sismique et les études de terrain montrent que la géométrie interne des SDR est analogue aux strates de croissance trouvées dans les sédiments syn-rift des blocs basculés aux marges passives sédimentaires. De même, l'existence des détachements en tant que structures d'amincissement principales est aujourd'hui attesté par les observations sismiques les plus récentes (*Blaich et al.,* 2013 ; *Quirk et al.,* 2014 ; *Clerc et al.,* 2015 ; *Geoffroy et al.,* 2015). Le débat le plus récent porte donc sur le rôle de ces détachements dans le break-up. Permettent-ils d'exhumer la croûte inférieure avant de provoquer une remontée adiabatique du manteau pour mettre en place la croûte océanique (comme suggéré dans *Aslanian et al.,* 2009 et *Blaich et al.,* 2013) ? Ou bien existent-ils en réponse à un *flow* actif dans le manteau et isolent-ils un bloc continental central, progressivement démantelé et intrudé qui constituera la proto-dorsale (comme proposé dans *Geoffroy et al.,* 2015) ?

Nos données apportent des éléments de réponse à ce questionnement. Nous avons montré que l'amincissement crustal et la structure en bloc basculés vers les rifts d'Afar Central était compatible avec le jeu de grands détachements plats dans la croûte continentale. Sur ce détachement viennent s'enraciner les multiples failles normales à pendage vers le continent que l'on a observé de façon systématique, dont celles qui relèvent de la flexure. Il est intéressant de souligner que cette flexure en Afar Central se produit à l'aplomb de la zone d'amincissement maximale imprimée par le jeu du détachement. La flexure serait donc contrôlée par une (ou plusieurs) failles majeures en roll-over, comme il a été proposé ailleurs (à Disko par exemple, i.e *Geoffroy et al.,* 1998). Nous avons proposé que la plus grande quantité de sous-plaquage devait se mettre en place là où les détachements ont le plus aminci la croûte continentale. Cela veut dire qu'à ces zones particulière, le « budget » total de croûte correspond à (i) entre 1 à 3 km de laves extrudées en surface et (ii) jusqu'à ~10 km de sous plaquage mafique ; c'est-à-dire qu'au niveau de ces zones particulières, la croûte est remplacée (ou ré-épaissie par elle, comme nous l'avons dit, au travers du mécanisme de magma *compensated-thinning* évoqué dans le chapitre 3) par une composante dite transitionnelle, plus mafique, intermédiaire entre une croûte continentale et océanique.

Ainsi, nous en conclurons que l'amincissement est localisé et est moteur de la «transformation » de la croûte continentale en une croûte transitionnelle plus mafique. A ce stade, nous pouvons faire l'analogie avec le modèle de *Quirk et al.,* 2014, qui prédit que la transition entre croûte continentale et océanique se fait par « dilution » du matériau continental initial par des injections mafiques pour former la proto-croûte océanique. En revanche, le point le plus important est que les détachements de notre modèle sont plats ou très faiblement pentés. C'est-à-dire que la partie active des détachements est située aux niveaux intra-crustaux, à la différence des détachements dans les *core-complexes* qui sont en fait des failles normales (donc raides) progressivement mises à plat au fur et à mesure de

l'extension. Ainsi, notre modèle exclut *a priori* qu'il puisse y avoir exhumation de la croûte inférieure, car cette structure plate distribue l'extension *de manière égale en surface* et pas seulement à l'apex du *necking*, et donc aura plutôt tendance à faire « glisser » les blocs supérieurs et inférieurs l'un contre l'autre.

Notre modèle pourrait donc ressembler à ceux de *Quirk et al.,* 2014 et *Geoffroy et al.,* 2015 en ce sens qu'il n'a pas besoin d'exhumation crustale pour arriver au break-up. En revanche, il en diffère profondément puisqu'il ne requiert pas de créer un bloc central isolé (« bloc C » dans *Geoffroy et al.* (2015)) qui jouerait le rôle de précurseur de la première croûte océanique. Nos interprétations montrent même l'inverse, puisque les zones de modification crustale majeures sont situées *sous* Manda Hararo et Tat'Ale, c'est à dire là où l'extension se localise. De même, les blocs crustaux les moins modifiés sont situés dans des parties qui ne sont plus soumises à l'extension et au magmatisme depuis la fin de l'éruption de la Stratoïde, il y a ~1 Ma. D'aucuns pourraient argumenter que le bloc de Danakil en Afar joue le rôle de Bloc C. Alors, les deux marges séparées par Danakil seraient hautement asymétriques, à la manière dont cela est décrit dans le chapitre 5, ce qui va à l'encontre même du modèle du bloc C (qui prédit des marges symétriques, sans *simple shear* (*Geoffroy et al.,* 2015)).

4. Construction des SDR

Il est établi que les SDR se forment de façon épisodique, c'est-à-dire en plusieurs épisodes éruptifs plutôt courts (*Hinz et al.,* 1998 ; *Lenoir et al.,* 2003). Cela est attesté notamment par le fait que les SDR ne retiennent pas une signature magnétique bien exprimée, car les différentes coulées de lave qui les composent enregistrent successivement une polarité différente (*Hinz et al.,* 1999). Ces coulées sont par la suite basculées progressivement donnant lieu à des discordances angulaires – qui sont progressives lorsque les éruptions sont syn-tectoniques. La question qui se pose est : comment ces différents épisodes se répartissent au cours de l'histoire syn-rift *s.l.* Le manque de datation direct des SDR impose de choisir des analogues terrestres.

A terre, la flexure monoclinale est l'analogue le mieux daté des SDR (e.g. *Geoffroy et al.,* 1998 *; Lenoir et al.,* 2003). La littérature s'accorde sur le caractère épisodique de la formation des ces objets (*Lenoir et al.,* 2003), mais le débat porte sur leur relation temporelle avec le break-up. La majeure partie de la flexure est-elle produite *au moment* du break-up lorsque les volumes émis sont importants (*Klausen,* 2008) ? Ou bien la formation de la flexure est-elle prolongée dans le temps, sous la forme d'épisodes magmatiques rapides et discontinus depuis le *début* du rifting (e.g. *Abdelmalak et al.,* 2015) ?

Nos données sur l'Afar Central indiquent que la morphologie en flexure monoclinale que nous avons documentée dans la zone d'Arabati est tardive dans l'histoire du rifting. Sa formation a lieu en même temps que la phase principale

d'amincissement crustal entre 7 et 5 Ma, soit quelques 20 Ma après le début de l'extension post-Trapps. On pourrait donc qualifier cette flexure monoclinale en Afar Central, associée à l'amincissement, de *tectonique*, par opposition aux flexures *magmatiques* décrites par *Klausen* (2008), dans lesquelles une grande partie du développement du monoclinal se fait par dilatation et injection de dykes. Cela veut dire qu'en Afar, la flexure est *complètement exprimée* avant la mise en place de la Stratoïde à 4 Ma. Les données de géochimie sur la Stratoïde montrent bien que celle-ci se met en place par la décompression de manteau suite à l'amincissement lithosphérique, et que cet amincissement lithosphérique est certainement concomitant de l'amincissement crustal (voir à ce sujet le chapitre 4). Ainsi, le pulse de décompression peut être qualifié de post-amincissement, ou *inter-tectonique* du point de vue des phases d'extensions plus récente que la Stratoïde. Ainsi, nous proposons que la flexure et la Stratoïde pourrait former un SDR.

La situation est différente au Yémen (Mer Rouge et Aden), où l'on trouve des prismes *syn-tectoniques*. Ils semblent s'être mis en place sur une période de temps assez longue, comme l'atteste le prisme de SDR daté entre 40-16 Ma à la marge volcanique du Golfe d'Aden (*Tard et al.,* 1991). En revanche, il semble y avoir, au sein d'un même SDR, une superposition continue d'épisodes éruptifs depuis le pré-rift jusqu'au break-up (voir figure 4 chapitre 5).

La première explication possible de cette différence est peut-être qu'il y a un biais d'observation, lié à l'échelle, entre les objets imagés en sismique et l'Afar Central. La résolution des images sismiques pourrait ne pas permettre de faire la distinction entre des strates de croissance et des discordances angulaires type *onlap*, comme celle entre la Stratoïde et le Miocène de la marge Ouest Afar. Il est incontestable qu'à terre, par exemple au Groenland ou à Djibouti, l'on observe des prismes flexurés syn-tectoniques (*Geoffroy et al.,* 1999, 2014 ; *Abdelmalak et al.,* 2015). Mais ces affleurements n'ouvrent qu'une fenêtre réduite sur la pile volcanique complète, puisqu'ils atteignent des épaisseurs de l'ordre du kilomètre au maximum. De fait, un prisme de 5 à 10 km d'épaisseur pourrait peut-être être également composé de strates *inter-tectoniques*, comme nous l'avons décrit pour l'Afar Central dans le chapitre 3. Si cela est vrai, alors le retard entre formation de la flexure et pulse de décompression serait une caractéristique majeure dans le processus de formation des SDR, qui a été préservé en Afar.

Une seconde explication est qu'il y a peut-être un vrai lien chronologique entre le moment où se font l'amincissement et la flexure et le moment où le magma est mis en place à la surface. Il pourrait y avoir un mécanisme qui bloquerait le magma en profondeur pendant le développement de la flexure sous forme de sous-plaquage et ferait de cette dernière une structure apparemment pré-magmatique, même si le magma est stocké en base de croûte. Et ce serait l'inverse aux marges où la partie syn-tectonique du prisme est la mieux exprimée.

Ainsi, la flexure telle qu'on l'a décrite en Afar Central pourrait-être le « début » du SDR, qui signe le moment de l'amincissement de la croûte. Ce début est bien exprimé en Afar Central, là où l'essentiel des volumes de laves Miocène ont été retenues en base de croûte, et où la décompression du manteau a eu lieu tardivement. Les SDR « classiques » exprimeraient alors plutôt le fait que l'amincissement et la décompression mantellique sont synchrones, ce qui pourrait-être dû au break-up lithosphérique. La description que nous avançons ici présente l'avantage de répondre au problème de la différence d'échelle d'observation entre sismique et terrain posé plus haut, puisque l'on peut maintenant considérer que la phase de « début » serait d'autant plus difficile à observer que le break-up produit de grande quantité de magma qui le masque.

En résumé, la part *syn-tectonique*, ou partie « *haute* » des SDR est exprimée par de grands volumes de laves agencés en strates de croissance, dont la mise en place est provoquée par un pulse majeur de décompression dû à une phase importante d'amincissement pendant le break-up lithosphérique. La partie *inter-tectonique*, ou partie « *basse* » des SDR est exprimée par des volumes de laves agencés en *onlap* sur des formations plus anciennes déjà flexurées au cours d'un épisode d'amincissement crustal et lithosphérique précédent. Cela signifie que moins la partie « basse » est exprimée, plus le début du rifting et le break-up sont rapprochés dans le temps, et plus l'amincissement crustal et lithosphérique nécessaire à la mise en place de grands volumes de laves doit être « *final* », c'est à dire, mener à la rupture lithosphérique et à la mise en place de la croûte océanique.

CHAPITRE 7
-
CONCLUSIONS ET PERSPECTIVES

1. Conclusions

Afin de mieux comprendre les processus d'amincissement et de break-up des marges passives volcaniques, nous nous étions fixé pour objectif de documenter les interactions tectono-magmatiques lors des phases précoces de la divergence en utilisant comme laboratoire naturel le rift Afar ; ce qui était la condition requise et manquante à l'interprétation de cette zone en tant qu'analogue aux marges volcaniques. Nos principaux résultats suggèrent que l'extension est accommodée de façon distribuée en surface en Afar Central pendant le Miocène. Ceci est compatible avec l'existence de grands détachements dans la croûte qui l'amincissent et contrôlent la mise en place d'importants volumes de sous-plaquage. Au stade précoce du rifting, de l'Oligocène au Miocène, nous montrons que des phases tectoniques ponctuelles alternent avec des périodes de magmatisme prolongées. Nous proposons que le système flexure + Stratoïde en Afar Central est analogue au début de la formation des SDR. Au Pliocène, la production de grands volumes de *flood basalts* se produit après l'amincissement crustal et lithosphérique tardif, ce qui suggère que la formation des SDR en Afar Central est contrôlée par des épisodes tectoniques antérieurs. Nous montrons qu'il existe une différence entre l'Afar Central, marge longue, asymétrique et fortement sous-plaquée, et les marges volcaniques de la Mer Rouge et du Golfe d'Aden, plus courtes et symétriques et où l'amincissement et la mise en place des prismes de SDR sont synchrones. Nous suggérons que cette différence est due en premier lieu à l'absence ou la présence de manteau lithosphérique sous ces deux types de marges et en second lieu à la segmentation précoce héritée de l'initiation du rifting qui renforce cet effet en distribuant inégalement le magma sous-plaqué et érupté. Enfin, nous proposons que le break-up aux marges volcaniques se traduit par l'amincissement extrême de la croûte continentale initiale, qui est progressivement remplacé par du sous-plaquage mafique et des laves subaériennes pour finir par former la première croûte océanique.

2. Perspectives

Nous proposions une distinction partie hautes et basses des SDR : syn- ou inter-tectonique. Comme nous l'avion remarqué dans le chapitre précédent, la distinction « architecturale » est peut-être un biais d'observation, c'est-à-dire que si nous pouvions obtenir une coupe sismique de l'Afar Central, peut-être verrions nous

le même type de prisme que dans les autres marges volcaniques. Dans le cas de marges Afar et Yéménites, un tel biais ne poserait pas de problèmes dans la distinction syn- et inter-tectonique, puisque celle-ci est essentiellement temporelle. En revanche, s'il était avéré que l'architecture des laves Mio-Pliocènes d'Afar Central était l'équivalent exact de ce qu'on voit de manière générale en sismique, alors il faudrait repenser la définition du terme syn-rift : lui retirer sa signification architecturale première pour ne lui laisser que sa signification temporelle. De plus, des profils sismiques pourraient confirmer ou infirmer notre hypothèse de détachement et de polyphase faulting.

Nous suggérions que la construction d'un SDR en Afar Central impliquait d'avoir d'abord flexuré la croûte au moment de l'amincissement crustale et lithosphérique, qui se produirait avant la mise en place de flood basalts (Stratoïdes). Nous nous basions pour partie sur un argument pétrogénétique qui était une forte signature type 'lid effect' enregistrée par la série Stratoïde, avec des rapports (La/Sm) et (Sm/Yb) bas. Il serait intéressant de voir si, au sein d'un même prisme de SDR l'on trouve une relation similaire à celle documentée en Afar Centrale, c'est-à-dire des basal flows qui enregistrent une grande profondeur de fusion partielle et des top flows qui enregistreraient ou non un « lid effect ». Si cette distinction existe, la question qui se poserait serait de savoir si la transition entre les deux signatures géochimiques est progressive ou brutale, et dans quelle mesure elle est associée à une phase d'extension. Pour cela, plus d'analyses des basaltes des SDR sont requises.

Notre d'hypothèse de la génération d'asymétrie des marges volcaniques est que le 1) panache initial affaibli la lithosphère de manière inégale sous le deux marges conjuguées et 2) l'amincissement est diachrone d'une marge à l'autre, ce qui se traduit par le fait que la marge amincie le plus tardivement est celle qui est le plus sous-plaqué par une arrivée progressive de matériel mafique encore chaud (celui-ci aurai une fonction rhéologique de distribution de la déformation). Vérifier cette hypothèse est difficile, car nous superposons deux paramètres potentiellement délocalisants qui sont 1) un manteau faible et 2) une croûte ductile faible et chaude. Il serait sans doutes intéressant de modéliser une distribution inégale de ces deux paramètres dans le temps et l'espace par rapports aux deux marges. Ceci permettrait entre autre de mieux préciser l'effet rhéologique du sous-plaquage.

BIBLIOGRAPHIE

Abdelmalak, M. M. (2010), Transition spatio-temporelle entre rift sédimentaire et marge passive volcanique: l'exemple de la baie de Baffin, Centre Ouest Groenland, Le Mans.

Abdelmalak, M. M., T. B. Andersen, S. Planke, J. I. Faleide, F. Corfu, C. Tegner, G. E. Shephard, D. Zastrozhnov, and R. Myklebust (2015), The ocean-continent transition in the mid-Norwegian margin: Insight from seismic data and an onshore Caledonian field analogue, *Geology*, G37086.1, doi:10.1130/G37086.1.

Acocella, V. (2010), Coupling volcanism and tectonics along divergent plate boundaries: Collapsed rifts from central Afar, Ethiopia, *Geological Society of America Bulletin*, *122*(9-10), 1717–1728.

Acocella, V., B. Abebe, T. Korme, and F. Barberi (2008), Structure of Tendaho Graben and Manda Hararo Rift: Implications for the evolution of the southern Red Sea propagator in Central Afar, *Tectonics*, *27*(4), doi:10.1029/2007TC002236.

d'Acremont, E., S. Leroy, M. Maia, P. Patriat, M.-O. Beslier, N. Bellahsen, M. Fournier, and P. Gente (2006), Structure and evolution of the eastern Gulf of Aden: insights from magnetic and gravity data (Encens-Sheba MD117 cruise), *Geophysical Journal International*, *165*(3), 786–803, doi:10.1111/j.1365-246X.2006.02950.x.

d'Acremont, E., S. Leroy, M. Maia, P. Gente, and J. Autin (2010), Volcanism, jump and propagation on the Sheba ridge, eastern Gulf of Aden: segmentation evolution and implications for oceanic accretion processes, *Geophysical Journal International*, *180*(2), 535–551, doi:10.1111/j.1365-246X.2009.04448.x.

Ahmed, A., C. Tiberi, S. Leroy, G. W. Stuart, D. Keir, J. Sholan, K. Khanbari, I. Al-Ganad, and C. Basuyau (2013), Crustal structure of the rifted volcanic margins and uplifted plateau of Western Yemen from receiver function analysis, *Geophysical Journal International*, *193*(3), 1673–1690, doi:10.1093/gji/ggt072.

Ajay, K. K., A. K. Chaubey, K. S. Krishna, D. G. Rao, and D. Sar (2010), Seaward dipping reflectors along the SW continental margin of India: Evidence for volcanic passive margin, *Journal of earth system science*, *119*(6), 803–813.

Albarede, F. (1992), How deep do common basaltic magmas form and differentiate?, *Journal of Geophysical Research: Solid Earth (1978–2012)*, *97*(B7), 10997–

11009.

Ali, M. Y. (2015), Petroleum geology and hydrocarbon potential of the Gurban Basin, Northern Somaliland, *Journal of Petroleum Geology*, *38*(4), 433–457.

Anderson, D. L. (1994), Superplumes or supercontinents?, *Geology*, *22*(1), 39, doi:10.1130/0091-7613(1994)022<0039:SOS>2.3.CO;2.

Anderson, D. L., T. Tanimoto, and Y. Zhang (1992), Plate tectonics and hotspots: the third dimension, *Science*, *256*(5064), 1645–1651.

Armitage, J. J., T. J. Henstock, T. A. Minshull, and J. R. Hopper (2009), Lithospheric controls on melt production during continental breakup at slow rates of extension: Application to the North Atlantic, *Geochemistry, Geophysics, Geosystems*, *10*(6), doi:10.1029/2009GC002404.

Armitage, J. J., J. S. Collier, and T. A. Minshull (2010), The importance of rift history for volcanic margin formation, *Nature*, *465*(7300), 913–917, doi:10.1038/nature09063.

Armitage, J. J., D. J. Ferguson, S. Goes, J. O. S. Hammond, E. Calais, C. A. Rychert, and N. Harmon (2015), Upper mantle temperature and the onset of extension and break-up in Afar, Africa, *Earth and Planetary Science Letters*, *418*, 78–90, doi:10.1016/j.epsl.2015.02.039.

Aslanian, D. et al. (2009), Brazilian and African passive margins of the Central Segment of the South Atlantic Ocean: Kinematic constraints, *Tectonophysics*, *468*(1-4), 98–112, doi:10.1016/j.tecto.2008.12.016.

Audin, L., X. Quidelleur, E. Coulié, V. Courtillot, S. Gilder, I. Manighetti, P.-Y. Gillot, P. Tapponnier, and T. Kidane (2004), Palaeomagnetism and K-Ar and 40Ar/39Ar ages in the Ali Sabieh area (Republic of Djibouti and Ethiopia): constraints on the mechanism of Aden ridge propagation into southeastern Afar during the last 10 Myr, *Geophysical Journal International*, *158*(1), 327–345.

Ayalew, D., and S. A. Gibson (2009), Head-to-tail transition of the Afar mantle plume: Geochemical evidence from a Miocene bimodal basalt–rhyolite succession in the Ethiopian Large Igneous Province, *Lithos*, *112*(3-4), 461–476, doi:10.1016/j.lithos.2009.04.005.

Ayalew, D., P. Barbey, B. Marty, L. Reisberg, G. Yirgu, and R. Pik (2002), Source, genesis, and timing of giant ignimbrite deposits associated with Ethiopian continental flood basalts, *Geochimica et Cosmochimica Acta*, *66*(8), 1429–

1448.

Baker, J., L. Snee, and M. Menzies (1996a), A brief Oligocene period of flood volcanism in Yemen: implications for the duration and rate of continental flood volcanism at the Afro-Arabian triple junction, *Earth and Planetary Science Letters*, *138*(1), 39–55.

Baker, J. A., M. F. Thirlwall, and M. A. Menzies (1996b), Sr-Nd-Pb isotopic and trace element evidence for crustal contamination of plume-derived flood basalts: Oligocene flood volcanism in western Yemen, *Geochimica et Cosmochimica Acta*, *60*(14), 2559–2581.

Ballmer, M. D., J. van Hunen, G. Ito, P. J. Tackley, and T. A. Bianco (2007), Non-hotspot volcano chains originating from small-scale sublithospheric convection, *Geophysical Research Letters*, *34*(23), doi:10.1029/2007GL031636.

Barberi, F., and R. Santacroce (1980), The Afar stratoid series and the magmatic evolution of East African rift system, *Bulletin de la Société Géologique de France*, (6), 891–899.

Barberi, F., H. Tazieff, and J. Varet (1972), Volcanism in the Afar depression: Its tectonic and magmatic significance, *Tectonophysics*, *15*(1), 19–29.

Barberi, F., G. Ferrara, R. Santacroce, and J. Varet (1975), Structural evolution of the Afar triple junction, *Afar Depression of Ethiopia*, *1*, 38–54.

Barrat, J. ., J. . Joron, R. . Taylor, S. Fourcade, R. . Nesbitt, and B. . Jahn (2003), Geochemistry of basalts from Manda Hararo, Ethiopia: LREE-depleted basalts in Central Afar, *Lithos*, *69*(1-2), 1–13, doi:10.1016/S0024-4937(03)00044-6.

Barrat, J. A., B. M. Jahn, S. Fourcade, and J. L. Joron (1993), Magma genesis in an ongoing rifting zone: the Tadjoura Gulf (Afar area), *Geochimica et cosmochimica acta*, *57*(10), 2291–2302.

Bastow, I. D., and D. Keir (2011), The protracted development of the continent–ocean transition in Afar, *Nature Geoscience*, *4*(4), 248–250, doi:10.1038/ngeo1095.

Bastow, I. D., A. A. Nyblade, G. W. Stuart, T. O. Rooney, and M. H. Benoit (2008), Upper mantle seismic structure beneath the Ethiopian hot spot: Rifting at the edge of the African low-velocity anomaly, *Geochemistry, Geophysics, Geosystems*, *9*(12), doi:10.1029/2008GC002107.

Bauer, K., S. Neben, B. Schreckenberger, R. Emmermann, K. Hinz, N. Fechner, K.

Gohl, A. Schulze, R. B. Trumbull, and K. Weber (2000), Deep structure of the Namibia continental margin as derived from integrated geophysical studies, *Journal of Geophysical Research, vol. 105, B11*, 25829–25853.

Beccaluva, L., G. Bianchini, C. Natali, and F. Siena (2009), Continental Flood Basalts and Mantle Plumes: a Case Study of the Northern Ethiopian Plateau, *Journal of Petrology*, *50*(7), 1377–1403, doi:10.1093/petrology/egp024.

Bellahsen, N., C. Faccenna, F. Funiciello, J. M. Daniel, and L. Jolivet (2003), Why did Arabia separate from Africa? Insights from 3-D laboratory experiments, *Earth and Planetary Science Letters*, *216*(3), 365–381, doi:10.1016/S0012-821X(03)00516-8.

Bellahsen, N., S. Leroy, J. Autin, P. Razin, E. d'Acremont, H. Sloan, R. Pik, A. Ahmed, and K. Khanbari (2013a), Pre-existing oblique transfer zones and transfer/transform relationships in continental margins: New insights from the southeastern Gulf of Aden, Socotra Island, Yemen, *Tectonophysics*, *607*, 32–50, doi:10.1016/j.tecto.2013.07.036.

Bellahsen, N., L. Husson, J. Autin, S. Leroy, and E. d'Acremont (2013b), The effect of thermal weakening and buoyancy forces on rift localization: Field evidences from the Gulf of Aden oblique rifting, *Tectonophysics*, *607*, 80–97, doi:10.1016/j.tecto.2013.05.042.

Benoit, M. H., A. A. Nyblade, and J. C. VanDecar (2006), Upper mantle P-wave speed variations beneath Ethiopia and the origin of the Afar hotspot, *Geology*, *34*(5), 329–332.

Berckhemer, H., B. Baier, H. Bartelsen, A. Behle, H. Burkhardt, H. Gebrande, J. Makris, H. Menzel, H. Miller, and R. Vees (1975), Deep seismic soundings in the Afar region and on the highland of Ethiopia, *Afar Depression of Ethiopia*, *1*, 89–107.

Berktold, A., V. Haak, and G. Angenheister (1975), Magnetotelluric measurements in the Afar area, *Afar Depression of Ethiopia*, *1*, 66–79.

Bertrand, H., G. Chazot, J. Blichert-Toft, and S. Thoral (2003), Implications of widespread high-μ volcanism on the Arabian Plate for Afar mantle plume and lithosphere composition, *Chemical Geology*, *198*(1-2), 47–61, doi:10.1016/S0009-2541(02)00418-7.

Beyene, A., and M. G. Abdelsalam (2005), Tectonics of the Afar Depression: A review and synthesis, *Journal of African Earth Sciences*, *41*(1-2), 41–59,

doi:10.1016/j.jafrearsci.2005.03.003.

Blaich, O. A., F. Tsikalas, and J. I. Faleide (2008), Northeastern Brazilian margin: Regional tectonic evolution based on integrated analysis of seismic reflection and potential field data and modelling, *Tectonophysics*, *458*(1-4), 51–67, doi:10.1016/j.tecto.2008.02.011.

Blaich, O. A., J. I. Faleide, and F. Tsikalas (2011), Crustal breakup and continent-ocean transition at South Atlantic conjugate margins, *Journal of Geophysical Research*, *116*(B1), doi:10.1029/2010JB007686.

Blaich, O. A., J. I. Faleide, F. Tsikalas, A. C. Gordon, and W. Mohriak (2013), Crustal-scale architecture and segmentation of the South Atlantic volcanic margin, *Geological Society, London, Special Publications*, *369*(1), 167–183, doi:10.1144/SP369.22.

Bonini, M., G. Corti, F. Innocenti, P. Manetti, F. Mazzarini, T. Abebe, and Z. Pecskay (2005), Evolution of the Main Ethiopian Rift in the frame of Afar and Kenya rifts propagation, *Tectonics*, *24*(1), doi:10.1029/2004TC001680.

Bosworth, W., and K. McClay (2001), Structural and stratigraphic evolution of the Gulf of Suez rift, Egypt: a synthesis, *Mémoires du Muséum National d'Histoire Naturelle*, *186*, 567–606.

Bosworth, W., P. Crevello, R. D. Winn Jr, and J. Steinmetz (1998), Structure, sedimentation, and basin dynamics during rifting of the Gulf of Suez and north-western Red Sea, in *Sedimentation and Tectonics in Rift Basins Red Sea:-Gulf of Aden*, pp. 77–96, Springer.

Bourgeois, O., O. Dauteuil, and E. Hallot (2005), Rifting above a mantle plume: structure and development of the Iceland Plateau, *Geodinamica acta*, *18*(1), 59–80.

Bown, J. W., and R. S. White (1995), Effect of finite extension rate on melt generation at rifted continental margins, *Journal of Geophysical Research: Solid Earth (1978–2012)*, *100*(B9), 18011–18029.

Bridges, D. L., K. Mickus, S. S. Gao, M. G. Abdelsalam, and A. Alemu (2012), Magnetic stripes of a transitional continental rift in Afar, *Geology*, *40*(3), 203–206, doi:10.1130/G32697.1.

Brun, J. P. (1999), Narrow rifts versus wide rifts: inferences for the mechanics of rifting from laboratory experiments, *Philosophical Transactions-Royal Society of London, Series A, Mathematical, Physical and Engineering Sciences*, 695–

709.

Buck, W. R. (1991), Modes of continental lithospheric extension, *Journal of Geophysical Research: Solid Earth*, *96*(B12), 20161–20178.

Buck, W. R. (2004), Consequences of asthenospheric variability on continental rifting, *Rheology and deformation of the lithosphere at continental margins*, *62*, 1–30.

Buck, W. R. (2006), The role of magma in the development of the Afro-Arabian Rift System, *Geological Society, London, Special Publications*, *259*(1), 43–54.

Buck, W. R., L. L. Lavier, and A. N. Poliakov (1999), How to make a rift wide, *Philosophical Transactions-Royal Society of London; series A Mathematical Physical and Engineering Sciences*, 671–689.

Callot, J. P., C. Grigné, L. Geoffroy, and J. P. Brun (2001), Development of volcanic passive margins: Two-dimensional laboratory models, *Tectonics*, *20*(1), 148–159.

Callot, J.-P., L. Geoffroy, and J.-P. Brun (2002), Development of volcanic passive margins: Three-dimensional laboratory models, *Tectonics*, *21*(6), 2–1–2–13, doi:10.1029/2001TC901019.

Campbell, I. H. (2007), Testing the plume theory, *Chemical Geology*, *241*(3-4), 153–176, doi:10.1016/j.chemgeo.2007.01.024.

Carignan, J., P. Hild, G. Mevelle, J. Morel, and D. Yeghicheyan (2001), Routine Analyses of Trace Elements in Geological Samples using Flow Injection and Low Pressure On-Line Liquid Chromatography Coupled to ICP-MS: A Study of Geochemical Reference Materials BR, DR-N, UB-N, AN-G and GH, *Geostandards Newsletter*, *25*(2-3), 187–198.

Chapman, D. S., and K. P. Furlong (1992), Thermal state of the continental lower crust, *Continental lower crust*, *23*, 179–199.

Chorowicz, J., B. Collet, F. Bonavia, and T. Korme (1999), Left-lateral strike-slip tectonics and gravity induced individualisation of wide continental blocks in the western Afar margin, *Eclogae Geologicae Helvetiae*, *92*(1), 149–158.

Civiero, C. et al. (2015), Multiple mantle upwellings in the transition zone beneath the northern East-African Rift system from relative P-wave travel-time tomography, *Geochemistry, Geophysics, Geosystems*, n/a–n/a, doi:10.1002/2015GC005948.

Clerc, C., L. Jolivet, and J.-C. Ringenbach (2015), Ductile extensional shear zones in the lower crust of a passive margin, *Earth and Planetary Science Letters*, *431*, 1–7, doi:10.1016/j.epsl.2015.08.038.

Coffin, M. F., and O. Eldholm (1994), Large igneous provinces: crustal structure, dimensions, and external consequences, *Reviews of Geophysics*, *32*(1), 1–36.

Collet, B., H. Taud, J. F. Parrot, F. Bonavia, and J. Chorowicz (2000), A new kinematic approach for the Danakil block using a Digital Elevation Model representation, *Tectonophysics*, *316*(3), 343–357.

Corti, G. (2009), Continental rift evolution: From rift initiation to incipient break-up in the Main Ethiopian Rift, East Africa, *Earth-Science Reviews*, *96*(1-2), 1–53, doi:10.1016/j.earscirev.2009.06.005.

Corti, G., M. Bonini, S. Conticelli, F. Innocenti, P. Manetti, and D. Sokoutis (2003a), Analogue modelling of continental extension: a review focused on the relations between the patterns of deformation and the presence of magma, *Earth-Science Reviews*, *63*(3-4), 169–247, doi:10.1016/S0012-8252(03)00035-7.

Corti, G., M. Bonini, F. Innocenti, P. Manetti, F. Mazzarini, and T. Abebe (2003b), Volcano-tectonic evolution of the Main Ethiopian Rift, in *EGS-AGU-EUG Joint Assembly*, vol. 1, p. 9405.

Coulié, E. (2001), *Chronologie 40Ar/39Ar et K^Ar de la de¤chirure continentale en Afar depuis 30 Ma, Ph.D*, Université Paris Sud.

Coulié, E., X. Quidelleur, P.-Y. Gillot, V. Courtillot, J.-C. Lefèvre, and S. Chiesa (2003), Comparative K–Ar and Ar/Ar dating of Ethiopian and Yemenite Oligocene volcanism: implications for timing and duration of the Ethiopian traps, *Earth and Planetary Science Letters*, *206*(3), 477–492.

Courtillot, V., C. Jaupart, I. Manighetti, P. Tapponnier, and J. Besse (1999), On causal links between flood basalts and continental breakup, *Earth and Planetary Science Letters*, *166*(3), 177–195.

Courtillot, V., A. Davaille, J. Besse, and J. Stock (2003), Three distinct types of hotspots in the Earth's mantle, *Earth and Planetary Science Letters*, *205*(3), 295–308.

Cox, K. G. (1980), A model for flood basalt vulcanism, *Journal of Petrology*, *21*(4), 629–650.

Cox, K. G. (1993), Continental magmatic underplating, *Philosophical Transactions*

of the Royal Society of London. Series A: Mathematical, Physical and Engineering Sciences, *342*, 155–166.

Craig, T. J., J. A. Jackson, K. Priestley, and D. McKenzie (2011), Earthquake distribution patterns in Africa: their relationship to variations in lithospheric and geological structure, and their rheological implications: Earthquake distribution patterns in Africa, *Geophysical Journal International*, *185*(1), 403–434, doi:10.1111/j.1365-246X.2011.04950.x.

Daoud, M. A., B. Le Gall, R. C. Maury, J. Rolet, P. Huchon, and H. Guillou (2011), Young rift kinematics in the Tadjoura rift, western Gulf of Aden, Republic of Djibouti, *Tectonics*, *30*(1), n/a–n/a, doi:10.1029/2009TC002614.

Daradich, A., J. X. Mitrovica, R. N. Pysklywec, S. D. Willett, and A. M. Forte (2003), Mantle flow, dynamic topography, and rift-flank uplift of Arabia, *Geology*, *31*(10), 901–904.

Davis, M., and N. J. Kusznir (2004), Depth-dependent lithospheric stretching at rifted continental margins, *Proceedings of NSF Rifted Margins Theoretical Institute*, 92–136.

Davison, I. A. N., M. Al-Kadasi, S. Al-Khirbash, A. K. Al-Subbary, J. Baker, S. Blakey, D. Bosence, C. Dart, R. Heaton, and K. E. N. McClay (1994), Geological evolution of the southeastern Red Sea Rift margin, Republic of Yemen, *Geological Society of America Bulletin*, *106*(11), 1474–1493.

Debayle, E., J.-J. Lévêque, and M. Cara (2001), Seismic evidence for a deeply rooted low-velocity anomaly in the upper mantle beneath the northeastern Afro/Arabian continent, *Earth and Planetary Science Letters*, *193*(3), 423–436.

Deniel, C., P. Vidal, C. Coulon, P.-J. Vellutini, and P. Piguet (1994), Temporal evolution of mantle sources during continental rifting: the volcanism of Djibouti (Afar), *Journal of Geophysical Research: Solid Earth (1978–2012)*, *99*(B2), 2853–2869.

Desissa, M., N. E. Johnson, K. A. Whaler, S. Hautot, S. Fisseha, and G. J. K. Dawes (2013), A mantle magma reservoir beneath an incipient mid-ocean ridge in Afar, Ethiopia, *Nature Geoscience*, *6*(10), 861–865, doi:10.1038/ngeo1925.

Dessai, A. G., and H. Bertrand (1995), The “Panvel Flexure” along the Western Indian continental margin: an extensional fault structure related to Deccan magmatism, *Tectonophysics*, *241*(1), 165–178.

Dick, H. J. B., and H. Zhou (2014), Ocean rises are products of variable mantle composition, temperature and focused melting, *Nature Geoscience*, *8*(1), 68–74, doi:10.1038/ngeo2318.

Dick, H. J. B., M. A. Tivey, and B. E. Tucholke (2008), Plutonic foundation of a slow-spreading ridge segment: Oceanic core complex at Kane Megamullion, 23°30′N, 45°20′W: Plutonic foundation of a slow-spreading ridge segment, *Geochemistry, Geophysics, Geosystems*, *9*(5), doi:10.1029/2007GC001645.

Driscoll, N. W., and G. D. Karner (1998), Lower crustal extension across the Northern Camarvon basin, Australia: Evidence for an eastward dipping detachment, *Journal of Geophysical Research: Solid Earth*, *103*(B3), 4975–4991.

Dugda, M. T. (2005), Crustal structure in Ethiopia and Kenya from receiver function analysis: Implications for rift development in eastern Africa, *Journal of Geophysical Research*, *110*(B1), doi:10.1029/2004JB003065.

Dugda, M. T., A. A. Nyblade, and J. Julia (2007), Thin Lithosphere Beneath the Ethiopian Plateau Revealed by a Joint Inversion of Rayleigh Wave Group Velocities and Receiver Functions, *Journal of Geophysical Research*, *112*(B8), doi:10.1029/2006JB004918.

Eagles, G., R. Gloaguen, and C. Ebinger (2002), Kinematics of the Danakil microplate, *Earth and*, *203*(2), 607–620.

Ebinger, C. (2005), Continental break-up: the East African perspective, *Astronomy & Geophysics*, *46*(2), 2–16.

Ebinger, C., and N. J. Hayward (1996), Soft plates and hot spots: Views from Afar, *Journal of Geophysical Research*, *101*(B10), 21859–21876.

Ebinger, C. J., and M. Casey (2001), Continental breakup in magmatic provinces: An Ethiopian example, *Geology*, *29*(6), 527–530.

Ebinger, C. J., and N. H. Sleep (1998), Cenozoic magmatism throughout east Africa resulting from impact of a single plume, *Nature*, *395*(6704), 788–791.

Ebinger, C. J., D. Keir, A. Ayele, E. Calais, T. J. Wright, M. Belachew, J. O. S. Hammond, E. Campbell, and W. R. Buck (2008), Capturing magma intrusion and faulting processes during continental rupture: seismicity of the Dabbahu (Afar) rift, *Geophysical Journal International*, *174*(3), 1138–1152, doi:10.1111/j.1365-246X.2008.03877.x.

Ebinger, C. J., J. van Wijk, and D. Keir (2013), The time scales of continental rifting: Implications for global processes, *Geological Society of America Special Papers*, *500*, 371–396.

Eldholm, O., and K. Grue (1994), North Atlantic volcanic margins: dimensions and production rates, *Journal of Geophysical Research: Solid Earth (1978–2012)*, *99*(B2), 2955–2968.

Elliott, G. M., and L. M. Parson (2008), Influence of margin segmentation upon the break-up of the Hatton Bank rifted margin, NE Atlantic, *Tectonophysics*, *457*(3-4), 161–176, doi:10.1016/j.tecto.2008.06.008.

Ernst, R. E., M. T. D. Wingate, K. L. Buchan, and Z. X. Li (2008), Global record of 1600–700Ma Large Igneous Provinces (LIPs): Implications for the reconstruction of the proposed Nuna (Columbia) and Rodinia supercontinents, *Precambrian Research*, *160*(1-2), 159–178, doi:10.1016/j.precamres.2007.04.019.

Faccenna, C., T. W. Becker, L. Jolivet, and M. Keskin (2013), Mantle convection in the Middle East: Reconciling Afar upwelling, Arabia indentation and Aegean trench rollback, *Earth and Planetary Science Letters*, *375*, 254–269, doi:10.1016/j.epsl.2013.05.043.

Ferguson, D. J., J. Maclennan, I. D. Bastow, D. M. Pyle, S. M. Jones, D. Keir, J. D. Blundy, T. Plank, and G. Yirgu (2013), Melting during late-stage rifting in Afar is hot and deep, *Nature*, *499*(7456), 70–73, doi:10.1038/nature12292.

Fernandes, R. M. ., B. A. . Ambrosius, R. Noomen, L. Bastos, L. Combrinck, J. . Miranda, and W. Spakman (2004), Angular velocities of Nubia and Somalia from continuous GPS data: implications on present-day relative kinematics, *Earth and Planetary Science Letters*, *222*(1), 197–208, doi:10.1016/j.epsl.2004.02.008.

Field, L., J. Blundy, R. A. Brooker, T. Wright, and G. Yirgu (2012), Magma storage conditions beneath Dabbahu Volcano (Ethiopia) constrained by petrology, seismicity and satellite geodesy, *Bulletin of Volcanology*, *74*(5), 981–1004, doi:10.1007/s00445-012-0580-6.

Fournier, M., N. Chamot-Rooke, C. Petit, P. Huchon, A. Al-Kathiri, L. Audin, M.-O. Beslier, E. d'Acremont, O. Fabbri, and J.-M. Fleury (2010), Arabia-Somalia plate kinematics, evolution of the Aden-Owen-Carlsberg triple junction, and opening of the Gulf of Aden, *Journal of Geophysical Research: Solid Earth (1978–2012)*, *115*(B4).

Fram, M. S., and C. E. Lesher (1997), Generation and polybaric differentiation of east Greenland early Tertiary flood basalts, *Journal of Petrology*, *38*(2), 231–275.

Franke, D. (2013), Rifting, lithosphere breakup and volcanism: Comparison of magma-poor and volcanic rifted margins, *Marine and Petroleum Geology*, *43*, 63–87, doi:10.1016/j.marpetgeo.2012.11.003.

Franke, D., S. Neben, S. Ladage, B. Schreckenberger, and K. Hinz (2007), Margin segmentation and volcano-tectonic architecture along the volcanic margin off Argentina/Uruguay, South Atlantic, *Marine Geology*, *244*(1-4), 46–67, doi:10.1016/j.margeo.2007.06.009.

Gac, S., and L. Geoffroy (2009), 3D Thermo-mechanical modelling of a stretched continental lithosphere containing localized low-viscosity anomalies (the soft-point theory of plate break-up), *Tectonophysics*, *468*(1-4), 158–168, doi:10.1016/j.tecto.2008.05.011.

Geoffroy, L. (2001), The structure of volcanic margins: some problematics from the North-Atlantic/Labrador–Baffin system, *Marine and Petroleum Geology*, *18*(4), 463–469.

Geoffroy, L. (2005), Volcanic passive margins, *Comptes Rendus Geoscience*, *337*(16), 1395–1408, doi:10.1016/j.crte.2005.10.006.

Geoffroy, L., P. Huchon, and K. Khanbari (1998a), Did Yemeni Tertiary granites intrude neck zones of a stretched continental upper crust?, *Terra Nova*, *10*(4), 196–200.

Geoffroy, L., J. P. Gélard, C. Lepvrier, and P. Olivier (1998b), The coastal flexure of Disko (West Greenland), onshore expression of the "oblique reflectors," *Journal of the Geological Society*, *155*(3), 463–473.

Geoffroy, L., B. Le Gall, M. A. Daoud, and M. Jalludin (2014), Flip-flop detachment tectonics at nascent passive margins in SE Afar, *Journal of the Geological Society*, 2013–135.

George, R., and N. Rogers (2002), Plume dynamics beneath the African plate inferred from the geochemistry of the Tertiary basalts of southern Ethiopia, *Contributions to Mineralogy and Petrology*, *144*(3), 286–304, doi:10.1007/s00410-002-0396-z.

Gernigon, L., J.-C. Ringenbach, S. Planke, and B. Le Gall (2004), Deep structures and breakup along volcanic rifted margins: insights from integrated studies

along the outer Vøring Basin (Norway), *Marine and Petroleum Geology*, *21*(3), 363–372, doi:10.1016/j.marpetgeo.2004.01.005.

Gernigon, L., F. Lucazeau, F. Brigaud, J.-C. Ringenbach, S. Planke, and B. Le Gall (2006), A moderate melting model for the Vøring margin (Norway) based on structural observations and a thermo-kinematical modelling: Implication for the meaning of the lower crustal bodies, *Tectonophysics*, *412*(3-4), 255–278, doi:10.1016/j.tecto.2005.10.038.

Gernigon, L., A. Blischke, A. Nasuti, and M. Sand (2015), Conjugate volcanic rifted margins, seafloor spreading, and microcontinent: Insights from new high-resolution aeromagnetic surveys in the Norway Basin, *Tectonics*, *34*(5), 907–933, doi:10.1002/2014TC003717.

Ghebreab, W. (1998), Tectonics of the Red Sea region reassessed, *Earth-Science Reviews*, *45*(1), 1–44.

Ghebreab, W., and C. J. Talbot (2000), Red Sea extension influenced by Pan-African tectonic grain in eastern Eritrea, *Journal of Structural Geology*, *22*(7), 931–946.

Ghiorso, M. S., and R. O. Sack (1995), Chemical mass transfer in magmatic processes IV. A revised and internally consistent thermodynamic model for the interpolation and extrapolation of liquid-solid equilibria in magmatic systems at elevated temperatures and pressures, *Contributions to Mineralogy and Petrology*, *119*(2-3), 197–212.

Gibson, I. L., and A. D. Gibbs (1987), Accretionary volcanic processes and the crystal structure of Iceland, *Tectonophysics*, *133*(1), 57–64.

Gladczenko, T. P., K. Hinz, O. Eldholm, H. Meyer, S. Neben, and J. Skogseid (1997), South Atlantic volcanic margins, *Journal of the Geological Society*, *154*(3), 465–470.

Grandin, R., A. Socquet, E. Jacques, N. Mazzoni, J.-B. de Chabalier, and G. C. P. King (2010), Sequence of rifting in Afar, Manda-Hararo rift, Ethiopia, 2005–2009: Time-space evolution and interactions between dikes from interferometric synthetic aperture radar and static stress change modeling, *Journal of Geophysical Research*, *115*(B10), doi:10.1029/2009JB000815.

Gualda, G. A., M. S. Ghiorso, R. V. Lemons, and T. L. Carley (2012), Rhyolite-MELTS: a modified calibration of MELTS optimized for silica-rich, fluid-bearing magmatic systems, *Journal of Petrology*, *53*(5), 875–890.

Guo, P. et al. (2014), Lithosphere thinning beneath west North China Craton: Evidence from geochemical and Sr–Nd–Hf isotope compositions of Jining basalts, *Lithos*, *202-203*, 37–54, doi:10.1016/j.lithos.2014.04.024.

Hack, P. J., R. L. Nielsen, and A. D. Johnston (1994), Experimentally determined rare-earth element and Y partitioning behavior between clinopyroxene and basaltic liquids at pressures up to 20 kbar, *Chemical Geology*, *117*(1), 89–105.

Halldórsson, S. A., D. R. Hilton, P. Scarsi, T. Abebe, and J. Hopp (2014), A common mantle plume source beneath the entire East African Rift System revealed by coupled helium-neon systematics, *Geophysical Research Letters*, *41*(7), 2304–2311, doi:10.1002/2014GL059424.

Hammond, J. O. S., J.-M. Kendall, G. W. Stuart, D. Keir, C. Ebinger, A. Ayele, and M. Belachew (2011), The nature of the crust beneath the Afar triple junction: Evidence from receiver functions, *Geochemistry, Geophysics, Geosystems*, *12*(12), doi:10.1029/2011GC003738.

Hammond, J. O. S. et al. (2013), Mantle upwelling and initiation of rift segmentation beneath the Afar Depression, *Geology*, *41*(6), 635–638, doi:10.1130/G33925.1.

Hammond, J. O. S., J.-M. Kendall, J. Wookey, G. W. Stuart, D. Keir, and A. Ayele (2014), Differentiating flow, melt, or fossil seismic anisotropy beneath Ethiopia, *Geochemistry, Geophysics, Geosystems*, *15*(5), 1878–1894, doi:10.1002/2013GC005185.

Harding, D. J., C. J. Ebinger, and J. . Heirtzler (1990), Lateral displacements on intersecting fault sets of the Afar depression, *Eos (Transactions, American Geophysical Union)*, *71*(617).

Hart, W. K., G. WoldeGabriel, R. C. Walter, and S. A. Mertzman (1989), Basaltic volcanism in Ethiopia: constraints on continental rifting and mantle interactions, *Journal of Geophysical Research: Solid Earth (1978–2012)*, *94*(B6), 7731–7748.

Hauri, E. H., T. P. Wagner, and T. L. Grove (1994), Experimental and natural partitioning of Th, U, Pb and other trace elements between garnet, clinopyroxene and basaltic melts, *Chemical Geology*, *117*(1), 149–166.

Hayward, N. J., and C. J. Ebinger (1996), Variations in the along-axis segmentation of the Afar Rift system., *Tectonics*, *15*(2), 244–257.

Herzberg, C., and P. D. Asimow (2008), Petrology of some oceanic island basalts: PRIMELT2.XLS software for primary magma calculation, *Geochemistry,*

Geophysics, Geosystems, *9*(9), doi:10.1029/2008GC002057.

Herzberg, C., and P. D. Asimow (2015), PRIMELT3 MEGA.XLSM software for primary magma calculation: Peridotite primary magma MgO contents from the liquidus to the solidus, *Geochemistry, Geophysics, Geosystems*, *16*(2), 563–578, doi:10.1002/2014GC005631.

Herzberg, C., and E. Gazel (2009), Petrological evidence for secular cooling in mantle plumes, *Nature*, *458*(7238), 619–622, doi:10.1038/nature07857.

Herzberg, C., and J. Zhang (1996), Melting experiments on anhydrous peridotite KLB-1: Compositions of magmas in the upper mantle and transition zone, *Journal of Geophysical Research: Solid Earth (1978–2012)*, *101*(B4), 8271–8295.

Herzberg, C., P. D. Asimow, N. Arndt, Y. Niu, C. M. Lesher, J. G. Fitton, M. J. Cheadle, and A. D. Saunders (2007), Temperatures in ambient mantle and plumes: Constraints from basalts, picrites, and komatiites, *Geochemistry, Geophysics, Geosystems*, *8*(2), doi:10.1029/2006GC001390.

Hill, R. I., I. H. Campbell, G. F. Davies, and R. W. Griffiths (1992), Mantle plumes and continental tectonics, *Science*, *256*(5054), 186–193.

Hinz, K. (1981), *A Hypothesis on Terrestrial Catastrophes Wedges of Very Thick Oceanward Dipping Layers Beneath Passive Continental Margins: Their Origin and Pleoenvironmental Significance*, Schweizerbart.

Hinz, K., S. Neben, B. Schreckenberger, H. A. Roeser, M. Block, K. G. de Souza, and H. Meyer (1999), The Argentine continental margin north of 48 S: sedimentary successions, volcanic activity during breakup, *Marine and Petroleum Geology*, *16*(1), 1–25.

Hofmann, C., V. Courtillot, G. Feraud, P. Rochette, G. Yirgu, E. Ketefo, and R. Pik (1997), Timing of the Ethiopian flood basalt event and implications for plume birth and global change, *Nature*, *389*(6653), 838–841.

Huchon, P., F. Jestin, J. M. Cantagrel, J. M. Gaulier, S. Al Khirbash, and A. Gafaneh (1991), Extensional deformations in Yemen since Oligocene and the Africa-Arabia-Somalia triple junction, in *Annales Tectonicae*, vol. 5, pp. 141–163.

Hugues, G. W., D. Perincek, D. J. Grainger, A.-J. Abu-Bshait, and A.-R. M. Jarad (1999), Lithostratigraphy and depositional history of part of the Midyan region, northwestern Saudi Arabia, *GeoArabia*, *4*, 503–541.

Huismans, R. S., and C. Beaumont (2014), Rifted continental margins: The case for depth-dependent extension, *Earth and Planetary Science Letters*, *407*, 148–162, doi:10.1016/j.epsl.2014.09.032.

Huismans, R. S., Y. Y. Podladchikov, and S. Cloetingh (2001), Transition from passive to active rifting: Relative importance of asthenospheric doming and passive extension of the lithosphere, *Journal of Geophysical Research: Solid Earth (1978–2012)*, *106*(B6), 11271–11291.

Humphreys, E. R., and Y. Niu (2009), On the composition of ocean island basalts (OIB): The effects of lithospheric thickness variation and mantle metasomatism, *Lithos*, *112*(1-2), 118–136, doi:10.1016/j.lithos.2009.04.038.

Irving, A. J., and F. A. Frey (1984), Trace element abundances in megacrysts and their host basalts: constraints on partition coefficients and megacryst genesis, *Geochimica et Cosmochimica Acta*, *48*(6), 1201–1221.

Jaupart, C., and J. C. Mareschal (1999), The thermal structure and thickness of continental roots, *Developments in Geotectonics*, *24*, 93–114.

Jourdan, F., H. Bertrand, U. Scharer, J. Blichert-Toft, G. Feraud, and A. B. Kampunzu (2007), Major and Trace Element and Sr, Nd, Hf, and Pb Isotope Compositions of the Karoo Large Igneous Province, Botswana-Zimbabwe: Lithosphere vs Mantle Plume Contribution, *Journal of Petrology*, *48*(6), 1043–1077, doi:10.1093/petrology/egm010.

Karson, J. A., C. K. Brooks, M. Storey, and M. S. Pringle (1998), Tertiary faulting and pseudotachylytes in the East Greenland volcanic rifted margin: Seismogenic faulting during magmatic construction, *Geology*, *26*(1), 39–42.

Katz, R. F., M. Spiegelman, and C. H. Langmuir (2003), A new parameterization of hydrous mantle melting, *Geochemistry, Geophysics, Geosystems*, *4*(9), doi:10.1029/2002GC000433.

Kelemen, P. B., and W. S. Holbrook (1995), Origin of thick, high-velocity igneous crust along the US East Coast Margin, *Journal of Geophysical Research: Solid Earth (1978–2012)*, *100*(B6), 10077–10094.

Kendall, J.-M., G. W. Stuart, C. J. Ebinger, I. D. Bastow, and D. Keir (2005), Magma-assisted rifting in Ethiopia, *Nature*, *433*(7022), 146–148.

Keranen, K. M., S. L. Klemperer, J. Julia, J. F. Lawrence, and A. A. Nyblade (2009), Low lower crustal velocity across Ethiopia: Is the Main Ethiopian Rift a narrow rift in a hot craton?, *Geochemistry, Geophysics, Geosystems*, *10*(5),

doi:10.1029/2008GC002293.

Kidane, T., V. Courtillot, I. Manighetti, L. Audin, P. Lahitte, X. Quidelleur, P.-Y. Gillot, Y. Gallet, J. Carlut, and T. Haile (2003), New paleomagnetic and geochronologic results from Ethiopian Afar: Block rotations linked to rift overlap and propagation and determination of a ~2 Ma reference pole for stable Africa, *Journal of Geophysical Research*, *108*(B2), doi:10.1029/2001JB000645.

Kieffer, B. (2004), Flood and Shield Basalts from Ethiopia: Magmas from the African Superswell, *Journal of Petrology*, *45*(4), 793–834, doi:10.1093/petrology/egg112.

Klausen, M. B. (2009), The Lebombo monocline and associated feeder dyke swarm: Diagnostic of a successful and highly volcanic rifted margin?, *Tectonophysics*, *468*(1-4), 42–62, doi:10.1016/j.tecto.2008.10.012.

Klein, E. M., and C. H. Langmuir (1987), Global correlations of ocean ridge basalt chemistry with axial depth and crustal thickness, *J. geophys. Res*, *92*(8), 8089–8115.

Klein, E. M., and C. H. Langmuir (1989), Local versus global variations in ocean ridge basalt composition: A reply, *J. geophys. Res*, *94*(B4), 4.

Kogan, L., S. Fisseha, R. Bendick, R. Reilinger, S. McClusky, R. King, and T. Solomon (2012), Lithospheric strength and strain localization in continental extension from observations of the East African Rift, *Journal of Geophysical Research: Solid Earth*, *117*(B3), n/a–n/a, doi:10.1029/2011JB008516.

Koopmann, H., S. Brune, D. Franke, and S. Breuer (2014), Linking rift propagation barriers to excess magmatism at volcanic rifted margins, *Geology*, doi:10.1130/G36085.1.

Korostelev, F. et al. (2014), Crustal and upper mantle structure beneath south-western margin of the Arabian Peninsula from teleseismic tomography, *Geochemistry, Geophysics, Geosystems*, doi:10.1002/2014GC005316.

Korostelev, F., S. Leroy, D. Keir, A. Ahmed, L. Boschi, F. Rolandone, G. W. Stuart, M. Obrebski, K. Khanbari, and I. El-Hussain (2015), Upper mantle structure of the southern Arabian margin: Insights from teleseismic tomography, *Geosphere*, *11*(5), 1262–1278, doi:10.1130/GES01159.1.

Kunz, K., H. Kreuzer, and P. Müller (1975), Potassium-Argon age determinations of the Trap basalt of the south-eastern part of the Afar Rift, *Afar Depression of*

Ethiopia, *1*, 370–374.

Lagabrielle, Y., E. Garel, O. Dauteuil, and M.-H. Cormier (2001), Extensional faulting and caldera collapse in the axial region of fast spreading ridges: Analog modeling, *Journal of Geophysical Research: Solid Earth (1978–2012)*, *106*(B2), 2005–2015.

Lahitte, P. (2003), New age constraints on the timing of volcanism in central Afar, in the presence of propagating rifts, *Journal of Geophysical Research*, *108*(B2), doi:10.1029/2001JB001689.

Lahitte, P., E. Coulié, N. Mercier, T. Kidane, and P.-Y. Gillot (2001), Chronologie K–Ar et TL du volcanisme aux extrémités sud du propagateur mer Rouge en Afar depuis 300 ka, *Comptes Rendus de l'Académie des Sciences-Series IIA-Earth and Planetary Science*, *332*(1), 13–20.

Lahitte, P., P.-Y. Gillot, and V. Courtillot (2003), Silicic central volcanoes as precursors to rift propagation: the Afar case, *Earth and Planetary Science Letters*, *207*(1-4), 103–116, doi:10.1016/S0012-821X(02)01130-5.

Langmuir, C. H., E. M. Klein, and T. Plank (1993), Petrological systematics of mid-ocean ridge basalts: Constraints on melt generation beneath ocean ridges, *Mantle flow and melt generation at mid-ocean ridges*, 183–280.

Lavier, L. L., and G. Manatschal (2006), A mechanism to thin the continental lithosphere at magma-poor margins, *Nature*, *440*(7082), 324–328, doi:10.1038/nature04608.

Le Bas, M. J. (1987), Ultra-alkaline magmatism with or without rifting, *Tectonophysics*, *143*(1), 75–84.

Lee, C.-T. A., P. Luffi, T. Plank, H. Dalton, and W. P. Leeman (2009), Constraints on the depths and temperatures of basaltic magma generation on Earth and other terrestrial planets using new thermobarometers for mafic magmas, *Earth and Planetary Science Letters*, *279*(1-2), 20–33, doi:10.1016/j.epsl.2008.12.020.

Le Gall, B., M. A. Daoud, R. C. Maury, J. Rolet, H. Guillou, and C. Sue (2010), Magma-driven antiform structures in the Afar rift: The Ali Sabieh range, Djibouti, *Journal of Structural Geology*, *32*(6), 843–854, doi:10.1016/j.jsg.2010.06.007.

Le Gall, B., M. A. Daoud, J. Rolet, and N. M. Egueh (2011), Large-scale flexuring and antithetic extensional faulting along a nascent plate boundary in the SE Afar rift: Structure of a nascent plate boundary in SE Afar, *Terra Nova*,

23(6), 416–420, doi:10.1111/j.1365-3121.2011.01029.x.

Lenoir, X., G. Féraud, and L. Geoffroy (2003), High-rate flexure of the East Greenland volcanic margin: constraints from 40Ar/39Ar dating of basaltic dykes, *Earth and Planetary Science Letters*, *214*(3-4), 515–528, doi:10.1016/S0012-821X(03)00392-3.

Le Pichon, X., and J.-C. Sibuet (1981), Passive margins: a model of formation, *Journal of Geophysical Research: Solid Earth*, *86*(B5), 3708–3720.

Leroy, S., E. d'Acremont, C. Tiberi, C. Basuyau, J. Autin, F. Lucazeau, and H. Sloan (2010), Recent off-axis volcanism in the eastern Gulf of Aden: Implications for plume–ridge interaction, *Earth and Planetary Science Letters*, *293*(1-2), 140–153, doi:10.1016/j.epsl.2010.02.036.

Leroy, S. et al. (2012), From rifting to oceanic spreading in the Gulf of Aden: a synthesis, *Arabian Journal of Geosciences*, *5*(5), 859–901, doi:10.1007/s12517-011-0475-4.

Li, C., R. D. van der Hilst, E. R. Engdahl, and S. Burdick (2008), A new global model for P wave speed variations in Earth's mantle, *Geochemistry, Geophysics, Geosystems*, *9*(5), doi:10.1029/2007GC001806.

Lister, G. S., and G. A. Davis (1989), The origin of metamorphic core complexes and detachment faults formed during Tertiary continental extension in the northern Colorado River region, USA, *Journal of Structural Geology*, *11*(1), 65–94.

Lucassen, F., G. Franz, R. L. Romer, D. Pudlo, and P. Dulski (2008), Nd, Pb, and Sr isotope composition of Late Mesozoic to Quaternary intra-plate magmatism in NE-Africa (Sudan, Egypt): high-μ signatures from the mantle lithosphere, *Contributions to Mineralogy and Petrology*, *156*(6), 765–784, doi:10.1007/s00410-008-0314-0.

Mackenzie, G. D., H. Thybo, and P. K. H. Maguire (2005), Crustal velocity structure across the Main Ethiopian Rift: results from two-dimensional wide-angle seismic modelling, *Geophysical Journal International*, *162*(3), 994–1006, doi:10.1111/j.1365-246X.2005.02710.x.

Maguire, P. K. H. et al. (2006), Crustal structure of the northern Main Ethiopian Rift from the EAGLE controlled-source survey; a snapshot of incipient lithospheric break-up, *Special Publication-Geological Society of London*, *259*, 269.

Makris, J., and A. Ginzburg (1987), The Afar Depression: transition between continental rifting and sea-floor spreading, *Tectonophysics*, *141*(1), 199–214.

Manatschal, G., and D. Bernoulli (1999), Architecture and tectonic evolution of nonvolcanic margins: Present-day Galicia and ancient Adria, *Tectonics*, *18*(6), 1099–1119.

Manighetti, I., P. Tapponnier, P. Y. Gillot, E. Jacques, V. Courtillot, R. Armijo, J. C. Ruegg, and G. King (1998), Propagation of rifting along the Arabia-Somalia plate boundary: Into Afar, *Journal of Geophysical Research: Solid Earth (1978–2012)*, *103*(B3), 4947–4974.

Marty, B., R. Pik, and Y. Gezahegn (1996), Helium isotopic variations in Ethiopian plume lavas: nature of magmatic sources and limit on lower mantle contribution, *Earth and Planetary Science Letters*, *144*(1), 223–237.

McClusky, S. et al. (2010), Kinematics of the southern Red Sea-Afar Triple Junction and implications for plate dynamics, *Geophysical Research Letters*, *37*(5), doi:10.1029/2009GL041127.

McDade, P., J. D. Blundy, and B. J. Wood (2003), Trace element partitioning on the Tinaquillo Lherzolite solidus at 1.5GPa, *Physics of the Earth and Planetary Interiors*, *139*(1-2), 129–147, doi:10.1016/S0031-9201(03)00149-3.

McDonough, W. F., and S.-S. Sun (1995), The composition of the Earth, *Chemical geology*, *120*(3), 223–253.

McKenzie, D. (1978), Some remarks on the development of sedimentary basins, *Earth and Planetary science letters*, *40*(1), 25–32.

McKenzie, D., and M. J. Bickle (1988), The volume and composition of melt generated by extension of the lithosphere, *Journal of petrology*, *29*(3), 625–679.

McKenzie, D. A. N., and R. K. O'nions (1991), Partial melt distributions from inversion of rare earth element concentrations, *Journal of Petrology*, *32*(5), 1021–1091.

Medynski, S. et al. (2013), Controls on magmatic cycles and development of rift topography of the Manda Hararo segment (Afar, Ethiopia): Insights from cosmogenic 3He investigation of landscape evolution, *Earth and Planetary Science Letters*, *367*, 133–145, doi:10.1016/j.epsl.2013.02.006.

Medynski, S. et al. (2015), Stability of rift axis magma reservoirs: Spatial and temporal evolution of magma supply in the Dabbahu rift segment (Afar,

Ethiopia) over the past 30 kyr, *Earth and Planetary Science Letters*, *409*, 278–289, doi:10.1016/j.epsl.2014.11.002.

Mège, D., and T. Korme (2004), Dyke swarm emplacement in the Ethiopian Large Igneous Province: not only a matter of stress, *Journal of Volcanology and Geothermal Research*, *132*(4), 283–310, doi:10.1016/S0377-0273(03)00318-4.

Menzies, M., K. Gallagher, A. Yelland, and A. J. Hurford (1997), Volcanic and nonvolcanic rifted margins of the Red Sea and Gulf of Aden: crustal cooling and margin evolution in Yemen, *Geochimica et Cosmochimica Acta*, *61*(12), 2511–2527.

Menzies, M. A., J. Baker, D. Bosence, C. Dart, I. Davison, A. Hurford, M. Al'Kadasi, K. McClay, G. Nichols, and A. Al'Subbary (1992), The timing of magmatism, uplift and crustal extension: preliminary observations from Yemen, *Geological Society, London, Special Publications*, *68*(1), 293–304.

Menzies, M. A., S. L. Klemperer, C. J. Ebinger, and J. Baker (2002), Characteristics of volcanic rifted margins, *Special Papers - Geological Society of America*, 1–14.

Meyzen, C. M., M. J. Toplis, E. Humler, J. N. Ludden, and C. Mével (2003), A discontinuity in mantle composition beneath the southwest Indian ridge, *Nature*, *421*(6924), 731–733.

Mjelde, R., T. Raum, Y. Murai, and T. Takanami (2007), Continent–ocean-transitions: Review, and a new tectono-magmatic model of the Vøring Plateau, NE Atlantic, *Journal of Geodynamics*, *43*(3), 374–392, doi:10.1016/j.jog.2006.09.013.

Mjelde, R., J. I. Faleide, A. J. Breivik, and T. Raum (2009), Lower crustal composition and crustal lineaments on the Vøring Margin, NE Atlantic: A review, *Tectonophysics*, *472*(1-4), 183–193, doi:10.1016/j.tecto.2008.04.018.

Mohr, P. (1978), Afar, *Annual Review of Earth and Planetary Sciences*, *6*, 145–172.

Mohr, P. (1983), The Morton-Black hypothesis for the thinning of continental crust—revisited in western Afar, *Tectonophysics*, *94*(1), 509–528.

Mohr, P. (1989), Nature of the crust under Afar: new igneous, not thinned continental, *Tectonophysics*, *167*(1), 1–11.

Mohr, P., and B. Zanettin (1988), The Ethiopian flood basalt province, in *Continental flood basalts*, pp. 63–110, Springer.

Montelli, R., G. Nolet, F. A. Dahlen, and G. Masters (2006), A catalogue of deep mantle plumes: New results from finite-frequency tomography, *Geochemistry, Geophysics, Geosystems*, *7*(11), doi:10.1029/2006GC001248.

Morency, C., M.-P. Doin, and C. Dumoulin (2002), Convective destabilization of a thickened continental lithosphere, *Earth and Planetary Science Letters*, *202*(2), 303–320.

Morgan, W. J. (1972), Deep mantle convection plumes and plate motions, *AAPG Bulletin*, *56*(2), 203–213.

Morton, W. H., and R. Black (1975), Crustal attenuation in Afar, *Afar Depression of Ethiopia*, 55–61.

Moucha, R., and A. M. Forte (2011), Changes in African topography driven by mantle convection, *Nature Geoscience*, *4*(10), 707–712, doi:10.1038/ngeo1235.

Mulibo, G. D., and A. A. Nyblade (2013), The P and S wave velocity structure of the mantle beneath eastern Africa and the African superplume anomaly: Mantle Structure Beneath Eastern Africa, *Geochemistry, Geophysics, Geosystems*, *14*(8), 2696–2715, doi:10.1002/ggge.20150.

Mutter, J. C., M. Talwani, and P. L. Stoffa (1982), Origin of seaward-dipping reflectors in oceanic crust off the Norwegian margin by "subaerial sea-floor spreading," *Geology*, *10*(7), 353–357.

Nikishin, A. M., P. A. Ziegler, D. Abbott, M.-F. Brunet, and S. Cloetingh (2002), Permo–Triassic intraplate magmatism and rifting in Eurasia: implications for mantle plumes and mantle dynamics, *Tectonophysics*, *351*(1), 3–39.

Niu, Y., and M. J. O'Hara (2007), Global Correlations of Ocean Ridge Basalt Chemistry with Axial Depth: a New Perspective, *Journal of Petrology*, *49*(4), 633–664, doi:10.1093/petrology/egm051.

Niu, Y., M. Wilson, E. R. Humphreys, and M. J. O'Hara (2011), The Origin of Intra-plate Ocean Island Basalts (OIB): the Lid Effect and its Geodynamic Implications, *Journal of Petrology*, *52*(7-8), 1443–1468, doi:10.1093/petrology/egr030.

Nobile, A., C. Pagli, D. Keir, T. J. Wright, A. Ayele, J. Ruch, and V. Acocella (2012), Dike-fault interaction during the 2004 Dallol intrusion at the northern edge of the Erta Ale Ridge (Afar, Ethiopia), *Geophysical Research Letters*, *39*(19), doi:10.1029/2012GL053152.

Ono, S. (2008), Experimental constraints on the temperature profile in the lower mantle, *Physics of the Earth and Planetary Interiors*, *170*(3), 267–273.

O'Reilly, B. M., F. Hauser, A. B. Jacob, and P. M. Shannon (1996), The lithosphere below the Rockall Trough: wide-angle seismic evidence for extensive serpentinisation, *Tectonophysics*, *255*(1), 1–23.

Pagli, C., T. J. Wright, C. J. Ebinger, S.-H. Yun, J. R. Cann, T. Barnie, and A. Ayele (2012), Shallow axial magma chamber at the slow-spreading Erta Ale Ridge, *Nature Geoscience*, *5*(4), 284–288, doi:10.1038/ngeo1414.

Pasyanos, M. E., W. R. Walter, and E. M. Matzel (2009), A simultaneous multiphase approach to determine P-wave and S-wave attenuation of the crust and upper mantle, *Bulletin of the Seismological Society of America*, *99*(6), 3314–3325.

Pérez-Gussinyé, M., M. Metois, M. Fernández, J. Vergés, J. Fullea, and A. R. Lowry (2009), Effective elastic thickness of Africa and its relationship to other proxies for lithospheric structure and surface tectonics, *Earth and Planetary Science Letters*, *287*(1-2), 152–167, doi:10.1016/j.epsl.2009.08.004.

Peron-Pinvidic, G. (2006), Morphotectonique et architecture sédimentaire de la transition océan-continent de la marge ibérique, Strasbourg 1.

Péron-Pinvidic, G., and G. Manatschal (2009), The final rifting evolution at deep magma-poor passive margins from Iberia-Newfoundland: a new point of view, *International Journal of Earth Sciences*, *98*(7), 1581–1597, doi:10.1007/s00531-008-0337-9.

Péron-Pinvidic, G., G. Manatschal, and P. T. Osmundsen (2013), Structural comparison of archetypal Atlantic rifted margins: A review of observations and concepts, *Marine and Petroleum Geology*, *43*, 21–47, doi:10.1016/j.marpetgeo.2013.02.002.

Pik, R. (2011), Geodynamics: East Africa on the rise, *Nature Geoscience*, *4*(10), 660–661.

Pik, R., C. Deniel, C. Coulon, G. Yirgu, C. Hofmann, and D. Ayalew (1998), The northwestern Ethiopian Plateau flood basalts: classification and spatial distribution of magma types, *Journal of Volcanology and Geothermal Research*, *81*(1), 91–111.

Pik, R., C. Deniel, C. Coulon, G. Yirgu, and B. Marty (1999), Isotopic and trace element signatures of Ethiopian flood basalts: evidence for plume–lithosphere interactions, *Geochimica et Cosmochimica Acta*, *63*(15), 2263–2279.

Pik, R., B. Marty, J. Carignan, and J. Lavé (2003), Stability of the Upper Nile drainage network (Ethiopia) deduced from (U–Th)/He thermochronometry: implications for uplift and erosion of the Afar plume dome, *Earth and Planetary Science Letters*, *215*(1-2), 73–88, doi:10.1016/S0012-821X(03)00457-6.

Pik, R., B. Marty, and D. R. Hilton (2006), How many mantle plumes in Africa? The geochemical point of view, *Chemical Geology*, *226*(3-4), 100–114, doi:10.1016/j.chemgeo.2005.09.016.

Pik, R., B. Marty, J. Carignan, G. Yirgu, and T. Ayalew (2008), Timing of East African Rift development in southern Ethiopia: Implication for mantle plume activity and evolution of topography, *Geology*, *36*(2), 167–170.

Pik, R., N. Bellahsen, S. Leroy, Y. Denèle, P. Razin, A. Ahmed, and K. Khanbari (2013), Structural control of basement denudation during rifting revealed by low-temperature (U–Th–Sm)/He thermochronology of the Socotra Island basement—Southern Gulf of Aden margin, *Tectonophysics*, *607*, 17–31, doi:10.1016/j.tecto.2013.07.038.

Pinzuti, P., E. Humler, I. Manighetti, and Y. Gaudemer (2013), Petrological constraints on melt generation beneath the Asal Rift (Djibouti) using quaternary basalts: Melt Generation Beneath the Asal Rift, *Geochemistry, Geophysics, Geosystems*, *14*(8), 2932–2953, doi:10.1002/ggge.20187.

Planke, S., P. A. Symonds, E. Alvestad, and J. Skogseid (2000), Seismic volcanostratigraphy of large-volume basaltic extrusive complexes on rifted margins, *Journal of Geophysical Research*, *105*(B8), 19335–19351.

Prodehl, C., K. Fuchs, and J. Mechie (1997), Seismic-refraction studies of the Afro-Arabian rift system—a brief review, *Tectonophysics*, *278*(1), 1–13.

Putirka, K. (2008), Excess temperatures at ocean islands: Implications for mantle layering and convection, *Geology*, *36*(4), 283–286.

Quirk, D. G., A. Shakerley, and M. J. Howe (2014), A mechanism for construction of volcanic rifted margins during continental breakup, *Geology*, *42*(12), 1079–1082, doi:10.1130/G35974.1.

Ranero, C. R., and M. Pérez-Gussinyé (2010), Sequential faulting explains the asymmetry and extension discrepancy of conjugate margins, *Nature*, *468*(7321), 294–299, doi:10.1038/nature09520.

Redfield, T. F., W. H. Wheeler, and M. Often (2003), A kinematic model for the

development of the Afar Depression and its paleogeographic implications, *Earth and Planetary Science Letters*, *216*(3), 383–398, doi:10.1016/S0012-821X(03)00488-6.

Reed, C. A., S. Almadani, S. S. Gao, A. A. Elsheikh, S. Cherie, M. G. Abdelsalam, A. K. Thurmond, and K. H. Liu (2014), Receiver function constraints on crustal seismic velocities and partial melting beneath the Red Sea rift and adjacent regions, Afar Depression, *Journal of Geophysical Research: Solid Earth*, *119*(3), 2138–2152, doi:10.1002/2013JB010719.

Reston, T. (2007), Extension discrepancy at North Atlantic nonvolcanic rifted margins: Depth-dependent stretching or unrecognized faulting?, *Geology*, *35*(4), 367, doi:10.1130/G23213A.1.

Reston, T. J. (2005), Polyphase faulting during the development of the west Galicia rifted margin, *Earth and Planetary Science Letters*, *237*(3-4), 561–576, doi:10.1016/j.epsl.2005.06.019.

Richards, M. A., R. A. Duncan, and V. E. Courtillot (1989), Flood basalts and hot-spot tracks: plume heads and tails, *Science*, *246*(4926), 103–107.

Ritsema, J., and R. M. Allen (2003), The elusive mantle plume, *Earth and Planetary Science Letters*, *207*(1-4), 1–12, doi:10.1016/S0012-821X(02)01093-2.

Ritsema, J., A. Deuss, H. J. van Heijst, and J. H. Woodhouse (2011), S40RTS: a degree-40 shear-velocity model for the mantle from new Rayleigh wave dispersion, teleseismic traveltime and normal-mode splitting function measurements: S40RTS, *Geophysical Journal International*, *184*(3), 1223–1236, doi:10.1111/j.1365-246X.2010.04884.x.

Robinet, J., P. Razin, J. Serra-Kiel, A. Gallardo-Garcia, S. Leroy, J. Roger, and C. Grelaud (2013), The Paleogene pre-rift to syn-rift succession in the Dhofar margin (northeastern Gulf of Aden): stratigraphy and depositional environments, *Tectonophysics*, *607*, 1–16.

Rochette, P., E. Tamrat, G. Féraud, R. Pik, V. Courtillot, E. Ketefo, C. Coulon, C. Hoffmann, D. Vandamme, and G. Yirgu (1998), Magnetostratigraphy and timing of the Oligocene Ethiopian traps, *Earth and Planetary Science Letters*, *164*(3), 497–510.

Rooney, T. O., I. D. Bastow, and D. Keir (2011), Insights into extensional processes during magma assisted rifting: Evidence from aligned scoria cones, *Journal of Volcanology and Geothermal Research*, *201*(1-4), 83–96,

doi:10.1016/j.jvolgeores.2010.07.019.

Rooney, T. O., C. Herzberg, and I. D. Bastow (2012), Elevated mantle temperature beneath East Africa, *Geology*, *40*(1), 27–30.

Rooney, T. O., P. Mohr, L. Dosso, and C. Hall (2013), Geochemical evidence of mantle reservoir evolution during progressive rifting along the western Afar margin, *Geochimica et Cosmochimica Acta*, *102*, 65–88, doi:10.1016/j.gca.2012.08.019.

Rooney, T. O., I. D. Bastow, D. Keir, F. Mazzarini, E. Movsesian, E. B. Grosfils, J. R. Zimbelman, M. S. Ramsey, D. Ayalew, and G. Yirgu (2014a), The protracted development of focused magmatic intrusion during continental rifting: focused magma intrusion during rifting, *Tectonics*, *33*(6), 875–897, doi:10.1002/2013TC003514.

Rooney, T. O., W. R. Nelson, L. Dosso, T. Furman, and B. Hanan (2014b), The role of continental lithosphere metasomes in the production of HIMU-like magmatism on the northeast African and Arabian plates, *Geology*, *42*(5), 419–422, doi:10.1130/G35216.1.

Rosenbaum, G., R. F. Weinberg, and K. Regenauer-Lieb (2008), The geodynamics of lithospheric extension, *Tectonophysics*, *458*(1-4), 1–8, doi:10.1016/j.tecto.2008.07.016.

Royden, L., and C. E. Keen (1980), Rifting process and thermal evolution of the continental margin of eastern Canada determined from subsidence curves, *Earth and Planetary Science Letters*, *51*(2), 343–361.

Ruppel, C. (1995), Extensional processes in continental lithosphere, *Journal of Geophysical Research: Solid Earth (1978–2012)*, *100*(B12), 24187–24215.

Rychert, C. A., J. O. S. Hammond, N. Harmon, J. Michael Kendall, D. Keir, C. Ebinger, I. D. Bastow, A. Ayele, M. Belachew, and G. Stuart (2012), Volcanism in the Afar Rift sustained by decompression melting with minimal plume influence, *Nature Geoscience*, *5*(6), 406–409, doi:10.1038/ngeo1455.

Savoyat, E., A. Shiferaw, and T. Balcha (1989), Petroleum exploration in the Ethiopian Red Sea, *Journal of Petroleum Geology*, *12*(2), 187–204.

Schilling, J.-G., R. H. Kingsley, B. B. Hanan, and B. L. McCully (1992), Nd-Sr-Pb isotopic variations along the Gulf of Aden: evidence for Afar mantle plume-continental lithosphere interaction, *Journal of Geophysical Research: Solid Earth (1978–2012)*, *97*(B7), 10927–10966.

Sengör, A. M., and K. Burke (1978), Relative timing of rifting and volcanism on Earth and its tectonic implications, *Geophysical Research Letters*, *5*(6), 419–421.

Shaw, J. E., J. A. Baker, A. J. R. Kent, K. M. Ibrahim, and M. A. Menzies (2007), The geochemistry of the Arabian lithospheric mantle—a source for intraplate volcanism?, *Journal of Petrology*, *48*(8), 1495–1512.

Shen, Y., and D. W. Forsyth (1995), Geochemical constraints on initial and final depths of melting beneath mid-ocean ridges, *Journal of Geophysical Rsearch: Solid Earth*, *100*(B2), 2211–2237, doi:10.1029/94JB02768.

Sheth, H. C. (1999), Flood basalts and large igneous provinces from deep mantle plumes: fact, fiction, and fallacy, *Tectonophysics*, *311*(1), 1–29.

Simmons, N. A., A. M. Forte, and S. P. Grand (2007), Thermochemical structure and dynamics of the African superplume, *Geophysical Research Letters*, *34*(2), doi:10.1029/2006GL028009.

Skogseid, J. (2001), Volcanic margins: geodynamic and exploration aspects, *Marine and Petroleum Geology*, *18*(4), 457–461.

Sokoutis, D., G. Corti, M. Bonini, J. Pierre Brun, S. Cloetingh, T. Mauduit, and P. Manetti (2007), Modelling the extension of heterogeneous hot lithosphere, *Tectonophysics*, *444*(1-4), 63–79, doi:10.1016/j.tecto.2007.08.012.

Stab, M., N. Bellahsen, R. Pik, X. Quidelleur, D. Ayalew, and S. Leroy (2015), Modes of rifting in magma-rich settings: Tectono-magmatic evolution of Central Afar, *Tectonics*.

Stamps, D. S., L. M. Flesch, and E. Calais (2010), Lithospheric buoyancy forces in Africa from a thin sheet approach, *International Journal of Earth Sciences*, *99*(7), 1525–1533, doi:10.1007/s00531-010-0533-2.

Stica, J. M., P. V. Zalán, and A. L. Ferrari (2014), The evolution of rifting on the volcanic margin of the Pelotas Basin and the contextualization of the Paraná–Etendeka LIP in the separation of Gondwana in the South Atlantic, *Marine and Petroleum Geology*, *50*, 1–21, doi:10.1016/j.marpetgeo.2013.10.015.

Stork, A. L., G. W. Stuart, C. M. Henderson, D. Keir, and J. O. S. Hammond (2013), Uppermost mantle (Pn) velocity model for the Afar region, Ethiopia: an insight into rifting processes, *Geophysical Journal International*, *193*(1), 321–328, doi:10.1093/gji/ggs106.

Stuart, G. W., I. D. Bastow, and C. J. Ebinger (2006), Crustal structure of the northern Main Ethiopian Rift from receiver function studies, *Geological Society, London, Special Publications*, *259*(1), 253–267.

Tard, F., P. Masse, F. Walgenwitz, and P. Gruneisen (1991), The volcanic passive margin in the vicinity of Aden, Yemen, *Bulletin des Centres de Recherches Exploration-Production Elf Aquitaine*, *15*(1), 1–9.

Tessema, A., and L. A. G. Antoine (2004), Processing and interpretation of the gravity field of the East African Rift: implication for crustal extension, *Tectonophysics*, *394*(1-2), 87–110, doi:10.1016/j.tecto.2004.07.057.

Thybo, H., and I. M. Artemieva (2013), Moho and magmatic underplating in continental lithosphere, *Tectonophysics*, *609*, 605–619, doi:10.1016/j.tecto.2013.05.032.

Thybo, H., and C. A. Nielsen (2009), Magma-compensated crustal thinning in continental rift zones, *Nature*, *457*(7231), 873–876, doi:10.1038/nature07688.

Ukstins, I. A., P. R. Renne, E. Wolfenden, J. Baker, D. Ayalew, and M. Menzies (2002), Matching conjugate volcanic rifted margins: 40Ar/39Ar chrono-stratigraphy of pre-and syn-rift bimodal flood volcanism in Ethiopia and Yemen, *Earth and Planetary Science Letters*, *198*(3), 289–306.

Van Wijk, J. W., R. S. Huismans, M. Ter Voorde, and S. Cloetingh (2001), Melt generation at volcanic continental margins: no need for a mantle plume?, *Geophysical Research Letters*, *28*(20), 3995–3998.

Varet, J. (1978), Geology of central and southern Afar (Ethiopia and Djibouti Republic), map and 124 pp. report,

Wang, K., T. Plank, J. D. Walker, and E. I. Smith (2002), A mantle melting profile across the Basin and Range, SW USA, *Journal of Geophysical Research*, *106*(B1), doi:10.1029/2001JB000209.

Weinberg, R. F., K. Regenauer-Lieb, and G. Rosenbaum (2007), Mantle detachment faults and the breakup of cold continental lithosphere, *Geology*, *35*(11), 1035, doi:10.1130/G23918A.1.

White, R., and D. McKenzie (1989), Magmatism at rift zones: the generation of volcanic continental margins and flood basalts, *Journal of Geophysical Research: Solid Earth (1978–2012)*, *94*(B6), 7685–7729.

White, R. S. (1992), Magmatism during and after continental break-up, *Geological*

Society, London, Special Publications, *68*(1), 1–16.

White, R. S., G. D. Spence, S. R. Fowler, D. P. McKenzie, and G. K. Westbrook (1987), Magmatism at rifted continental margins, *Nature*, *330*, 439–444.

White, R. S. et al. (2008), Lower-crustal intrusion on the North Atlantic continental margin, *Nature*, *452*(7186), 460–464, doi:10.1038/nature06687.

Wolfenden, E., C. Ebinger, G. Yirgu, A. Deino, and D. Ayalew (2004), Evolution of the northern Main Ethiopian rift: birth of a triple junction, *Earth and Planetary Science Letters*, *224*(1-2), 213–228, doi:10.1016/j.epsl.2004.04.022.

Wolfenden, E., C. Ebinger, Y. Gezahegn, P. R. Renne, and S. P. Kelley (2005), Evolution of a volcanic rifted margin: Southern Red Sea, Ethiopia, *Geological Society of America Bulletin*, *117*(7-8), 846–864, doi:10.1130/B25516.1.

Wright, T. J., C. Ebinger, J. Biggs, A. Ayele, G. Yirgu, D. Keir, and A. Stork (2006), Magma-maintained rift segmentation at continental rupture in the 2005 Afar dyking episode, *Nature*, *442*(7100), 291–294, doi:10.1038/nature04978.

Zanettin, B., and E. Justin-Visentin (1975), Zanettin, B., & Justin-Visentin, E. (1975). Tectonical and volcanological evolution of the western Afar margin (Ethiopia). E., *Afar Depression of Ethiopia*, 300–309.

Ziegler, P. A., and S. Cloetingh (2004), Dynamic processes controlling evolution of rifted basins, *Earth-Science Reviews*, *64*(1-2), 1–50, doi:10.1016/S0012-8252(03)00041-2.

Ziegler, P. A., S. Cloetingh, R. Guiraud, and G. M. Stampfli (2001), Peri-Tethyan platforms: constraints on dynamics of rifting and basin inversion, *Mémoires du Muséum national d'histoire naturelle*, *186*, 9–49.

Zumbo, V., G. Féraud, H. Bertrand, and G. Chazot (1995a), 40Ar39Ar chronology of Tertiary magmatic activity in southern Yemen during the early Red Sea-Aden rifting, *Journal of volcanology and geothermal research*, *65*(3), 265–279.

Zumbo, V., G. Féraud, P. Vellutini, P. Piguet, and J. Vincent (1995b), First 40Ar39Ar dating on early pliocene to plio-pleistocene magmatic events of the Afar—Republic of Djibouti, *Journal of volcanology and geothermal research*, *65*(3), 281–295.

ANNEXE

Article en révisions à *Geostandards and Geoanalytical Research*
(manuscript n° GGR-0375-R1)

An alternative protocol for single zircon dissolution with application to (U-Th-Sm)/He thermochronometry.

Bouchaïb **Tibari** (1), Arnaud **Vacherat** (1,2,3), Martin **Stab** (1,2,3), Raphaël **Pik** (1), Delphine **Yeghicheyan** (1,4) and Pascal **Hild** (1,4)

(1) CRPG, UMR 7358, CNRS- Université de Lorraine, BP20, 54501 Vandoeuvre-Lès-Nancy Cedex, France
(2) Sorbonne Université. UPMC Univ Paris 06, CNRS, UMR 7193, Institut des Sciences de la Terre Paris (iSTeP), 4 Place Jussieu, F-75005 Paris, France
(3) CNRS, UMR 7193, Institut des Sciences de la Terre Paris (iSTeP), 4 Place Jussieu, F-75005 Paris, France
(4) Service d'Analyse des Roches et des Minéraux (SARM), CNRS-CRPG, 15 rue Notre-Dame des Pauvres, BP 20, 54501 Vandoeuvre-lès-Nancy, France

Abstract
Zircon (U-Th-Sm)/He (ZHe) thermochronometry is a powerful tool that has been widely used in geology to constrain the exhumation histories of orogens. In this study, we present an alternative protocol for dissolving zircon grains for determination of parent nuclides. This new alkali fusion procedure, developed at the SARM (Service d'Analyse des Roches et des Minéraux) in Nancy, France, is fast (requiring only 2 days, including cleaning steps), and offers several advantages by avoiding: (1) use of HF pressure dissolution and (2) complete removing of grains from the metal microvials. After dissolution, U, Th and Sm are measured using an ICP-MS. We tested the new procedure on two different reference materials, Fish Canyon Tuff and Buluk Tuff. These exhibited standard precision and accuracy for ZHe age estimations (9 % and 6 %, respectively, 1s). In addition, zircons from Buluk Tuff are shown to be chemically more homogenous and more suitable for assessing the confidence interval of the entire integrated procedure.
Keywords: (U-Th-Sm)/He thermochronometry, zircon, ICP-MS, Fish Canyon Tuff, Buluk Tuff.

Résumé
La thermochronometrie (U-Th-Sm)/He sur zircon est un puissant outil largement utilisé en géologie pour contraindre les histoires d'exhumation des orogènes. Dans cette étude, nous présentons un protocole alternatif pour la dissolution des grains de zircon pour la détermination de nucléides parents.
Cette nouvelle méthode de fusion alcaline, développée au SARM (Service d'Analyse des Roches et des Minéraux), Nancy, France, est plus rapide (nécessite seulement 2 jours, nettoyage inclus), et offre plusieurs avantages en évitant: (1) d'utiliser la dissolution HF haute pression et (2) de retirer complètement les grains de leur microtubes métalliques. Après dissolution, U, Th et Sm sont déterminés à l'aide d'un ICP-MS. Nous avons testé cette nouvelle procédure sur deux matériaux standards différents: Fish Canyon Tuff et Buluk Tuff, qui présentent une précision sur l'estimation des âges ZHe de 9% et 6% respectivement, (1s). Nous démontrons en outre que les zircons de Buluk Tuff sont chimiquement plus homogènes et offrent une meilleure reproductibilité pour évaluer les intervalles de confiance de cette procédure.
Mots-clés: Themochronometrie (U-Th-Sm)/He, zircon, ICP-MS, Fish Canyon Tuff, Buluk Tuff.

Introduction

Over the last two decades, considerable advances have been made in our understanding of the principles of (U-Th-Sm)/He thermochronometry and its use in tectonic/erosion/exhumation studies. In particular, ^{4}He diffusivity in apatites (Shuster et al., 2006; Flowers et al., 2009; Gautheron et al., 2009) and zircons (Guenthner et al., 2013) has been shown to be dependent on the degree of radiation damage, which is proportional to U and Th concentration (effective Uranium : eU = U + 0.24 Th). In order to calculate the ages themselves, and to take this eU dependency into account high precision U and Th measurements on single grains are essential. Moreover, the use of zircon (U-Th-Sm)/He detrital thermochronology to reconstruct the denudation history of orogens (Reiners et al., 2005 ; Filleaudeau et al., 2011; Tochilin et al., 2012 ; Saylor et al., 2012 ; Mouthereau et al., 2014; Vacherat et al., 2014) requires an ability to rapidly perform large numbers of single-grain analyses. Recent advances of in situ (U-Th-Sm)/He dating should allow measuring such large batches of single grains routinely in the future (J. Boyce et al., 2009 ; Tripathy-Lang et al., 2013 ; Evans et al., 2015). However, in situ measurements in the core of abraded single grains potentially provide only partial thermochronological information by favoring documentation of rapid cooling episodes, and will therefore not be able to completely replace conventional bulk single grain measurements.
The conventional bulk single grain analytical technique used for (U-Th-Sm)/He thermochronometry typically consists of two consecutive steps: (1) *in vacuo* heating of the sample to enable complete outgassing of the ^{4}He, which is then purified in a

dedicated high-vacuum system before measurement in a noble gas mass spectrometer; and (2) dissolution of the sample in order to measure U, Th and Sm contents in solution by ICP-MS. The duration of the dissolution step depends on the mineral analyzed. Around one hour is required for apatite (Gautheron et al., 2013), but dissolution takes several days for zircon (Reiners et al., 2002, Evans et al., 2005, Wolfe and Stockli, 2010). Laboratories have each developed their own, largely similar, in-house protocols for zircon dissolution and these have generally been inherited from those used for U/Pb geochronology (Krog, 1973). After ^{4}He measurement of single crystals, samples are spiked with non naturally occurring isotopes of U, Th and Sm, and dissolved in a HF-HNO_3 mixture for several days (Tagami et al., 2003; Reiners, 2005) at 220 to 235°C in a pressure dissolution vessel. At this point complete evaporation of HF is necessary. A second pressure dissolution step, using concentrated HCl for 12 to 24 hours at 200°C, is sometimes required in order to dissolve fluoride salts. Moreover, when zircon grains have been loaded for gas extraction in Pt tubes, it is necessary to remove the crystals prior to dissolution to avoid the pervasive PtAr interference on every parent/spike isotope. Alternatively, zircon grains may be loaded in Nb microvials which can be dissolved along with the crystals to reduce handling. The overall time for this dissolution protocol is up to 4 days (Harangi and al., 2015) for each series of samples.

In this study, we detail an alternative protocol to dissolve single zircon grains, which offers several advantages by avoiding: (1) use of HF pressure dissolution and (2) complete removing of grains from the metal microvials. The protocol is tested on two different reference materials: Fish Canyon Tuff (FCT) and Buluk Fm Tuff.

Experimental procedures

The routine preparation protocol developed at the SARM (Service d'Analyse des Roches et des Minéraux) for REEs, Pb, U and Th analysis, consists of alkali fusion. The amounts of reactants and fluxes used for refractory minerals (zircon, olivine) are reported in Table 1. To test the routine protocol of the SARM procedure, 100-mg samples were first weighed into the custom-made Pt crucibles routinely used in the laboratory (12g in weight; 95%Pt and 5%Au; 20 mm in height, 20 mm in diameter and 0.40 mm in basal thickness). Samples were then fused at 990°C for 2 hours in a mixture of home-made ultra-pure $LiBO_2$ (1:9 ratio of flux to BR reference material) and ultra-pure $B(OH)_3$ (1:6 ratio of flux to BR). After cooling to room temperature, each Pt crucible was then plunged into 100mL of acid solution (HNO_3 7% v/v) for 12 hours in order to dissolve the fusion bead. The sample solution was then diluted with HNO_3 (2% v/v) to reach the dilution coefficient of the routine protocol.

	BR (mg)	$LiBO_2$ (mg)	$B(OH)_3$ (mg)	Acid solution (ml) (*)	Final dilution	Dilution coefficient
SARM routine protocol	100	900	600	100	1 ml / 9 ml HNO_3 2% v/v	1000
This study (small Pt crucible)	6.66	60	40	6.6 HNO_3 2% v/v + 6.6 acid dilution	1 ml /4 ml HNO_3 2% v/v	500*2 = 1000
Ratio routine / this study	15	15	15	7.5	2	

Table 1. *Quantities and ratios of material, fluxes, and reactants, and calculated dilution coefficient used in the routine protocol and in the new protocol proposed in this study at the SARM laboratory. (*) Acid solution = HNO_3 (0.7% v/v) suprapure (Carlo Erba). BR corresponds to the SARM Basalt reference material, from Essey-la-Côte, near Nancy, Meurthe-et-Moselle.*

This procedure is used specifically for refractory minerals such as olivines and zircons and differs from that used for bulk rock, which uses only $LiBO_2$. The importance of mixing $LiBO_2$ with $B(OH)_3$ for complete dissolution of zircons was tested on various granulometric sizes of the #91500 zircon standard used for SIMS and La-ICP-MS calibration (Wiedenbeck et al., 1995, 2004). Results are presented in Figure 1 and clearly demonstrate that whatever the grain size (from powder to 250 mm), complete dissolution cannot be achieved in experiments carried out with Li-metaborate alone. The incomplete dissolution also appears to be associated with a large fractionation of the U/Th ratio. Whereas about half of the U is retrieved when only Li-metaborate is used, only a fifth of the Th is measured. The complex behavior of Th in the possible presence of remaining crystal structure during incomplete dissolution likely explains this large fractionation between U and Th. In future routine measurements, such fractionation of the U/Th ratio could be used as an indicator of accidental incomplete dissolution of individual aliquots from a single sample population.

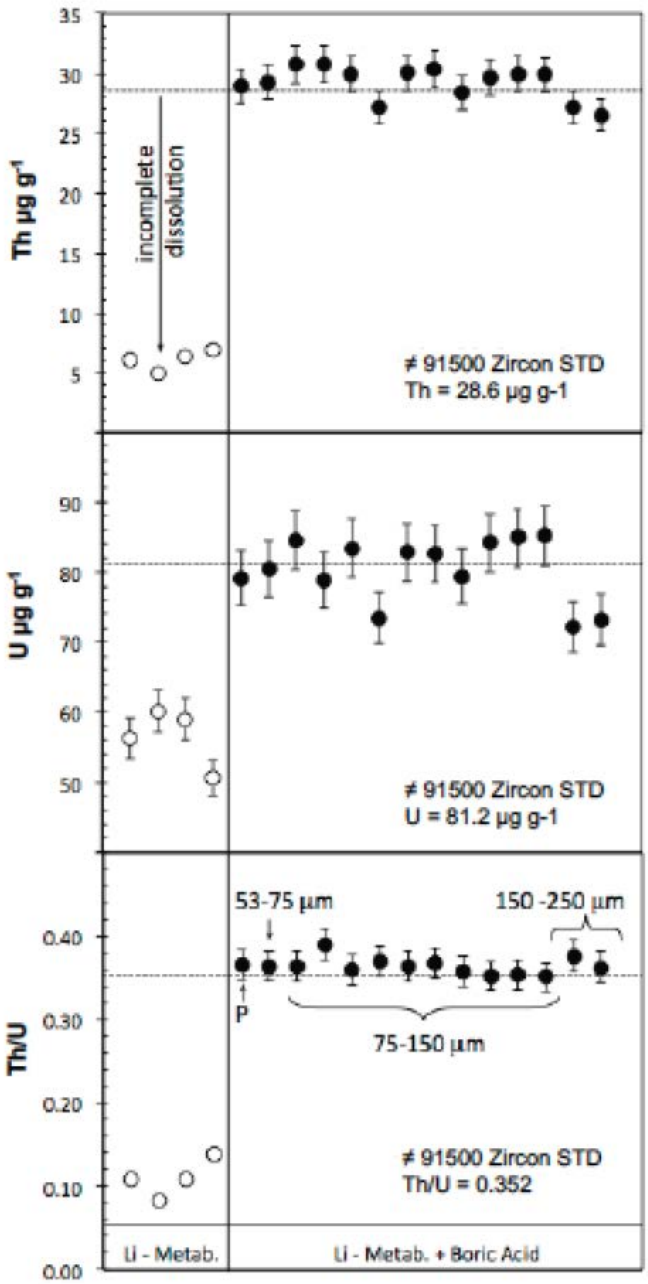

Figure 1. *Comparison of zircon dissolution procedure using Li-metaborate and a mixture of Li-metaborate with boric acid. These tests were carried out on powder remaining after preparation of SIMS standard #91500, for which the concentration of U and Th is well known and has been shown to be particularly homogeneous (Wiedenbeck et al., 1995, 2004). Reported concentrations are mean concentrations in the samples.*

Nevertheless, these experiments highlight the very efficient and complete dissolution of zircons when Li-metaborate is mixed with boric acid. Whatever the grain size (from powder to 250 mm), the concentrations measured for U and Th are reproducible within about 5 % and the mean concentrations are in agreement with the recommended values for this standard within 2 %.

To take into account the very small amounts of material processed for ZHe thermochronometry compared to those used for routine analyses (~ 1/15 to 1/10), the quantities of reactants and solutions, as well as the Pt crucible size, were adapted in order to reduce the levels of the background (blank). This adjustment was based on the proportions of fluxes/solutions routinely used by the SARM to give the same dilution coefficient before analysis (Table 1). Thus, after complete dissolution of the fusion bead, the solution was diluted by a factor of 10 with ultrapure HNO_3 (2% v/v) for analysis.

After He extraction at CRPG (Nancy, France: Pik et al., 2003; Godard et al., 2009), grains were retrieved from their Pt capsules and placed into small Pt-crucibles. A set of 25 custom crucibles with polished surfaces was specifically designed for this new procedure. Each crucible weighs 6g and is made from 95% Pt and 5% Au (dimensions: 10 mm diameter, 10.5 mm height and 0.7 mm basal thickness). These are hereafter referred to as "small" crucibles in order to distinguish them from the larger "routine" crucibles.

In each batch, one of the 25 small crucibles was used to determine the environmental blank, i.e chemical contributions and crucible deterioration due to aging. This blank was used to calculate the ICP-MS detection limit. The BR alkali basalt reference material (Carignan et al., 2001) was also fused three times per batch. Two 66.66 mg aliquots were prepared using the larger SARM routine crucibles in order to calibrate the instrument. One of these aliquots was doped with U and Th (with mono elementary 1000 µg ml^{-1} Accustandards solutions) in order to obtain a high calibration point at 200 µg g^{-1} for the ICP-MS. The second aliquot was used as a quality control for the routine procedure. The third aliquot of basalt reference material (6.66 mg) was weighed into a small crucible in order to assess the new procedure described in this study. The blank, quality controls and samples were then analyzed by ICP-MS (Thermo Fischer Scientific X7) using a two points "linear through blank" calibration. Individual analyses lasted 26s with a washing delay of 120s using the blank solution. A linear regression calibration was performed after every five samples in order to correct for instrumental drift. All results are reported in ng g^{-1} according to basalt reference material calibration.

#Series	^{238}U	^{232}Th	^{147}Sm
1	20.9	3.6	0.0
2	37.3	4.8	3.9
3	28.0	5.4	2.6
4	20.7	0.0	3.5
5	38.1	0.0	0.0
6	29.8	0.9	2.2
7	25.2	0.5	0.0
8	32.2	0.0	6.9
9	31.4	1.2	2.0
Mean	29.3	1.8	2.4
SD*	6.3	2.2	2.3
% RSD **	*21*	*119*	*97*
LOQ ***	92.3	23.8	25.4

Values are given in ng g-1
* 1 standard deviation
** Relative standard deviation
*** Limit of quantification. LOQ = Mean + 10*SD

Table 2. *Concentrations of blanks measured in the solution during this study (new protocol) and calculation of the running LOQ (limit of quantification, ng g^{-1}) for this procedure.*

Typical blanks obtained in the measured solution with this procedure are listed in Table 2 and are significantly higher for U (29.3 ± 6.3 ng g^{-1}) than for Th (1.8 ± 2.2 ng g^{-1}) and Sm (2.4 ± 2.3 ng g^{-1}). These concentrations correspond to the following amounts of elements, U (0,193 ± 0,041 ng), Th (0,011 ± 0,014 ng), Sm (0,015 ± 0,015). These reproducible blank values were obtained only after significant cleaning of the new small crucible set and performing repeated blank procedures (see Appendix for cleaning process details: fig 4 and 5).

Analyses were considered valid if the analyzed concentrations are above the limit of quantification (LOQ, ng g^{-1}) for a given element. The LOQ for U, Th and Sm is calculated using the mean of the nine fusion blanks (ng g^{-1}) presented in Table 2, plus 10 times the standard deviation. The calculated LOQ for this small-crucible procedure are much lower than those calculated for the routine crucibles (170 ng g^{-1} for U and 210 ng g^{-1} for Th). The LOQ for U and Th are 92.2 ng g^{-1} and 23.5 ng g^{-1}, respectively. Because the contribution of Sm to the total He budget is only about 0.0001% for FCT zircons (Table 3), the Sm LOQ was not taken into account in this study. Interferences were checked on 238, 232 and 147 mass and were insignificant. U is monitored at mass 238 and cannot be interfered by argides formation.

Sample	Nbr of grains	Width µm	Lenght µm	FT [a]	Mass [b] µg	Blank [c] #	^{4}He nmol g^{-1}	U µg g^{-1}	Th µg g^{-1}	Sm µg g^{-1}	eU µg g^{-1}	He age Ma	Corrected He age [d] Ma	±
FC Tuff-2-SG-Zr-a	1	119	193	0.82	7.5	1	19.4	155	108	1	181	20.1	24.5	1.5
FC Tuff-9-SG-Zr-a	1	157	243	0.86	15.9	1	21.5	151	78	3	170	23.7	27.5	1.7
FC Tuff-8-SG-Zr	1	117	353	0.85	17.5	1	36.1	254	142	4	288	23.4	27.6	1.7
FC Tuff-1-SG-Zr-a	1	108	189	0.81	6.4	1	37.0	250	206	1	300	23.1	28.5	1.7
FC Tuff-4-SG-Zr	1	88	230	0.80	6.2	1	45.9	296	170	1	337	25.5	31.9	1.9
FC Tuff-7-SG-Zr-a	1	127	188	0.83	7.8	1	44.9	276	137	7	309	27.2	32.8	2.0
FC Tuff-6-SG-Zr-a	1	157	214	0.85	12.5	1	61.0	349	221	1	402	28.4	33.4	2.0
FC Tuff-5-SG-Zr-a	1	110	184	0.81	6.2	1	37.6	198	153	7	235	29.9	37.0	2.2
FC Tuff-3-SG-Zr-a	1	79	156	0.75	3.0	1	44.3	236	220	4	289	28.7	38.2	2.3
FC Tuff-10-SG-Zr	1	169	219	0.86	14.1	1	44.7	224	105	2	249	33.5	39.0	2.3
FC Tuff-15-SG-Zr-a	1	109	213	0.82	7.8	2	19.0	148	72	2	166	21.4	26.1	1.6
FC Tuff-17-SG-Zr-a	1	206	543	0.91	79.7	3	15.1	101	75	2	119	23.7	26.0	1.6
FC Tuff-1-SG-Zr-b	1	95	234	0.81	7.2	4	84.7	743	390	15	837	18.9	23.4	1.4
FC Tuff-2-SG-Zr-b	1	77	166	0.76	3.2	4	79.1	689	361	15	776	19.1	25.1	1.5
FC Tuff-11-SG-Zr	1	128	460	0.86	28.4	5	46.7	312	227	4	367	23.8	27.7	1.7
FC Tuff-8-SG-Zr	1	197	476	0.90	62.0	5	33.6	186	195	7	233	27.0	30.0	1.8
FC Tuff-10-SG-Zr	1	275	384	0.91	70.6	5	20.8	118	85	4	139	28.0	30.8	1.8
FC Tuff-18-SG-Zr	1	186	374	0.89	40.2	8	16.3	120	70	2	137	22.3	25.0	1.5
FC Tuff-3-Zr-b	2	55	110	0.66	1.0	4	88.6	895	662	711	1054	15.7	23.8	1.4
FC Tuff-17-Zr-b	2	125	288	0.85	14.8	8	68.3	519	286	19	588	21.7	25.6	1.5
FC Tuff-5-Zr-b	3	144	344	0.87	23.8	5	51.5	372	227	10	427	22.6	25.9	1.6
FC Tuff-9-Zr-b	3	163	304	0.88	24.2	5	104.5	665	360	13	751	26.0	29.6	1.8
FC Tuff-6-Zr-b	3	130	265	0.85	14.0	5	124.2	803	509	11	925	25.1	29.6	1.8
FC Tuff-7-Zr-b	3	163	301	0.87	23.7	5	100.7	617	391	23	711	26.5	30.4	1.8
FC Tuff-15-Zr-b	3	110	218	0.82	8.1	8	125.7	936	495	8	1055	22.3	27.2	1.6
FC Tuff-16-Zr	3	87	171	0.78	4.0	8	115.2	862	497	65	981	22.0	28.2	1.7
FC Tuff-5-Zr-c	4	113	247	0.83	10.2	7	116.6	848	568	33	984	22.2	26.7	1.6
FC Tuff-4-Zr-d	4	125	272	0.85	13.7	7	148.1	996	601	20	1140	24.3	28.6	1.7
FC Tuff-4-Zr-a	4	113	271	0.84	11.7	7	202.9	1338	702	25	1506	25.2	30.0	1.8
FC Tuff-5-Zr-e	5	81	197	0.78	4.4	7	162.8	1317	622	16	1467	20.8	26.6	1.6
Buluk-5-SG-Zr-a	1	124	378	0.86	21.1	1	7.0	83	66	39	99	13.2	15.3	0.9
Buluk-9-SG-Zr	1	159	344	0.88	27.9	1	8.9	106	68	37	123	13.6	15.5	0.9
Buluk-12-SG-Zr-a	1	157	389	0.88	32.5	1	2.6	31	16	28	35	14.0	15.9	1.0
Buluk-6-SG-Zr-a	1	137	387	0.87	25.7	1	4.5	52	29	52	59	14.3	16.4	1.0
Buluk-11-SG-Zr-a	1	132	324	0.86	19.0	1	10.8	119	73	28	136	14.8	17.2	1.0
Buluk-2-SG-Zr	1	186	428	0.90	49.0	5	3.3	42	22	24	48	12.8	14.2	0.9
Buluk-08-SG-Zr	1	211	492	0.91	72.7	5	6.7	76	57	54	90	13.9	15.2	0.9
Buluk-01-SG-Zr	1	246	439	0.91	77.2	5	8.3	91	81	106	110	14.0	15.4	0.9
Buluk-5-SG-Zr-b	1	227	380	0.91	54.8	5	8.4	91	61	31	106	14.9	16.4	1.0
Buluk-03-SG-Zr	1	205	352	0.90	42.0	5	12.9	136	109	119	163	14.8	16.5	1.0
Bluk-04-SG-Zr	1	169	400	0.89	38.3	5	5.1	53	30	41	61	15.6	17.5	1.1
Buluk-12-SG-Zr-b	1	170	405	0.89	39.1	6	3.2	36	23	27	42	14.1	15.8	1.0
Buluk-14-SG-Zr	1	212	436	0.91	61.6	6	9.7	100	97	124	123	14.7	16.2	1.0
Buluk-13-SG-Zr	1	202	411	0.90	52.3	6	10.9	94	189	437	140	14.6	16.2	1.0
Buluk-16-SG-Zr	1	185	411	0.89	45.9	6	4.0	45	26	28	51	14.8	16.6	1.0
Buluk-15-SG-Zr	1	225	347	0.90	46.4	6	8.9	90	77	74	109	15.2	16.9	1.0
Buluk-10-Zr	3	122	319	0.87	16.4	1	11.5	117	82	36	137	15.7	18.1	1.1
Buluk-6-Zr-b	3	132	417	0.87	26.6	5	15.0	170	118	61	199	14.1	16.2	1.0
Buluk-7-Zr	3	162	353	0.88	30.0	5	20.1	215	165	148	255	14.8	16.8	1.0
Buluk-11-Zr-b	3	124	157	0.80	5.3	6	26.7	284	271	311	349	14.3	17.9	1.1
Buluk-19-Zr	3	243	407	0.91	67.1	9	8.7	104	77	83	123	13.3	14.6	0.9
Buluk-17-Zr	3	143	266	0.86	16.2	9	23.1	284	209	111	335	12.9	15.0	0.9
Buluk-20-Zr	3	44	88	0.59	0.5	9	373.7	5778	2785	3273	6447	10.8	18.4	1.1

Table 3. *Results of (U-Th-Sm)/He analyses on FCT and Buluk geostandards. (a) FT correction factor calculated from Ketcham et al. (2011). (b) Mass of zircons calculated using a mean density of 4.65. (c) Blank sessions detailed in Table 2. (d) Corrected age = Raw He age /F_T.*

Standard analysis

In order to test the validity of this new protocol, we measured the He ages of zircons from two well-known (U-Th-Sm)/He thermochronometry standards: Fish Canyon Tuff (FCT) and Buluk Tuff (Naese C. W. and al., 1981, Hurford and al., 1987).

We analyzed 30 aliquots of FCT (18 single grains and 12 multi grain aliquots) and 23 aliquots of Buluk (16 single grains and 7 multi grain aliquots). Aliquots of single and multiple grains were carefully selected to ensure that grains were similar in size.
Both single and multiple grains were loaded in order to test the sensitivity of the dissolution method and to validate the routine use of single grains. The zircon grains were then analyzed and He, U, Th and Sm extracted and measured following the protocol described above. Results are reported in Table 3. He ages and F_T correction factors were calculated following Ketcham et al. (2011).

Results

The (U-Th-Sm)/He ages of 23 Buluk Tuff zircons ranged from 14.1 to 18.0 Ma with a mean of 16.0 ± 1.0 Ma (1s). The (U-Th-Sm)/He ages of 30 FCT zircons ranged from 22.5 to 38.8 Ma with a mean of 28.0 ± 4.0 Ma (1s). These ages are in good agreement with the reported ages of these standards in the literature (Table 4).

Age	Dating method	References
Fish Canyon Tuff		
27.08 ± 0.2	Biotite Ar/Ar	Hurford and Hammerschmidt, 1985
26.8 ± 4.2	Apatite fission tracks	
27.0 ± 2.2	Zircon fission tracks	Carpéna and Mailjé, 1987
28.03 ± 0.18	Feldspar Ar/Ar	Renne et al., 1994
30.1 ± 1.0		Reiners and Farley, 1999
27.9 ± 1.1	Titanite He age	House et al., 2000
27.8 ± 0.7	Zircon He age	Tagami et al., 2002
28.2 ± 0.05	Sanidine Ar/Ar	Kuiper et al., 2008
Buluk		
16.3 ± 0.2	Sanidine K/Ar	McDougall and Watkins, 1985
16.2 ± 0.6	Zircon fission tracks	Hurford and Watkins, 1987
16.1 ± 0.8	Zircon He age	Tagami et al., 2002

Table 4. *Compilation of published ages for Fish Canyon Tuff and Buluk Fm Tuff.*

In Figure 2, the ZHe-age values are plotted against U concentration measured in the solution. Dissolution of zircon grains with this procedure yields typical U concentrations in the solution for Buluk and FCT that are far higher than the Pt crucible blanks and significantly higher than the calculated LOQ, even for single grains. The corresponding mass of U for the blank and for the LOQ are ~ 0,2 ng and ~ 0,7 ng respectively. Moreover, the observed scatter in the ages of the single grain analyses is not significantly greater than that of the multi-grain ages. There does not appear to be any specific correlation between the ZHe-ages and the concentration of U in the solution, which indicates that (i) the quantity of elements present in the solution for a single grain is not a limitation of this dissolution procedure, and (ii)

that the proposed LOQ value is reasonable. Even in the case of the FCT data, which exhibited the worst reproducibility, the oldest outlier ages do not seem to be specifically linked to low concentrations which might have led to less precise U and Th measurements.

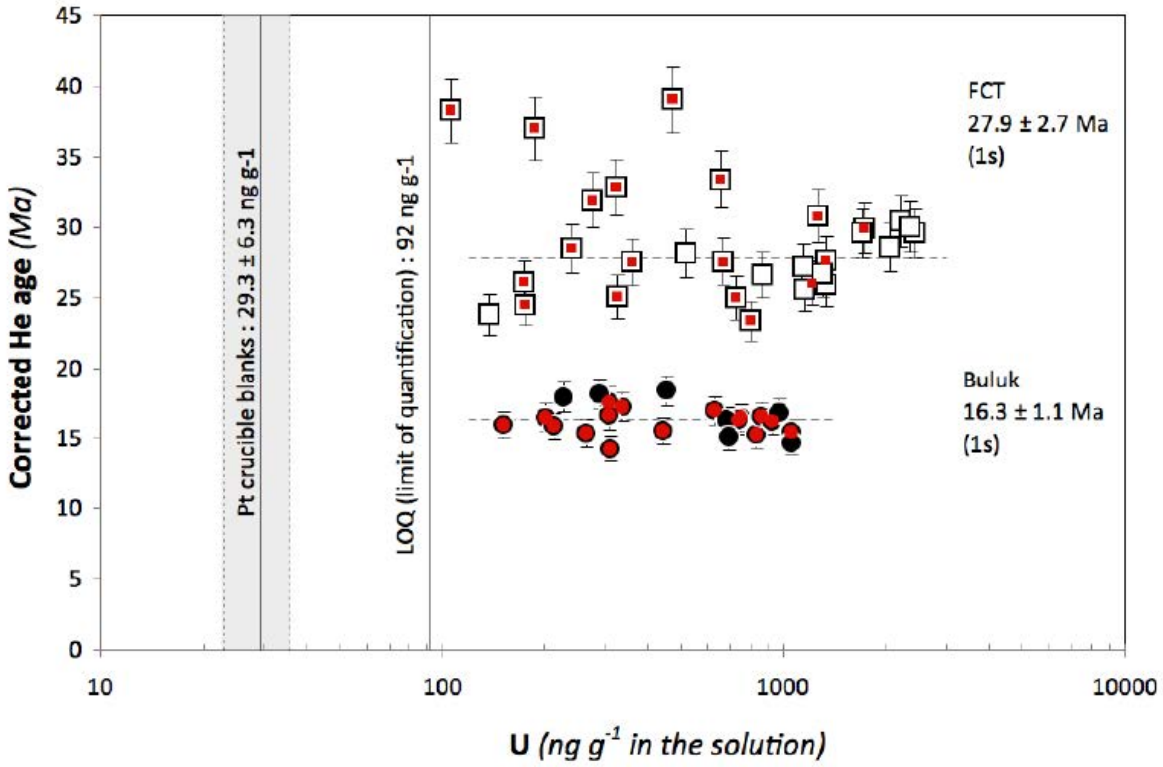

Figure 2. *Comparison of final ZHe-age determinations with the concentration of U injected in the IC-PMS for FCT and Buluk zircons. Red symbols represent single grain analyses. The dispersion of ages does not show any correlation with U concentration. The concentrations of U in both single and multi grain solutions are significantly higher than the proposed Limit of Quantification (LOQ), which is used as a criterion for selection of valid analyses. The corresponding mass of U for the blank and for the LOQ are 0,2 +/- 0,03 ng and 0,7 ng respectively.*

The S-shaped curve in Figure 3A, which illustrates the dispersion around the average age, is more pronounced for FCT zircons than it is for Buluk Tuff zircons, thus demonstrating the better age reproducibility of Buluk Tuff (~ 6%) compared to FCT (~ 14% with all data and ~ 9% excluding the 3 older outlier). Th/U values (Fig. 3B) present significant scatter and are similar for the two standards, ranging from 0.47 to 1.05, with the exception of a single outlier for Buluk Tuff at 2.02. The three FCT outliers with ages above 35 Ma encompass the whole range of Th/U values and are not associated with particularly low Th/U values that might be indicative of accidental incomplete dissolution, as observed in Figure 1. We note that there is no correlation between ages and grain dimension. This indicates successful dissolution of

zircon grains over the entire size range and is also consistent with the observed wide scatter in Th/U values.

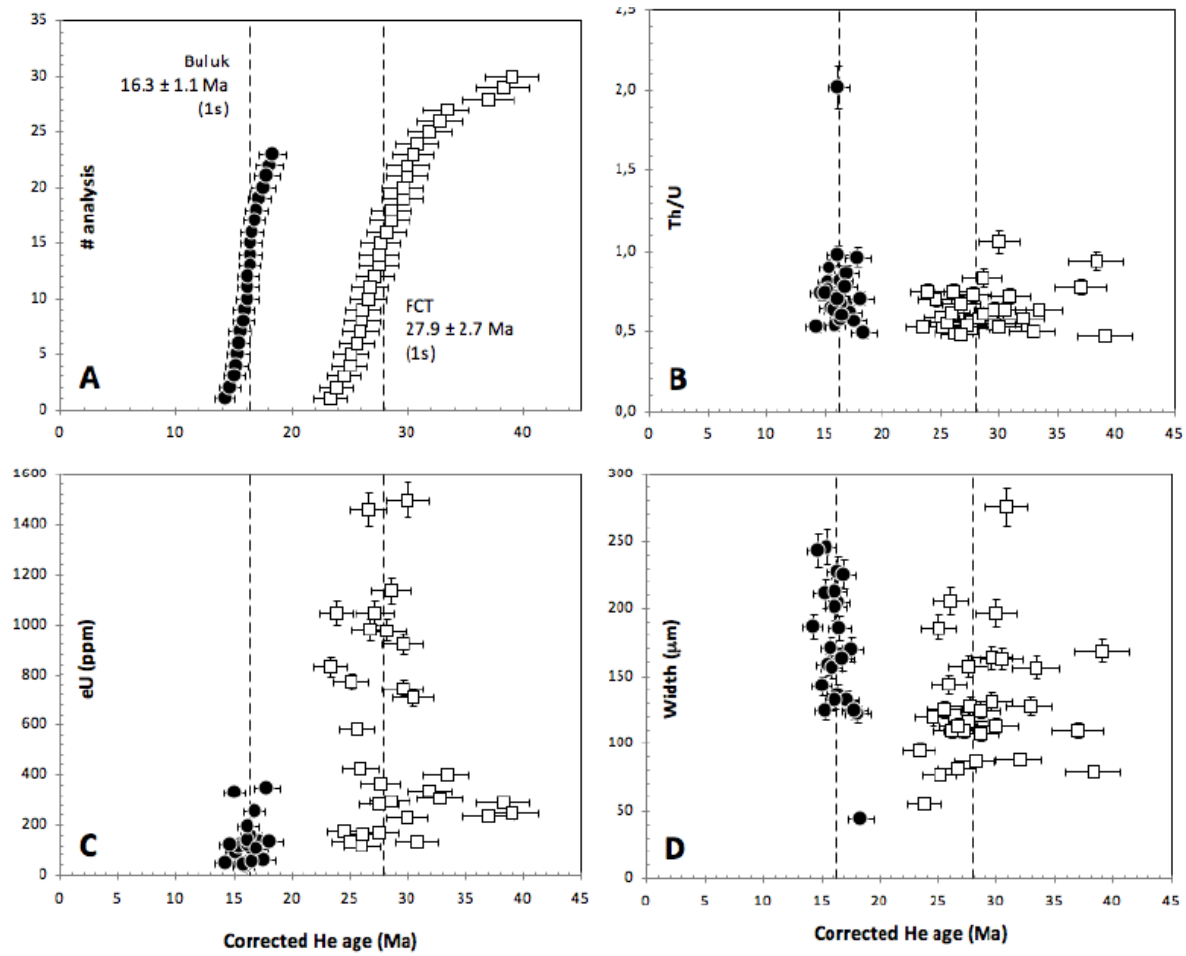

Figure 3. *Corrected (U-Th-Sm)/He ages plotted against the number of analyses (upper left panel, A), Th/U ratio (upper right panel, B), eU concentration (bottom left panel, C) and grain diameters (bottom right panel, D). Individual error bars are given at 6% based on the reproducibility of Buluk.*

The eU values range from 45 to 271 µg g^{-1} for Buluk and from 50 to 1278 µg g^{-1} for FCT (Fig. 3c), indicating that Buluk Tuff has a better chemical homogeneity than FCT and could therefore represent a more suitable reference material. Even though no direct correlation can be seen in Figure 3C, the wider dispersion of FCT ages could be related to complex zoning, as was previously shown by Dobson et al. (2008).
The reproducibility of ages for the Buluk Tuff reference material with this dissolution method is about 6 % (1s). This is comparable to the value obtained using other dissolution methods for zircons (Reiners, 2005; Dobson et al., 2008) and apatites (Farley, 2002; Kraml et al., 2006).
The external reproducibility for the entire dating procedure incorporates not only the analytical uncertainty and precision for the determination of He and U and Th concentrations, but also the uncertainties linked to the alpha ejection correction. This

correction is fundamentally based on the assumption that U and Th are uniformly distributed in the minerals, and it therefore represents the largest source of uncertainty for zircons, which are frequently zoned. For thermochronological applications, a reproducibility of ~ 6 % is not particularly problematic because interpretations are usually model dependent, leading to higher uncertainties and therefore less precision in the determination of the dates of geological events. However, for (U-Th-Sm)/He dating, such relatively poor precision for a reference material prevents use of our new method for bulk dissolution of zircons in studies that requires precise (U-Th-Sm)/He ages of volcanic material such as rhyolites. For this specific application, new technical advances in in-situ (Evans et al., 2015) measurement should lead to better precision in the future.

Conclusions

In this study we detail a new procedure for single zircon dissolution applied to (U-Th-Sm)/He geochronology. The new alternative preparation protocol is fast (two days, cleaning included) and yields comparable measurement accuracy and reproducibility than traditional dissolution procedures. It could therefore present significant advantages for studies that require analysis of large datasets such as in detrital thermochronology.

We have also demonstrated that the Buluk Tuff standard exhibits a better reproducibility than Fish Canyon Tuff, and we consider it to be a more suitable standard for assessing the confidence interval of the entire integrated procedure.

Acknowledgments

We would like to thank Yves Marrocchi for sampling the Fish Canyon Tuff and Etienne Deloule for providing the #91500 zircon standard powder, as well as the CRPG staff and SARM laboratory for their precious help during data acquisition. This is CRPG contribution # GGR-0375.

References

Boyce, J. W., K. V. Hodges, D. King, J. L. Crowley, M. Jercinovic, N. Chatterjee, S. A. Bowring, and M. Searle (2009). Improved confidence in (U-Th)/He thermochronology using the laser microprobe: An example from a Pleistocene leucogranite, Nanga Parbat, Pakistan, Geochemistry Geophysics Geosystems, 10, QAA01.

Carignan J., Hild P., Mevelle G., Morel J., and Yeghicheyan D. (2001). Routine analyses of trace element in geological samples using flow injection and low pressure on-line liquid chromatography coupled to ICP-MS: a study of geochemical reference materials BR, DR-N, UB-N, AN-G and GH. Geostandards Newsletter, 25, 187-198.

Carpena J. and Mailhe D. (1987). Fission-track dating calibration of the Fish Canyon Tuff standard in French reactors. Chemical Geology, 66, 53–59.

Dobson K.J., Stuart F., Dempster T.J., EIMF (2008). U and Th zonation in Fish Canyon Tuff zircons: Implications for a zircon (U)Th)/He standard. Geochimica et Cosmochimica Acta, 72, 4745-4755.

Evans, N. J., Byrne, J. P., Keegan, J. T., & Dotter, L. E. (2005). Determination of uranium and thorium in zircon, apatite, and fluorite: Application to laser (U-Th)/He thermochronology. Journal of Analytical Chemistry, 60(12), 1159-1165.

Evans, N.J., McInnes, B.I.A., McDonald, B., Danisik, M., Becker, T., Vermeesch, P., Shelley, M., Marillo-Sialer, E. and Patterson, D.B (2015). An in situ technique for (U-Th-Sm)/He and U-Pb double dating. Journal of Analytical Atomic Spectroscopy, 30(7), 1636-1645.

Filleaudeau P.Y., Mouthereau F., and Pik R. (2011). Thermo-tectonic evolution of south-central Pyrenees from rifting to orogeny: insights from detrital zircon U/Pb and (U-Th)/He thermochronometry. Basin Research, 23, 1-17.

Flowers R.M., Ketcham R.A., Shuster D.L., and Farley K.A. (2009). Apatite (U-Th)/He thermochronometry using a radiation damage accumulation and annealing model. Geochimica et Cosmochimica Acta, 73, 2347-2365.

Gautheron C., Barbarand J., Ketcham R. A., Tassan-Got L., Van der Beek P., Pagel M., Pinna-Jamme R., Couffignal F., and Fialin M. (2013). Chemical influence on α-recoil damage annealing in apatite: Implications for (U-Th)/He dating. Chemical Geology, 351, 257-267.

Gautheron C., Tassan-Got L., Barbarand J. and Pagel M. (2009). Effect of alpha-damage annealing on apatite (U–Th)/He thermochronology. Chemical Geology, 266, 157-170.

Godard V., Pik R., Lavé J., Cattin R., Tibari B., de Sigoyer J., Pubelier M., and Zhu J. (2009). Exhumation History of the Central Longmen Shan (Eastern Tibet) from (U-Th)/He Thermochronometry. Tectonics, 28, TC5009.

Govindaraju K. (1995). Working values with confidence limits for twenty-six CRPG, ANRT and IWG-GIT geostandards. Geostandards Newsletter, 19, 1-32.

Guenthner W.R., Reiners P.W., Ketcham R.A., Nasdala L., and Giester G. (2013). Helium diffusion in natural zircon: Radiation damage, anisotropy, and the interpretation of zircon (U-Th)/He thermochronology. American Journal of Science, 313, 145-198.

Harangi S., Lukács R., Schmitt A.K., Dunkl I., Molnár K., Kiss B., Seghedi I., Novothny Á., Molnár M. (2015). Constraints on the timing of Quaternary volcanism and duration of magma residence at Ciomadul volcano, east–central Europe, from combined U–Th/He and U–Th zircon geochronology. Journal of Volcanology and Geothermal Research, 301, 66–80.

House M.A., Farley K.A., and Stockli D.F. (2000).
Helium chronometry of apatite and titanite using Nd-YAG laser heating. Earth and Planetary Science Letters, 183, 365-368.

Hurford A.J. and Hammerschmidt K. (1985).
40Ar-39Ar and K/Ar dating of the Bishop and Fish Canyon Tuffs: Calibration of ages for fission-track dating standards. Chemical Geology, 58, 23-32.

Hurford A.J. and Watkins R.T. (1987).
Fission-track age of the tufts of the Buluk Member, Bakate Formation, Northern Kenya: a suitable fission-track standard. Chemical Geology, 66, 209-216.

Ketcham R.A., Gautheron C. and Tassan-Got L. (2011).
Accounting for long alpha-particle stopping distances in (U-Th-Sm)/He geochronology: Refinement of the baseline case. Geochemica et Cosmochimica Acta, 75, 7779-7791.

Kraml M., Pik R., Rahn M., Selbeck R., Carignan J., and Keller J. (2006).

A potential single grain 40Ar/39Ar, (U-Th)/He and FT age standard: the Limberg t3 tuff, Geostandard Geological Research, 30, 73-86.

Krog, T.E. (1973). A low contamination method for hydrothermal decomposition of zircon and extraction of U and Pb for isotopic age determination. Geochimica et Cosmochimica Acta , 37, 485-494.

Kuiper K.F., Deino A., Hilgen F.J., Krijgsman W., Renne P.R., and Wijbrans J.R. (2008). Synchronizing Rock Clocks of Earth. History Science, 320, 500-504.

McDougall I. and Watkins R. T. (1988). Potassium–argon ages of volcanic rocks from northeast of Lake Turkana, northern Kenya. Geological Magazine, 125, 15-23.

Mouthereau F., Filleaudeau P.Y., Vacherat A., Pik R., Lacombe O., Giuditta Fellin M., Castelltort S., Christophoul F., and Masini E. (2014). Placing limits to shortening evolution in the Pyrenees: Role of margin architecture and implications for the Iberia/Europe convergence. Tectonics, 33, 1-32.

Naeser C. W., R. A. Zimmermann and G. T. Cebula (1981). Fission-track dating of apatite and zircon: an interlaboratory comparison, Nuclear Tracks, 5, 65-72.

Pik R., Marty B., Carignan J., and Lavé J. (2003). Stability of the Upper Nile drainage network (Ethiopia) deduced from (U-Th)/He thermochronometry: implications for uplift and erosion of the Afar plume dome. Earth and Planetary Science Letters, 215, 73-88.

Reiners P.W. (2005). Zircon (U-Th)/He thermochronometry. Reviews in Mineralogy and Geochemistry, 58, 151-179

Reiners, P.W., Campbell, I.H., Nicolescu, S., Allen, C.M., Hourigan, J.K., Garver, J.I., Mattinson, J.M., Cowan, D.S. (2005). (U-Th)/(He-Pb) double dating of detrital zircons, American Journal of Science, 305, 259-311.

Reiners P. W. and Farley K. A. (1999). Helium diffusion and (U-Th)/He thermochronometry of titanite. Geochimica et Cosmochimica Acta, 63, 3845–3859.

Reiners P. W., Farley K. A. and Hickes H. J. (2002). He diffusion and (U-Th)/He thermochronometry of zircon: initial results from Fish Canyon Tuff and Gold Butte. Tectonophysics, 349, 297-308.

Renne P.R., Deino A.L., Walter R.C., Turrin B.D., Swisher III C.C., Becker T.A., Curtis G.H., Sharp W.D., and Jaouni A.R. (1994). Intercalibration of astronomical and radioisotopic time. Geology, 22, 783-786.

Saylor, J.E., Stockli, D.F., Horton, B.K., Nie, J., and Mora, A. (2012). Discriminating rapid exhumation from syndepositional volcanism using detrital zircon double dating: Implications for the tectonic history of the Eastern Cordillera, Colombia. Bulletin of the Geological Society of America, 124, 762-779.

Shuster D. L., Flowers R. M., and Farley K. A. (2006). The influence of natural radiation damage on helium diffusion kinetics in apatite. Earth and Planetary Science Letters, 249, 148-161.

Tagami T., Farley K.A., and Stockli D.F. (2003). (U-Th)/He geochronology of single zircon grains of known Tertiary eruption age.Earth and Planetary Science Letters, 207, 57-67.

Tochilin, C.J., Reiners, P.W., Thomson, S., Hemming, S.R., Gehrels, G., and Pierce, E.L. (2012). Erosional history of the Prydz Bay sector of East Antarctica from detrital apatite and zircon geo- and thermochronology multidating, Geochemistry Geophysics Geosystems, 13, Q11015.

Tripathy-Lang, A., K. V. Hodges, B. D. Monteleone, and M. C. van Soest (2013). Laser (U-Th)/He thermochronology of detrital zircons as a tool for studying surface processes in modern catchments. Journal Geophysical Research Earth Surface, 118, 1333–1341.

Vacherat A., Mouthereau F., Pik R., Bernet M., Gautheron C., Masini E., Le Pourhiet L., Tibari B., and Lahfid A. (2014). Thermal imprint of rift-related processes in orogens as recorded in the Pyrenees. Earth and Planetary Science Letters, 408, 296-306.

Wiedenbeck, M., Allé, P., Corfu, F., Griffin, W.L., Meier, M., Oberli, F., von Quadt, A., Roddick, J.C., and Spiegel, W. (1995). Three natural zircon standards for U-Th-Pb, Lu-Hf, trace element and REE analyses. Geostandards Newsletter, 19, 1-23.

Wiedenbeck, M., Hanchar, J.M., Peck, W.H., Sylvester, P., Valley, J., Whitehouse, M., Kronz, A., Morishita, Y., Nasdala, L., Fiebig, J., Franchi, I., Girard, J.P., Greenwood, R.C., Hinton, R., Kita, N., Mason, P.R.D., Norman, M., Ogasawara, M., Piccoli., P.M. , Rhede, D., Satoh, H., Schulz-Dobrick, B., Skår, Ø., Spicuzza, M.J., Terada, K., Tindle, A., Togashi, S., Vennemann, T., Xie, Q. and Zheng, Y.F. (2004).

Further characterisation of the 91500 zircon crystal. Geostandards and Geoanalytical Research, 28, 9-39.

Wolfe M.R. and Stockli D.F. (2010). Zircon (U-Th)/He thermochronometry in the KTB drill hole, Germany, and its implications for bulk He diffusion kinetics in zircon. Earth and Planetary Science Letters, 295, 69- 82.

APPENDIX

Cleaning of the Platinum crucibles is as follows: Lithium tetraborate is weighed into each small crucible and fused at 1000°C during 3 hours. Then, they are boiled for 3 hours in a solution of 2 liters of distilled water and 300 ml of HCl 65%.
Next, they are cleaned with distilled water and put in an oven at 100°C for at least 12 hours.

Just before the routine utilization of small Pt crucibles, we verified their U-Th-Sm blanks alcali fusion as descibed before (Fig. 4 and 5).

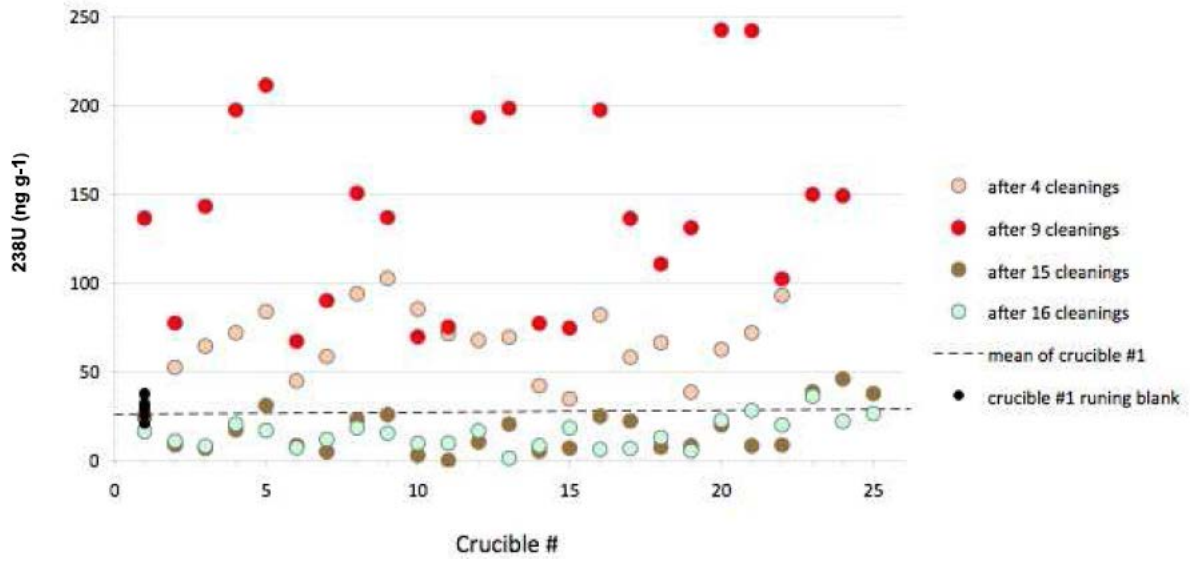

Figure 4. ^{238}U (ng g^{-1}) blanks. First analysis performed after 4 sequences of cleaning, second analysis after 9 sequences, third analysis after 15 sequences and fourth analysis after 16 sequences of cleaning.

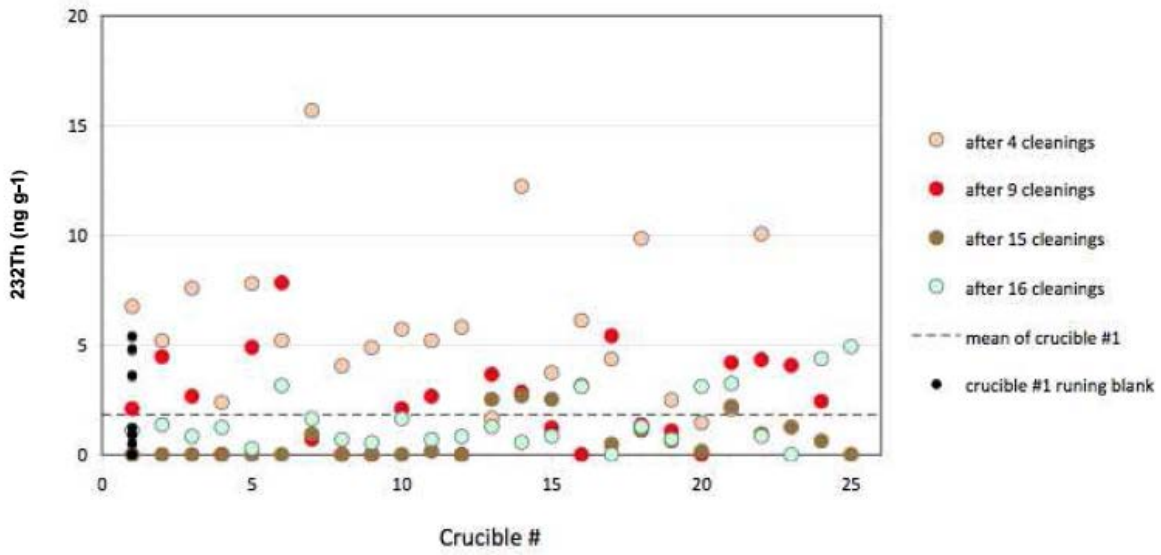

Figure 5. ^{232}Th (ng g^{-1}) blanks. First analysis performed after 4 sequences of cleaning, second analysis after 9 sequences, third analysis after 15 sequences and fourth analysis after 16 sequences of cleaning.